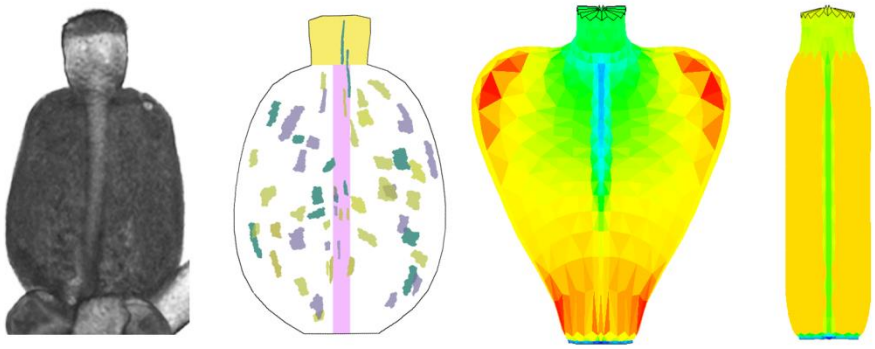

An Integrative Analysis of Fruit Shape in *Capsella rubella* and *Arabidopsis thaliana*

Tilly Eldridge

Thesis submitted for the Degree of Doctor of Philosophy

University of East Anglia

John Innes Centre

September 2014

Abstract

Plant organs develop from a small number of cells into a wide variety of shapes. This development is coordinated by underlying genetic factors that control the organisation and patterning of growth. The *Arabidopsis* fruit has been studied in detail and genes involved in fruit shape development and organisation have been uncovered. Related species that have divergent fruit forms have not been studied in the same detail and it remains unclear if the mechanisms and genes controlling growth organisation and patterning in fruit are common. Here, I give a general description of fruit shape changes within a time framework for *Capsella rubella*, which has an elaborate heart-shaped fruit. I used clonal analysis to generate a description of regional growth dynamics within the tissue. Using this data, I generated computational models to explore the coordination of growth and polarity in the *Capsella* fruit. Based on observations of morphology, growth dynamics and model outputs, *Capsella* fruit development can be divided into three phases. It is likely that there is a proximodistal polarity field that deforms locally as the fruit grows. Changes in growth rates and orientations parallel and perpendicular to this polarity field during the different phases can account for the morphology and clonal patterns of the *Capsella* fruit. In addition, I investigated factors important for the development of the heart-shaped fruit of *Capsella* through forward and reverse genetic approaches. I found *FRUITFULL* is an important factor for the development of the heart-shape fruit of *Capsella* but may not be important for the evolutionary differences in fruit shape within the family. Simplified versions of the *Capsella* fruit model accounted for fruit shapes of related species including *Arabidopsis*. This indicates that the *Capsella* fruit is a more elaborate form of the evolutionary conserved mechanisms that underlie fruit development in the Brassicaceae.

Acknowledgements

I started my PhD off the back of a year's travelling around the world with total freedom and adventure. So the idea of settling in one place for four years, with the knowledge that I would have to commute every weekend to keep my newly found relationship going was a truly daunting task. Luckily for me, Nathan Sukhnandan has stuck with me throughout this time, being ever encouraging, enthusiastic and interested in my project. His support has kept me on track, mentally and he has jumped to my need experimentally on many occasions too. I cannot thank him enough, because without him I probably would't have completed my PhD and I certainly wouldn't have been as happy.

I am deeply grateful for the support that I have received from my two exceptional supervisors, Lars Ostergaard and Enrico Coen. This partnership has been a great combination for me, allowing me the freedom to move between their areas of expertise. Lars has provided me with much encouragement and enthusiasm, and he has given me the space to explore my ideas. Rico has taught me so much from computational modelling, to presentations skills to scientific writing. Although I couldn't always answer his probing questions, he always made me think of my work in a different and more interesting way.

Thank you to my examiners Miltos Tsantis and Stan Maree for the interesting discussions we had in the viva and for all the helpful suggestions that you have made to help me improve my thesis and future work.

I have had lots of help with my experiments from members of both labs. One special individual who has been my Capsella guru is Nicola Stacey. We had many an interesting chat while drinking tea, sewing, princking out, harvesting, sieving, sterilising seeds, collecting DNA, screening mutants all on a massive and tedious scale. But somehow it wasn't a chore when working with Nicola. Many other people have helped me especially with the harvesting and threshing seeds for the TILLING population, including Nathan Sukhnandan, Friederike Jansen, Pauline Stephenson, Aisling Cooke, George Averill, Joyita Deb and Andre Kuhn.

Many people at JIC have shown me great patience in teaching me varied techniques. I am sincerely grateful to all of them and I will mention but a few. Firstly I would like to thank Susana Sauret-Gueto who as the beginning of my project really helped me get set up, taught me as much as she could about Sector analysis in flowers and has been a constant source of discussion even after she left JIC. Karen Lee has given me terrific

training on the OPT which has allowed me to generate some breathtaking images. Grant Caulder has tirelessly helped me with imaging and answered all me microscope needs.

There are many services at JIC that deserve acknowledgement as without them I think my PhD would have taken twice as long. Horticultural services has been great at looking after my mountains of plants especially Lesley Phillips who was incredibly helpful while the TILLING population was growing. Secondly, the mediaprep ladies have provided a constant source of sterile equipment, clean glassware and chinwags.

I started my PhD on the rotation programme, moving around different labs until I settled with Lars and Rico. A big thank you goes to Nick Brewin, the coordinator of this programme, who provided us with all the tools to make a success of a PhD and has continued to help me beyond my studentship, helping me to secure a further years funding to go to Africa. The fellow rotation students were my first group of friends in Norwich, helping me settle into the JIC lifestyle. I would especially like to thank Joyita Deb and Sonali Roy who have remained close friends throughout and gone through every step of the fun (and pain) with me.

I have not been short of friendship or support from lots of wonderful people at JIC. These are just a few inidividuals who have made my experience fun and worthwhile: Elaine Barclay and Paul Budd for the footy fun, Xana Rebocho and family for company on days out and evenings in and Claire Bushell and Rob Green for games and food. Outside of JIC my family could not have been more supportive. I am truly grateful to my mum and dad for supporting me through my whole education and helping me reach this point.

I would like to dedicate this thesis to three people who passed away during my PhD: my Nan and Grandad, George and Peggy Eldridge, who were always so enthusiastic and amazed at what I was up. Finally, Andrew Bangham, who always showed me so much excitement when I spoke about my project and is deeply missed by all that knew him.

Contents

List of Figures

1. Introduction

Plant organs display a wide variety of shapes and forms, from simple leaves to complex flowers and fruits. All this complexity of form begins as a small number of cells and through different developmental programmes propagates the variety of shapes all around us. The developmental pathways are under different selective constraints depending on the function of the organ. For example the Antirrhinum flower starts as a symmetrical lobed bud and develops into a complex 3D flower with dorso-ventral asymmetry and an opening mouth allowing bees to collect nectar (Green et al., 2010).

The fruit is arguably the most complex structure of flowering plants, the innovation of which characterises the angiosperms and lead to the explosion of plant diversity almost 180 million years ago. The fruit begins as a small group of cells in the centre of a young flower bud as the fourth whorl. At the start of its development, before fertilisation, the organ is termed the gynoecium, which can be composed of multiple carpels. The gynoecium grows as a protective organ for the developing ovules and directs efficient fertilisation. Once fertilised, the fruit acts as a protective organ for the developing seeds and promotes effective seed dispersal once the seeds are mature. These selective and developmental constraints have generated a wide variety of fruit forms and structures from the dry dehiscent pods of *Arabidopsis* to fleshy fruits such as tomatoes.

Within a single family, or even a single genus there can be a significant variety of fruit shapes. Within the Camilinae tribe of the Brassicaceae family, fruit shape varies from elongated siliques of *Arabidopsis* to the more elaborate heart-shaped fruit of *Capsella*. Shape differences generated through growth are controlled by genetic factors. A few genes have been identified that are important for the fruit shape in *Arabidopsis* but none have been identified in *Capsella*.

In *Arabidopsis*, the interaction of some of these genes has been studied to generate a genetic network for fruit development (Gonzalez-Reig et al., 2012; Roeder and Yanofsky, 2006). Some of these factors have also been found to be important for fruit development in other Brassicaceae genera such as Brassica and Lepidium (Girin et al., 2010; Lenser and Theissen, 2013). The dynamic expression patterns of some of these genes have also been documented (Roeder and Yanofsky, 2006). However, this picture is not complete and is complicated by genetic redundancies in the network (Dinneny et al., 2006). Many of these genes have been studied in context of fruit opening and tissue patterning and so the

contribution of these genes to fruit shape is less well understood. Also little is known about which genes are important for controlling the differences in fruit shapes between species.

To understand how fruit growth patterns are established and maintained it is important to make a detailed description of fruit growth. Within this context, the contribution of genes can be assessed. The growth of plant organs can be studied by a variety of methods. These include: time-lapse imaging (Kuchen et al., 2012; Schmundt et al., 1998), fate mapping (Bossinger and Smyth, 1996) and clonal analysis (Green et al., 2010; Rolland-Lagan et al., 2003). Using these methods growth rates and orientations can be quantified. There are very few examples of such studies in fruit with the possible exception of maize (Johri and Coe Jr, 1983). Many studies have looked at whole-organ growth dynamics such as fruit length, width and diameter over time but not looked at regional growth patterns within the fruit.

Understanding how the activities of individual genes can influence shape is complex and difficult to predict. Computational modelling can be used as a tool to bridge this gap between genetic influences at a regional level and whole organ shape (Bassel et al., 2014; Kennaway et al., 2011). Computational models of the Antirrhinum flower (Green et al., 2010), *Arabidopsis* leaf (Kuchen et al., 2012), *Arabidopsis* petal (Sauret-Gueto et al., 2013) have generated relatively simple frameworks where experimental observations can be tested on organ shape development.

In this work, the *Capsella* and *Arabidopsis* fruit were studied to understand how different fruit forms can be generated. The morphological changes through development were described and growth dynamics were studied by clonal analysis. Computational modelling was used to hypothesise the underlying growth and polarity patterns that control fruit shape. The identities of factors involved in fruit-shape development were investigated through forward and reverse genetics.

1.1 Growth

The developmental processes that give rise to characteristic shapes involve a huge change in scale which is associated with changes in cell numbers and cell size. For instance, the first leaf of *Arabidopsis* which starts from two initial cells is estimated to have ~132,000 cells at maturity (Asl et al., 2011; Pyke et al., 1991). Also, plant cells can increase by 1000 fold in volume (Pyke et al., 1991; Roeder et al., 2010). In cucumbers after anthesis a 30 fold

increase in cell area is associated with a 100 fold increase in fruit weight, an important agronomic trait (Yang et al., 2013).

1.1.1 Growth anisotropy

In plants, where cells do not move, orientations of growth at a cellular level occur through modification of cell wall properties. The plant cell wall is a lattice of biopolymers that provide mechanical strength to the tissue. In the cell wall, strong cellulose microfibrils are cross linked with hemicellulose and embedded in a pectin matrix (Cosgrove, 2005). The alignments of the cellulose microfibrils bias the orientation of cell expansion. Cell expansion is driven by turgor pressure (Lockhart, 1965) which causes stresses on the cell wall, modulated through rearrangements in the cell wall network and adding new material (Cosgrove, 2005). This modulation of cell expansion is driven by cell wall loosening enzymes known as expansins (Cosgrove et al., 2002; McQueen-Mason et al., 1992). In this way the rates of growth of an individual cell is controlled at a mechanical and a genetic level.

Another level of complexity has been added recently. A 3D model of the germinating root tip of an *Arabidopsis* embryo has been generated with an accurate representation of cells (Bassel et al., 2014). In this model, it has been shown that potential for cell expansion is influenced greatly by the geometry of the cell.

At a tissue level, growing complex shapes involves growing differentially along axes (local axiality can be represented as a field of lines). There are two hypotheses of how the orientations of growth in a tissue could be specified. In a stress-based axiality system mechanical stresses in the tissue specify the orientations of growth through positioning of cytoskeleton components such as microtubules to modify the the mechanical properties of the cell. (Heisler et al., 2010). This modulates growth orientations and in turn may feed back to influence patterns of tissue stresses. Alternatively, in a polaritybased axiality system the tissue is orientated through local molecular gradients (Green et al., 2010; Kennaway et al., 2011). Varying concentrations at a local level provides an axiality and directionality to cells (can be represented at a field of arrows). Using a polarity-based axiality system, the generation of complex biological forms such as the Antirrhinum flower can be explained through interactions of tissue growth and polarity, both modulated by genetic components (Green et al., 2010). Using this system, important morphological differences between the *Arabidopsis* leaf and petal can be explained (Kuchen et al., 2012;

Sauret-Gueto et al., 2013). These models are based on a quasi-3D tissue that deforms in 3D and abstracts away from the level of cells (Kennaway et al., 2011).

1.2 Polarity and auxin

Polarised growth in plants has been tightly linked with auxin dynamics and cellular PIN polarities. For example the new leaf primordia outgrowths at the shoot apical meristem (SAM) are correlated with high *DR5rev::GFP* expression (marker of auxin signalling) and PIN polarities pointing towards the presumptive primordia (Heisler et al., 2005).

There are several hypotheses on how PIN polarities in individual cells are coordinated at a tissue level. One hypothesis is that cells position their PINs in the cell membrane adjacent to the neighbouring cell with the highest level of auxin (Bayer et al., 2009; Sahlin et al., 2009; Smith et al., 2006). This Up-the-gradient hypothesis can account for the patterns of PIN localisations to establish spacing between new organ primordia (Jonsson et al., 2006). An alternative hypothesis is that cells can detect a net flux of auxin across the cell and position the PINs on the cell membrane with the largest net efflux (Bayer et al., 2009; Rolland-Lagan and Prusinkiewicz, 2005). This hypothesis can explain vein patterns with strands of PIN expression following the route of a presumptive vein.

A more recent hypothesis is the intracellular partitioning, in which individual cells can generate polarity without asymmetric cues (Abley et al., 2013). Cell polarities are coordinated across a tissue by cell-cell coupling by a diffusible molecule such as auxin. In this hypothesis, organisers of polarity at the boundaries of organs fix the polarity across the tissue (Abley et al., 2013). This hypothesis has made several predictions that distinguish it from the above models, and these predictions are currently being tested experimentally (Katie Abley, unpublished).

1.3 *Arabidopsis* fruit morphology and development

The most detailed characterisation of a developmental series of gynoecium and fruit growth to date has been carried out in *Arabidopsis*. The mature fruit shape of *Arabidopsis* is an elongated cylindrical silique. The fruit is composed of several specialised tissue types which are derived from the gynoecium (Figure 1.1). The gynoecium consists of two carpels that are congenitally united in the medial region and develops as a cylinder (Figure 1.1). The carpels are thought to have originated from leaves that carried spore-producing organs or sporophylls (Scutt et al., 2006).

The tissues of the gynoecium can be characterised along three orthogonal axes: proximodistal axis (Figure 1.1A), mediolateral axis and abaxial-adaxial axis (Figure 1.1B).

The proximal base of the fruit is connected to the rest of the flower by a short stalk or gynophore. The ovary makes up the majority of the fruit length which is composed of two valves (fruit walls) joined at a central replum at the valve margins. At the distal apex the fruit has a style and stigmatic tissue (Figure 1.1A).

The medial tissue of the fruit includes the two repla joined by a septum which divides the fruit into two separate halves. The ovule placentae align along the inner side of the repla (Figure 1.1B). The style and stigmatic tissue are also medial tissues. The valves make up the lateral tissue of the gynoecium.

The adaxial surface is the inner-epidermis which consists of two layers, endocarp *a* and endocarp *b* which become lignified in later stages of development (Spence et al., 1996). Three layers of cells make up the mesocarp and the outer (abaxial) epidermis is the exocarp, made up of large rectangular cells interspersed with stomata.

The features of *Arabidopsis* gynoecium development have been staged using

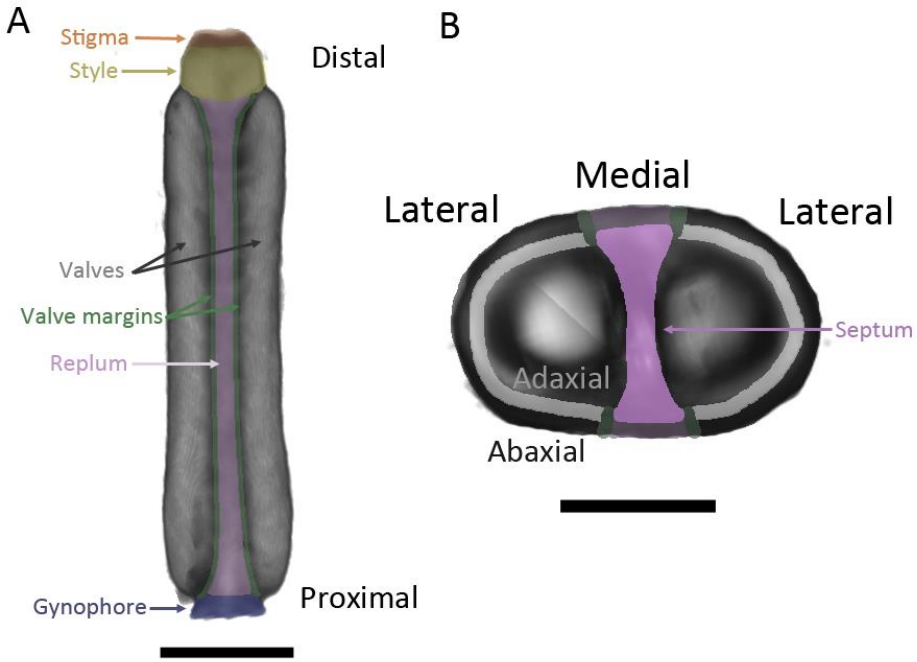

Figure 1.1 Patterning of the Arabidopsis fruit (A) Longitudinal view of the Arabidopsis fruit just after anthesis. Image taken by Susana Sauret-Gueto (B) Cross section view of a mature Arabidopsis fruit. Images taken by optical projection tomography. Scale bars 500µm

Flower stage	Gynoecium and fruit development	Landmark features	Reference
6	The gynoecium develops as an oval ridge with a cleft in the centre. 16 progenitor cells of the flower bud give rise to the gynoecium, 8 for each carpel	Sepals close round the flower bud	(Bossinger and Smyth, 1996; Smyth et al., 1990)
7	The ridge grows up to produce a hollow cylinder	Medial stamens become stalked at the base	(Sessions, 1997)
8	The gynoecium continues to grow as a cylinder. The septum begins to form and the medial ridges become flanked by placentae	Locules form in the anthers	(Smyth et al., 1990)
9	The gynoecium apex start to close and the first stigmatic papillae appear. The style becomes morphologically distinct.	Petal primordia become stalked	(Roeder and Yanofsky, 2006; Smyth et al., 1990)
10	The gynoecium reaches ~400µm.	Petal primorida reach the length of the short stamens	(Sessions et al., 1997)
11	The stigmatic papillae cover the surface of the stigma. The surface of the style develops wax crenulations		(Roeder and Yanofsky, 2006)
12	The valves, valve margins and replum become morphologically distinct and the gynoecium becomes ready for fertilisation	The petals reach the length of the long medial stamens	(Roeder and Yanofsky, 2006)
13		Anthesis, the flower opens and self-fertilises	(Smyth et al., 1990)
14	Pollen tubes grow down the transmitting tract and fertilise the ovules.	The anthers extend above the stigma	(Roeder and Yanofsky, 2006)
15	Gynoecium elongates above the anthers		(Roeder and Yanofsky, 2006)
16	The fruit continues to elongate	Sepals, petals and anthers fall from the fruit	(Smyth et al., 1990)
17A	The fruit elongates to its mature size		(Roeder and Yanofsky, 2006)
17B	The valve margin differentiates into the dehiscence zone. The lignified layer becomes lignified		(Roeder and Yanofsky, 2006)
18	The silique turns yellow and the separation layer disintegrates		(Roeder and Yanofsky, 2006; Vivian-Smith and Koltunow, 1999)
19	The valves separate from the replum and fall away from the fruit		(Roeder and Yanofsky, 2006)
20	The seeds fall from the replum		(Smyth et al., 1990)

Table 1.1 The key developmental stages of the Arabidopsis gynoecium and fruit. The fruit is defined as when fertilisation has taken place (green).

landmark features of early flower development (Sessions, 1997; Smyth et al., 1990). The developmental stages of the fruit have also been described in detail (Roeder and Yanofsky, 2006). Table 1.1 details the key developmental stages in the *Arabidopsis* fruit and gynoecium development.

1.4 Polarity, Growth and Patterning in the fruit

1.4.1 Proximodistal axis

The growth of the *Arabidopsis* gynoecium is anisotropic from a very early stage (Smyth et al., 1990), suggesting that it has a polarity at or shortly after initiation. There are several pieces of evidence that auxin or polar auxin transport may coordinate the proximodistal axis of the *Arabidopsis* fruit. During the earliest stages of gynoecium development (stage 5-6) there is expression of the auxin biosynthesis genes YUCCA1 and YUC4 at the base of the gynoecium primordia (Cheng et al., 2006). The double mutant *yuc1yuc4* have severe disruption of gynoecium patterning along the proximodistal axis with a stalk-like gynoecium with no valve tissue (Cheng et al., 2006). In addition, the auxin efflux carrier PIN1 is apically localised on the epidermal cells of the gynoecium at an early stage (Moubayidin and Ostergaard, in revision). PIN localisations and auxin dynamics could determine the proximodistal polarity of the gynoecium, or may be a read out of the underlying polarity.

It has been hypothesised that a gradient in auxin is responsible for the proximodistal patterning of the *Arabidopsis* gynoecium (Nemhauser et al., 2000). In this model the highest concentration of auxin (internal or external auxin is not specified) at the apex of the gynoecium generates style differentiation, medium levels of auxin give rise to valve differentiation and the lowest levels of auxin generate the gynophore (Nemhauser et al., 2000). However, several recent pieces of evidence contradict this hypothesis (Hawkins and Liu, 2014).

An auxin gradient has not been visualised with the auxin signalling marker *DR5rev::GFP*. Expression is initiated as two foci at the apex in the lateral regions of the young gynoecium, then two additional foci initiate in the medial regions before a continual ring of *DR5rev::GFP* expression around the apex at stage 8 (Girin et al., 2011; Grieneisen et al., 2013; Larsson et al., 2013). This ring of high auxin signalling overlaps with high expression of PIN3 at the apex (Moubayidin and Ostergaard, in revision). The ring of *DR5rev::GFP* expression is disrupted in several mutants of genes important for style identity

and growth. For example *NGATHA* and *STYLISH* genes are essential for proper style development and both drive *YUC4* in the presumptive style (Sohlberg et al., 2006). A *nga* quadruple mutant has severe defects in the style, and no longer produces a WT *DR5rev::GFP* ring of expression. However, the valve tissue develops as normal (Martinez-Fernandez et al., 2014) indicating that the proximodistal axis has been established prior to the expression of *DR5rev::GFP* at the gynoecium apex. NGA is also essential for style development in other species including basal eudicot *Eschscholzia californica* (Fourquin and Ferrandiz, 2014). The expression of *YUC1 YUC4* at the earliest stages of gynoecium development is at the base. Only at later stages, from stage 8, *YUC4* expression is concentrated at the apex, in the presumptive style (Cheng et al., 2006; Trigueros et al., 2009). Given that the disruption of this auxin synthesis pattern does not greatly alter the proximodistal patterning of the gynoecium it is possible that early synthesis of auxin at the base is more important for the early proximodistal patterning of the gynoecium.

1.4.2 Ad-abaxial axis

The ad/abaxial axis, which is orientated from the inside to the outside of the gynoecium, is also defined at a very early stage in development. The ad/abaxial axis is defined by the polar expression of transcription factors.

Abaxial fate of the gynoecium (outside) is determined by the GARP transcription factors *KANADI1/2* which are also important from abaxial identity in other lateral organs (Eshed et al., 2001; Kerstetter et al., 2001). *kan1 kan2* mutants have ovules on the outside of the gynoecium (Eshed et al., 2001). *ETTIN*, a member of the auxin response factor (ARF) family of transcriptional regulators is also important for the abaxial identity (Hunter et al., 2006; Sessions, 1997). *KAN1* and *ETT* have been shown to interact (Kelley et al., 2012) and it has been suggested that *KAN-ETT* complex acts as a module to promote abaxial fate (Pekker et al., 2005).

ett gynoecia have much reduced valve tissue and longer gynophore and style regions. From this evidence (Nemhauser et al., 2000) hypothesised that *ETT* was required for tissue boundary formation in an auxin concentration dependent manner, by mediating a ‘middle-level’ auxin response generating the ovary and excluding the high and low level auxin responses of the style and gynophore, respectively. Recently, the *ett* mutant phenotype has been reinterpreted to that valve growth along the proximodistal axis

requires the juxtaposition of adaxial and adaxial identity (Hawkins and Liu, 2014). However, little is known about how the components of ad/abaxial patterning coordinate growth.

Adaxial fate in lateral organs is driven by *PHABULOSA (PHB), PHAVOLUTA (PHV)* and *REVOLUTA (REV)* members of the class III homeodomain leucine zipper (HD-ZIP III) family (McConnell et al., 2001; Nole-Wilson et al., 2010). Gain of function alleles of *PHB* cause ectopic growth of ovules at the base of the gynoecium (McConnell and Barton, 1998).

1.4.3 Mediolateral axis

Patterning along the mediolateral axis is caused by the antagonistic activities of lateral and medial factors. The lateral factors *FILAMENTOUS FLOWER*/*JAGGED*/*YABBY3* and *ASSYMETRIC LEAVES1/2* are important for establishing the boundary between the valve and the replum (Alonso-Cantabrana et al., 2007; Gonzalez-Reig et al., 2012). *FIL/JAG/YAB3* act upstream of *FUL* which specifies valve identity in late stages of fruit development. The positioning and size of the replum is specified by the medial factors *BREVIPEDICELLUS* (*BP*), *REPLUMLESS* (*RLP*) and *WOX13* (Alonso-Cantabrana et al., 2007; Gonzalez-Reig et al., 2012; Roeder et al., 2003; Romera-Branchat et al., 2012).

The valve margin is controlled by *SHATTERPROOF1/2* upstream of two bHLH transcription factors: *INDEHSCENT* and *ALCATRAZ* (Liljegren et al., 2004; Rajani and Sundaresan, 2001). The expression of these genes is restricted to the valve margins by *FRUITFULL (FUL)* and *RLP* from stage 12 (Gu et al., 1998; Roeder et al., 2003). The interactions of FUL and SHP1/2, two MADS-box transcription factors, have been shown to be important for fruit growth and lignification in many species (Ferrandiz and Fourquin, 2014). *SHP* genes in Medicago are important for the spiral form of the fruit in some species (Fourquin et al., 2013).

Thus, many factors and interactions important for the patterning along the mediolateral axis in the gynoecium have been identified. Again, little work has been done to understand how this patterning influences growth and shape of the fruit.

1.5 Fertilisation

Growth of the fruit is complicated by the coordination with the growth of the seeds. If the seeds are not fertilised it is not beneficial for the plant to waste resources on growing an empty fruit. When this process is uncoupled, the fruits can expand without fertilisation, a phenomenon known as parthenocarpy. Moreover, as soon as the seeds are

fertilised, it is important that the growth of the fruit stops when the seeds reach maturity. This function of the fruit involves seed to fruit communications that have been studied in great detail.

Hormones play a key role in seed to fruit communication. Exogenous application of Gibberellins (GA), auxin and cytokinin can all induce parthenocarpy in *Arabidopsis* (Vivian-Smith and Koltunow, 1999). GA causes the degradation of growth inhibitor proteins DELLAs, and this process is essential for the post fertilisation growth of the fruit (Fuentes et al., 2012). In agreement with the role of DELLAs in repressing growth in the absence of fertilisation, reduced levels of DELLAs in fruits have a parthenocarpic phenotype in tomato and *Arabidopsis* (Fuentes et al., 2012; Marti et al., 2007). Mutants in the auxin response factor *ARF8* also induce parthenocarpy, showing that *ARF8* is also a repressor of fruit growth in the absence of fertilisation in both *Arabidopsis* and tomato (Goetz et al., 2007).

Overexpression of a cytochrome P450 CYP78A9 also generates parthenocarpic fruit in *Arabidopsis* (Ito and Meyerowitz, 2000). The fruit are also much wider and slightly longer than wildtype when fertilised. Multiple knockouts of P450s (*cyp78a9* and its closest paralogues *cyp78a6, cyp78a8*) resulted in smaller fruits even after fertilisation, and CYP78A9 is expressed in the ovules, seeds and septum (Sotelo-Silveira et al., 2013). CYP78A9 overexpression does not influence any known hormonal pathways and this has led to speculation that it produces a novel signal important for reproductive signalling (Sotelo-Silveira et al., 2013).

1.6 Fruit shape

As well as CYP78A9, a few genes have been identified in *Arabidopsis* that influence fruit shape. A mutation in the gene *PEAPOD* (*PPD*) causes over proliferation of meristemoid cells which results in shorter, triangular-shaped siliques that are wider at the distal end of the valves (White, 2006). A family of small polypeptides named *DEVIL* or *ROTUNDIFOLIA* can also influence silique shape in *Arabidopsis* when overexpressed (Larue et al., 2010; Narita et al., 2004; Wen et al., 2004). A variety of shapes can be generated with the overexpression of the *DVL*/*ROT* peptides, generally triangular in shape being wider at the top or wider at the bottom or horn-looking outgrowths at the top of the valves (Wen et al., 2004). These factors that can influence fruit shape in *Arabidopsis* have been speculated to be important for fruit shape differences in the Brassicaceae (Bowman, 2006). However, there is little information on how fruit shape in other Brassicaceae species is established.

1.7 Phylogeny of the Brassicaceae

The Brassicaceae is a large family, consisting of 338 genera and 3700 species (Al-Shehbaz et al., 2006). In the past, species were characterised on morphological features such as fruit shape and seed embryo type. Since the advent of molecular phylogenetics, the species, genera and tribes of Brassicaceae have been revised and it was found that characteristics such as fruit shape are evolutionary very plastic, and species previously classified together because of these features may not belong to monophyletic groups (Al-Shehbaz et al., 2006; Al-Shehbaz et al., 2002; Bailey et al., 2006; Beilstein et al., 2006). This apparent evolutionary plasticity could be result of high selective pressures on particular fruit forms in different environments. Alternatively genetic drift could fix different fruit shapes between populations.

The Camelineae tribe consists of 12 genera including: *Arabidopsis*, *Capsella*, *Camelina*, *Neslia* and *Catabolous* (Bailey et al., 2006). The fruit shape within this tribe varies significantly, for example *Arabidopsis* have elongated siliques, *Capsella* have heart-shaped sillicles and *Neslia* have rounded sillicles (Al-Shehbaz et al., 2006). This diversity in fruit shape provides good models to understand how differences in fruit shape is generated and the genetic control that leads to this variation.

Capsella represents an interesting model as it has a unique fruit shape from the rest of the Brassicaceae with flattened heart-shaped fruit. The genus contains three species, *Capsella bursa-pastoris*, *Capsella grandiflora* and *Capsella rubella*. *C. bursa-pastoris* is the fifth most widely spread flowering plant species in the world (Coquillat, 1951) and has been of scientific interest for over one hundred years (Shull, 1914). *C. bursa-pastoris* is a tetraploid which explains segregation ratios of recessive traits observed by Shull (1914) of 15:1. *C. grandiflora* is an outcrossing species and *C. rubella* is a selfing species that was thought to have arisen from a major bottleneck, where one individual gave rise to the entire *C. rubella* lineage only 20-50,000 years ago (Foxe et al., 2009; Guo et al., 2009). This interesting evolutionary history and reproductive biology has led to extensive studies on mating systems in *Capsella* (Agren et al., 2014; Hintz et al., 2006; Sicard et al., 2011) and the generation of a lot of genetic information including an annotated genome sequence for *C. rubella* (Slotte et al., 2013).

C. rubella has been used as a model to identify factors important for leaf morphology (Sicard et al., 2014). The homeobox gene *REDUCED COMPLEXITY* (*RCO*) was

shown to be important for the differences in leaf morphology between *C .rubella* and *C. grandiflora* (Sicard et al., 2014). *RCO* was first reported to be responsible for controlling the differences in leaf complexity between *Arabidopsis* and *Cardamine hirsuta* (Vlad et al., 2014). Factors important for morphological evolution of fruit shape in Brassicaceae have yet to be identified.

1.8 Modelling

Shape development is highly complex and involves the coordination of growth and polarity at a range of scales including at a whole tissue level and within individual cells. The control of shape development is likely to come from biochemical factors, operating within the constraints of physical factors. It is also possible that physical factors play a more direct role in coordinating growth and polarity.

With such a high level of complexity, it is difficult to decipher the key principles underlying the developmental process. Moreover, with increasing knowledge of developmental dynamics, mathematical formulations of growth are becoming more complex. Thus, computational modelling is increasingly used to test if hypotheses or experimental measurements can account for developmental observations. Even when a vast amount of information is available on a developmental process, the outcome is often not intuitive due to the complex interactions. For example in the *Arabidopsis* embryo root, the expression of growth factors is displaced from the centre of cell expansion. It was found that mechanical constraints of 3D cell geometry directs where genetically controlled growth can occur through the use of a 3D cellular computational model (Bassel et al., 2014).

Many modelling tools are becoming available to model systems on a variety of different scales (Walpole et al., 2013). As computational power increases the number of scales that can be incorporated into a single model is increasing. For example (Chew et al., 2014) have integrated four existing models into a multiscale model that predicts growth of individual organs and the whole organism.

When modelling tissues, they can be treated as either discrete or continuous systems. In discrete systems, tissues are composed of discrete entities which in a biological system generally represent cells. In a continuous system the tissue is treated as a continuum and for computational purposes is discretised into smaller regions. The type of model that is used is dependent on the specific biological question that is being addressed.

For example a discrete system is suitable for modelling *Dictyostelium discoideum*, the slime mould which undergoes cellular rearrangements (Marée et al., 1999). Also a model of auxin transport in a tissue involves the polar distribution of PIN proteins on the cell membranes. Therefore models are generally discrete (Abley et al., 2013; Grieneisen et al., 2007).

Generally, to model biological systems on a tissue scale, continuous systems are used. For example, the finite element method (FEM) is a continuous system which has been used to model the tissue dynamics of many different biological systems such as the insect wings (Kesel et al., 1998) and *Arabidopsis* leaf and petal development (Kuchen et al., 2012; Sauret-Gueto et al., 2013).

1.9 This work

A large number of developmental genes and pathways have been identified in the *Arabidopsis* gynoecium and fruit. However, how these genes and pathways relate to fruit shape is unclear. In addition, very few factors important for divergent fruit shapes in the Brassicaceae have been identified. Therefore, in this work I have used a combination of imaging, growth analysis, computational modelling and forward and reverse genetics to understand the key factors important for fruit shape determination in *Capsella rubella* and *Arabidopsis thaliana*.

To understand how fruit shape develops a description of fruit growth is necessary. In *Arabidopsis* the development of the gynoecium and fruit has been described in great detail (Roeder and Yanofsky, 2006; Smyth et al., 1990). However, in *Capsella* a detailed description of developmental shape changes is lacking. Also data on growth dynamics on a whole organ and on a regional tissue scale is not available for either species. Here, I use clonal analysis to estimate growth rates and visualise growth orientations in *Capsella* and *Arabidopsis* gynoecia and fruit.

I have generated computational models of fruit shape development using a framework termed Growing Polarised Tissue (GPT) framework (Kennaway et al., 2011). This framework has been used to generate models for the Antirrhinum flower (Green et al., 2010), the *Arabidopsis* leaf (Kuchen et al., 2012) and the *Arabidopsis* petal (Sauret-Gueto et al., 2013). This framework is implemented in a tool box, called *GFTbox* in MATLAB and tissues are treated as a continuum, based on FEM. This method has been chosen as tissue deformations can be studied on an organ scale without having to consider the large number of biological cells individually.

To identify genetic factors that are important for the growth of heart-shaped fruit in *Capsella* I have generated a mutant population in *Capsella rubella* by chemical mutagenesis. This population was also developed as a TILLING population to use as a reverse genetics resource. Here, I investigate and characterise a candidate gene for fruit shape development, *FRUITFULL*.

This work aims to understand the key factors that underlie fruit shape in *Capsella* and *Arabidopsis*. I will use imaging, clonal analysis and *GFTbox* to show how the *Capsella* fruit develops in three phases through changes in local growth orientations. I will show how *FUL* is important for the development of the heart-shape fruit in *Capsella* through mutant analysis. In addition, I will investigate the role of *FUL* in the evolution of divergent fruit shapes in the Brassicaceae by a transgenic approach. Finally I will use the model developed for *Capsella* fruit to investigate divergent fruit shapes in the Brassicaceae, including *Arabidopsis*.

2. Capsella Fruit Growth

2.1 Introduction

In the Brassicaceae there is an array of distinct fruit shapes that each grow from a small group of cells or primordia. The developmental series and shape changes that occur from the primordia to the final fruit has been studied in detail in *Arabidopsis* (Roeder and Yanofsky, 2006). However, the development and growth of a divergent fruit shapes has not been explored.

Comparative studies between *Arabidopsis* and other Brassicaceae species have been powerful in identifying key characteristics and genetic players controlling divergent leaf shapes (Hay et al., 2014; Vlad et al., 2014). For fruit shape studies the genus *Capsella* represents a good comparative model against *Arabidopsis* due to the distinct heart-shaped form and its close evolutionary proximity.

2.1.1 Growth dynamics

To understand fruit growth first a detailed picture of growth dynamics has to be generated. Growth dynamics have been calculated in a variety of ways. Live imaging and cell tracking has been used in the *Arabidopsis* leaf to get a detailed picture of leaf growth (Kuchen et al., 2012). The limitation of this technique is the accessibility of the organ for imaging and also the size. The gynoecium is protected within the developing flower bud which makes it unsuitable for live imaging with current technologies.

A second method that has been utilised in many biological systems for decades is clonal or sector analysis. Clonal analysis is a technique that marks somatic cells in various ways to determine rate and orientation of cell divisions within an organ. The value of this approach to study developmental processes was first recognised by (Stadler, 1930). The first clonal analysis in plants was carried out in maize where coloured sectors caused by chromosome deletions were used to reconstruct the development of the shoot apex (Steffensen, 1968; Stein and Steffensen, 1959). These early studies used x-rays to induce sectors; today transgenic lines are commonly used. Cre/LoxP systems involve expression of the Cre site specific recombinase of bacteriophage P1 (Sternberg and Hamilton, 1981) under an inducible promoter such as a heat shock promoter (Sieburth et al., 1998). Induction leads to a recombination event at specific Lox sites specifically designed to activate expression of either a colour gene (Gallois et al., 2002) or a gene of interest

(Sieburth et al., 1998) or both (Wachsman et al., 2011). Heat shock inducible GFP sectors (or clones) have been successfully used to generate growth maps in *Arabidopsis* leaves and petals (Kuchen et al., 2012; Sauret-Gueto et al., 2013) through different stages of development.

2.1.2 Organ shape

It has been shown that shapes of the Antirrhinum and *Arabidopsis* petals depend on directions of growth rather than differences in local growth rates (Rolland-Lagan et al., 2003; Sauret-Gueto et al., 2013). In both cases clonal patterns showed that orientations of growth that were evident from the earliest stages were maintained throughout development. In contrast, growth rates are non-uniform along the proximal distal axis of the *Arabidopsis* leaf and principle orientations of growth change through development (Kuchen et al., 2012). However, differences in the appendage shapes can be accounted for in the same basic framework involving a polarity field and patterns of growth rates specified parallel and perpendicular to the polarity (Kennaway et al., 2011; Kuchen et al., 2012; Sauret-Gueto et al., 2013). To date a similar study has not been carried out on the fruit, which is thought to be the most complex organ of flowering plants.

Here, the *Capsella rubella* gynoecium/fruit was studied to explore development of a divergent fruit form. The stages of development were imaged using SEM and whole organ dynamics were measured from OPT images. Clonal analysis was performed at different stages of development to investigate local growth dynamics from primordium stage to a mature heart-shape fruit. The observed dynamics were used to generate a computational model of *Capsella* fruit development.

Although the *Capsella* fruit is a 3D volumetric structure the model represents it as a 2D cylindrical sheet that can deform in 3D but has no internal tissue. This can be representative as the layers of the *Arabidopsis* gynoecium valves are established in the earliest stages of development and the epidermal layer does not seem to contribute cells to the underlying layer. Also, most growth of the valves occurs along the mediolateral and proximodistal axis and so can be represented as a 2D cylindrical sheet. The medial tissue including the septum, ovules and style also grow along the abaxial-adaxial axis; however, this growth cannot be captured in the 2D modelling framework.

2.2 Results

2.2.1 Fruit growth dynamics

To investigate how the *Capsella* fruit shape changes, it was first necessary to describe the timing and pattern of these shape changes. *Capsella* plants were grown in standardised conditions and whole inflorescences were collected at two day intervals starting from 19 to 32 days after sowing. This method was developed from a protocol for staging *Arabidopsis* flower buds (Sauret-Gueto et al., 2013).

To standarise each inflorescence, the timing of the first flower of the main inflorescence was given in exact hours after sowing (HAS). The timing for subsequent flowers on the same inflorescence was calculated using the plastochron (timing interval between initiation of successive flower primordia) and the flower position. The plastochron was calculated by counting the number of newly open flowers in a 24h period on 10 inflorescences and averaged over several days. Under these conditions the plastochron of *Capsella* was 4.8h. The position of the individual flowers is the order that the flowers were initiated; so that the first flower on the inflorescence (oldest) would be at position 1, the second flower (second oldest) would be at position 2. Since, the flower at position 2 is initiated one plastochron after the first flower (456 HAS), the timing of the second flower would be 456 h – 4.8 h = 451.2 HAS. It is important that every flower can be standardised in time so that the growth rates of the flowers and floral organs can be estimated.

I measured the length and width of multiple gynoecia/fruit from each sample. The length was measured along the longest axis of the gynoecium from the gynophore to top of the style; stigmatic hairs were not included in the length measurement as they are variable depending on the fertilisation status. Width was measured at the widest point across the mediolateral axis. A better idea of gynoecium age was gained by classifying the gynoecium according to timing after gynoecium initiation rather than HAS. Gynoecium initiation, 0 days after initiation (0 DAI) was assumed to be when the gynoecium is a simple cylindrical shape and ~40µm in length which corresponds to ~450 HAS.

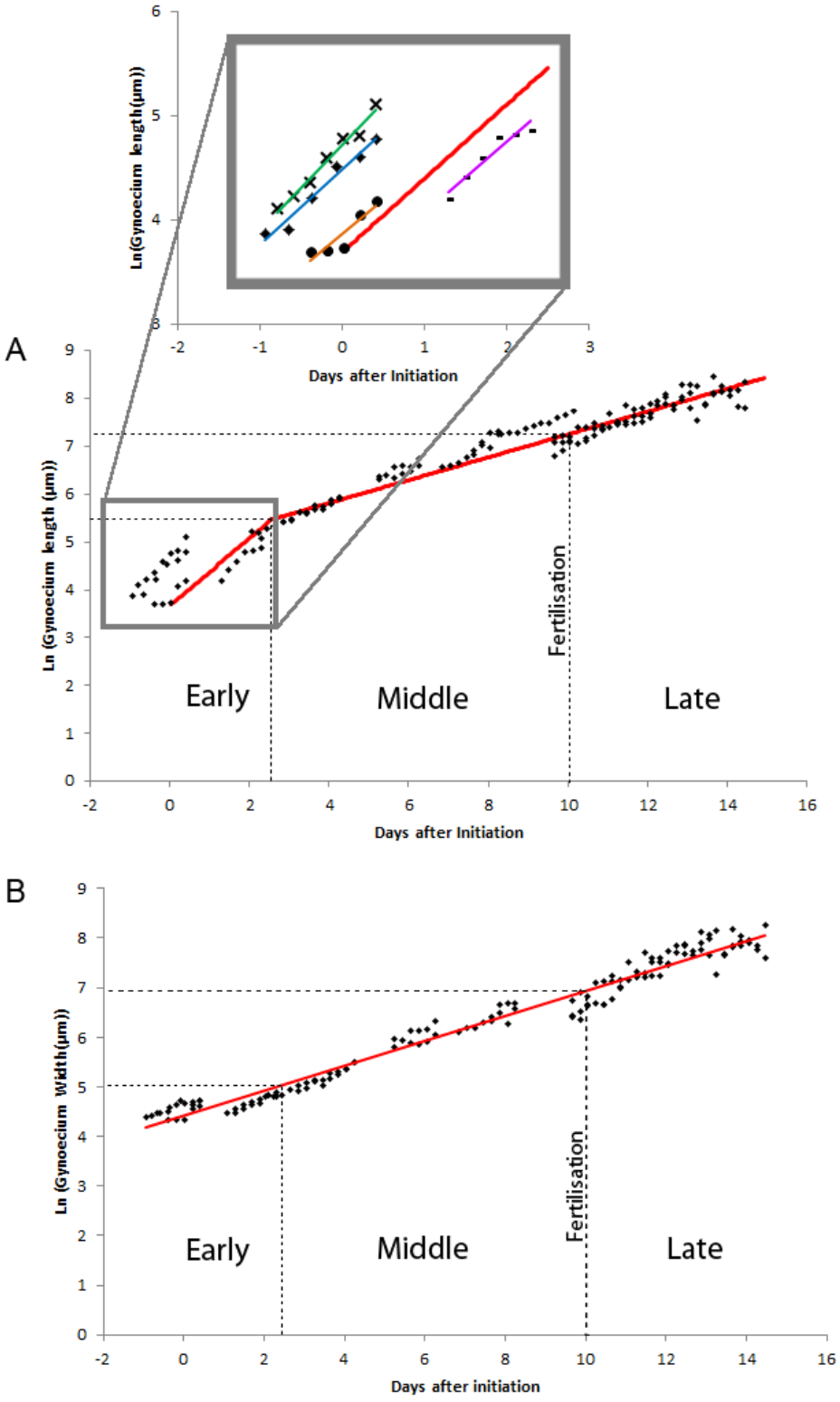

Figure 2.1 Growth of *Capsella rubella* fruit. Natural logarithm of gynoecium length (A) and width (B) at days after initiation. A straight line was fitted to the data (red lines). (A) Grey inset shows individual inflorescences (green, blue, pink and orange lines) with variation of 2 days. The growth is divided into three phases marked by dotted lines: 0-2.5 DAI early phase where rate of growth in length is 3%/h (A –red line inset) and width 1.15%/h, 2.5-10 DAI middle phase up to fertilisation and 10-15 DAI after fertilisation , rate of growth in length is 1%/h and width 1.15%/h.

The natural logarithm of gynoecium length and width was plotted against DAI (Figure 2.1). From ~0-2.5 DAI the rate of growth in gynoecium length is greater than in later stages, this period is designated early phase. The middle phase begins at 2.5 DAI and lasts until fertilisation at ~10 DAI. After fertilisation (10-15 DAI) is designated late phase.

The measurements of the early phase gynoecium show some discrepancy in timings (Figure 2.1A). Four inflorescences were measured and between them is a two day variation in time of initiation. This may be due to the initiation of the inflorescence meristem not being completely uniform. In each sample the time of initiation was variable but the rate of growth in gynoecium length was ~3%/h (Figure 2.1A). The rate of growth in gynoecium length in the middle phase and late phase is drops to ~1%/h. In Figure 2.1A a straight line was fitted to the data, with a 3 %/h growth rate in length from 0-2.5 DAI (starting length is 40µm) and a 1 %/h growth rate from 2.5-15 DAI.

The rate of growth in gynoecium width remains at a constant level of ~1.15%/h from 0-15 DAI (Figure 2.1B). An early, middle or late phase cannot be distinguished from this data.

To compare growth rates in length versus width the natural logarithm of length was plotted against the natural logarithm of width (Figure 2.2). A gradient of 1 would mean length is growing at an equal rate to width, in Figure 2.2 this is represented by a red dotted line. Deviation from 1 would mean growth is anisotropic with one axis growing more than the other. Using this plot two phases of growth are observed. During early stages of development gynoecium length is growing more than width (green line); this is from 0-2 DAI when the gynoecium is between 40µm and 200µm in length. At around 2DAI the whole organ growth pattern changes and width grows slightly faster than length (blue line).

2.2.2 Morphology of *Capsella* fruit

I have established a time framework for the growth of the *Capsella* fruit from 0-15 DAI. Next, to investigate the patterns of shapes within this framework it was necessary to describe the fruit morphology throughout development. A standard method for looking at developmental stages is scanning electron microscopy (SEM). SEM produces detailed images of organ surfaces allowing cell types to be distinguished. However, SEM does not always provide an accurate 3D perspective of organ shape.

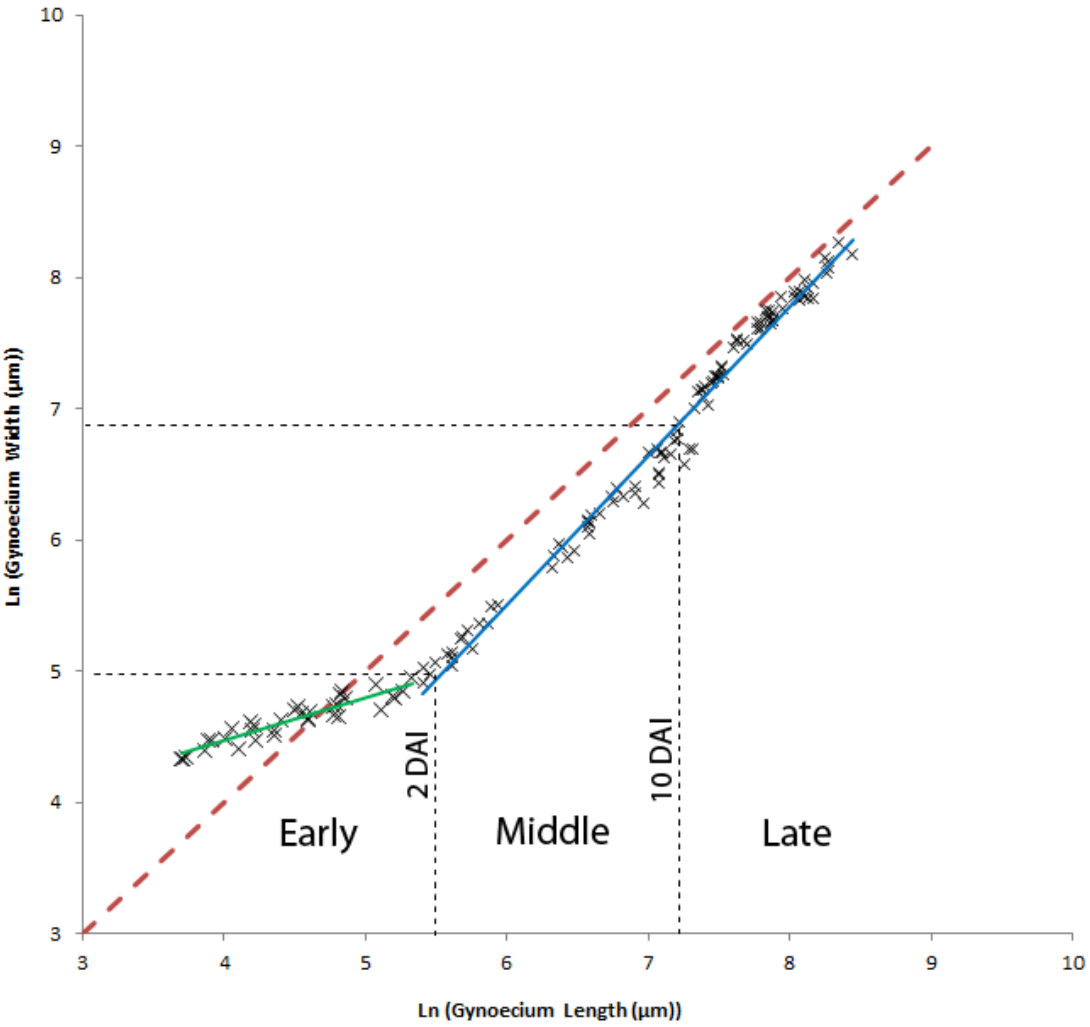

Figure 2.2 Natural logarithm of length vs. width during Capsella gynoecium development. Each cross represents one gynoecium. The red dotted line plots length and width growing at an equal rate. The gradient of the green fitted line is 0.33 showing that the growth rate in length is greater than width at early stages of development. The gradient of the blue fitted line is 1.14 showing that in later stages of development the growth rate is greater in width than length.

Optical projection tomography (OPT) can be used to look at structures in 3D. OPT shines various wavelengths of light through cleared tissue. The projection of the remaining light is detected at 400 angles and then reconstructed into a 3D image (Lee et al., 2006; Sharpe et al., 2002). Volviewer is software developed in the lab to visualise these images in 3D. OPT does not provide cellular detail but is an effective complement to SEM images.

Here, I dissected prepared and imaged using SEM *Capsella* flower buds and fruits of all different sizes. Complementary to this, I dissected whole inflorescences and dissected gynoecia and fruit imaged them using OPT. Included in the description is the corresponding

floral developmental stage (Smyth et al., 1990), which uses landmark features to stage floral development in *Arabidopsis*.

2.2.3 Shape changes of the *Capsella* fruit

The gynoecium primordium, 0 DAI (flower stage 6), was difficult to dissect without damaging the tissue due to its small size (~40µm in length). For this reason SEM (Figure 2.3A) does not give us a clear picture of the initial gynoecium shape. However, there is clearly a groove in the centre of the primordia with a ridge all the way round. OPT confirms this (Figure 2.3C) and shows that the distal end of the gynoecium at 0 DAI is wider than the proximal end (Figure 2.3B). The primordium is oval in cross section (Figure 2.3C).

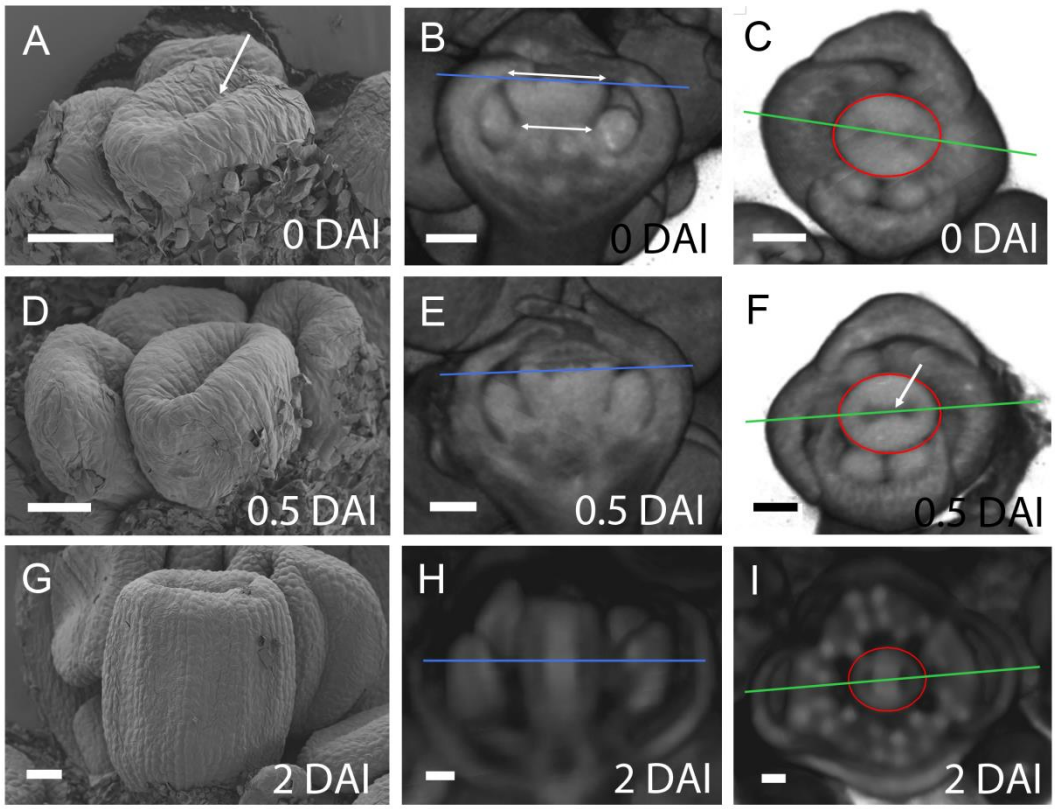

Figure 2.3 Early phase of Capsella gynoecium development (A, D, G) SEM of dissected gynoecia. (B, E, H) OPT image of flower buds, virtual longitudinal sections through mediolateral plane indicated by green line in C, F, I, respectively. (C, F, I) OPT image of flower buds, virtual cross section indicated by blue line in B, E, H, respectively. (A, C) arrow shows central cleft. (B) Arrows show the top is wider than the base. (F) arrow marks the deepening central cleft. Red outlines show oval cross section of the gynoecium. (G) no tissues in gynoecium epidermis are differentiated, note cylindrical shape of gynoecium. Scale bars: 25µm (A, D, G) and 50µm (B, C, E, F, H, I).

0-0.5 DAI corresponds to flower stage 7, marked by the medial anthers becoming stalked at the base. The gynoecium develops as a hollow cylindrical tube as the ridge around the primordia grows and the central groove deepens (Figure 2.3D, F). The oval cross section shape is maintained and the gynoecium elongates (Figure 2.3F).

At 2 DAI the gynoecium is at flower stage 8, characterised by the anthers forming locules. The gynoecium reaches ~200µm and there is no obvious differentiation of tissues in the epidermis (Figure 2.3G). The gynoecium is cylindrically shaped throughout this stage (Figure 2.3H) and has an oval cross section (Figure 2.3I).

From 2-6 DAI a distinct change in gynoecium shape is observed. At 3 DAI (early flower stage 9) the cylindrical shape rounded with a tapered distal apex (Figure 2.4A). By 4DAI the tapered apex becomes morphologically distinct as the style and becomes covered in immature stigmatic papillae (Figure 2.4B). The rounded shape becomes more pronounced 6 DAI with the style becoming much narrower than the ovary (Figure 2.4C-F). The perspective of the SEM images show a flat gynoecium but the OPT images show an oval cross-section (Figure 2.4D). The central cleft of the style begins to close (Figure 2.4C).

At 8.5 DAI cell types on the gynoecium epidermis are morphologically distinct: the style, stigma, a central replum and the valves are observed (Figure 2.5E). In the cross-section plane the ovary is slightly flattened along the mediolateral axis (Figure 2.5B) compared to earlier stages (Figure 2.4D) and has a bilateral symmetry. The style is circular (Figure 2.5A) and is completely covered in stigmatic papillae (Figure 2.5E). The gynoecium shape is reminiscent of a Chinese snuff bottle (Figure 2.5F) as the style is narrow compared to the round ovary and slightly flattened in cross section (Figure 2.5C, D).

Once fertilisation has occurred at ~10 DAI there is a further change in shape as the fruit develops into a heart-shape. At 10 DAI (flower stage 14 as the anthers extend above the fruit), the base of the ovary begins to taper to give an almost triangular shape (Figure 2.6A).

By 11.5 DAI (flower stage 15 where the fruit extends above the anthers), the base of the fruit becomes increasingly tapered and the distal shoulders increasingly larger to produce a clear heart-shape (Figure 2.6B). The fruit has a much flatter cross-section (Figure 2.6D) which is consistent through all following stages of fruit development. The style remains circular in cross-section and becomes increasingly smaller relative to the ovary (Figure 2.6C) and the stigmatic papillae start to degrade (Figure 2.6B).

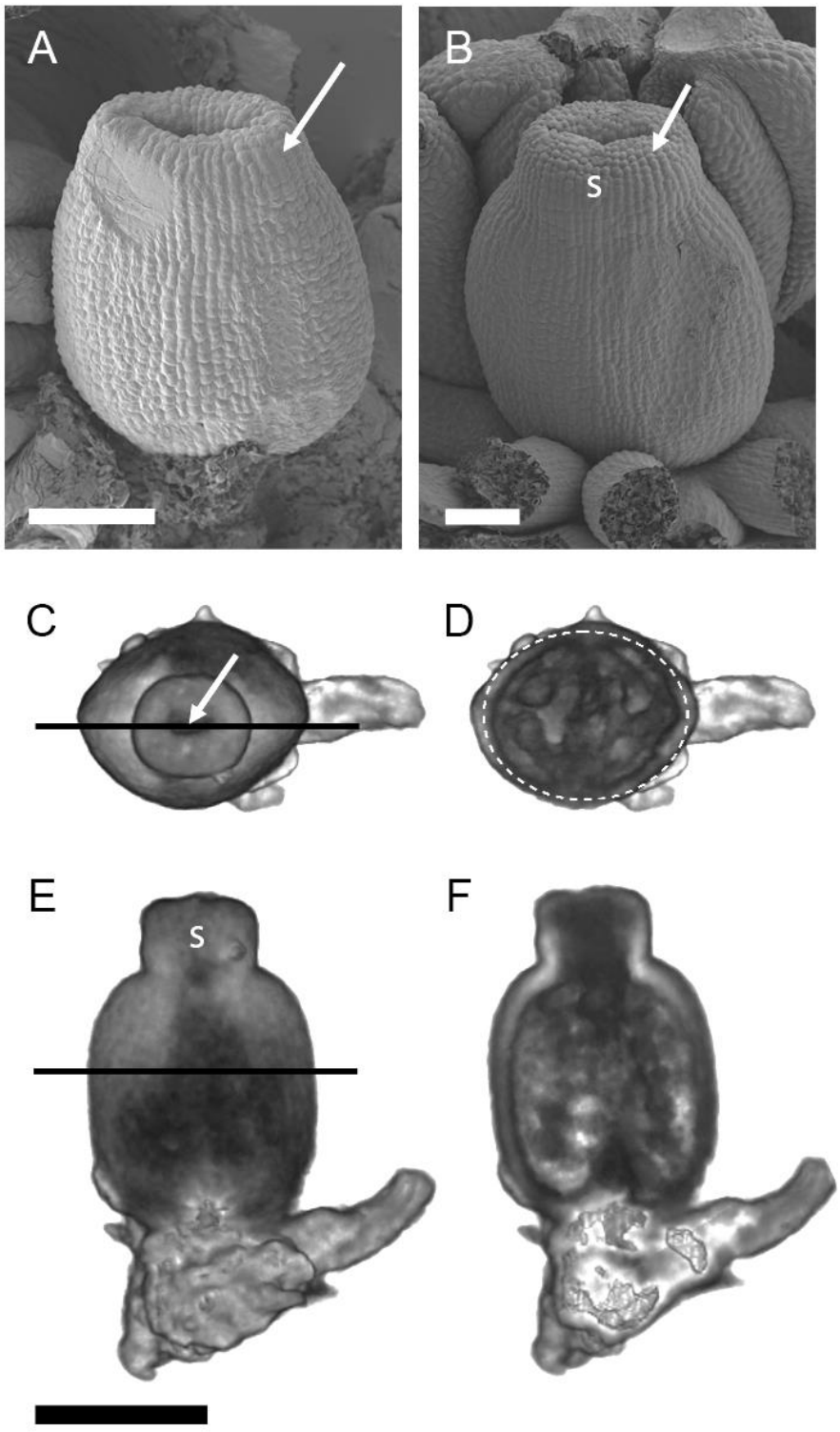

Figure 2.4 Middle phase of Capsella rubella gynoecium development. (A, B) SEM images of dissected gynoecium. (A) 3 DAI, arrow shows the tapered distal apex of the presumptive style. (B) 4 DAI, arrow points to rounded cells that newly forming stigmatic papillae cells. (C-F) OPT scans of gynoecium 6 DAI. (C) From above, arrow shows the central cleft of the style beginning to close. (D) Cross-section through the middle of the ovary at position marked by black line in (E), white dotted outline shows oval cross section shape. (E) Mediolateral view. (F) Longitudinal section marked by line in (C). s: style. Scale bars 50µm (A, B) and 250µm (C-F).

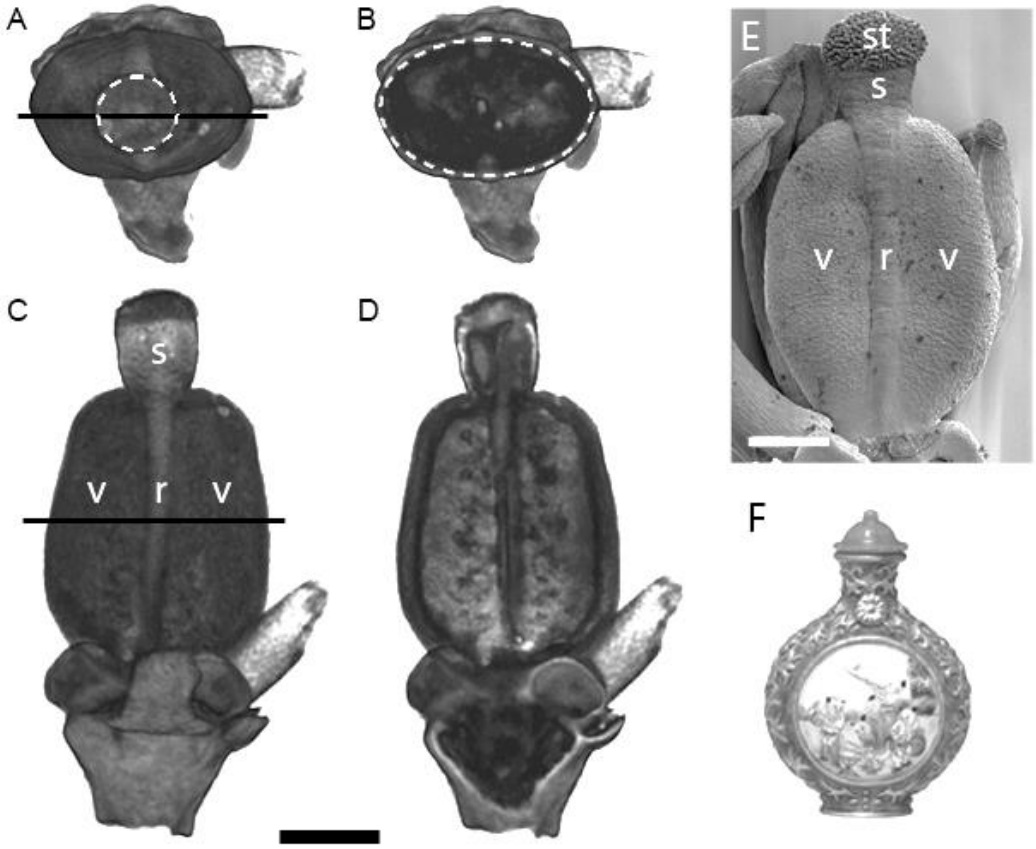

Figure 2.5 Middle phase (continued) *Capsella rubella* gynoecium (A-D) OPT scans of gynoecium 8.5 DAI. (A) From above, white dotted outline marks the circular cross section shape of the style. (B) Virtual cross section, position indicated by black line in (C). White dotted outline shows oval cross section, slightly flattened. (C) Mediolateral view (D) Longitudinal section, position shown by black line in (A). (E) SEM of gynoecium 9 DAI. (F) Chinese snuff bottle. Morphologically distinct tissue types s: style, r: replum, v: valve, st: stigma. Scale bars 250µm

The fruit continues to grow to maturity at around 8-10mm in length. At this stage the heart shape is more emphasised as the distal shoulders have extended above the style (Figure 2.7). The valve margin, where the fruit dehisces is clearly defined (Figure 2.7).

Thus, the growth of the *Capsella* gynoecium can be divided into three phases with whole organ growth data and morphology. During the early phase of growth the gynoecium develops from a cylindrical shape that becomes more elongated (0-2.5 DAI). During the middle phase (2.5-10 DAI) a snuff-bottle shape is generated as growth in length slows down; the rate of growth in width at the widest point is equal to the rate of growth in length. After fertilisation in the late phase (10-15 DAI) a heart-shaped fruit is generated and rate of growth in width continues to equal to rate of growth in length.

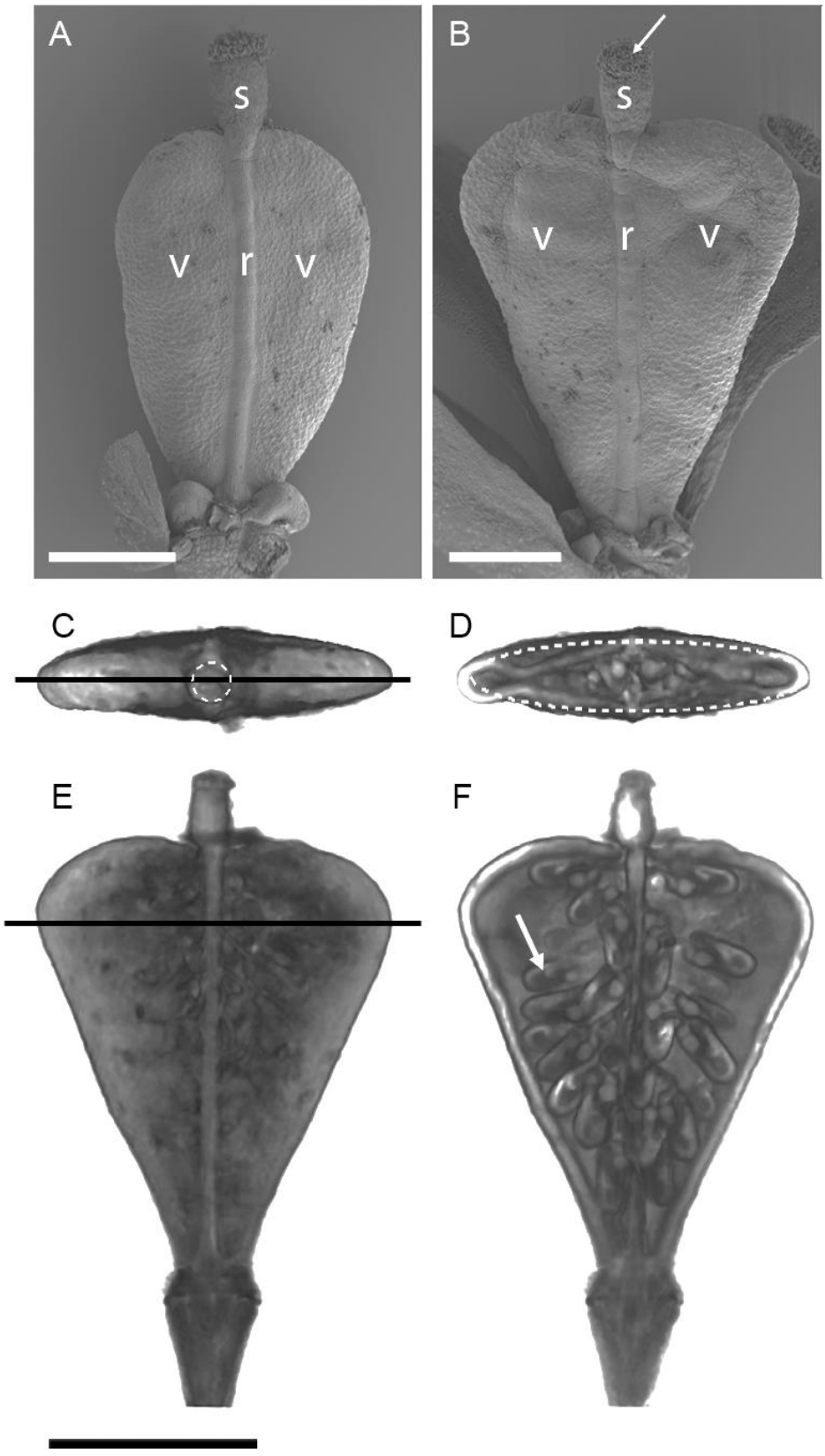

Figure 2.6 Late phases of Capsella rubella fruit development. (A, B) SEM of Capsella fruit. (A) 10 DAI (B) 11.5 DAI, arrow indicates degrading stigmatic papillae. (C-F) OPT scans of fruit 11.5 DAI. (C) from above, dotted circular outline marks the style. (D) Virtual cross-section, position indicated by black line in (E), white dotted outline marks flattened cross section of fruit. (E) Medio-lateral view. (F) Longitudinal section marked by black line in (C), white arrow indicates developing seeds. Distinct tissues s: style, r: replum, v: valve. Scale bars 500µm (A, B) and 1mm (C-F)

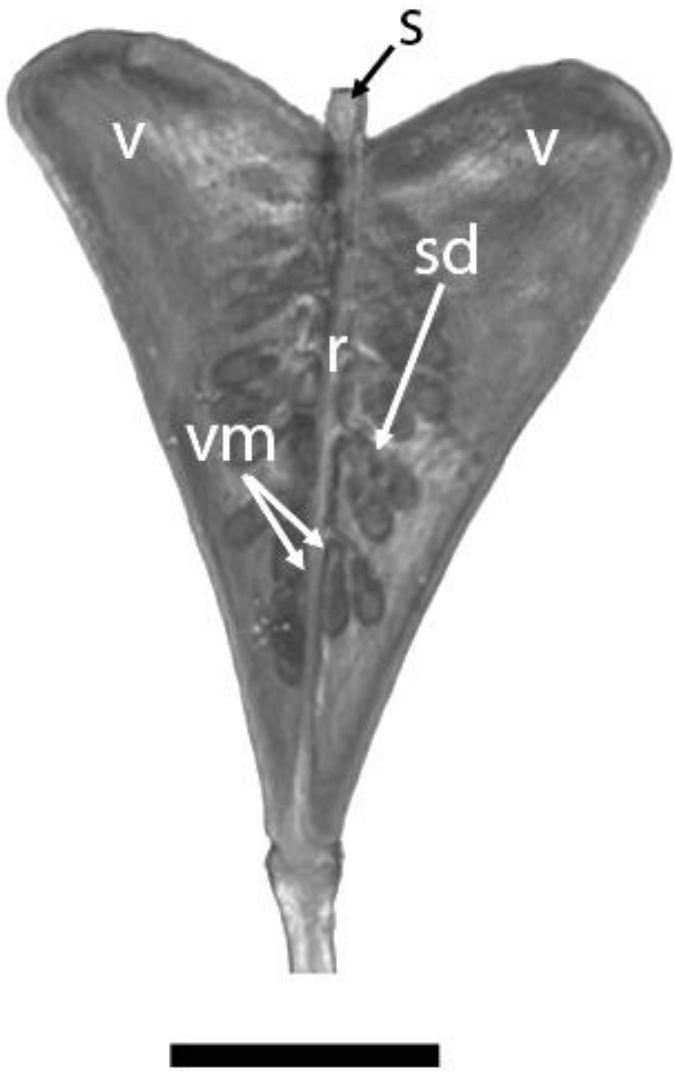

Figure 2.7 Mature Capsella WT fruit OPT image of Capsella fruit ~15 DAI. Distinct tissues s: style, r: replum, v: valve, vm: valve margin. The seeds (sd) can be seen lined up along the septum. Scale bar 2mm.

2.2.4 Clonal Analysis

Whole organ growth dynamics change through time and capture two distinct phases in growth. However, imaging reveals a third phase of growth where the organ develops from a snuff bottle shape to a heart-shaped fruit. This is not captured with measuring the growth in length and width of the whole organ, especially as the widest point changes relative position through time.

In this study, sector analysis was used to capture growth dynamics at a regional rather than whole organ level. I transformed *Capsella* with a *Cre* recombinase under the control of a heat shock promoter (Gallois et al., 2002) and *Brother of Brainbow* (*BOB*) construct (Wachsman et al., 2011). In *BOB*, YFP is driven by a 35S promoter followed by CFP and RFP spaced by mutually exclusive *lox* sites (Figure 2.8B). These plants under normal conditions express YFP everywhere and CFP and RFP are not expressed. Upon a heat shock at 37˚C, or above, *Cre* is expressed and causes recombination at the *lox* sites to initiate expression of CFP or RFP (Figure 2.8D, E). This process occurs randomly in individual cells and as the cells divide the florescent marker is passed down to all descendent cells. This creates clonal sectors of different colours (Figure 2.8F). The orientation and size of these sectors reflect the local growth dynamics over the period analysed (Rolland-Lagan et al., 2003; Sauret-Gueto et al., 2013).

To heat shock the plants, whole inflorescences were dipped at around 1-3cm in length into a water bath set to 38.5°C. The plants were returned to the growth room for 4,

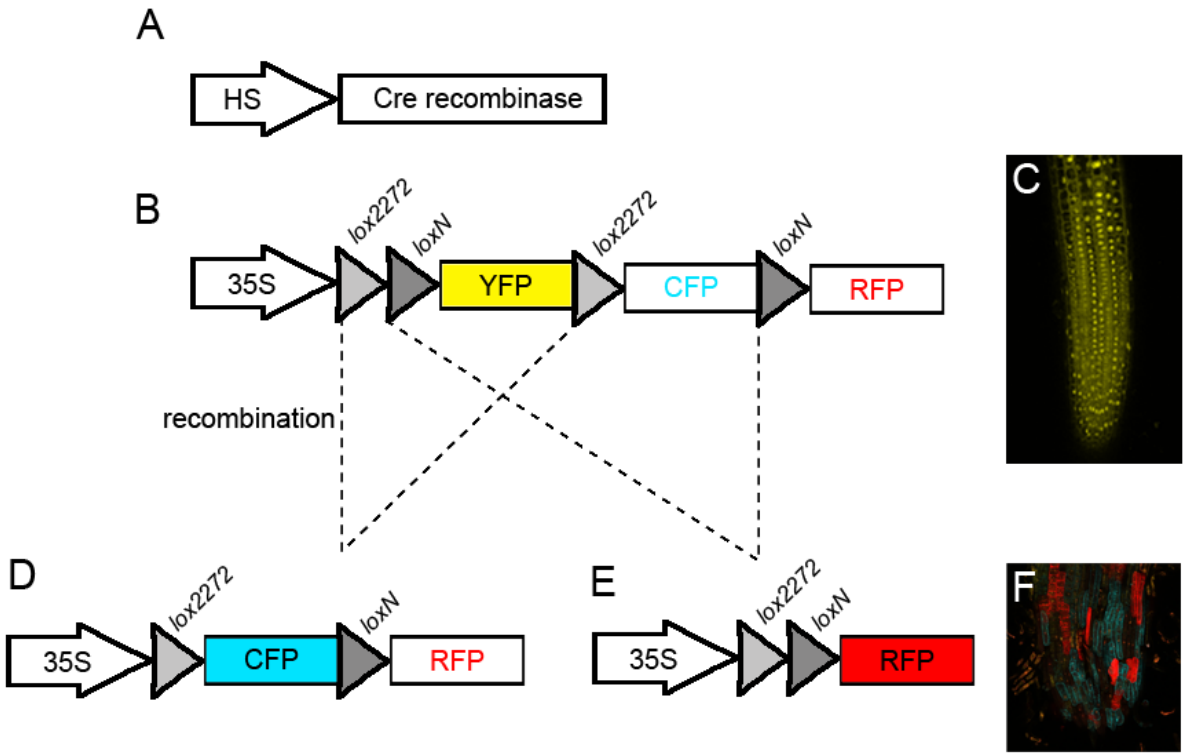

Figure 2.8 Expression of clones in Capsella rubella BOB (A) Cre recombinase under the control of heat shock (HS) promoter (Gallois et al., 2002). (B) BOB construct before Cre mediated recombination. (C) Root of *C. rubella* with no HS. (D, E) BOB construct after one of two possible Cre mediated recombination events. (F) Root of *C. rubella* after HS treatment. BOB construct from (Wachsman et al., 2011).

6, or 8 days before imaging. I dissected flowers and selected gynoecium/fruit at lengths of 300µm, 500µm, 1mm, 2mm and 4mm and imaged the sectors in the epidermis with confocal or fluorescent microscopy. The clonal sectors represent the period of growth prior to the stage of the gynoecium that is imaged. For example, the clonal sectors imaged 6 days after HS on a 1mm long gynoecium represent 6 days of growth prior to that stage.

These five sizes of gynoecium were chosen as they represent the period it takes the gynoecium to double in length, except 300µm as this is ~4DAI and is the first size possible to image. The time interval between each size is not equal but was calculated using the fitted line in Section 3.2.1. The gynoecium reaches 300µm, 500µm, 1mm, 2mm and 4mm at approximately 4 DAI, 6 DAI, 8.5 DAI, 11.5 DAI and 14 DAI, respectively.

For each experiment, between 4 and 10 individual gynoecia were imaged. Using Image J all clonal sectors in the epidermis of the gynoecia and the whole gynoecia were outlined manually. The epidermal clones were distinguishable from clones in other layers as the cells were large and had a brighter florescent signal. The outlines of the whole gynoecia and clones were analysed using software developed in the lab called *Sector Analysis Toolbox*. In the software a mean organ shape was calculated for each stage; 4 DAI, 6 DAI, 8.5 DAI, 11.5 DAI and 14 DAI. Secondly, the manually segmented clones for each experiment were warped onto the calculated mean shape giving a clear map of regional growth patterns.

The major axis, minor axis and area of the clonal sectors were measured from the confocal images in Image J. This data was used to calculate growth rates using the following equation:

$$k = \frac{\left[ln\left(\frac{N_{t1}}{N_{t0}}\right)\right]}{\Delta t}$$

Where k is the growth rate, N_{t1} is the dimension of the sector, N_{t0} is the dimensions of the cell at time of heat treatment and Δt is time in hours from heat treatment to imaging. It is assumed that the cells at time of heat shock are uniform in size and isodiametric in shape.

The dimensions of epidermal cells (N_{t0}) were measured and averaged from clones of 300µm gynoecia (4 DAI, Figure 2.9) to 6.67µm (length and width as the cells are almost circular) and 51.7µm^2 (cell area). For L/W ratio the length (parallel to long axis of the gynoecium), width (perpendicular to the long axis of the gynoecium) of the clones were

measured in Image J. The cell dimensions in gynoecia 500µm in length were similar to the dimensions at 300µm gynoecia. For this reason it was assumed that the cells dimensions of the earlier stages were also consistant, when clones were induced. Therefore the initial cell shapes and sizes were determined from the cells of the 300µm gynoecia.

2.2.4.1 Clones imaged at 4 DAI

Gynoecia at 4 DAI (300µm) are almost cylindrical in shape but the distal apex is slightly tapered where the style will probably form (Figure 2.4, Figure 2.9). The gynoecium at this stage is delicate and easily damaged when imaged, no smaller stages were examined. Growth prior to this stage represents the early phase of growth where the rate of growth in length is greater than width (0-2.5 DAI, Figure 2.1) and the first 1.5 days of the middle phase. Clones were induced 4 days prior to this stage (0 DAI).

The results show that the clones during this earliest stage (0-4 DAI) have an anisotropic shape, elongated more along the proximodistal axis (Figure 2.9). At 4 DAI it is difficult to define the position of the replum as the cell types have not differentiated. The clones are similar sizes and shapes across the body of the gynoecium. The clones at the proximal end and the distal end (in the presumptive style) are shorter than the middle region (Figure 2.9).

The average length-to-width ratio (L/W) of the clones was 5.2. Based on the dimensions of the clones and the average cell size (assuming the cell size doesn't change in the early phase of growth) the average growth rate along the major axis of the clones is 2%/h and 0.4%/h along the minor axis. The anisotropic shape of the clones correlates with cell division rates along the two axes. The clones are 4-10 cells long and 1-2 cells wide indicating 2-3 rounds of cell division along the major axis and ~1 round of cell division along the minor axis. The mean areal growth rate is 2.2%/h.

In Summary, growth in the interval 0 to 4 DAI is highly anisotropic in a proximal distal direction. These regional growth patterns correlate with the whole organ growth in the early phase of growth (0-2.5 DAI) where growth in length is greater than growth in width (Figure 2.2).

2.2.4.2 Clones imaged at 6 DAI

Gynoecia at 6 DAI are round in shape and the style is beginning to differentiate as a narrower distal tissue. The replum can also be distinguished at this stage. Clones were

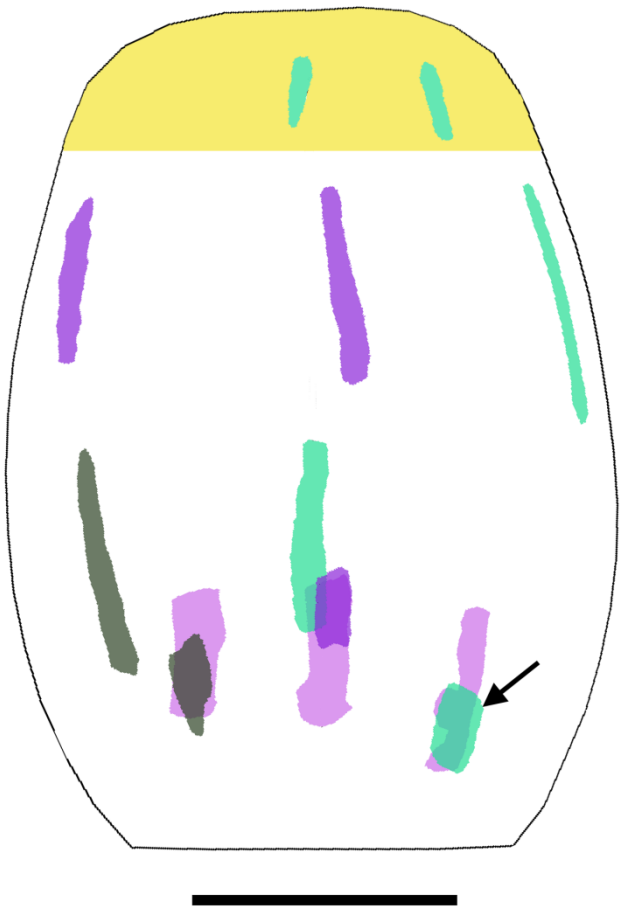

Figure 2.9 Capsella gynoecium 4 DAI. Black outline shows mean shape calculated from multiple samples of gynoecia 4 DAI. Clones were induced at 0 DAI and imaged using confocal microscopy. Coloured regions represent individual clones that have been warped onto the mean shape. The yellow area represents the position of the probable style and the remaining white region represents the valve and replum. Arrow indicates shorter clones in the basal region of the gynoecium. Scale bar 50µm

induced 6 and 4 days prior to this stage at 0 DAI and 2 DAI, respectively. Clones induced 6 days prior to imaging capture the early phase and the middle phase. Clones induced 4 days prior to imaging capture mostly the middle phase. For simplicity the clones have been separated for the following analysis into regions style, replum and valve (Figure 2.10).

2.2.4.2.1 Style

In the style the clones are highly anisotropic along the proximal distal axis (Figure 2.10). The average L/W ratio is 8.9 and 5.4 for 6 and 4 days growth respectively. The

average growth rate of the major and minor axis of the clones is 1.8%/h and 0.2%/h respectively for both time points. This anisotropic growth is reflected in different cell division rates across the axes. The clones are 8-12 and 4-7 cells long indicating 3 and 2 rounds of cell division along the major axis for 6 and 4 days respectively. The clones are 1 cell wide showing that there is no cell division along the minor axis. Therefore the areal growth rate of the style of 1.8%/h is correlated with cell division along the proximodistal axis.

2.2.4.2.2 Replum

In the replum the clones also have an anisotropic shape along the proximodistal axis, however they look smaller in comparison to the style clones (Figure 2.10). The L/W ratio of replum clones are 3.3 and 2.4 for 6 and 4 days respectively. Growth rates along the major and minor axis are 1.2%/h and 0.3%/h respectively for both time points. Again this anisotropy is correlated with differential cell division rates across the two axes with clones 4-5 and 2-4 cells long indicating 2 and 1-2 rounds of cell division along the major axis for 6 and 4 days respectively. The clones were 1-2 cells wide for both time points showing that there is an occasional round of cell division along the minor axis. The areal growth rate of replum clones of 1.3%/h is reflected in the multiple rounds of cell divisions along the major axis and few rounds of cell divisions along the minor axis. The replum clones have a lower growth rate than clones in the style which correlates with lower cell division rates along the proximal distal axis.

2.2.4.2.3 Valve

In the valve the clones are anisotropic when induced 6 days prior to this stage and more of isotropic when induced 4 days prior to this stage (Figure 2.10). This is reflected in the average L/W ratio of 2.5 and 1.4, respectively. Growth along the major axis is approximately 1.4%/h and 1.3%/h and along the minor axis is 0.8%/h and 0.9%/h for 6 and 4 days, respectively. However for clones induced 4 days prior to imaging, the major axis is not always the proximodistal axis but sometimes the mediolateral axis. This suggests that clones induced 6 days prior to this stage overlap with the early phase of growth (Figure 2.9) when growth along the proximodistal axis is greater than growth along the mediolateral axis.

Cell division rates along the axes are correlated with the clone shape. After 6 days, the clones were 6-10 cells long and 2-4 cells wide indicating 3 rounds and 1-2 rounds of cell

divisions along the major and minor axis respectively. After 4 days the clones were 2-5 cells long and 2-4 cells wide indicating 1-2 rounds of cell divisions along both axes.

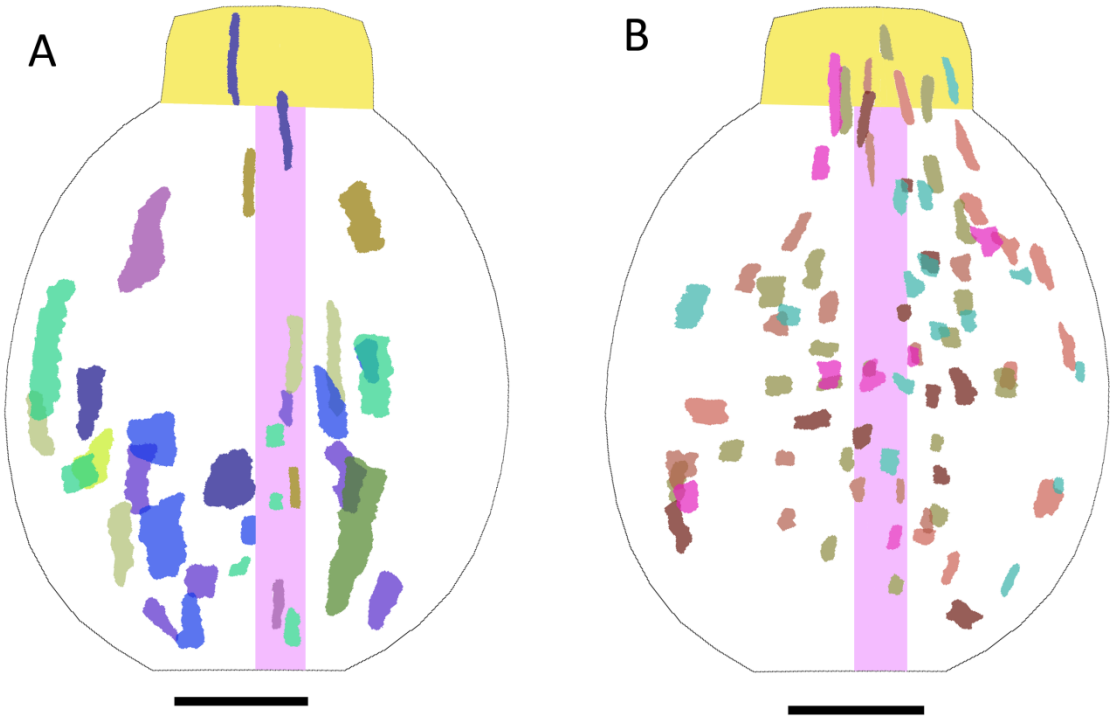

Figure 2.10 Capsella gynoecium 6 DAI. Black outline shows mean shape calculated from multiple samples of gynoecia 6 DAI (500µm in length). Clones were induced at 0 DAI (A) and 2 DAI (B) and imaged using confocal microscopy. Coloured patches represent individual clones that have been warped onto the mean shape. The yellow region represents the style and the pink region in the middle roughly marks the replum, the remaining white area represents the valves. Scale bar 100µm

The areal growth rate is 2.1%/h and 2.0%/h for 6 and 4 days, respectively. These areal growth rates are comparable to growth rates of clones induced 4 days prior to gynoecia 3 DAI (2.2%/h). However the contribution to areal growth rate of growth along the proximodistal axis is much greater in the period leading to the 250µm gynoecia (3 DAI). Clones induced 6 days prior to 5 DAI gynoecia overlap with the early phase of growth 4 days prior to the 3 DAI gynoecia reflected by anisotropy along the proximodistal axis.

In summary, growth in the style and replum continues to be anisotropic in the 6 and 4 day interval prior to 6 DAI gynoecia, preferentially along the proximodistal axis. In the valves the 4 day interval prior to 6 DAI growth is almost isotropic whereas in the 6 day interval prior to this stage the growth is anisotropic along the proximodistal axis. This is because the 6 days of growth overlaps with the early phase of proximodistal growth.

2.2.4.3 Clones imaged at 8.5 DAI

Gynoecia at 8.5 DAI are rounded in shape and have a narrow style. The replum and the style cells are morphologically distinct at this stage and the style is covered by stigmatic papillae. Here, gynoecia of 1mm (8.5 DAI) were imaged at 8, 6 and 4 days after heat shock treatment. Clones induced 8 days prior to imaging capture early and middle phases of growth. Clones induced 6 and 4 days prior to imaging capture the middle phase. The quantative sector analysis focuses on 6 and 4 day treatments and the gynoecia are divided into regions style, replum and valve (Figure 2.11).

2.2.4.3.1 Style

The style clones are similar to clones in earlier stages with a highly anisotropic shape elongated along the proximal distal axis (Figure 2.11). The L/W ratio of the clones is 8.4 and 3.6 for 6 and 4 days respectively. The areal growth is maintained at 2%/h and 1.7%/h which can be mostly accounted for growth along the major axis of the clones: 1.8%/h and 1.6%/h for 6 and 4 days respectively. Clones are 4-6 and 1-2 cells long indicating that there are 2 and 1 rounds of cell divisions for 6 and 4 days respectively. Cell division is lower in comparison to earlier stages but areal growth rates are maintained. This can be accounted for by cell expansion: the average cell area doubles from 64μm^2 at 6 DAI to 145μm^2 at 8.5 DAI.

2.2.4.3.2 Replum

The replum clones are much smaller than clones across the rest of the gynoecium (Figure 2.11). The shape of the clones is anisotropic along the proximodistal axis with L/W ratio of 2.3 and 1.74 for 6 and 4 days, respectively. Areal growth rate is lower than previous stages at 1.0%/h and 0.7%/h (6 and 4 days respectively), mostly accounted for by growth along the major axis. The clones are 2-4 and 1-2 cells long indicating 2 and 1 round of cell division: lower than previous stages. Cell size is maintained at approximately 50μm^2 in 6 DAI and 8.5 DAI repla. The lower cell division rate correlates with the slower areal growth of the replum clones.

2.2.4.3.3 Valve

The valve clones that were induced 6 and 4 days prior to imaging 8.5 DAI gynoecia have some key differences in shape (Figure 2.11B,C). The clones induced at 6 days prior to this stage are isotropic with a L/W ratio of 1.0. The clones do not have a major axis with growth rates of each axis of 0.9%/h accounting for the 1.7%/h areal growth. The clones at 4 days are anisotropic and have a L/W ratio of 0.6, showing that the major axis of the clones is the mediolateral axis. The growth rates of the major and minor axis are 1.4%/h and 0.8%/h respectively maintaining an areal growth rate of 1.9%/h. The areal growth rate has been maintained however the orientation of growth has changed from principally proximodistal in the early phase of growth (0 to 4 DAI) to mediolateral in the interval prior to 8.5 DAI (4.5 to 8.5 DAI).

The pattern of cell divisions has changed from mostly symmetrical division to both symmetrical and asymmetric divisions which look like stomata precursors (Robinson et al., 2011). Some cells that do not have stomatal identity at this stage are no longer rounded in shape but have a major and minor axis. The sizes of the cells in the clones are mixed from large cells up to 200μm^2 to cells as small as 15μm^2. Therefore the areal growth of the valve is not totally correlated with by cell division but also by changes in cell size.

At the base of the valve there is a region where clones have an anisotropic shape along the proximodistal axis, 4 days after induction. In this region the L/W ratio of the clones is 1.6 and the growth rate along the major and minor axis is 1.6%/h and 1.2%/h respectively. This indicates that growth in the valve is not uniform and direction of anisotropic growth is different across the tissue.

Valve clones induced at 0.5 DAI and imaged at 8.5 DAI are anisotropic along the proximodistal axis (Figure 2.11A). This indicates that this interval of growth overlaps with the early phase of growth where growth along the proximodistal axis is greater than growth along the mediolateral axis (Figure 2.9).

In summary, the style and replum continue to grow in a proximodistal orientation however the areal growth rate replum is lower than the rest of the gynoecia. In the valve during the 6 day interval prior to 9 DAI growth is isotropic and in the 4 day interval prior to 8.5 DAI growth is anisotropic along the mediolateral axis. A region at the base of the valve growth is greater along the proximodistal axis in the 4 day interval prior to 8.5 DAI.

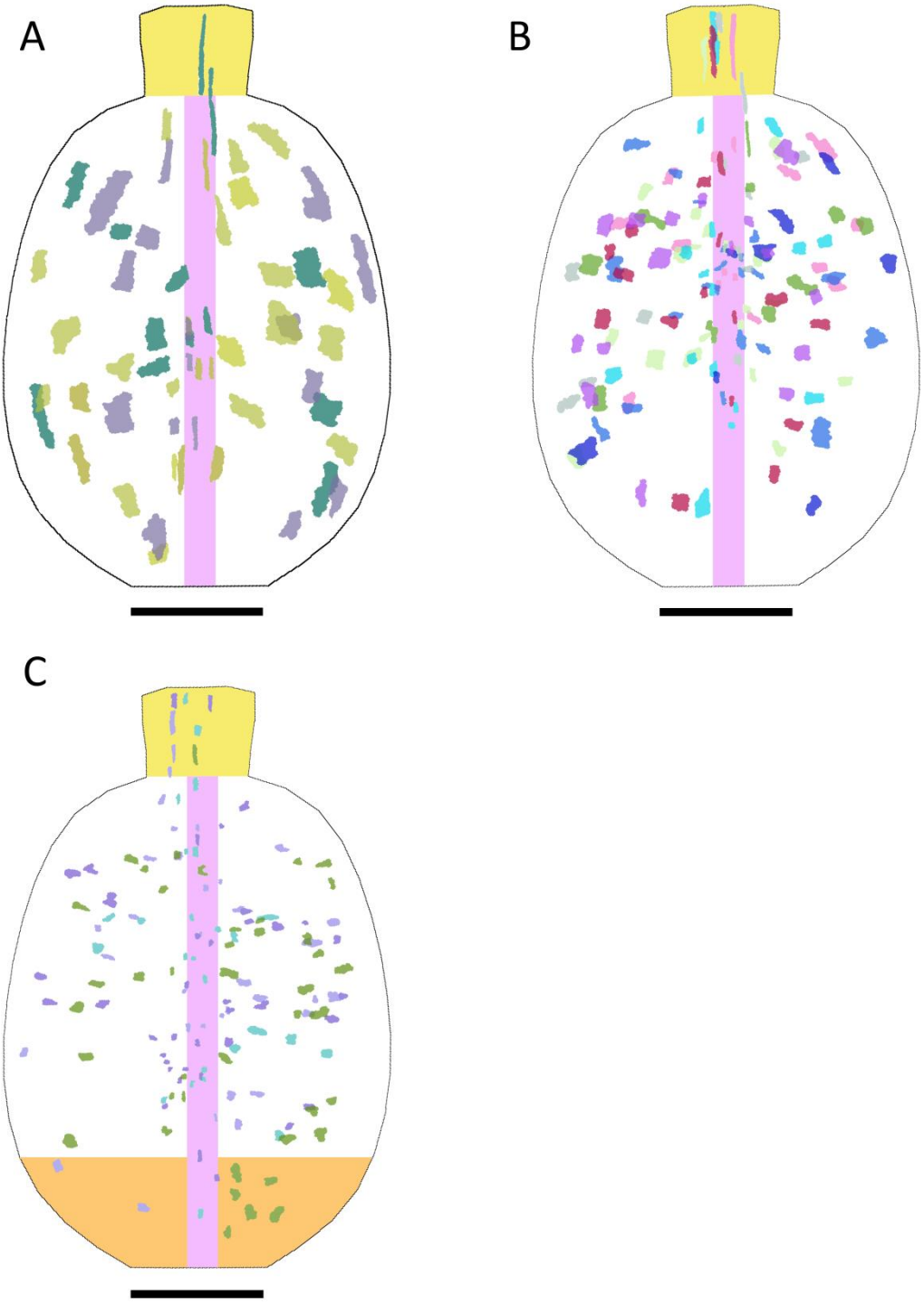

Figure 2.11 Capsella gynoecium 8.5 DAI. Black outline shows mean shape calculated from multiple samples of gynoecia 8.5 DAI (1000µm in length). Clones were induced at 0.5 DAI (A), 2.5 DAI (B) and 4.5 DAI (C) and imaged using confocal microscopy. Coloured patches represent individual clones that have been warped onto the mean shape. Yellow region represents the style, pink region in the centre represents the replum, the remaining area is the valves and the orange region represents a region in the valve where growth is preferentially proximodistal. Scale bar 250µm

2.2.4.4 Clones imaged at 11.5 DAI

At 11.5 DAI, the *Capsella* fruit are 2mm in length and have been fertilised. The shape of the organ is a triangular with wider distal shoulders and a tapered proximal end (Figure 2.6). Fruits were imaged 8, 6 and 4 days after heat shock treatment at 3.5 DAI, 5.5 DAI and 7.5 DAI, respectively. Clones induced 8, 6 and 4 days prior to imaging capture the middle and late phases of growth. The clones induced 4 days prior to imaging (at 7.5 DAI) cannot be used in this quantitative analysis since cells at this time of induction are a variety of sizes and some have a major axis. Here clones induced at 6 days prior to this stage (5.5 DAI) are analysed (Figure 2.12B).

2.2.4.4.1 Style

As in all previous stages the style clones are narrow and anisotropic in shape along the proximodistal axis (Figure 2.12). The L/W ratio of the sectors is 5.7 with a growth rate along the major and minor axes of 1.5%/h and 0.3%/h. The clones are mostly 2 cells long and 1 cell wide indicating only one round of cell division along the major axis. The areal growth rate is 1.6%/h which does not correlate with cell divisions but can be accounted for by cell expansion as cell area increases from 145μm^2 at 8 DAI to 384μm^2 at 11 DAI.

2.2.4.4.2 Replum

Replum clones are smaller in comparison to sectors in other parts of the fruit (Figure 2.12). The replum clones have a narrow anisotropic shape as previously described. L/W ratio of the clones at this stage is 3.2 and the growth rates along the major and minor axes are 1.0% and 0.3%, respectively. Areal growth rate is maintained at 1.1% however cell division is lower with sectors only 1-3 cells long. Growth by cell expansion can account for the maintenance of areal growth from ~50μm^2 at 8 DAI to ~130 μm^2 at 11 DAI.

2.2.4.4.3 Valve

The valve clones show a change in orientation at this stage (Figure 2.12). In the middle and distal regions of the valves the clones are narrow and anisotropic in shape along the mediolateral axis. The clones are no longer perpendicular to the long axis of the fruit but splay out towards the distal shoulders at ~30° from the long axis of the fruit (Figure 2.12B). In the proximal region of the fruit the clones are anisotropic along the proximal-distal axis (Figure 2.12B). The clones are orientated ~15˚ from the long axis of the fruit and also splay towards the distal shoulders.

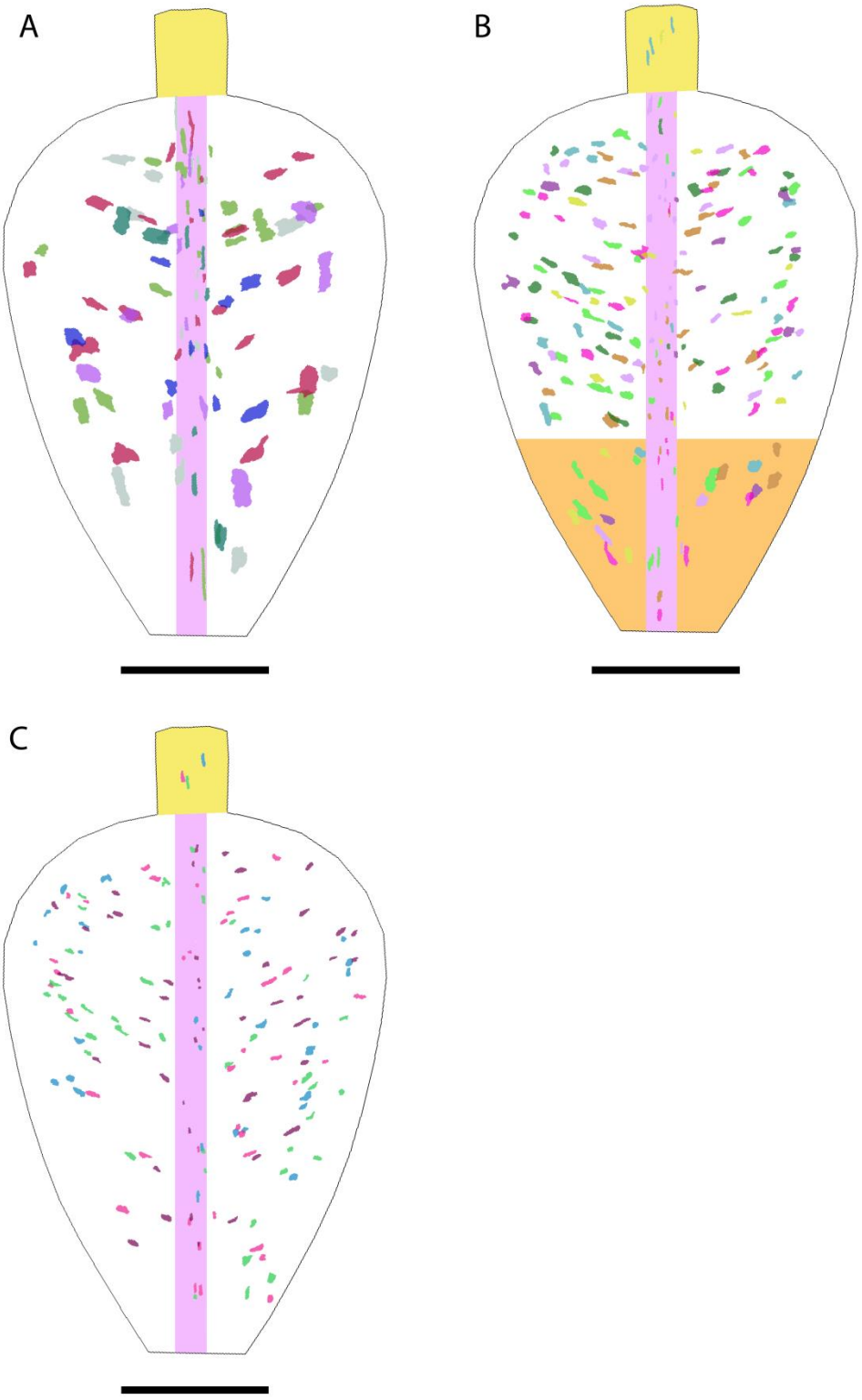

Figure 2.12 Capsella gynoecium 11.5 DAI. Black outline shows mean shape calculated from multiple samples of gynoecia 11.5 DAI. Clones were induced at 7.5 DAI (A), 5.5 DAI (B) and 3.5 DAI (C) and imaged using confocal microscopy. Coloured patches represent individual clones that have been warped onto the mean shape. Yellow region represents the style, pink region the replum, orange region where clones are anisotropic along the proximodistal axis in the valve and white regions where clones are anisotropic along the mediolateral axis in the valve. Scale bar 500µm

To visualise the regional differences, growth rates of major (Kmax) and minor axis (Kmin) of individual clones were plotted directly onto the sector map of fruit 11.5 DAI, 6 days after induction (Figure 2.13). The value of Kmax is uniform across the valves at ~1.3 - 1.6%/h however the axis that Kmax is parallel to differs from proximodistal near the base of the fruit (Figure 2.13 orange region) to mediolateral in the middle and upper part of the fruit (Figure 2.13 white region). Kmin in the upper and middle region (parallel to the proximodistal axis in the white region) of the fruit is ~0.6-0.8%/h whereas Kmin in the region nearest the base (parallel to the mediolateral axis in the orange region) is slightly greater at ~1.0-1.3%/h. This means that the areal growth rate in the basal region of the fruit is greater at ~2.5-3%/h compared to the upper and middle region areal growth rate at ~2-2.5%/h.

In summary, growth prior to 11.5 DAI in style and replum is anisotropic along the proximodistal axis. Growth in the valves from 5.5 to 11.5 DAI has mixed orientations, generally splaying out to the distal shoulders. The basal region has higher growth rates along the proximodistal axis during the 5.5-11.5 DAI interval whereas the middle and upper region of the fruit has a higher growth rate along the mediolateral axis in this interval.

2.2.4.5 Clones imaged a 14 DAI

The *Capsella* fruit at 14 DAI (4mm in length) is heart-shaped with distal shoulders extending to the top of the style with a tapered base (Figure 2.14). I induced clones at 6 DAI and imaged at 14 DAI. The clones capture some middle phase growth and most late phase growth. The clones cannot be used in a quantitative analysis since cells at this time of induction (6 DAI) are a variety of sizes and some have a major axis. The map of clones for this interval (6-14 DAI) shows that replum cells are smaller than clones in the valves and anisotropic along the proximodistal axis (Figure 2.14). Clones in the valves splay out towards the distal shoulders. A basal and upper region cannot be distinguished by clone orientation as in fruits imaged at 11.5 DAI (Figure 2.13).

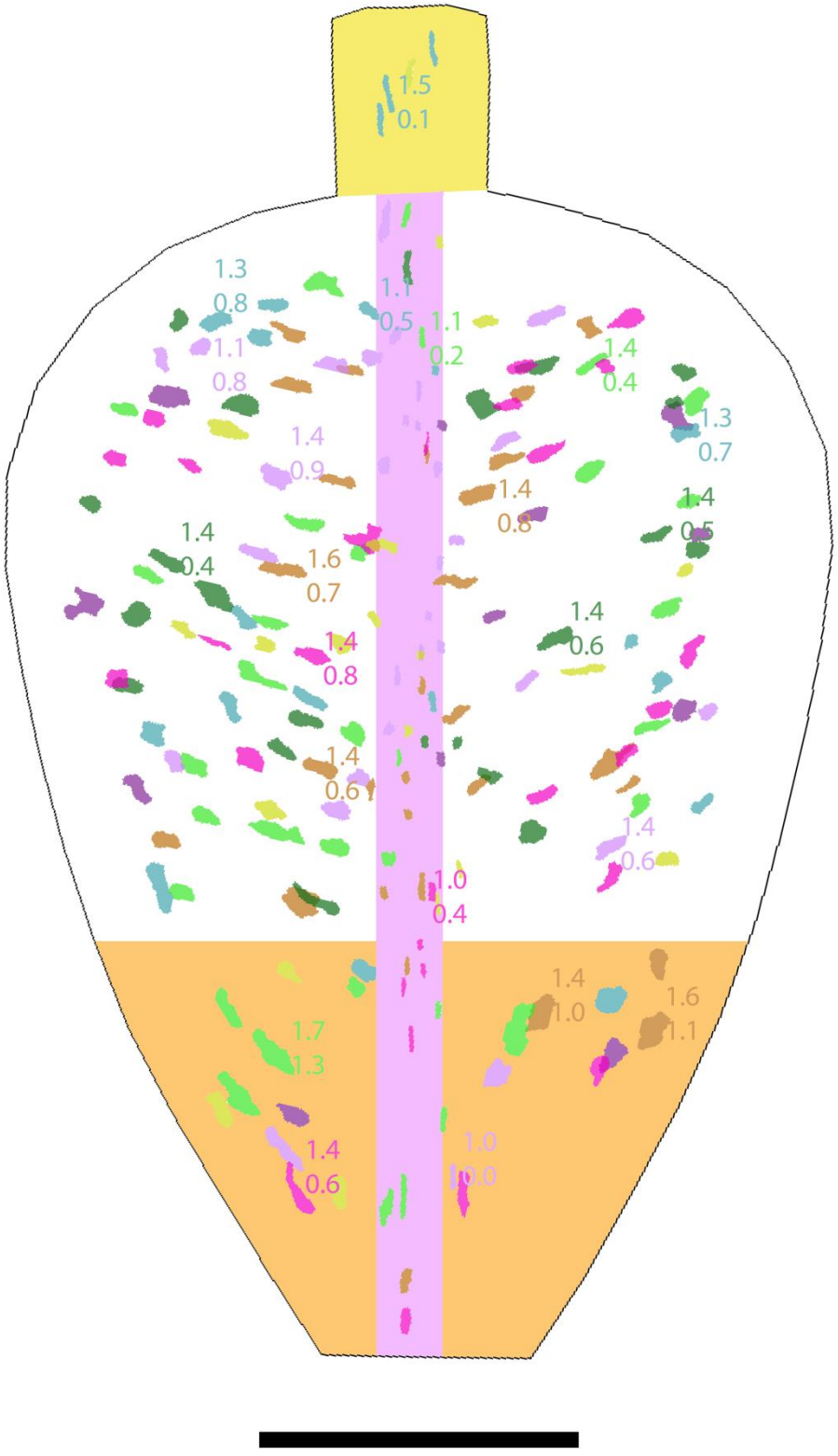

Figure 2.13 Kmax and Kmin of clones from interval 5.5 DAI to 11.5 DAI. Black outline shows the mean shape calculated from multiple gynoecia at 11.5 DAI. Coloured patches represent individual clones induced at 5.5 DAI. The numbers correspond to Kmax (top) and Kmin (bottom) of the nearest clone to the left with the same colour as the number (%/h). Yellow region represents the style, pink region the replum, the orange region is the valve where Kmax is the proximodistal axis and the white region is the valve where kmax is the mediolateral axis. Scale bar 500µm

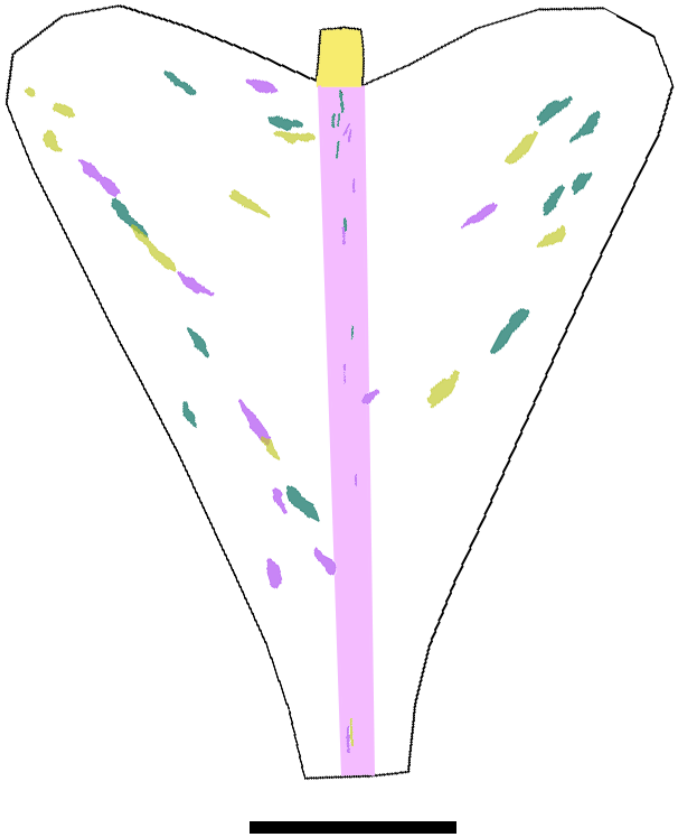

Figure 2.14 Capsella gynoecium 14 DAI. Black outline shows mean shape calculated from multiple samples of gynoecia 14 DAI. Clones were induced at 6 DAI imaged using florescent microscopy. Coloured patches represent individual clones that have been warped onto the mean shape. Yellow region represents the style, pink region the replum and white regions the valves. Scale bar 1mm

Clonal analysis of the *Capsella* fruit has revealed regional differences in growth rates and orientations through development. In the style and replum, growth is orientated in a proximodistal direction throughout development (0-14 DAI). However, growth orientations in the valves change through development. In the time interval (0-4 DAI) growth in the valves is mostly along the proximodistal axis of the gynoecium (Figure 2.9). This changes in the interval 4-9 DAI where growth rates are greater along the mediolateral axis (Figure 2.11C). Finally from 5.5-11.5 DAI growth orientations in the valves are mixed with higher growth rates along the proximodistal axis in the basal region of the fruit and higher growth rates along the mediolateral axis in the middle and upper regions (Figure 2.13).

2.2.5 Growing Polarised Tissue Framework

The sector analysis has revealed the regional growth patterns through the different stages of *Capsella* fruit development. It has given us a dynamic picture of local growth while organ measurements have shown how the whole fruit changes through time. However, from this data it is difficult to extract the key principles that are necessary to generate the final fruit form.

To understand the dynamics of fruit shape development a modelling framework is required. Growth Polarised Tissue (GPT) Framework developed by Kennaway et al. (2011) was used here to model fruit growth. The GPT framework is implemented in a toolbox, *GFtbox*, in MATLAB and is based on a finite element method. In GPT framework, biological tissues are represented as a continuous sheet of material with two surfaces and a thickness, termed the canvas. Growth is computed for discrete prisms which together form a continuous canvas. In this framework a biological tissue is treated as a continuous sheet and ignores individual cells. In plants, the behaviour of individual cells is heavily constrained by the cell walls of their neighbours. In this way plant tissues could be regarded as continuous tissue and allows shape to be explored at a whole-organ level without having to model for large numbers of cells individually.

At each time step the deformation of the canvas is calculated using the elasticity theory. Growth is controlled by identity or signalling factors that have a value for each vertex, as the canvas grows regions where the factors are expressed will expand and distort with growth. The growth properties of biological tissues are controlled by several components such as gene expression patterns and material properties of the tissue. In these models for simplicity, it is assumed that material properties are uniform across the canvas. Residual stresses that build up as the canvas grows are reset at every timestep.

2.2.5.1 Specified and Resultant growth

In *GFtbox* there are two types of growth: (1) Specified growth is how growth is input into the model and is how much a region of the canvas would grow if it were independent of its neighbours. However the canvas is a connected sheet and so regions are mechanically constrained, giving rise to the notion of (2) Resultant growth, which is the growth observed when these mechanical constraints are taken into consideration. Figure 2.15 shows a simple example using isotropic specified growth where a square canvas is grown more at the base as shown by the gradient (Figure 2.15A). Intuitively, this

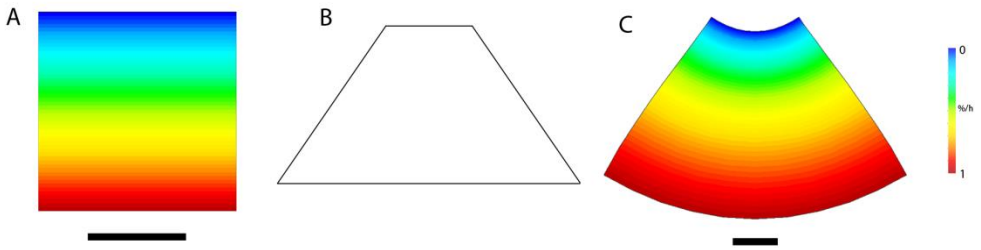

Figure 2.16 2D example with isotropic growth (A) Specified linear gradient of areal growth rates on initial starting shape. (B) Expected outcome of specified growth in A is Trapezium. (C) Resultant shape is curved and resultant areal growth rates. Scale bars 1mm

distribution of isotropic growth would generate a trapezoid shape with straight edges (Figure 2.15B). However, the resultant shape of the canvas is curved and rotated (Figure 2.15C). This was not specified but is a result of the connectedness of the tissue.

In Figure 2.15C even for this simple shape it is difficult to predict, just by looking at the final outcome, what the specified pattern of growth was. It could be a result of isotropic growth increasing towards the base, or the result of boosted anisotropic growth towards the base of the canvas. To test these hypotheses in *GFtbox* it is possible to place clones in the model (Figure 2.16A). These clones will deform as the canvas grows and will give information on the local growth dynamics. In Figure 2.16B the clones are round, smaller at the top than the base showing a gradient in isotropic growth across the canvas. In Figure 2.16C the clones reveal a pattern of anisotropic growth as the clones have grown more along one axis than another increasingly towards the base. Since the resultant shapes are similar it is therefore important to place clones on the model to make this distinction. In a similar way clones can be induced in biological systems to test model predictions.

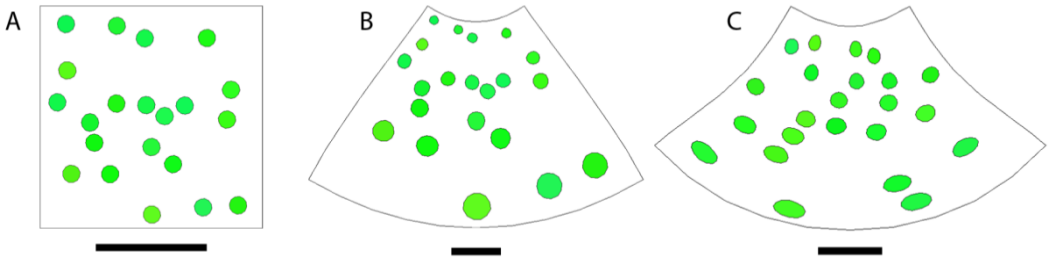

Figure 2.15 2D example with isotropic and anisotropic growth (A) Initial starting shape with clones plotted onto canvas and grown either with isotropic growth (B) or anisotropic growth (C). Scale bars 1mm.

2.2.6 Generating a *Capsella* Fruit Model

Capsella gynoecium starts as an oval cylindrical ridge. The starting shape for the model was loosely based on the size and shape on the gynoecium 0 DAI. At this stage the gynoecium is a short oval cylinder with no differentiated tissues. Thus a cylinder was chosen as the starting canvas shape. The dimensions at this stage were approximated from the OPT measurements as 40 µm length and 80µm x 60µm width (Figure 2.17). In *GFtbox* a finite element I created a canvas corresponding to these measurements (Figure 2.17). The canvas is orientated on a *xyz* coordinate system, with the canvas base being parallel to *xy*-axis and the long axis parallel to the *z*-axis. The gynoecium is anchored to the flower at the base so that growth in the baseline is constrained to be parallel to the *xy*-axis.

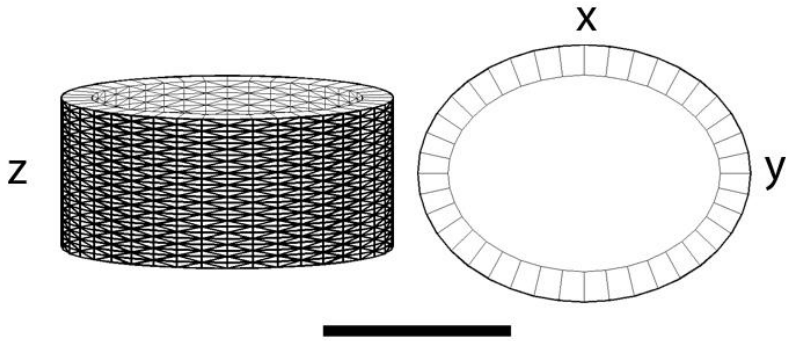

Figure 2.17 Starting canvas shape made up of a mesh of finite elements. Scale bar 100µm

In *GFtbox*, growth is driven by factors that either have a fixed value for each vertex of the tissue, termed identity factors ($\mathbf{i}_{FACTORNAME}$) or can propagate through the canvas, termed signalling factors ($\mathbf{s}_{FACTORNAME}$). It is assumed that levels of factors do not dilute as the canvas grows.

Signalling factors can be set up as a gradient across the canvas. To set up a linear gradient there has to be a region of production and a region of complete breakdown. This is specified in the canvas by a region $\mathbf{s}_{FACTORNAME}$ equal to 1 (production) and a region of $\mathbf{s}_{FACTORNAME}$ equal to 0 (breakdown). Exponential gradients can be set up through a region of production ($\mathbf{s}_{FACTORNAME}$ =1) and an overall decay rate of the whole canvas.

2.2.6.1 Modelling the early phase

In the early phase (0-2.5 DAI), the *Capsella* gynoecium primordia grows elongates from a short oval ridge to a longer cylinder. Whole organ growth dynamics has shown that during this phase, *Capsella* gynoecium grows more in length (~3%/h) than width (~1.15%/h). Clones in this early phase of growth have an anisotropic shape elongated more along the proximodistal axis.

2.2.6.2 Organiser-Based Polarity

To specify anisotropic growth in the model there has to be some form of directional information. In GPT-framework, this information is given by the polarity of the canvas, specified with a diffusible factor $\mathbf{s}_{POLARISER}$ ($\mathbf{s}_{POL}$) which propagates from regions of high to low concentrations. This polarity is organised by regions that produce $\mathbf{s}_{POL}$ (plus organisers) and regions that degrade $\mathbf{s}_{POL}$ (minus organisers). Arrows in the model show the direction of polarity by pointing away from plus organisers and towards minus organisers (Figure 2.18B). Growth rates can be specified parallel (K_{par}) and perpendicular (K_{per}) to this gradient of $\mathbf{s}_{POL}$ (Figure 2.18C).

I setup a gradient of $\mathbf{s}_{POL}$ parallel to the *z*-axis as the clones in the early phase are initially elongated in a proximodistal orientation. $\mathbf{i}_{PROXORG}$ produces $\mathbf{s}_{POL}$ is at the base which then propagates towards the top of the cylinder. As the canvas grows this polarity field will dynamically change with the growing canvas.

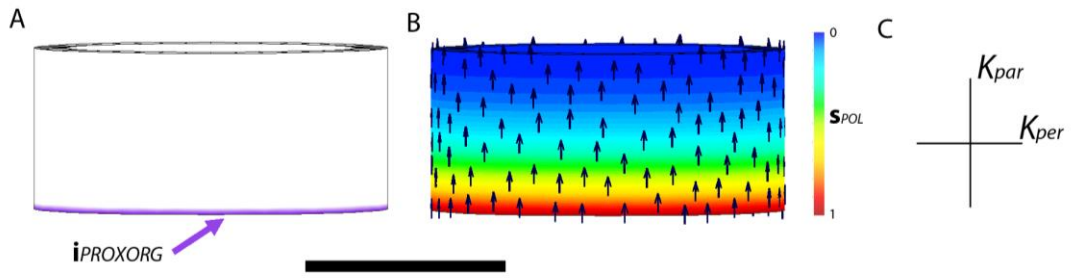

Figure 2.18 Specifying polarity (A) Distribution of $\mathbf{i}_{PROXORG}$ on the initial canvas. (B) Distribution of $\mathbf{S}_{POL}$ across the canvas after 3 time steps. (C) Growth orientations given this gradient of $\mathbf{S}_{POL}$. Scale bar 100µm

I used the polarity field to specify anisotropic growth of the canvas from 0-2 DAI by introducing a factor $\mathbf{i}_{EPHASE}$ which has a value of 1 from 0-2 DAI and a value of 0 after 2 DAI (Figure 2.19B). $\mathbf{i}_{EPHASE}$ promotes growth in the following way:

K_{par} = 0.014 .pro(p_{EPHASE} , $\mathbf{i}_{EPHASE}$)

K_{per} = 0.0115

K_{knor} = 0.01

Where pro(p_{EPHASE} , $\mathbf{i}_{EPHASE}$) = 1 + p_{EPHASE} +$\mathbf{i}_{EPHASE}$ and p_{EPHASE} is the amount of promotion by $\mathbf{i}_{EPHASE}$. Hence, if p_{EPHASE} and $\mathbf{i}_{EPHASE}$ are equal to one: K_{par} is doubled. The canvas becomes elongated parallel to the polarity (Figure 2.19C). To investigate if experimental clone patterns can be explained by this specified growth, I generated clones in the model at 0 DAI (Figure 2.19Di). The relative size of the starting clone on the canvas was estimated from biological cell size data at the different stages. The clones were introduced as circles in the model as the cells at these stages do not have a long axis. It is difficult to compare the exact shapes of the resultant clones as the biological cells are square not round, however the orientation of the clones is comparable.

The clones deform with the canvas and by 2 DAI were elongated parallel to polarity (Figure 2.19Dii), similar to experimental clones which elongate along the proximal distal axis (Figure 2.19E). The experimental clones are more elongated as they represent 4 days of growth (0 to 4 DAI).

2.2.6.3 Modelling the middle phase

During the middle phase (2-10 DAI) the *Capsella* gynoecium grows from an oval cylinder to a snuff bottle shape at fertilisation (~10 DAI). I used a factor, $\mathbf{i}_{MPHASE}$ to introduce a middle phase into the model. $\mathbf{i}_{MPHASE}$ has a valve of 0 everywhere at 0-2 DAI, a value of 1 at 2-8 DAI and 0 after 8 DAI. 8 DAI was chosen as the end of the middle phase in the model instead of 10 DAI as by 11 DAI the fruit has already developed a heart shape.

2.2.6.4 Style and base

During the middle phase of growth all clones in the style are narrow have a proximodistal orientation and clones in the valves are isotropic (Figure 2.20F,H). This suggests that there is more K_{per} in the valves than the style. Not many clones were imaged at the base of the gynoecium but given that the gynoecium is pinched at the bottom it is

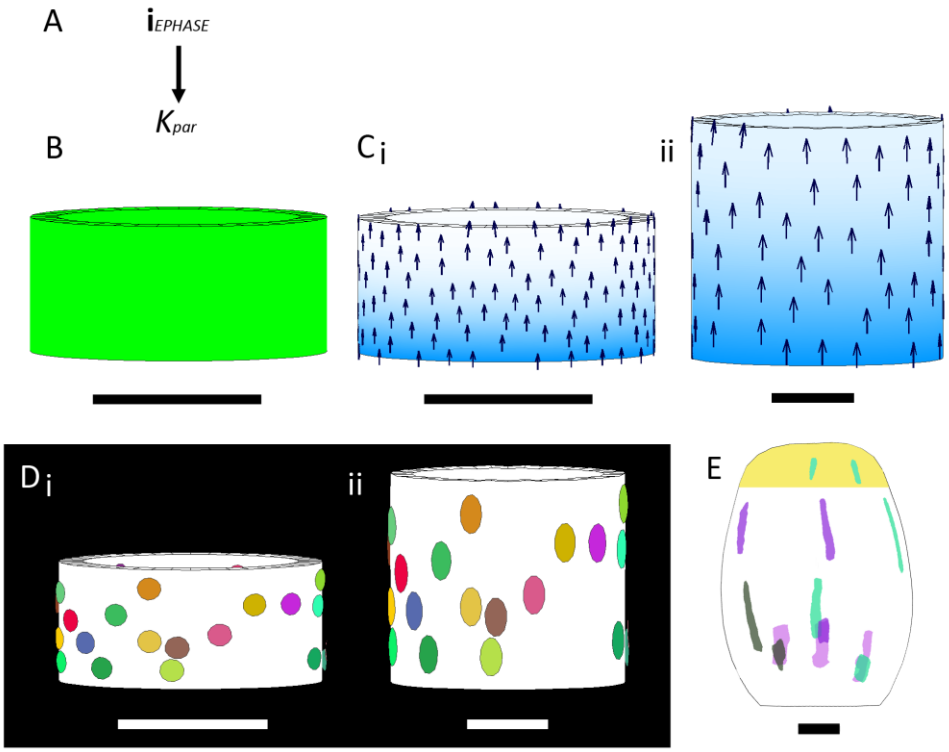

Figure 2.19 Early phase growth (0-2 DAI) (A) The Growth regulatory network (B) $\mathbf{i}_{EPHASE}$ (green colour) on starting canvas. (C) $\mathbf{S}_{POL}$ (blue colour) and polarity field (arrows) mapped onto canvas 0 DAI (i) and 2 DAI (ii). (D) Clones induced on canvas at 0 DAI (i). The clones deform with the growing canvas by 2 DAI (ii). (E) Experimental clones induced on gynoecium at 0 DAI and imaged at 4 DAI. Scale bars 50µm

likely that K_{per} is also restricted in the base region. To implement this in the model I introduced $\mathbf{i}_{STYLE}$ and $\mathbf{i}_{BASE}$ which are generated as an exponential gradient with values of between 0 and 1 (Figure 2.20B). These gradients are fixed during the initial setup phase before growth, and grow with the canvas. $\mathbf{i}_{STYLE}$ and $\mathbf{i}_{BASE}$ interact with the growth regulatory network in the following way:

$$K_{par} = 0.014 \text{ .pro}(p_{EPHASE}, \mathbf{i}_{EPHASE}) \text{ .inh}(h_{BASE}, \mathbf{i}_{BASE}. \mathbf{i}_{MPHASE})$$

$$K_{per} = 0.0115 \text{ .inh}(h_{STYLE}, \mathbf{i}_{STYLE}. \mathbf{i}_{MPHASE}) \text{ .inh}(h_{BASE}, \mathbf{i}_{BASE}. \mathbf{i}_{MPHASE})$$

$$K_{knor} = 0.01$$

Where $\text{inh}(h_{FACTOR} + \mathbf{i}_{FACTOR}) = 1 / (1 + h_{FACTOR} + \mathbf{i}_{FACTOR})$ and h_{FACTOR} is the amount of inhibition by $\mathbf{i}_{FACTOR}$. In this way if h_{FACTOR} and $\mathbf{i}_{FACTOR}$ are equal to one, growth is halved. $\mathbf{i}_{BASE}$ inhibits K_{par} as well as it was noted that the base does not elongate like the style.

The resultant shape 8 DAI is very rounded in longitudinal and transverse views (Figure 2.20C). In *Capsella* the gynoecium is partly flattened in cross section by 8 DAI. In this way the model differs from the *Capsella* gynoecium. However, clones induced at 0 and 2 DAI are similar to experimental clones. Clone induced at 0 DAI are elongated in parallel to the polarity like the proximodistal orientated experimental clones (Figure 2.20E,F). Clones induced at 2 DAI are isotropic in shape similar to experimental clones induced at 2 DAI and imaged at 8 DAI (Figure 2.20G,H).

The shape of the style does resemble that found in the gynoecium, which is round and narrow. Clones induced in the style are narrow in the model (Figure 2.20E,G) and match experimental clones (Figure 2.20F,H). This shows it is important to restrict growth in K_{per} to generate the narrow style.

In summary the specified growth in this model is sufficient to explain the clone orientations in the style and the valves. However, this model does not explain the overall gynoecium shape which is flattened in cross section by 8 DAI or clone shapes in the replum.

2.2.6.5 Replum

It is not clear how the gynoecium becomes flattened in cross section. Clone patterns show that growth is anisotropic in the replum (Figure 2.20), preferentially growing along the proximodistal axis. To test if this type of growth could contribute towards flattening the gynoecium shape I mapped a growth factor $\mathbf{i}_{REP}$ onto the canvas to represent the replum (Figure 2.22B). Growth was specified in the following way:

K_{par} = 0.014 .pro(p_{EPHASE} , $\mathbf{i}_{EPHASE}$) .inh(h_{BASE} , $\mathbf{i}_{BASE}$. $\mathbf{i}_{MPHASE}$)

K_{per} = 0.0115 .inh(h_{STYLE} , $\mathbf{i}_{STYLE}$. $\mathbf{i}_{MPHASE}$) .inh(h_{BASE} , $\mathbf{i}_{BASE}$. $\mathbf{i}_{MPHASE}$) .inh(h_{REP} , $\mathbf{i}_{REP}$. $\mathbf{i}_{MPHASE}$)

K_{knor} = 0.01

where h_{REP} is the amount of inhibition by $\mathbf{i}_{REP}$. The growth inhibitor $\mathbf{i}_{REP}$ is expressed in a stripe in the centre of the *x*-axis on both sides of the cylinder (Figure 2.22B). The resulting shape is not completely round but has a slightly oval cross section (Figure 2.22C). However, the canvas does not flatten like the *Capsella* gynoecium.

This specified growth can explain the clonal patterns observed in the replum which are narrower than clones in the valve and elongated along the proximodistal axis (Figure

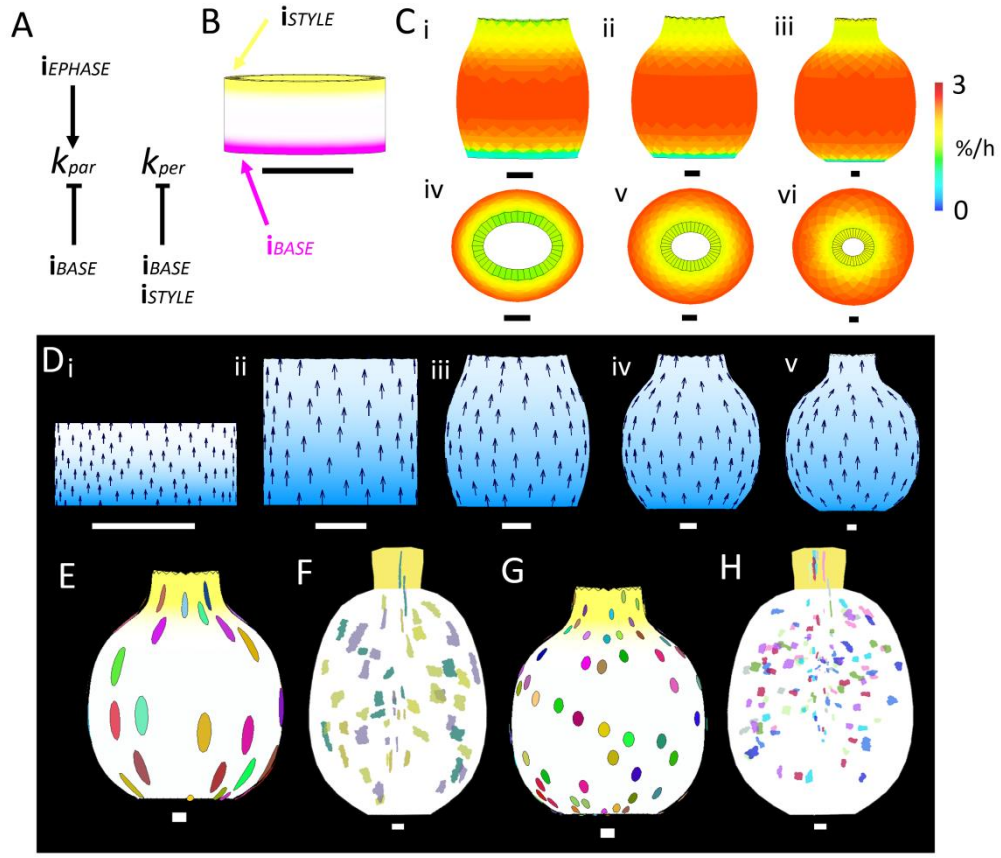

Figure 2.20 Modelling the middle phase (0-8 DAI) with i_{BASE} and i_{STYLE} (A) Growth regulatory network. (B) i_{STYLE} (yellow) and i_{BASE} (pink) on starting canvas. (C) Resultant shapes and resultant areal growth rates (colours) in %/h 4,6 and 8 DAI. (i-iii) longitudinal view, (iv-vi) view from above. Colour chart represents resultant areal growth rates. (D) Polariser (blue) and polarity field deforms with the canvas 0,2,4,6 and 8 DAI. (E-F) Clones induced at 0 DAI in the model (E) and 0.5 DAI experimentally (F) and imaged at 8 DAI and 8.5 DAI, respectively. (G-H) Clones induced at 2 DAI in the model (G) and at 2.5 DAI experimental (H) and imaged at 8 DAI and 8.5 DAI, respectively. The yellow region in E-H indicates the style. Scale bars 50µm.

2.22E,G). Likewise the clones in the region i_{REP} are elongated parallel to the polarity when induced at 0 or 2 DAI (Figure 2.22).

In summary by inhibiting K_{per} by i_{REP}, it is possible to explain the clonal patterns observed in *Capsella* gynoecium 0-8 DAI. However, it is not sufficient to explain the flattened cross section shape at 8 DAI.

2.2.6.6 Midvalve

It is not obvious how specified growth can flatten out the cylinder. To understand how flattening could be achieved it is useful to look at *Capsella* gynoecia 8 DAI from

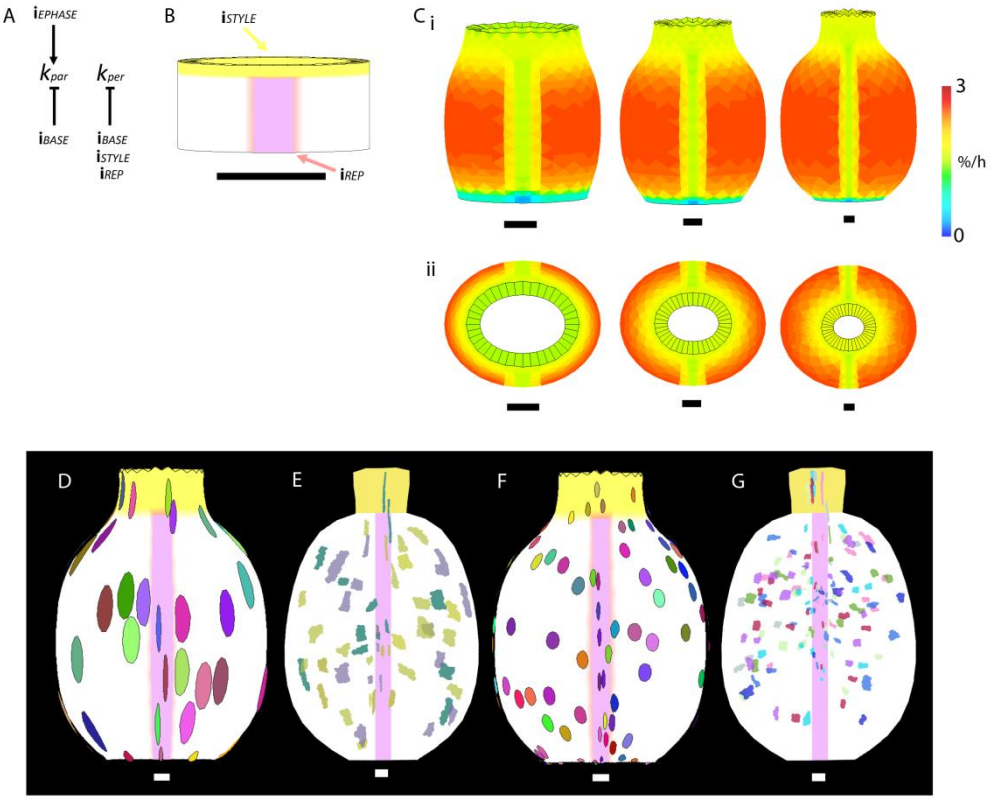

Figure 2.22 Inhibiting K_{per} in the replum (A) Growth regulatory network (B) The distribution of i_{REP} and i_{STYLE} on the initial canvas. (C) Resultant areal growth (colours) and resultant shapes shape of the canvas 4, 6 and 8 DAI from a longitudinal view (i) and a transverse view (ii). (D-E) Clones induced at 0 DAI in the model (E) and 0.5 DAI experimentally (F) and imaged at 8 DAI and 8.5 DAI, respectively. (F-G) Clones induced at 2 DAI in the model (G) and at 2.5 DAI experimental (H) and imaged at 8 DAI and 8.5 DAI, respectively. Yellow region: style and pink region: replum. Scale bars 50µm

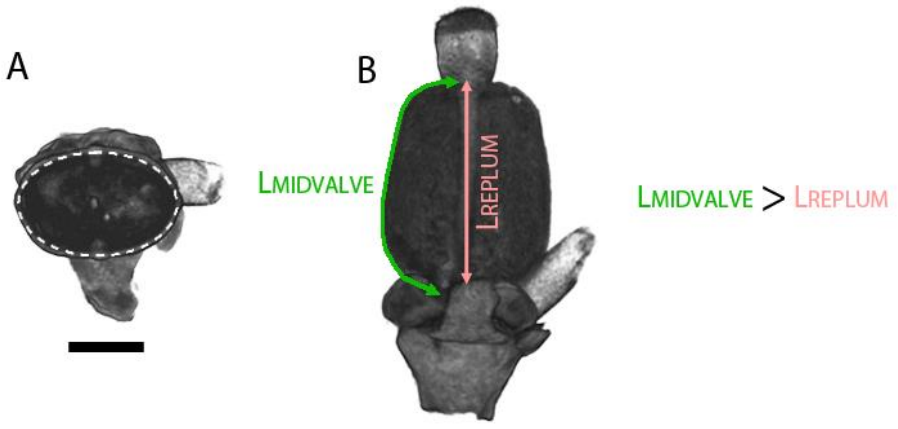

Figure 2.21 Length of midvalve and replum in Capsella gynoecia 8.5 DAI (A) Cross section view. White dotted line shows the cross section shape of the gynoecium (B) Line drawn down the middle of the valve is longer than a line drawn down the replum. Scale bar 500µm

different perspectives (Figure 2.21). If a line is drawn from the style to the base following the contour of the gynoecium at the replum and termed L_{REPLUM} and compared to a line drawn from the style to the base at the midvalve, termed $L_{MIDVALVE}$ then $L_{MIDVALVE} > L_{REPLUM}$ (Figure 2.21B). Hence, it is probable that the midvalve is growing more in length than the replum and this may contribute to the flattened shape. In the model this could be interpreted as higher K_{par} along the opposite sides of the cylinder. To test this idea, I introduced a growth factor to the canvas termed $\mathbf{i}_{MIDVALVE}$ which is expressed in the centre of the *y*-axis (Figure 2.23B):

$K_{par} = 0.014 .\text{pro}(p_{EPHASE} , \mathbf{i}_{EPHASE})$

$.\text{inh}(h_{BASE} , \mathbf{i}_{BASE}. \mathbf{i}_{MPHASE}) .\text{pro}(p_{MIDVALVE} , \mathbf{i}_{MIDVALVE}. \mathbf{i}_{MPHASE})$

$K_{per} = 0.0115 .\text{inh}(h_{STYLE} , \mathbf{i}_{STYLE}. \mathbf{i}_{MPHASE}) .\text{inh}(h_{BASE} , \mathbf{i}_{BASE}. \mathbf{i}_{MPHASE}) .\text{inh}(h_{REP} , \mathbf{i}_{REP}. \mathbf{i}_{MPHASE})$

$K_{knor} = 0.01$

where $p_{MIDVALVE}$ is the amount of promotion by $\mathbf{i}_{MIDVALVE}$. I tested three values of $p_{MIDVALVE}$: 0.1, 0.25 and 0.5. Figure 2.23shows that with increasing values of $p_{MIDVALVE}$ and thereby promoting K_{par} in the midvalve region results in the flattening of the canvas in the cross section.

Clones induced on the three models at 2 DAI and observed at 8 DAI show different characteristics. When K_{par} is promoted by 50%/h the clones in the valve become elongated parallel to the polarity (Figure 2.23F). This is not observed in the experimental clones (Figure 2.23C). When K_{par} is promoted by 10%/h or 20%/h the clones have a mostly isotropic shape (Figure 2.23D,E) similar to the experimental clones. However, the cross section shape is most similar to the *Capsella* gynoecium with 20%/h more K_{par} at $\mathbf{i}_{MIDVALVE}$ (Figure 2.23E,Figure 2.21A). To stop the midvalve region from expanding, in all subsequent models $\mathbf{i}_{MIDVALVE}$ also inhibits K_{per}. I have not been able to test these hypotheses in *Capsella* as the flattened shape of the gynoecium made imaging the midvalve region difficult.

In summary, using the principle of higher K_{par} at the midvalve to flatten the shape out and inhibition of K_{per} in the replum, style and base, a snuff bottle shape gynoecium can be recapitulated (Figure 2.23). This model can explain the experimental clone patterns observed in the gynoecium 0-8 DAI.

The polarity field deforms with the growing canvas (Figure 2.24A) and splays out to following the contours of the rounded shape and converges back towards the style. This

means that the orientations of K_{par} and K_{per} do not continue to be parallel and perpendicular to the proximodistal axis across the whole canvas but fan out with the polarity field.

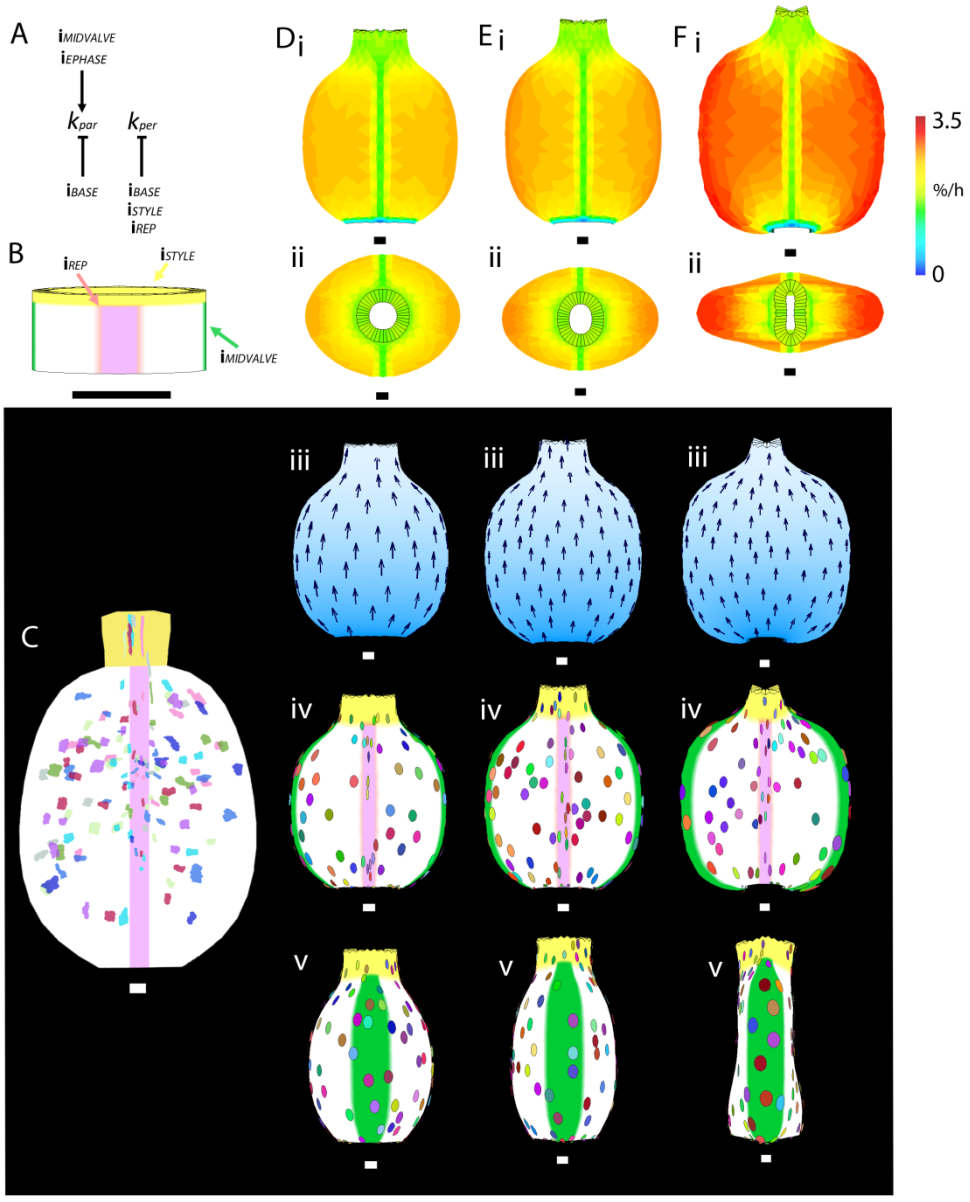

Figure 2.23 Promoting K_{par} by $i_{MIDVALVE}$ (A) Growth regulatory network (B) initial starting shape with $i_{MIDVALVE}$ i_{REP} and i_{STYLE} mapped. (C) Experimental clone induced 2 DAI and images at 8 DAI. (D-F) K_{par} promoted by 0.1 (D), 0.2 (E) or 0.5 (F). Resultant areal growth (colours) and shapes 8 DAI longitudinal view (i) and view from above (ii). Polariser and polarity field deforms with canvas (iii). Clones induced at 2 DAI and image at 8 DAI (iv,v). Yellow region: style, pink region: replum, green region: midvalve, white region: valves. Scale bars 100µm and coloured scale bar %/h resultant areal growth.

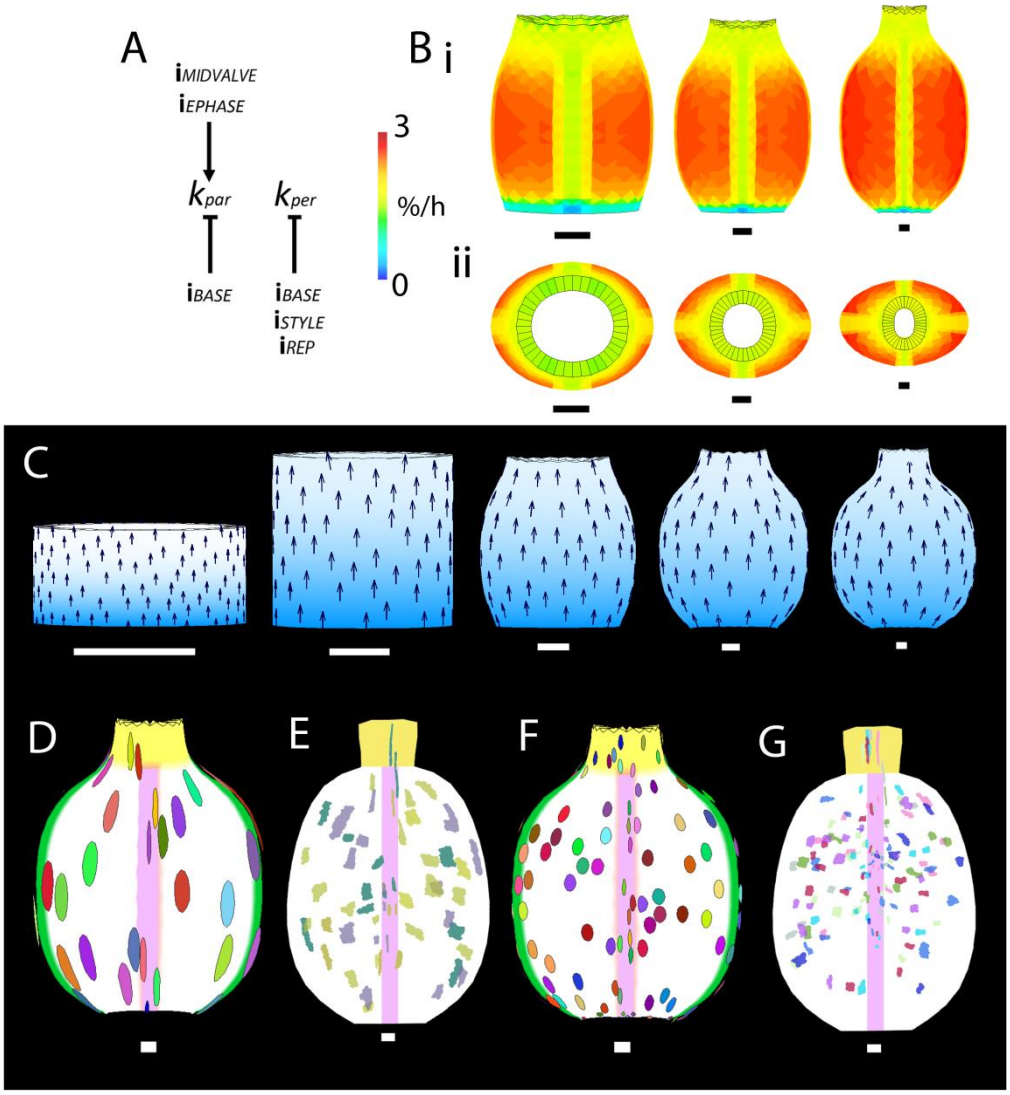

Figure 2.24 Modelling the snuff bottle phase. (A) Growth regulatory network (B) Resultant shapes with resultant areal growth rates (colours) of 4, 6 and 8 days of growth respectively from face view (**i**) and above (**ii**) (C) polarity field (arrows) specified by the signalling factor s_{POL} (blue) at 0,2,4,6 and 8 DAI. The polarity field deforms with the growing canvas. Yellow region: style, pink region: replum, green region: midvalve, white region: valves. Clone induced at 0.5 Scale bars 100µm.

The clones in the replum and style regions of the canvas have an anisotropic shape, orientated parallel to the polarity after 8 and 6 days of growth (Figure 2.24D,F), matching the biological clones (Figure 2.24E, G). The clones in the valve regions are isotropic in both model and biological examples. This simple model shows a fairly accurate representation 8days of growth from the cylindrical to the snuff bottle shaped gynoecium of *Capsella*. For simplicity all following models build from this stage and do not show the first 8 days.

2.2.6.7 Modelling the late phase

Following the snuff bottle stage the *Capsella* gynoecium starts to develop shoulders by 11 DAI and has a tapered base. The fruit also becomes progressively flatter. From observations of the morphology, the style seems to stop growing in later stages the style is relatively small in the mature fruit. Because of this observation, in the model I inhibit K_{par} in the style region for the later stages. Also I have observed in the model that the midvalve region becomes quite wide if the model continues into later stages (data not shown). For this reason I inhibit K_{per} in the midvalve region in the late stages (see function below).

2.2.6.8 Gradient in the midvalve

I have shown that higher K_{par} along the midvalve can be used in the model to develop a flattened shape (Figure 2.23). Another observation is that with greater values of K_{par} (Figure 2.23G) the top and bottom of the valves begin to bulge out beyond the length of the replum. In the heart shape fruit the shoulders bulge above the style so it is possible that the growth along the midvalve could be important for this. The base does not bulge out, so in order to test this a factor was introduced to the model ($\mathbf{i}_{GMIDVALVE}$) that has a linear gradient along the midvalve with the highest value of 1 just under the style and the lowest value of 0 at the base (Figure 2.25B). The gradient is fixed in the initial setup phase before growth and grows with the canvas. $\mathbf{i}_{GMIDVALVE}$ influences growth in the following way:

K_{par} = 0.014 .pro(p_{EPHASE} , $\mathbf{i}_{EPHASE}$)

.inh(h_{BASE} , $\mathbf{i}_{BASE}$. $\mathbf{i}_{MPHASE}$) .pro($p_{MIDVALVE}$, $\mathbf{i}_{MIDVALVE}$. $\mathbf{i}_{MPHASE}$)

.inh(h_{STYLE} , $\mathbf{i}_{STYLE}$. $\mathbf{i}_{LPHASE}$).pro($p_{GMIDVALVE}$, $\mathbf{i}_{GMIDVALVE}$. $\mathbf{i}_{LPHASE}$)

K_{per} = 0.011 .inh(h_{STYLE} , $\mathbf{i}_{STYLE}$. $\mathbf{i}_{MPHASE}$) .inh(h_{BASE} , $\mathbf{i}_{BASE}$. $\mathbf{i}_{MPHASE}$) .inh(h_{REP} , $\mathbf{i}_{REP}$. $\mathbf{i}_{MPHASE}$)

.inh($h_{MIDVALVE}$, $\mathbf{i}_{MIDVALVE}$. $\mathbf{i}_{LPHASE}$)

K_{knor} = 0.01

where $p_{GMIDVALVE}$ is the amount of promotion by $\mathbf{i}_{GMIDVALVE}$ (Figure 2.25A). This can be visualised in Figure 2.25C&D which maps the specified growth onto the canvas, where K_{par} is highest in the midvalve nearest the style.

The resultant shape is reminiscent of flattened apple (Figure 2.25E). The top part of the canvas has shoulders that bulge above the style. However, even though K_{par} is less in the midvalve at the base, the valve bulges downwards as well. This can be explained by the deforming polarity field as the canvas grows. The polarity field in the snuff bottle stage splurges out away from the base and then converges at the style. This becomes more pronounced as the canvas gets rounder, making a circular pattern. At the proximal base either side of the replum the polarity field is oblique to the proximal distal axis of the canvas. Since the rate of K_{per} is uniform across the valves the oblique orientation results in downward growth. At the distal shoulders the polarity field has a greater oblique orientation which results in growth above the style.

The clones generated in this model do not match the biological clones. The clones in the model are orientated parallel to the polarity in the valves (Figure 2.25G). Experimental clones of a similar stage are orientated perpendicular to the polarity in the valves (Figure 2.25H). Therefore, promoting growth in the midvalve cannot explain the resultant heart shape of the *Capsella* fruit or the clonal patterns.

2.2.6.9 Gradient of K_{per} in the valves

The apple shape is similar to a heart shape in the distal shoulders but dissimilar at the base where it bulges out compared to the tapered base of the heart. This difference seems to be the result of uniform rates of K_{per} in the valves. Clone patterns show growth is orientated perpendicular to the proximodistal axis in the later stages and clones at the proximal region of the fruit are orientated parallel to the polarity (Figure 2.25H). This could be interpreted as lower K_{per} in the proximal region and greater in the distal region. Here, I explored the distribution of K_{per} in the valve region.

To test the hypothesis that K_{per} is greater in the distal region, I introduced two factors into the model termed $\mathbf{i}_{GPROX}$ and $\mathbf{i}_{GDIST}$. $\mathbf{i}_{GPROX}$ is distributed as a linear gradient with a value of 1 at the base and a value of 0 at the style. $\mathbf{i}_{GDIST}$ is distributed as a linear gradient with a value of 1 in the valve near the style and a value of 0 at the base. The gradients were fixed in the initial setup phase and grow with the canvas. $\mathbf{i}_{GPROX}$ and $\mathbf{i}_{GDIST}$ influence growth in the following function:

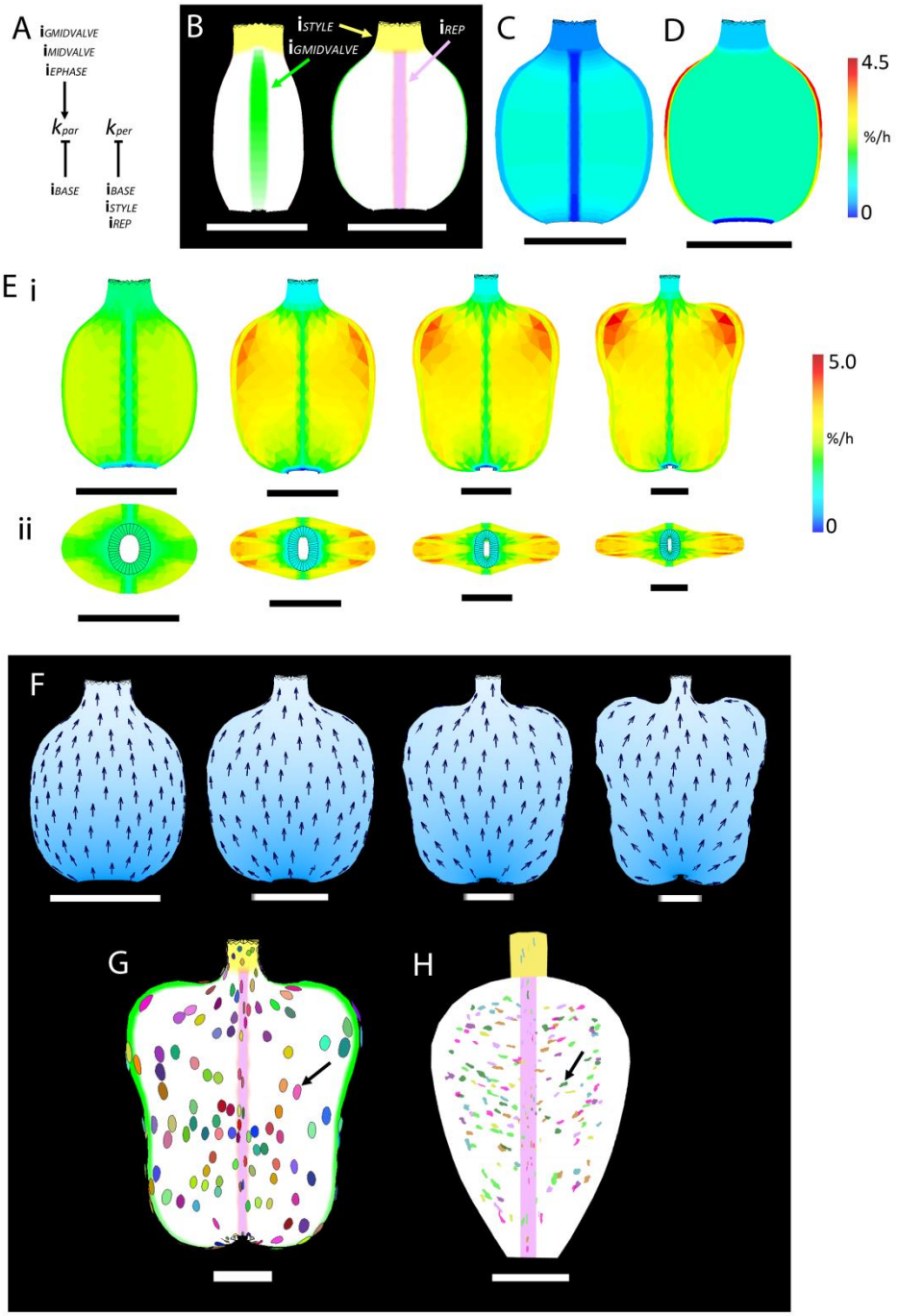

Figure 2.25 Promoting K_{par} by $i_{GMIDVALVE}$ (A) Growth regulatory network (B) Canvas at 8 DAI with $i_{GMIDVALVE}$ i_{REP} and i_{STYLE} mapped. (C) Specified K_{per} and (D) specified K_{par} (colours) mapped on to the canvas at 9 DAI, colour scale bar represents respective specified growth rate in %/h. (E) Resultant areal growth (colours) and shapes at 8, 9, 10 and 11 DAI from a longitudinal view (i) and view from above (ii). Coloured scale bar represents resultant areal growth rates in %/h (F) Polarity field (arrows) specified by the signalling factor s_{POL} (blue). (G) Clones induced at 5 DAI and imaged at 11 DAI in the model. (H) Clones induced at 5.5 DAI and imaged at 11.5 DAI experimentally. Black arrows indicate model and experimental clones have different orientations in the valve. Yellow region: style, pink region: replum, green region: $i_{GMIDVALVE}$, white region: valves. Scale bars 500µm

K_{par} = 0.014 .pro(p_{EPHASE} , $\mathbf{i}_{EPHASE}$)

.inh(h_{BASE} , $\mathbf{i}_{BASE}$. $\mathbf{i}_{MPHASE}$) .pro($p_{MIDVALVE}$, $\mathbf{i}_{MIDVALVE}$. $\mathbf{i}_{MPHASE}$)

.inh(h_{STYLE} , $\mathbf{i}_{STYLE}$. $\mathbf{i}_{LPHASE}$).pro($p_{GMIDVALVE}$, $\mathbf{i}_{GMIDVALVE}$. $\mathbf{i}_{LPHASE}$)

K_{per} = 0.011 .inh(h_{STYLE} , $\mathbf{i}_{STYLE}$. $\mathbf{i}_{MPHASE}$) .inh(h_{BASE} , $\mathbf{i}_{BASE}$. $\mathbf{i}_{MPHASE}$) .inh(h_{REP} , $\mathbf{i}_{REP}$. $\mathbf{i}_{MPHASE}$)

.inh($h_{MIDVALVE}$, $\mathbf{i}_{MIDVALVE}$. $\mathbf{i}_{LPHASE}$) .inh(h_{PROX} , $\mathbf{i}_{GPROX}$. $\mathbf{i}_{LPHASE}$) .pro(p_{GDIST} , $\mathbf{i}_{GDIST}$. $\mathbf{i}_{LPHASE}$)

K_{knor} = 0.01

where h_{GPROX} is the amount of inhibition by $\mathbf{i}_{GPROX}$ and p_{GDIST} is the amount of promotion by $\mathbf{i}_{GDIST}$. For this model K_{par} was kept uniform across the valve region accept for the midvalve where K_{par} is promoted by $\mathbf{i}_{GMIDVALVE}$, (the value of $h_{GMIDVALVE}$ is lower for this model compared to Figure 2.25). In Figure 2.26C the specified rates of K_{par} and K_{per} are mapped onto the canvas at 9DAI.

The resultant shape after 4 days of growth is heart shaped, with wider distal shoulders and a narrow tapered base (Figure 2.26E). The shape is also flat in cross section. This model at 11 DAI has a similar to the shape to the *Capsella* fruit at 11 DAI. The resultant areal growth rates are higher in the distal shoulders than the base (Figure 2.26E). The polarity field follows the contours of the heart shape; spreading out towards the shoulders and converging back towards the style (Figure 2.26D).

The resultant whole organ shape is similar to *Capsella*. However, clones induced in valve region of the model have an isotropic shape or are slightly elongated parallel to the polarity (Figure 2.26F). Experiment clone in the same area are anisotropic perpendicular to the polarity (Figure 2.26G). This difference in clone orientations between the experimental and the model clones shows that a non-uniform distribution of K_{per} in the valves is not sufficient to explain the regional growth of the *Capsella* heart-shaped fruit.

2.2.6.9 Gradient of K_{par} in the valves

The experimental clones in the distal half of the fruit are shorter along the proximal distal axis compared to the clones at the base (Figure 2.27G) or in other words are elongated more parallel to the polarity. This may be accounted for by higher values of K_{par} in the proximal region compared to the distal shoulders. To test this idea in the model, I used $\mathbf{i}_{GPROX}$ and $\mathbf{i}_{GDIST}$ to influence K_{par} in the following function:

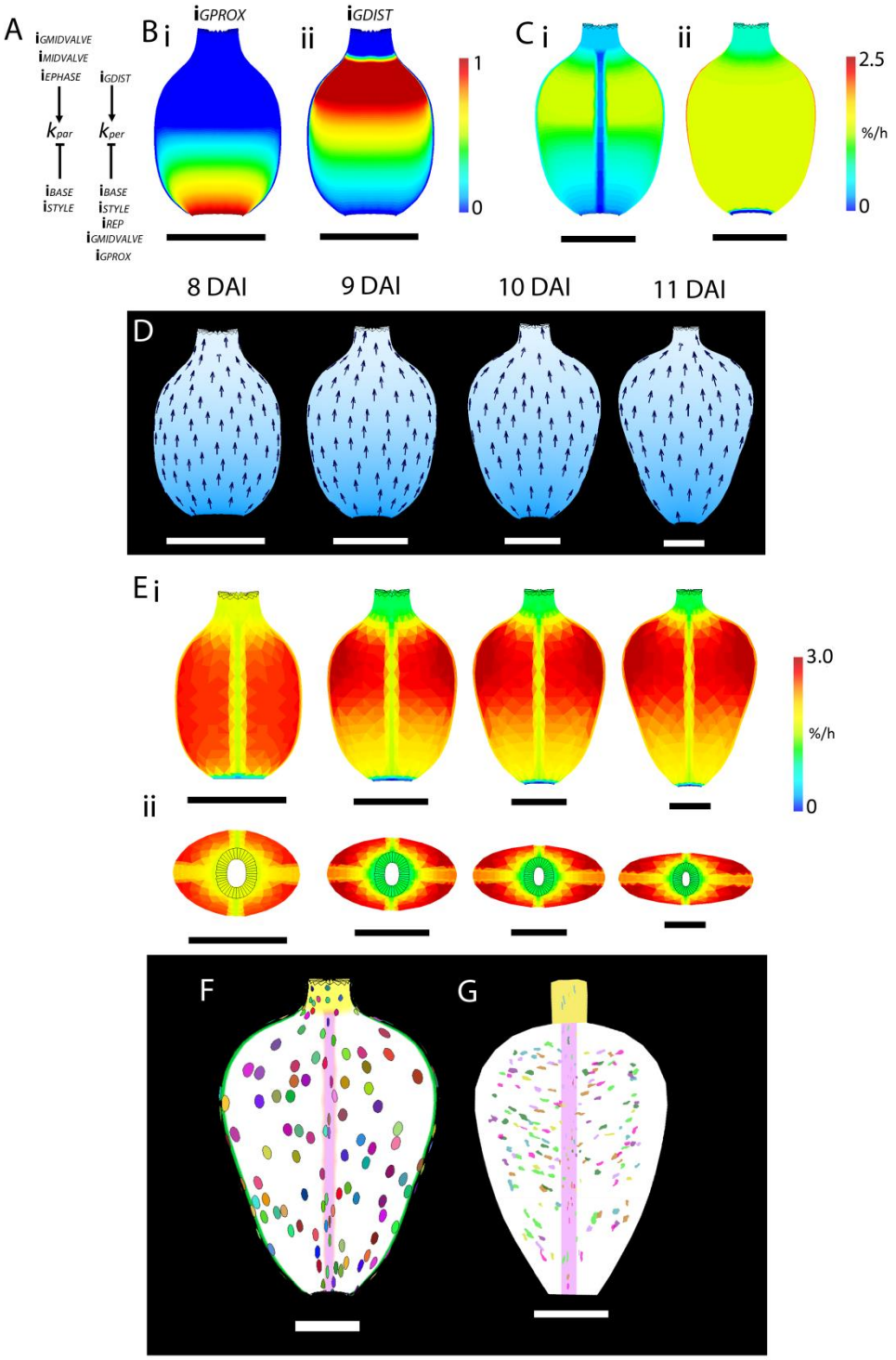

Figure 2.26 Generating a heart-shape with non-uniform distribution of Kper in the valves (A) The growth regulatory network. (B) Distributions of iGPROX (i) and iGDIST at 8 DAI. Coloured scale bar is parameter value. (C) Specified K_{par} (i) and K_{per} (ii) mapped onto canvas 9DAI. Coloured scale bar is specified growth in %/h. (D) Polarity field (arrows) and $\mathbf{s}_{POL}$ (blue) (E) Resultant shapes and areal growth rates from longitudinal view (i) and from above (ii). (F) Clone induced in the model at 5 DAI and imaged at 11 DAI. (H) Clones induced experimentally at 5.5 DAI and imaged at 11 DAI. Yellow region: style, pink region: replum, green region: midvalve, white region: valves. Scale bars 500µm.

K_{par} = 0.014 .pro(p_{EPHASE} , $\mathbf{i}_{EPHASE}$)

.inh(h_{BASE} , $\mathbf{i}_{BASE}$. $\mathbf{i}_{MPHASE}$) .pro($p_{MIDVALVE}$, $\mathbf{i}_{MIDVALVE}$. $\mathbf{i}_{MPHASE}$)

.inh(h_{STYLE} , $\mathbf{i}_{STYLE}$. $\mathbf{i}_{LPHASE}$).pro($p_{GMIDVALVE}$, $\mathbf{i}_{GMIDVALVE}$. $\mathbf{i}_{LPHASE}$) .pro(p_{PROX} , $\mathbf{i}_{GPROX}$. $\mathbf{i}_{LPHASE}$)

.inh(h_{GDIST} , $\mathbf{i}_{GDIST}$. $\mathbf{i}_{LPHASE}$)

K_{per} = 0.011 .inh(h_{STYLE} , $\mathbf{i}_{STYLE}$. $\mathbf{i}_{MPHASE}$) .inh(h_{BASE} , $\mathbf{i}_{BASE}$. $\mathbf{i}_{MPHASE}$) .inh(h_{REP} , $\mathbf{i}_{REP}$. $\mathbf{i}_{MPHASE}$)

.inh($h_{MIDVALVE}$, $\mathbf{i}_{MIDVALVE}$. $\mathbf{i}_{LPHASE}$) .inh(h_{PROX} , $\mathbf{i}_{GPROX}$. $\mathbf{i}_{LPHASE}$) .pro(p_{GDIST} , $\mathbf{i}_{GDIST}$. $\mathbf{i}_{LPHASE}$)

K_{knor} = 0.01

Where p_{GPROX} is the amount of promotion by $\mathbf{i}_{GPROX}$ and h_{GDIST} is the amount of inhibition by $\mathbf{i}_{GDIST}$. Specified K_{per} remains constant from the previous model (Figure 2.26). Hence, in this model, $\mathbf{i}_{GPROX}$ is promoting K_{par} and inhibiting K_{per} and $\mathbf{i}_{GDIST}$ is inhibiting K_{par} and promoting K_{per}. The specified growth rates have been mapped onto the canvas at 9DAI (Figure 2.27B, C).

The resultant shape of the model is heart-shaped by 11 DAI (Figure 2.27Ei). The shoulders have bulged up above the style and the base is tapered. The model is also flattened in cross section (Figure 2.27Eii). The polarity field again follows the contours of the heart shape spreading out toward the shoulders and converging at the style (Figure 2.27D). The resultant areal growth rates are highest at the base and at the very tip of the distal shoulders (Figure 2.27E).

Clone induced in the model are anisotropic in the distal region, orientated parallel to the polarity (Figure 2.27F). This matches the experimental clones which are orientated parallel to the proximodistal axis in proximal region of the fruit (Figure 2.27G). Clones in the more distal regions of the valves in the model are anisotropic perpendicular to the polarity field (Figure 2.27F), similar to experimental clones in the same region (Figure 2.27G).

The model resultant shape at 11 DAI has larger distal shoulders that the experimental mean shape at this stage (Figure 2.27F,G). However, exploring the parameters controlling the gradients of K_{par} and K_{per} in more depth would likely reach a more similar final shape. This model shows how alternative gradients in K_{par} and K_{per} can account for the orientations of clones and can generate a heart-shape.

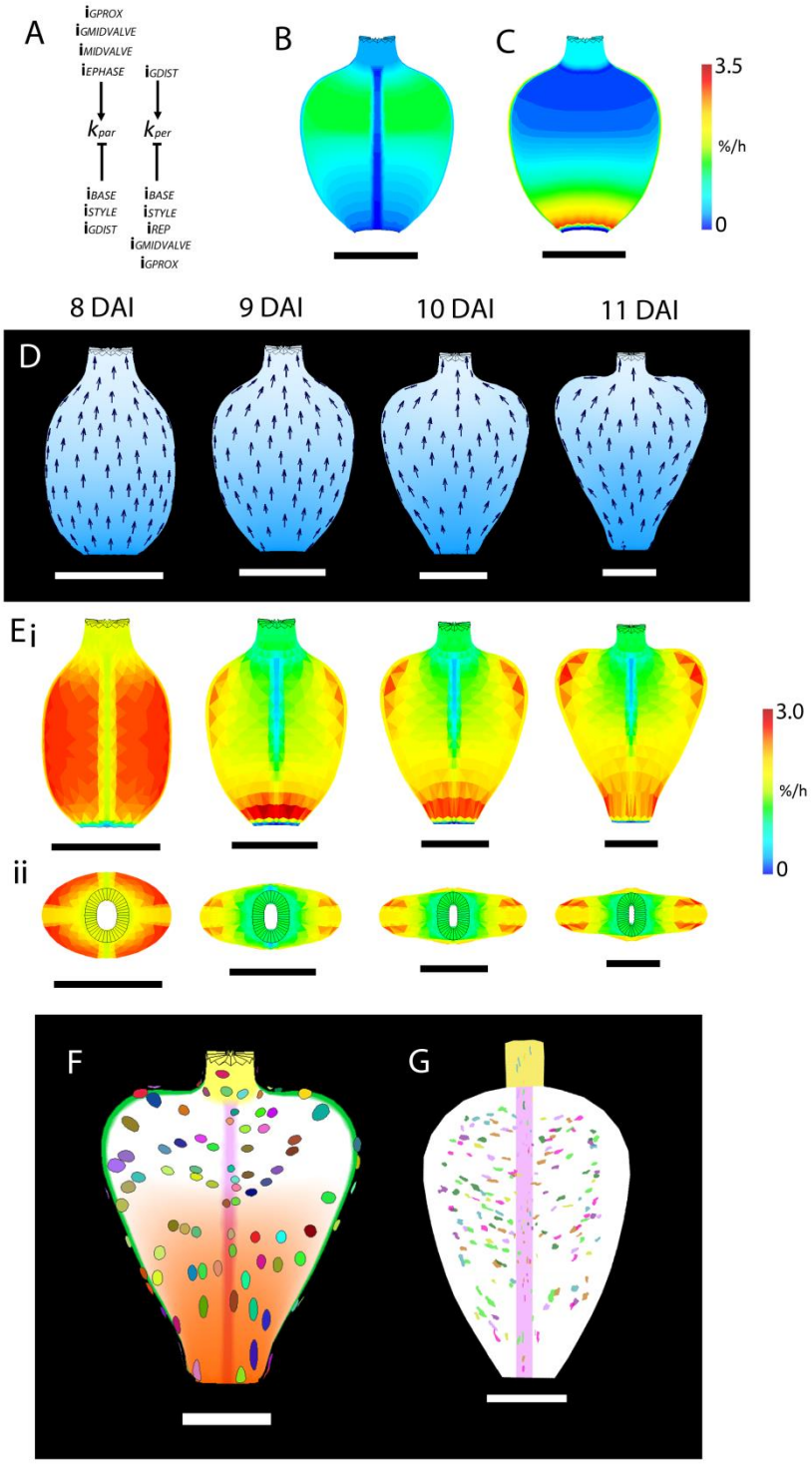

Figure 2.27 Generating a heart-shape with non-uniform distribution of Kper and Kpar in the valves (A) The growth regulatory network. (B) Specified K_{per} and (C) K_{par} mapped onto canvas 9DAI. Coloured scale bar is specified growth in %/h. (D) Polarity field (arrows) and distribution of $\mathbf{s}_{POL}$ (blue) (E) Resultant shapes and areal growth rates from longitudinal view (i) and from above (ii). (F) Clones induced in the model at 5 DAI and imaged at 11 DAI. (H) Clones induced experimentally at 5.5 DAI and imaged at 11 DAI. Yellow region: style, pink region: replum, green region: midvalve, white region: valves. Scale bars 500µm.

In summary, the clonal patterns in the early phase can be account for by higher growth parallel to the polarity. The snuff bottle shape can be generated and clonal patterns for the middle phase can be explained by inhibition of K_{per} in the style, base and replum. I hypothesise that the cross section shape is flattened by higher growth parallel to the polarity in the midvalve region. Finally, the clone patterns in the late phase can be accounted for by higher values of K_{par} in the proximal region and higher values of K_{per} in the distal regions of the valves.

2.3 Discussion

This study provides a detailed morphological description of *Capsella rubella* gynoecium and fruit development using SEMs and OPT to describe all stages. There is an early phase of growth, from 0-2.5 DAI, where the gynoecium grows as a hollow cylinder with a greater growth rate in length than width. During the middle phase a snuff bottle-shape gynoecium is produced before fertilisation with nearly isotropic growth in the valve regions. During the late phase the snuff-bottle shape grows into the heart-shaped fruit and the clones have different orientations across the valves. These clone patterns has been explored by computational modelling, where higher values of K_{par} in the proximal region of the fruit and higher values of K_{per} in the distal regions can explain the orientations of the experimental clones.

2.3.1 Imaging *Capsella* fruit development

In many morphological studies SEMs have provided beautiful details of development. However SEMs do not provide accurate 3D perspectives. In SEMs of the earliest developmental stages the *Capsella* gynoecium looks flattened in the mediolateral plain, however OPT reconstructions reveal it is round to oval until at least 6 DAI. OPT images have therefore provided accurate volumetric and shape data for all stages of development. The complementation of cellular detail from SEM images combined with the 3D information from OPT images has been really powerful in describing accurately the development of the *Capsella* gynoecium.

2.3.2 The 3 phases of *Capsella* fruit growth

In this study, *Capsella* fruit growth has been divided into three principle phases. The early phase and the middle phase are pre-fertilisation and late phase is post-

fertilisation. The phases are categorised by the orientations of growth which change dynamically through *Capsella* fruit development. Phases in fruit growth have been identified before in fleshy fruits (Gillaspy et al., 1993). Phase I is ovary development, fertilisation and fruit set, Phase II is characterised by fruit growth correlated with cell division and Phase III growth is primarily driven by cell expansion (Yang et al., 2013). In cucumber, for example, the orientation of growth is maintained throughout development regardless of the phase.

During the early phase, gynoecium growth rates in length are the highest. This initial growth is anisotropic, lengthening the cylindrical gynoecium. Initially high growth rates seems to be a common feature of developing organs for example in the *Arabidopsis* petal areal growth rates are initially 4.1%/h and at later stages drop and are maintained around 2.3%/h. Small cells and high cell division rates are correlated with a higher growth rate.

In the *Arabidopsis* petal, orientation of growth is maintained throughout the development (Sauret-Gueto et al., 2013), growth orientation changes in the *Capsella* gynoecium after the early phase. The orientation changes by a decrease in growth rate in length and a steady growth rate in width. This change in orientation signifies a switch to the middle phase of gynoecium development. It is likely that factors that promote growth in width are expressed by 2DAI and it would be interesting to identify the genetic players.

An early phase of gynoecium development has not been described in other Brassicaceae species to date. However it may be a key determinant of fruit shape differences; this will be discussed further in Chapter 5.

The late phase is characterised by mixed orientations of growth across the valves of the fruit and results in the transition from a snuff-bottle shape to a heart-shaped fruit in *Capsella*. The visible whole organ change in shape occurs after fertilisation however growth orientations may have changed before this stage. A change in shape of fruit following fertilisation is not uncommon. For example the wild relative of tomato (*Lycopersicon pimpinellifolium*) has similar shaped gynoecium to the domesticated relative (*L.* esculentum). However, after fertilisation the fruit shapes diverge to form spherical or elongated fruit (van der Knaap and Tanksley, 2001). Also in several species of Brassicaceae the gynoecium is rounded and only following fertilisation the fruits develop as a flattened form (Bowman, 2006). It is clear that changing growth patterns after fertilisation are

important for the final fruit form and fertilisation may act as a switch. A direct link between fertilisation and change in growth patterns was not proven in this study. However, this could be further explored by emasculation of the flowers, followed by a heat shock treatment and with and without subsequent hand pollination.

The model of *Capsella* fruit describes dramatic differences in growth properties between the three temporally distinct phases. The transition from the early to middle phase may be caused by cell differentiation as style region becomes distinct and in *Arabidopsis* the expression of *FUL* becomes restricted to the valves (Ferrandiz *et al.,* 1999) indicating a establishement of valve identity. The second transition from middle to late phase may be a result of hormonal cues, as ovules and pollen are reaching maturity hormonal signals are likely to change during this period.

In previous studies, fertilisation has been inferred as a cue for changing growth properties of the fruit (Bowman, 2006). However, the models described here reveal that the transition in the case of *Capsella* occurs before the point of fertilisation. This interesting observation suggests the existence of a pre-fertilisation cue which alters growth properties of the fruit. It also suggests that fertilisation doesn't alter growth properties of the fruit but maintains the growth patterns laid down before fertilisation.

2.3.3 Fruit growth dynamics

Whole organ dynamics have shown the contribution of length and width to overall growth of the *Capsella* gynoecium and fruit. However, whole fruit measurements of length and width were not enough to capture the changing shape of the fruit as the relative position of the widest part changed through development.

There are two models described that generate a good match to the organ shape. The first has a uniform rate of K_{par} and higher K_{per} in the distal regions of the valves but clones generated on the model do not match the experimental clones. Therefore, it is not enough to analyse only the whole organ shape as there may be multiple possibilities of generating it. The clonal analysis provides a rigorous test for the model predictions and has been used as such in the *Arabidopsis* leaf and petal (Kuchen et al., 2012; Sauret-Gueto et al., 2013).

I quantified growth rates in the experimental data using the clone data from clones induced when cells were assumed to be isodiametric and similar sizes. It is possible to

calculate growth tensors if cell shapes are initially not isodiametric and uniform in size. In order to do this an accurate map of cell shapes at the time of clone initation would be important. For example, cell shapes of the *Arabidopsis* leaf were superimposed onto the GFtbox model to more accurately predict the clone patterns (Kuchen et al., 2012). It may be possible to generate a map of cell shapes in the gynoecium epidermis, using propidium iodide staining and confocal imaging. However, this would be difficult to achieve around the full 3D structure.

In the model the clonal patterns were observed qualitatively. Quanitification of growth in the model can be done by observing the resultant areal growth (displayed in modelling figures) and resultant growth rates parallel and perpendicular to the polarity in a heat map. Although not carried out in this study, it could be useful to directly compare growth rates by generating a heat map based on clonal anaylsis (Green et al., 2010). This would allow for a more quantitative comparison of growth rates between the experimental and model data.

2.3.4 Polarity

In the models presented here an organiser based system has been used to establish and maintain polarity. An organiser-based model for *Arabidopsis* leaf and petal has given the most accurate predictions of growth orientations and organ shape (Kuchen et al., 2012; Sauret-Gueto et al., 2013). *PIN1* cell polarities in both cases are consistent with an organiser-based hypothesis. In the *Arabidopsis* gynoecium *PIN1* expression is apically localised in replum cells (Grieneisen et al., 2013). This is consistent with an organiser-based model for the gynoecium as growth orientations are specified depending on the axiality of the polarity field (Kennaway et al., 2011).

It is likely that *Capsella* and *Arabidopsis* have a similar polarity field during gynoecium development. To answer this, a *PIN1:GFP* line in *Capsella* has recently been made available (Adrien Sicard, unpublished) and will be examined throughout gynoecium development. Immunolocalistion studies of PIN proteins would also be very informative to understand if PIN localisation could be a component of polarity organisation in the *Capsella* gynoecium.

A candidate for + organiser at the base of the gynoecium is unclear but is likely to be a transcription factor. Auxin production is an expected property of a + organiser region (Abley et al., 2013). The auxin biosynthesis genes, *YUC1* and *YUC4*, are expressed at the

base of the earliest stage of *Arabidopsis* gynoecium development. *CUP-SHAPED COTYLEDON* (*CUC*) genes encode *NAC*-type transcription factors and are candidates for +organisers at the base of the leaf (Kuchen et al., 2012). *CUC* genes are expressed on the adaxial side of the medial tissue at the base of the gynoecium (Nahar et al., 2012). This expression does not match the predicted position of a + organiser of the models. However, the medial tissues grow in a different plane to the model as the medial ridges grow inwards to fuse as the septum and develop ovules. This growth plane cannot be captured by the model as GFtbox is not a 3D modelling framework. Once a 3D modelling framework is available it would be interesting to see how growth and polarity of the internal gynoecium tissues would affect overall organ shape and organisation.

An alternative hypothesis for the development of the shoulders of the heart-shaped fruit would be to change the organisation of the polarity. This could be done by having a – organiser in the midvalve during the late phase. Growth would then be anisotropic parallel to the polarity as it would splay out towards the shoulders. The model described in this work, demonstrates that is not necessary to reorganise the polarity field to generate a heart-shaped fruit. This is because the polarity field deforms with the growing tissue and non-uniform rates of K_{par} and K_{per} is sufficient to explain clonal patterns. To distinguish between these hypotheses it would be useful to follow *PIN* dynamics through development of the *Capsella* fruit.

In the Capsella model described here the + organiser is at the base of the gynoecium and polarity points apically. However, growth only uses the axiality of the predefined arrows, not the directional information. Therefore the polarity field could be flipped to the opposite orientation, with the + organiser at the apex and the polarity pointing basally. This can generate the same resultant shape.

2.3.5 Regions and factors

The factors introduced in the models are likely to represent multiple genetic factors in the gynoecium. The genes identified for different regions are often transcription factors that mark tissues for a specific developmental programme.

In the models I used gradients to set up different regions such as $\mathbf{i}_{STYLE}$, $\mathbf{i}_{BASE}$, $\mathbf{i}_{GPROX}$ and $\mathbf{i}_{GDIST}$. An alternative is to use defined boundaries representing the identities of the different cell types, I used this in for $\mathbf{i}_{REP}$ and $\mathbf{i}_{MIDVALVE}$. Gradients give a smootherboundary between growth properties of different regions and therefore smoother resultant shapes.

In the case of $\mathbf{i}_{GPROX}$ and $\mathbf{i}_{GDIST}$ in the *Capsella* model it was essential to use gradients to generate the smooth heat shape. In the valves of *Arabidopsis* gradients are observed in expression of factors such as *FUL* (Woods, 2010). For tissues such as the style and replum, which have very different growth properties and cell types there is an obvious defined boundary between these tissues. Instead of using gradients in this case it would be more accurate to use a sharp boundary. The use of a gradient for $\mathbf{i}_{STYLE}$ was an artefact of a previous model and would be better represented with a defined region. However, due to the short, sharp gradient set up initially for $\mathbf{i}_{STYLE}$ it is unlikely to make a significant difference to the model shape.

During the construction of the final *Capsella* fruit model I have added several factors to generate the final form. When any of these factors are removed the model no longer explains the fruit shape of *Capsella.* Removal of some of the factors gives rise to simpler fruit forms such as *Lepidium* and *Arabidopsis* (see chapter 4). Therefore, I suggest that the factors used in the *Capsella* model are the minimal necessary to explain the heart-shape fruit.

2.3.5.1 Replum

In the models $\mathbf{i}_{REP}$ is expressed centrally down the canvas separating the two valves. In the *Arabidopsis* gynoecium *REPLUMLESS* (*REP*) and *BREVIPEDICELLUS* (*BP*) are expressed in the medial region of the presumptive replum (Alonso-Cantabrana et al., 2007; Roeder et al., 2003). These medial factors act antagonistically with lateral factors (valve and valve margin) JAGGED/FILAMENTOUS/YABBY3 and ASYMETRIC LEAVES1 (Alonso-Cantabrana et al., 2007; Gonzalez-Reig et al., 2012) to specify the replum. Misexpression of the medial factors result in altered size of the replum, likewise changing the specified region of $\mathbf{i}_{REP}$ would alter the proportion of replum to valve in the model. Through evolution the size of the replum has changed dramatically between Brassicaceae species. For example a single point mutation in a cis element has been linked to the one cell file replum of members of the Brassica tribe and the domestication of certain Brassica crops (Arnaud et al., 2011). This robust relationship between the medial and lateral tissues can be manipulated in the modelling framework to understand the contribution to shape and morphology of different species.

2.3.5.2 Style

Many genes have been identified in *Arabidopsis* that have the expression pattern of i_{STYLE} and control style identity. To give a couple of examples *STYLISH* (*STY1,2*) and *NGATHA* (*NGA1-4*) genes have been shown to act synergistically in style development (Alvarez et al., 2009; Trigueros et al., 2009). *STY1* is expressed in the apical part of the gynoecium from the earliest stages of development. The sector analysis showed that the apical domain of the gynoecium has a distinctive cell division pattern from initiation, the expression of *STY1* at the earliest stages is in agreement with the fact that the apical domain has style identity from the earliest stages of organ development.

Auxin dynamics play a key role in style development. In *Arabidopsis NGA* genes are necessary to drive expression of auxin biosynthesis genes *YUCCA2* (*YUC2*) and *YUC4* in the style (Trigueros et al., 2009). *PIN3* expression is apolar in a ring around the top of the cylinder, this state of high auxin and apolar localisation of *PIN* is essential for the correct development of the style (Moubayidin and Ostergaard, in revision). The style fuses and becomes round in cross section. Modelling the 3D style growth is not possible in GFtbox but it would be interesting to understand how polarity and orientations of growth influence development of the style shape.

2.3.5.3 Valve

In the models valve identity is a default condition if one of the factors is not expressed ($\mathbf{i}_{REP}$, i_{STYLE}, i_{BASE}, $i_{MIDVALVE}$). Unlike the style and replum the orientations of growth change in the valve through the *Capsella* fruit development. This may indicate that different genetic players or different expression patterns are important for valve growth at different developmental stages. There is evidence of this from *Arabidopsis* where *JAG*/*FIL*/*YAB3*/*AS1*/*NUB* are expressed early in development and are important for lateral growth of the valves (Dinneny et al., 2006; Gonzalez-Reig et al., 2012) and later valve expansion is driven by the activity of the *FUL* gene (Gu et al., 1998).

In the *Arabidopsis* petal *JAG* promotes growth perpendicular to the proximodistal axis (Sauret-Gueto et al., 2013) while in the sepal *JAG* promotes growth parallel to the proximodistal axis (Schiessl et al., 2012). *JAG* is expressed in the valves and even though *jag* loss of function mutants do not have a strong phenotype, in an *as1* background the growth of the valves is severely compromised (Gonzalez-Reig et al., 2012). Therefore, it is possible that *JAG* could be important for the growth orientation of the lateral tissue in the young

Capsella gynoecium. The model predicts that a factor promotes growth perpendicular to the polarity after the early elongation phase of gynoecium growth. *JAG* is a potential candidate for this.

The model predicts that a change in growth orientations is important to generate the heart shape. There is evidence for this from the clonal analysis of later stages. A factor important for post fertilisation fruit growth in a wide range of species is *FUL* (Gu et al., 1998; Muhlhausen et al., 2013; Pabon-Mora et al., 2012). In *Arabidopsis FUL* is expressed in the gynoecium from as early as flower stage 6 and from flower stage 8 expression of *FUL* is restricted to the valve tissues (Ferrandiz et al., 1999). However, a phenotype of *ful* is only observed in later stages of gynoecium development at flower stages 11-12 (Ferrandiz et al., 1999). *ful* fruit do not have proper valve expansion leading to small shrunken fruit. Therefore *FUL* could be a candidate for $\mathbf{i}_{LPHASE}$ which controls all late phase growth. This will be discussed further in the following chapters.

In *Arabidopsis FUL* is expressed everywhere in the developing valve tissue and it is possible that other factors that are differentially expressed across the valve are important. Examples of differentially expressed genes are *SQUAMOSA PROMOTER BINDING PROTEIN-LIKE* (*SPL*) genes which have been implicated in apical basal patterning of the *Arabidopsis* gynoecium (Xing et al., 2013). A number of *SPL* genes are expressed in the apical part of the gynoecium including the style. *SPL8* is expressed in this manner until fertilisation when its expression is restricted below the style and to an area near the base of the fruit (Xing et al., 2013). *miRNA156* targets multiple members of the SPL family and when *35S:miRNA156 is* combined with *spl8* the gynoecium develops with a larger apical part and a narrow base. This phenotype is reminiscent of the tapered base in *Capsella*. The models implicate different zones of growth in the fruit valves through factors i_{GPROX} and i_{GDIST}. *SPL* expression data shows that there may be different zones within the valves that altering expression of *SPL* genes can alter the gynoecium shape.

The model predicts that the midvalve region grows more parallel to the polarity than the rest of the valve tissue to flatten the shape. Clonal analysis of the midvalve region would clarify the growth in this region and would test the model. Live cell tracking would give the clearest results on relative growth rates (Kuchen et al., 2012), early stages could not be tracked but later stages with floral organs removed would be very informative. To date no factors that are specifically expressed in the midvalve have been identified;

however the region does have a specific identity as vasculature marks this region (Roeder and Yanofsky, 2006).

Anisotropic growth is important for all stages of the *Capsella* gynoecium and fruit development. Anisotropic growth is controlled by the distribution of cellulose microfibrils in cell walls (Baskin, 2005). The clonal analysis evidence shows that much growth in the later stages of gynoecium and fruit growth is through cell expansion. It is possible that cell growth orientations have been established before fertilisation through cellulose distributions. After fertilisation growth orientations do not change but cell expansion maintains the existing pattern of growth orientations laid down in the cell walls.

The *Capsella* fruit represents an interesting model to understand the dynamics of fruit shape. This work has found that the *Capsella* fruit goes through three phases of growth. Changing growth orientation and rate during these different phases generates intermediate forms of cylindrical and snuff-bottle gynoecia and then the heart-shaped fruit. The factors important for such changing orientations of growth in the *Capsella* fruit are not known; in the following chapter potential candidates are explored.

3. *Capsella* mutants

3.1 Introduction

In the previous chapter a model for *Capsella* fruit growth was explored. The model made several predictions about potential factors controlling growth. To investigate the identity of some of these factors, in this chapter candidate genes are explored through mutagenesis and transgenics.

3.1.1 Forward and Reverse screens

Forward-genetic screens have been widely used throughout biology to identify novel genes in molecular pathways. In a forward screen, following a random mutagenesis, a phenotype is identified and the underlying genetic basis is studied. Forward screens are useful when few genetic players are known in a particular pathway. In contrast a reverse-genetic screen takes a more targeted approach by investigating the biological function of a particular gene. A reverse-screen is useful when candidate genes are already known but the biological relevance is not.

Both forward and reverse screening approaches begin with a random mutagenesis. Mutagens can be physical, biological or chemical (Koornneef, 2002) and the choice of mutagen used will depend on the experimental requirements. For example T-DNA insertion mutagenesis leads to insertion of large chunks of DNA randomly in the genome (Alonso et al., 2003). These insertions are likely to knock out genes (null alleles) and position of insertion can be easily detected by PCR in a reverse genetics approach. However, if an allelic series is required it is more effective to use a mutagen that generates point mutations.

A popular chemical mutagen that causes single point mutations is ethyl methanesulfonate (EMS). EMS causes G/C to A/T substitutions in more than 99% of cases (Greene et al., 2003). EMS alkylates guanine residues to produce an unusual base O^6-ethylguanine which pairs with T instead of C (Jansen et al., 1995). This introduces base changes following replication.

If a point mutation causes a truncation of the protein by introduction of a premature stop codon or splice site mutation the allele is likely to be a null allele and have a severe phenotype. It is expected that about 5% of mutations will produce protein

truncation (Greene et al., 2003; Kurowska et al., 2011) and these types of mutations are highly selected for in forward genetic screens. About 50% of mutations are expected to be missense mutations (Greene et al., 2003; Kurowska et al., 2011) where amino acid substitutions occur as a result. In a reverse genetic screen many missense mutations are found.

One widely used reverse screening approach is TILLING (*t*argeting *i*nduced *l*ocal *l*esions *in g*enomes). TILLING involves EMS mutagenesis followed by screening for point mutations in a gene of interest (Colbert et al., 2001; McCallum et al., 2000). Individuals' DNA is pooled and CEL 1 endonuclease cleaves at mismatches formed in heteroduplexes between mutant and wildtype strands (Oleykowski et al., 1998). This is a high-throughput method and powerful reverse genetics tool. As a result TILLING populations have been set up in many plant species such as wheat, *Brassica rapa*, *Arabidopsis* and maize (Stephenson et al., 2010; Till et al., 2003; Till et al., 2004; Uauy et al., 2009) and also has been adopted in animal research (Gilchrist et al., 2006; Winkler et al., 2005). Organisations have also been set up to provide TILLING services to the biologists for example RevGen UK (http://revegenuk.jic.ac.uk) and *Arabidopsis* TILLING Project (Till et al., 2003). Given the success in other species it would be useful to generate a TILLING resource in *Capsella*.

3.1.2 *Arabidopsis* fruit shape mutants

In *Arabidopsis* several genes have been identified through gain of function screens that can alter the shape of the narrow siliques. When overexpressed, ROTUNDIFOLIA/DEVIL (ROT/DVL) family of peptides can generate shorter wider fruit with outgrowths in the mediolateral plane (Narita et al., 2004; Wen et al., 2004). Likewise, the overexpression of a gene encoding a cytochrome P450, *CYP78A9* generates shorter rounded fruit in *Arabidopsis* (Ito and Meyerowitz, 2000). The architecture of these fruits have been compared to *Capsella* and it has been speculated that these genes could be important for variations in fruit shape in Brassicaceae family (Bowman, 2006; Ito and Meyerowitz, 2000). A mutant screen in *Capsella* may elucidate if these genes do play a role in fruit shape development.

3.1.3 *Capsella* fruit shape mutants

One fruit-shape mutant has been reported in *Capsella* by Shull (1914) who described a variant of *C. bursa-pastoris*, named *C. heegeri*, which had 'capsule' fruits. In the paper there are hand drawn pictures that depict the cross section views of *C. bursa-pastoris* WT and *Heegeri* variant fruit. The wildtype cross section of *C. bursa-pastoris* is

flattened along the mediolateral axis and has large spaces around the seeds (Figure 3.1A). This is comparable to the wildtype fruit of *Arabidopsis* (Figure 3.1C). The *Heergeri* variant has a circular cross section fruit and the seeds look squashed together (Figure 3.1B). These features are characteristic of a well described mutation in *Arabidopsis*, *fruitfull* (Gu et al., 1998), where the valves fail to expand after fertilisation leading to small rounded fruit and seeds tightly packed inside (Figure 3.1D).

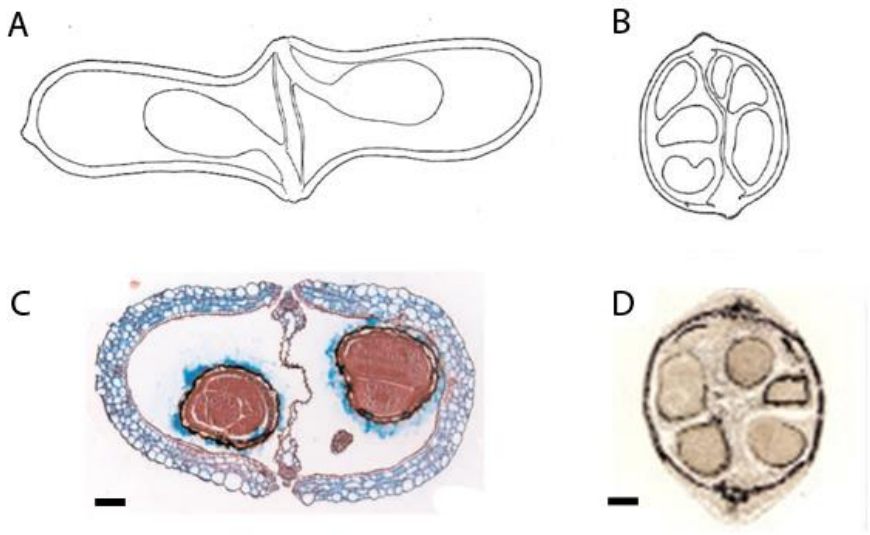

Figure 3.1 Heegeri variant is reminiscent of Arabidopsis *ful.* Cross sections of mature fruits of (A) Wild type *Capsella bursa-pastoris* (B) *C. bursa-pastoris Heegeri* variant (C) Arabidopsis WT and (D) Arabidopsis *ful*. A + B hand drawn images from Shull (1914). C + D from (Roeder and Yanofsky, 2006). Scale bars 100µm

This naturally occurring fruit mutant segregated in the F2 generation 15:1 indicating that two unlinked genes are responsible for the heart shaped fruit (Shull, 1914). These loci seem to act redundantly with only one dominant wild-type allele sufficient to produce heart-shaped fruits. *C. bursa-pastoris* is a tetraploid and genome duplication could explain this functional redundancy of the two loci. This would make it more difficult to re-identify the *heergeri* variant in *C. bursa-pastoris*, which was unfortunately lost many years ago.

To understand if *FUL* has a direct role in *Capsella* fruit shape it would be necessary to identify a mutant in *Capsella*. *C. rubella* is a self-compatible and diploid species, offering a great potential for forward genetic screens that could elucidate the underlying molecular mechanism of heart-shaped fruit by *FUL* or other genetic factors. Also *C. rubella* represents

a good model for comparative genetic analysis with *Arabidopsis* due to the recent publication of the genome (Slotte et al., 2013) and relatively small genome size of 219-250MB (Johnston et al., 2005; Slotte et al., 2013).

3.1.4 *FRUITFULL*

FRUITFULL (*FUL*) is a MADS-box transcription factor that is important for valve expansion and meristem maintenance in *Arabidopsis* (Ferrandiz et al., 2000; Gu et al., 1998). *FUL* is a MIKC type protein made up of four domains: MADS domain (M), Intervening domain (I), Kerratin-like domain (K) and a C-terminal domain (C) (Gramzow and Theissen, 2010). Each domain has some specific functions. The MADS domain interacts with the DNA through the MADS-box located on exon 1 (Honma and Goto, 2001). MADS box proteins interact with DNA by forming homo- or heterodimers which form through protein-protein interactions of the I and K domains (van Dijk et al., 2010). The C-terminal domain is known to interact with other transcriptional regulators (Kaufmann et al., 2005).

Members of the *FUL* family have many described roles in late fruit development across the eudicots including fruit ripening in tomato (Wang et al., 2014) and correct lignification in opium and Californian poppy (Pabon-Mora et al., 2012). Given that *FUL* expression and activity can influence fruit shape and the heegeri variant has *ful* features, it is a suitable candidate to target for a targeted reverse genetics approach in *Capsella*.

3.2 Results

3.2.1 EMS Mutagenesis

I took a forward genetic screen approach to identify novel regulators of fruit shape. *Capsella rubella* was chosen for this screen as it is a diploid species, self-fertile, its genome has been sequenced and has heart-shaped fruit characteristic of the genera. I treated approximately 10,000 seeds with one of three treatments: 0.2% EMS, 0.25% EMS or 0.3% EMS (30,000 seeds in total). 0.2% EMS is optimal for *Arabidopsis* (Till et al., 2003) and 0.3% EMS is optimal for *Brassica rapa* (Stephenson et al., 2010) which have smaller and larger seeds respectively than *C. rubella*. Therefore an intermediate dose was expected to be optimal for *C. rubella*.

Initially it was observed that the EMS treatment had been effective as germination was much reduced in 0.25% and 0.3% EMS treatments compared to 0.2% (data not shown). All seedlings that germinated from the 0.25% and 0.3% EMS treatments were transplanted

as they would most likely have the highest number of mutations and a selection of the 0.2% to make up 2,400 M1 lines.

The mutagensised seedlings were grown over the summer 2012 and given a line number that would carry through all subsequent generations. This number included the concentration of EMS treatment and a number from 1 to 1200, for example Cr.25 0001 is *Capsella rubella* 0.25% EMS treatment line number 1. As the M1 plants grew it was observed that some plants had somatic mutations such as fused leaves (Figure 3.2A) and bleached sectors (Figure 3.2B) indicating that the EMS treatment had been a success.

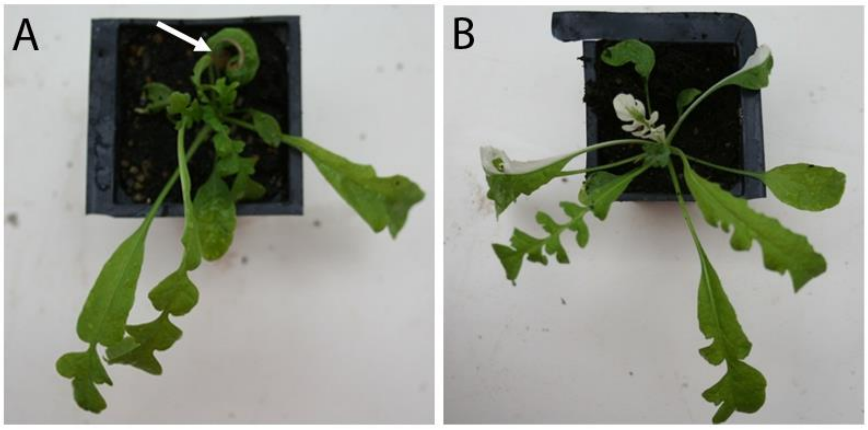

Figure 3.2 Somatic mutations in M1 generation. (A) Fused leaves indicated by white arrow and (B) bleached sectors are white in colour.

All plants were bagged and seeds threshed individually. To take the line on to the next generation for screening there had to be at least 15 seeds and so for each line it was recorded if there were more or less than 15 seeds or no seeds at all (infertile). Figure 3.3 shows a very sharp decrease in fertility of the M1 plants of the 0.3% treatment with only 30% of the lines suitable for continuing to the next generation compared to 75% of 0.25% EMS treatment (Figure 3.3).

3.2.2 Forward screening

I chose lines that produced more than 15 seeds from 0.25% and 0.3% EMS treatments for the forward screen as they had sufficient fertility but were likely to harbour a high mutation number. During the screen I identified some classic mutations such as three putative *pin* mutants with characteristic pin-like inflorescences (Figure 3.4A). I also identified a putative *agamous* mutant (Figure 3.4B) which produces no reproductive organs

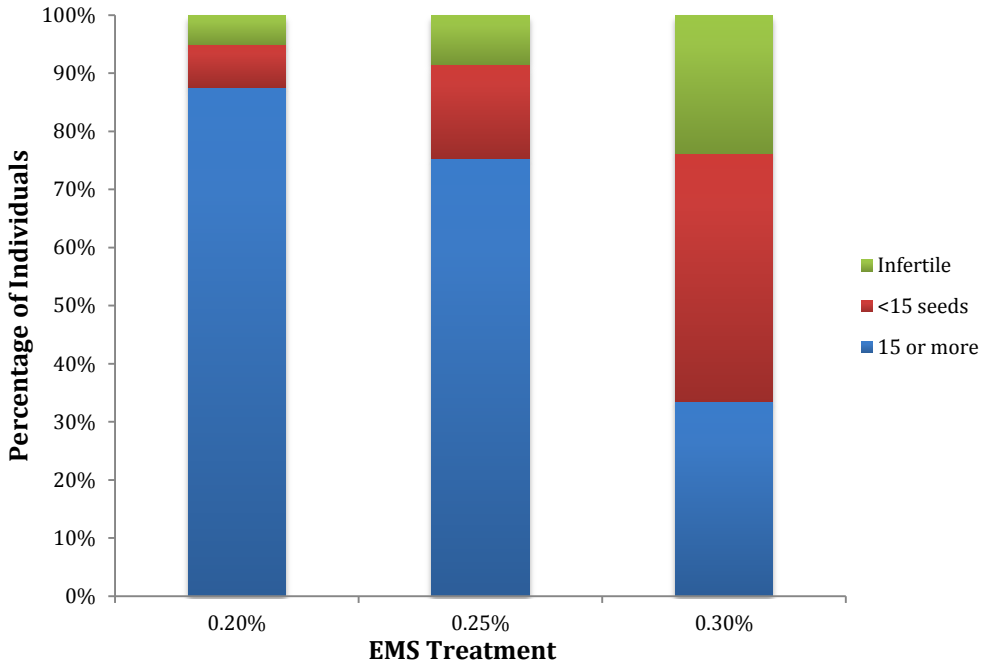

Figure 3.3 M1 Plants from 0.3% EMS seed treatment had much lower fertility. Infertile indicates plants that produced no seed. Lines producing more than 15 seeds could be taken on to the next generation for screening and TILLING.

but instead another flower inside the petal whorl (Bowman et al., 1989). These classic mutants provide further evidence that the EMS mutagenesis was a success.

Twelve plants from each line were screened by eye (no magnification) for differences in fruit shape. I recorded any lines with unusual fruit morphology; M3 seeds were collected from the mutants and sown out to check penetrance (whether all fruits displayed the phenotype) and heritability (if it was passed down to the next generation).

3.2.3 Valve identity mutants

A common fruit phenotype recorded was fruits with 'half-hearts' or fruits that have single valves (Figure 3.5A). This phenotype was never fully penetrant or passed on the subsequent generations and was likely caused by the valves not fusing to the central replum in the correct manner.

Also commonly observed were fruit that had multiple valves (Figure 3.5B) and often in these mutants the shoot apical meristem would terminate early (data not shown). These phenotypes are characteristic of mutants in the *clavata 1 /3* pathway. Multiple valve

phenotype is reported for *clavata2* in *Arabidopsis* caused by increased meristem size (Kayes and Clark, 1998).

Both single valve and multiple valve mutants were classified valve identity mutants as the number of valves was affected but not the shape of the valves.

Figure 3.4 Classic mutants identified in forward screen (A) Cr.25 0055 putative *pin* mutant with pin-like inflorescences (B) Cr.25 0480 putative *agamous* mutant with flowers produced inside flowers

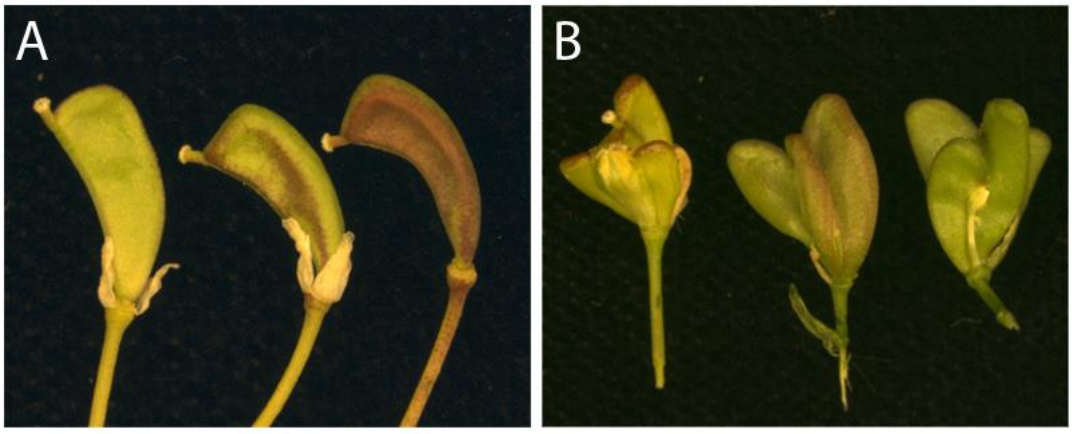

Figure 3.5 Fruit mutants that have problems with valve identity (A) Single-valved fruit or 'half-hearted' Cr.25 0032 (B) Multiple-valved fruit likely to be a putative *clavata 1/3* mutation Cr.25 0347

3.2.4 *Capsella* fruit shape mutants

I identified several fruit shape mutants as shown in Figure 3.6. Cr.25 500D (Figure 3.6A) reaches the same length as wildtype fruit but does not extend the shoulders to produce the heart-shape. This mutation was fully penetrant and passed on to subsequent generations. Lukasz Langowski (a postdoc in the lab) is currently continuing to characterise this mutant and decipher the gene responsible for this phenotype.

Another interesting mutant, Cr.25 307, growth in the wrong plane giving rise to a more 3D fruit shape and again did not extend the shoulders (Figure 3.6B). The base of the fruit looks flattened parallel to the septum whereas the top of the fruit is still flattened perpendicular to the septum. In Cr.25 890 the shoulders seemed to have extended too much giving the fruit a stretched and pointed phenotype (Figure 3.6C) whereas Cr.25 109 had small rounded fruit (Figure 3.6D). These mutants will be useful in future projects to identify novel genes involved in fruit-shape development but due to time constraints could not be characterised during this project.

Figure 3.6 Fruit shape mutants (A) Shoulders don't extend (white arrow) Cr.25 500 (B) Fruit flattened parallel to the septum at the base (red arrow) and top of the fruit flattened perpendicular to the septum (white arrow) Cr.25 0307 (C) Shoulders extended more giving rise to wrinkled fruit Cr.25 890 (D) Small rounded fruit Cr.25 109

3.2.5 Screening for *crful* alleles

Since, the *Heegeri* variant had close similarities to *ful* and *FUL* is known to be important for late fruit development it would be interesting to identify alleles of *crful* to elucidate if *FUL* has a role in determining fruit shape in *Capsella*. To accomplish this, I screened for the phenotype of *Heegeri* variant in the forward mutant screen by looking for plants with smaller shrunken fruits.

I did not identify alleles of *crful* in this screen. However, a forward screen running in parallel in the lab of Michael Lenhard (Potsdam University) found two mutants, mut313 and mut493, which had *crful* characteristics. Both mutations were identified as a likely allele of *crful* by sequencing (by Adrien Sicard and Nicola Stacey) and from now on will be referred to as *crful-1* and *crful-2*, respectively. *crful-1* had a G to A mutation leading to a substitution of glutamic acid to lysine at position 129 of the protein. This missense mutation is in the keratin domain of the protein known to be involved in dimerisation (Kaufmann et al., 2005). *crful-2* had a G to A mutation leading to a glutamic acid to lysine substitution at position 67.

3.2.6 TILLING population in *Capsella rubella*

To identify further alleles of *crful* and to generate a reverse genetics resource in *Capsella* I set up a TILLING population in collaboration with Nicola Stacey. Two plants from each line of all EMS treatments (0.2%, 0.25% and 0.3%) were selected for the TILLING population. Two M2 plants from each M1 family were chosen as it is the optimal combination for recovering maximum number of independent mutations from a population (Redei and Koncz, 1992). DNA was extracted by Richard Goram (JIC genotyping platform) from each M2 plant and M3 seeds collected making a population of 3072 individuals. The DNA was normalised and pooled into 4 x 8 pool 96 well plates by Nicola Stacey.

TILLING identifies point mutations by mismatches in a given amplicon of a gene of interest. So far 7 amplicons have been tested in this TILLING population: 4 amplicons of CrFUL, 2 amplicons of *PINOID* (*CrPID*) and one amplicon of *INDEHISCENT* (*CrIND*). All TILLING was carried out by Nicola Stacey. Table 3.1 shows the number of mutations found for each amplicon and the mutation density if calculated from the individual amplicon. Mutation density is calculated by:

$$\frac{\text{no. individuals screened} \times \text{size of amplicon (kb)}}{\text{no. mutations}}$$

The average mutation density of the population if all amplicons are taken into account on average there is 1 mutation every 259kb. With a genome size of 219MB (Slotte et al., 2013) there are on average 846 mutations per individual. Depending on the amplicon there is a lot of variation in number of mutations detected which greatly affects the calculated mutation density (Table 3.1). The reason for such high fluctuations between these amplicons is likely because the *CrFUL* amplicons contained regions of intron where mutations seen were not always recorded. Therefore it is likely that the mutation density of one mutation per 259kb is an under estimation.

All mutants identified by TILLING were tracked back to the corresponding seed packet and if seeds were available, plants were grown and genotyped by Nicola Stacey. In all cases the DNA sample matched the seed packet. In conclusion a TILLING population for *Capsella rubella* has been established and can be used as a reverse genetics resource.

amplicon	size in bp	number of mutations	mutation density (1mutation/kb)
CrFUL-1	744	10	229
CrFUL-2	859	10	264
CrFUL-3	984	11	275
CrFUL-4	935	5	574
CrPID-1	810	9	276
CrPID-2	980	24	125
CrIND-1	799	35	70

Table 3.1 Description of amplicons screened by TILLING in *Capsella rubella*

3.2.6 TILLING for *crful* alleles

To identify new alleles of *CrFUL* all exons were covered with four amplicons. Several mutations were isolated: the majority of the mutations were in the intron as *CrFUL* gene contains many small exons amongst large regions of intron. 10 mutations were identified in the exons and 6 of these mutations resulted in an amino acid substitution

(Table 3.2). These lines were grown up and genotyped by sequencing which confirmed the presence of the mutations by Nicola Stacey.

Two missense mutations were identified in the MADS domain of exon 1 (Table 3.2) which is a highly conserved domain through the entire superfamily of proteins. The mutations were C to T causing a substitution of serine to phenylalanine at position 22 and 26. This would be expected to show a phenotype as across the whole MADS box superfamily a phenylalanine is never present in this position (Gramzow and Theissen, 2010).

Two missense mutations were identified in the intervening domain (Table 3.2), one from TILLING and *crful-2* by the parallel mutant screen (Adrien Sicard). No phenotype was observed for the mutant identified by TILLING.

Amino acid Position	Amino acid substitution	Mutation	Phenotype	Protein domain	Line	Amplicon
22	S > F	C > T	No	MADS	Cr.3 0228 B	1
26	S > F	C > T	No	MADS	Cr.2 0500 A	1
59	T > T	C > T	No	MADS	Cr.25 0504 B	1
67	E > K	G > A	Yes	Intervening	Mut493 (*crful-2)*	
77	D > N	G > A	No	Intervening	Cr.3 0707 A, B	2
109	R > K	G > A	No	Keratin-like	Cr.25 717 A, B	2
109	R > K	G > A	No	Keratin-like	Cr.25 0720 A, B	2
129	E > K	G > A	Yes	Keratin-like	Mut313 *(crful-1)*	
140	R > R	G > A	No	Keratin-like	Cr.25 0473 A	3
143	K > K	G > A	Yes- partial	Keratin-like	Cr.25 0394 A (*crful-3*)	3
160	A > T	G > A	No	Keratin-like	Cr.2 0022 A	3
189	S > S	C > T	No	C-terminal	Cr.25 0089 B	4
234	M > I	G > A	No	C-terminal	Cr.3 0415 B	4

Table 3.2 Alleles of *crful* identified by TILLING and in a forward screen. Rows highlighted in green show a phenotype.

Five missense mutations were identified in the Kerratin-like domain (Table 3.2), four of which did not have a phenotype. *crful-1* has a mutation in this domain (identified by Adrien Sicard). Surprisingly, a mutation at position 143 which did not cause an amino acid change showed a phenotype. The amino acid substitution of G>A is at the last base of exon 4 (Table 3.2) caused a partial *ful* phenotype (data not shown). Nicola Stacey identified alternative splice variants in this line (personal communication) indicating that this mutation will lead to a truncated protein.

Two missense mutations were identified in the C-terminal domain but there was no phenotype in either line.

3.2.7 Characterisation of *crful* alleles

The most detailed analysis was carried out on *crful-1*. I dissected and prepared the gynoecia and fruits of all flower stages for SEM analysis. Growth dynamics were not determined for *crful-1* so the dissected gynoecia were compared to WT by flower stage using landmark features (Smyth et al., 1990) rather than DAI.Before stage 13 (anthesis) the gynoecium of *crful-1* is not clearly distinguishable from WT in shape and tissue patterning (Figure 3.7). Like WT, the cylindrical gynoecium elongates up to stage 8 (Figure 3.7D) and starts bulging out to produce a rounded shape during stage 9 (Figure 3.7E). By stage 12 the *crful-1* gynoecium has a snuff-bottle shape with defined replum, style, stigmatic papillae and valves (Figure 3.7F).

The *crful-1* gynoecium at stage 13 is snuff-bottle in shape but with a longer style than WT (Figure 3.8D). By stage 14, when in wildtype the shoulders begin to develop, the fruit of *crful-1* remains rounded (Figure 3.8E). This rounded shape becomes slightly elongated but is retained in all subsequent stages of fruit development (Figure 3.8F). The stigmatic papillae remain expanded for a longer period than wildtype. This may be due to the lower fertility of the mutant pollen.

The fertilised fruits become lumpy and in some cases burst due to the seeds expanding inside (data not shown) as also observed in *Arabidopsis ful* mutants (Gu et al., 1998).

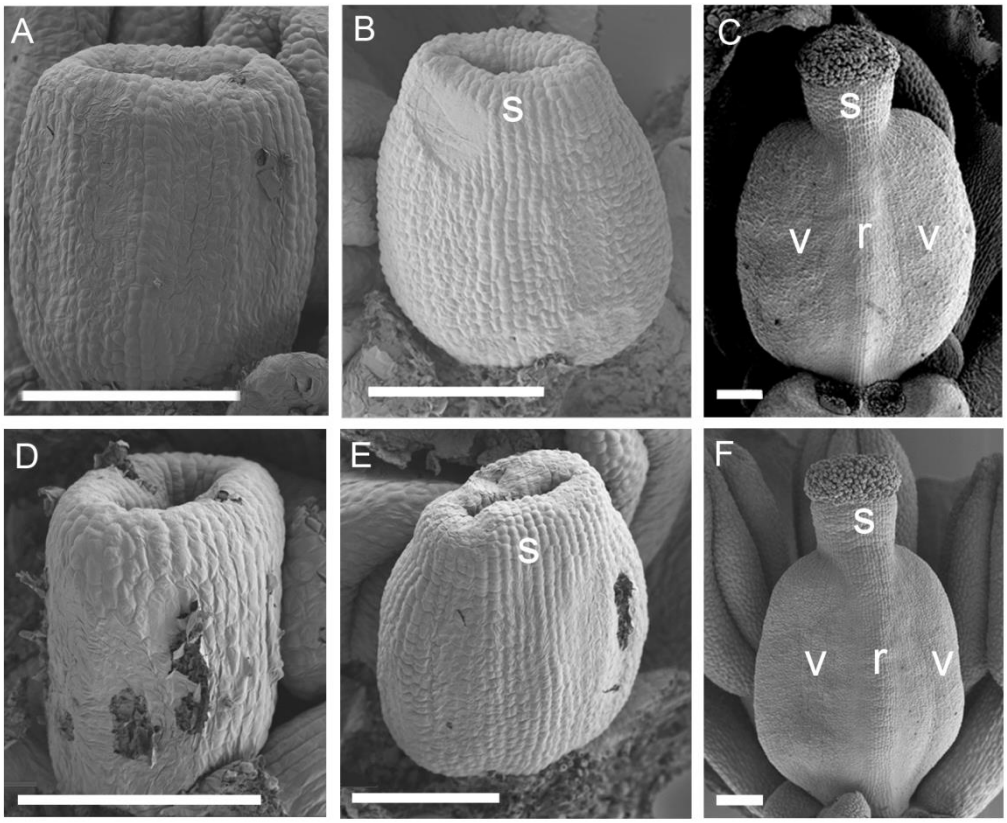

Figure 3.7 WT and *crful-1* gynoecium flower stages 8-12 (A-C) Wild type gynoecium stage 8 (A), stage 9 (B) and stage 12 (C). (D-F) *crful-1* dissected gynoecium (D) stage 8 (E) Stage 9 and (F) Stage 12. Defined regions are labelled: style (s), replum (r) and valves (v). Scale bars 100µm.

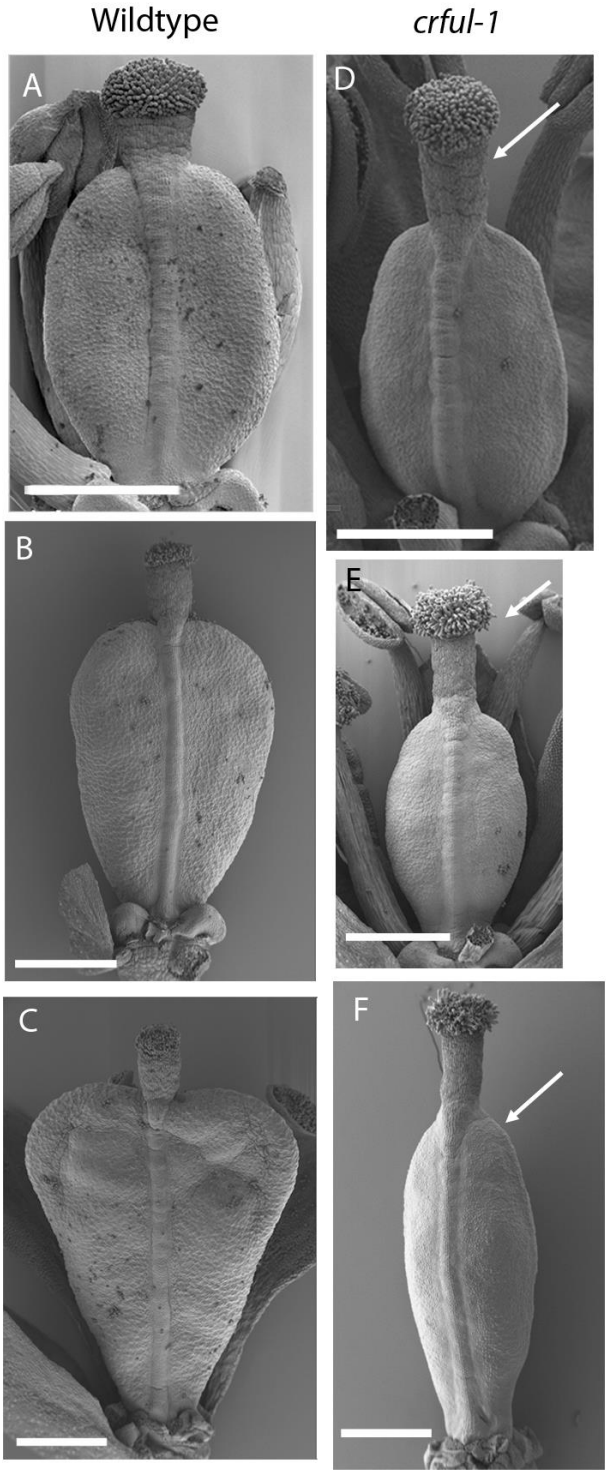

Figure 3.8 WT and *crful-1* fruit stages 13-15 (A-C) Wildtype fruit. (A) stage 12 gynoecium just before anthesis (B) Stage 14 the shoulders of the heart begin to grow. (C) Stage 15 the fruit has a distinct heart shape. (D-F) *crful-1* fruit (D) Stage 13 anthesis the style is longer than wildtype indicated by arrow. (E) Stage 14 Anthers extend above the stigma and fruit still rounded, arrow indicates the stigmatic papillae are still expanded. (F) Stage 15 elongated snuff bottle shape, note shoulders of heart have not extended (arrow) and stigmatic hairs still expanded (F). Equivalent stages are at the same scale. Scale bars 500µm

3.2.7.1 Lignification of *crful-1*

A characteristic of *ful* mutants in other species is ectopic lignification of the valves and indehiscent fruit due to the valve margin not forming properly (Gu et al., 1998; Lenser and Theissen, 2013). To analyse the lignification pattern and valve margin formation in *crful*, fruits of WT and *crful-1* were sectioned and stained with Alcian blue and Safranin to stain lignin and cell walls by André Kuhn. Lignin is stained pink in this protocol. There is more lignification of the valve tissues in all cell layers in *crful-1* (Figure 3.9B) compared to WT (Figure 3.9). In WT fruit there are two distinct layers of small cells between the replum and valve which make up the valve margin (Figure 3.9C). In *crful-1* the distinction between the replum and valve is less clear and the valve margin cells are not visible (Figure 3.9D).

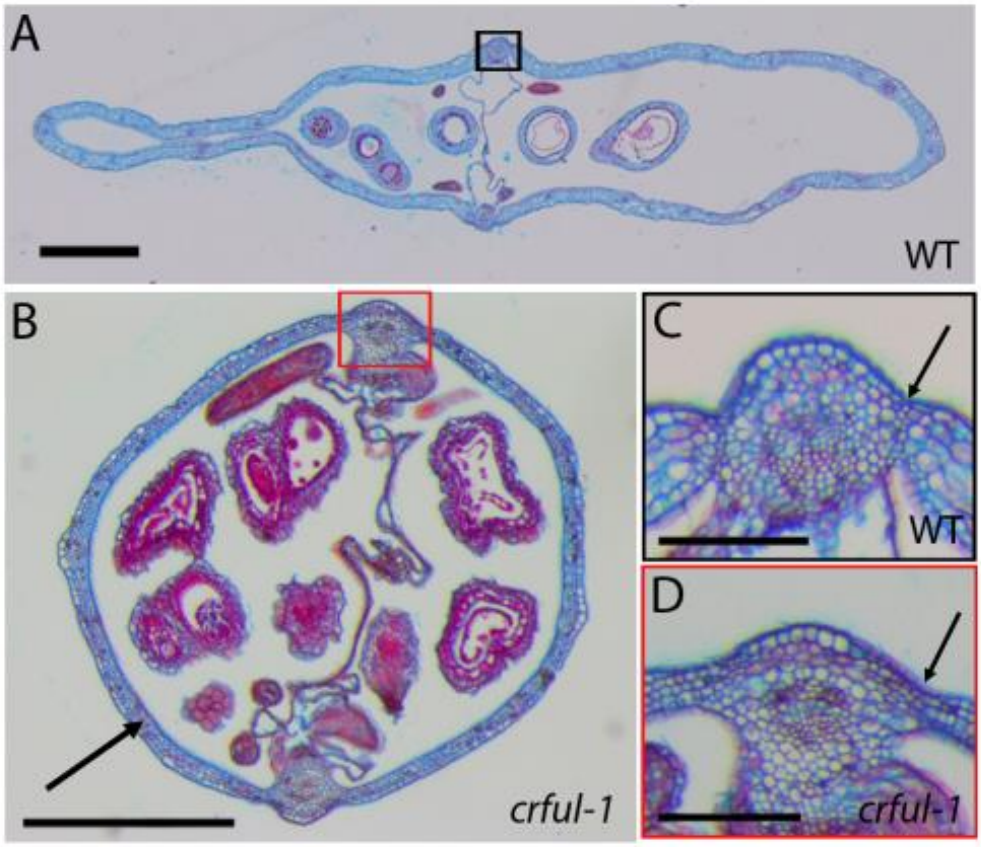

Figure 3.9 Cross section of Capsella WT and *crful1* Fruits collected were sectioned and stained with Alcian blue and Safranin (A) Cross section of WT Capsella fruit at ~15 DAI. (B) Cross section of *crful-1* at ~15 DAI. Arrow indicates the darker pink staining of lignin in the valves. (C, D) Zoomed in image of black outline in A, B respectively, arrow indicates valve margin or presumptive valve margin. Lignin is stained with pink. Scale bars 500µm (A, B) and 100µm (C, D).

Also the cross section shape of *crful-1* is rounded compared to the elongated cross section of WT which matches the observations of the Heegeri variant (Shull, 1914).

In summary, the role of *CrFUL* in *Capsella* fruit development is mainly in late phase of growth, post fertilisation. *CrFUL* is important for the formation of the heart-shaped and for flattening the fruit cross section.

3.2.8 Modelling *FUL* in GFtbox

In Chapter 3 I described a model for the growth of the *Capsella* fruit. A method for validating the model is to compare fruit shape mutants with the model predictions when factors are removed. In this way the biological relevance of the factors can be explored.

In the *Capsella* fruit model the factor i_{LPHASE} is necessary to switch from middle phase to late phase where a heart shape is generated. i_{LPHASE} is not necessary for specifying the orientations of growth to achieve this but it is required to switch rates and orientations. *FUL* is a possible candidate for i_{LPHASE} as it is necessary for valve expansion in the later stages of fruit development.

In the WT model i_{LPHASE} is 1 everywhere after 8 DAI and interacts with all other factors during 8-11 DAI:

K_{par} = 0.014 .pro(h_{EPHASE} , $\mathbf{i}_{EPHASE}$)

.inh(h_{BASE} , $\mathbf{i}_{BASE}$. $\mathbf{i}_{MPHASE}$) .pro($h_{MIDVALVE}$, $\mathbf{i}_{MIDVALVE}$. $\mathbf{i}_{MPHASE}$)

.pro($h_{GMIDVALVE}$, $\mathbf{i}_{GMIDVALVE}$. i_{LPHASE}) .inh(h_{BASE} , $\mathbf{i}_{BASE}$. i_{LPHASE}) .inh(h_{STYLE} , $\mathbf{i}_{STYLE}$. i_{LPHASE})

.inh(h_{GDIST} , $\mathbf{i}_{GDIST}$. i_{LPHASE}) .pro(h_{GPROX} , $\mathbf{i}_{GPROX}$. i_{LPHASE})

K_{per} = 0.0115 .inh(h_{STYLE} , $\mathbf{i}_{STYLE}$. $\mathbf{i}_{MPHASE}$) .inh(h_{BASE} , $\mathbf{i}_{BASE}$. $\mathbf{i}_{MPHASE}$) .inh(h_{REP} , $\mathbf{i}_{REP}$. $\mathbf{i}_{MPHASE}$)

.inh($h_{MIDVALVE}$, $\mathbf{i}_{MIDVALVE}$. $\mathbf{i}_{MPHASE}$)

.inh($h_{MIDVALVE}$, $\mathbf{i}_{MIDVALVE}$. i_{LPHASE}) .inh(h_{STYLE} , $\mathbf{i}_{STYLE}$. i_{LPHASE}) .inh(h_{BASE} , $\mathbf{i}_{BASE}$. i_{LPHASE})

.inh(h_{REP} , $\mathbf{i}_{REP}$. i_{LPHASE}) .pro(h_{GDIST} , $\mathbf{i}_{GDIST}$. i_{LPHASE}) .inh(h_{GPROX} , $\mathbf{i}_{GPROX}$. i_{LPHASE})

K_{knor} = 0.01

After 8 DAI in the *Capsella* WT fruit model, with i_{LPHASE} equal to 1, higher K_{par} at the base and higher K_{per} in the distal region generates a heart shape. This growth pattern

switched by i_{LPHASE} produces a heart shape by 11 DAI (Figure 3.10A). To investigate the effect of i_{LPHASE} on shape in the *Capsella* fruit model, I set i_{LPHASE} to be 0 at all time points. In this virtual mutant (i_{lphase}) the early (0-2 DAI) and middle (2-8 DAI) growth phases were unaffected.

In the virtual mutant i_{lphase}, all factors controlling growth are cancelled out 8 DAI, so K_{par} and K_{per} are the same everywhere (Figure 3.10B). Given that the basic rate of K_{par} is greater than the basic rate of K_{per}, the model becomes a slightly elongated snuff-bottle shape by 11 DAI (Figure 3.10B). This model superficially looks like the *crful-1* fruit at flower stage 15, with an elongated style (Figure 3.10H). However, there are some key differences which cannot be accounted for in i_{lphase} mutant: (1) in i_{lphase}, K_{par} and K_{per} are maintained at 1.4% and 1.15% everywhere, and the model reaches a similar length to WT (Figure 3.10A,B). A characteristic of *ful* fruits is that they are much smaller than WT. (2) The factors controlling the identity of the replum and the style are lost in the i_{lphase} mutant. It is known that in *Arabidopsis ful* fruits these identities are maintained (Gu et al., 1998). (3) The cross section of the i_{lphase} mutant is a flattened oval shape whereas in *crful1* fruits have a circular cross section (Figure 3.9).

These results suggest that the interactions of i_{LPHASE} in the model represent some of the interactions of *FUL* in *Capsella*. However, the key difference is that i_{LPHASE} switches growth in all regions of the model including the replum. *In Planta*, the replum does not seem to be under the control of *FUL*. However, this needs to be explored by whole organ growth dynamics and clonal analysis in *crful-1* fruits.

The model predicts that if *FUL* acts broadly in a similar way to i_{LPHASE}, clones would be isotropic in the valves (Figure 3.10F). I have crossed CrBOB with *crful-1* to investigate the how regional growth rates and orientation are influenced by *CrFUL,* but the lines are not ready for analysis.

In summary, *FUL* is an attractive candidate for i_{LPHASE}. However, the interactions of i_{LPHASE} in the model have to be revised as reducing i_{LPHASE} in the model does not account for all features of a *ful* mutant.

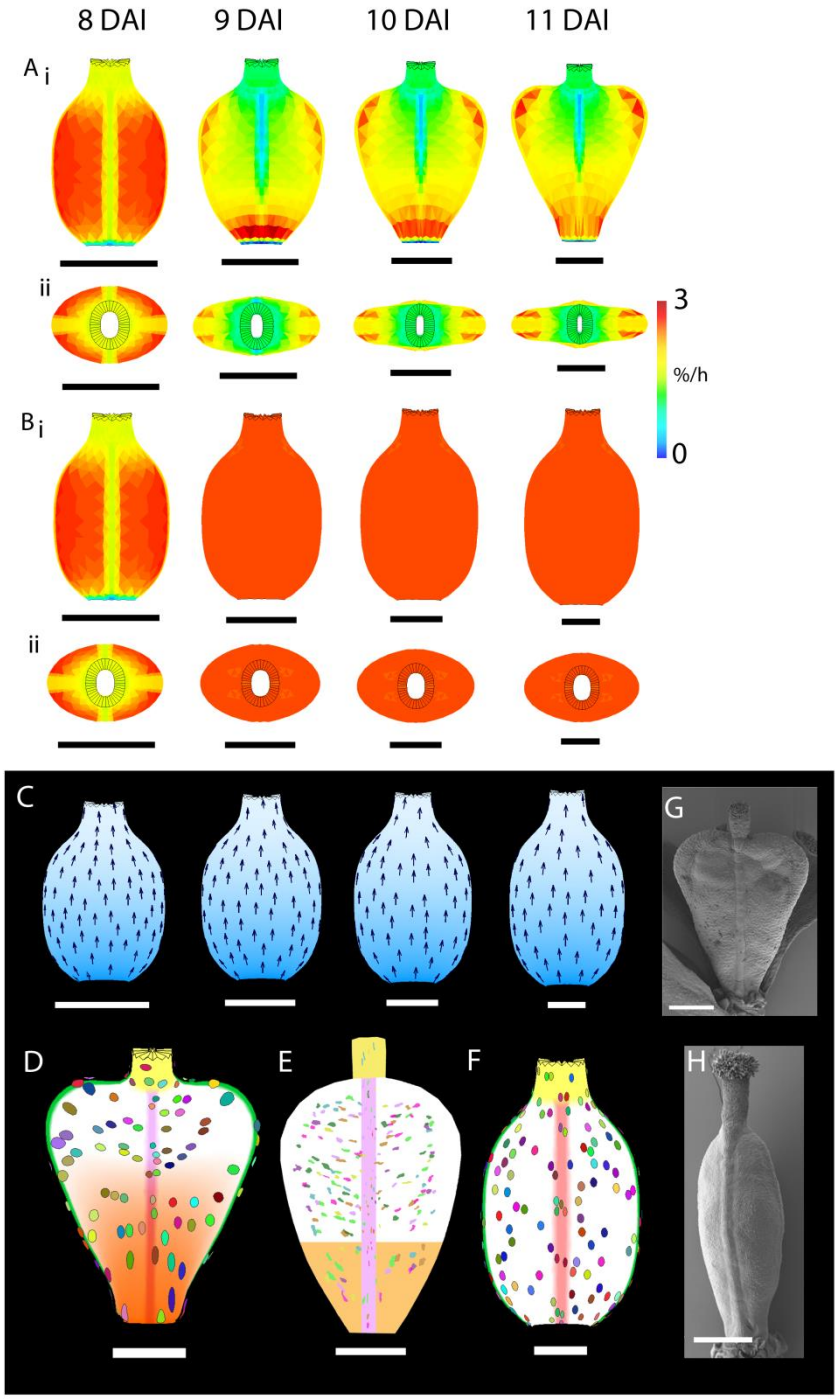

Figure 3.10 Modelling i_{LPHASE} mutant 8-11 DAI (A) Resultant areal growth and shapes of WT model from longitudinal view (i) and from above (ii). (B) Resultant areal growth and shapes of i_{LPHASE} mutant (C) Polariser (blue) and polarity field on i_{LPHASE} model. (D,E) Clones induced at 5 DAI and imaged at 11 DAI on WT (D) and i_{LPHASE} model (E). Style: yellow region, Replum: Pink region, Midvalve: Green and region with clone elongated parallel to polarity: Orange. (F) *crful-1* mutant at flower stage 15. Scale bars 500µm. Colour scale bar: resultant areal growth rate (%/h).

3.3 Discussion

Capsella rubella represents a good model to investigate the factors controlling fruit shape as it has interesting fruit morphology and established genetic tools. For this reason I carried out a forward screen in *C. rubella* and identified some fruit-shape phenotypes that may lead to the identification of novel factors. I also targeted a valve identity factor *FRUITFULL* in the forward screen and by a TILLING approach. *crful* plants develop gynoecia indistinguishable to WT but cannot generate a heart-shaped fruit and so is important for late phase fruit growth. I used the *Capsella* fruit model to investigate if a *FUL* could play a similar role to i_{LPHASE} and found that there are some important differences which will be discussed.

3.3.1 Mutant and TILLING populations in *Capsella rubella*

In this study, I used EMS mutagenesis to identify mutants in fruit shape and to set up a TILLING population in *C. rubella*. In previously described TILLING populations there is huge variation in mutation density from as high as 24 mutations^{-1}/kb in wheat to 3,297 mutations^{-1}/kb in a gamma radiated TILLING population of Barley (Kurowska et al., 2011). The ploidy level is an important factor in determining the mutation load that a species can carry. *C. rubella* is diploid and so the most useful comparison of mutation load is to other diploid species. *Arabidopsis* has multiple TILLING populations (Greene et al., 2003; Martin et al., 2009; Till et al., 2003) which range from one mutation every 84-300kb. TILLING populations available in rice (Suzuki et al., 2008; Till et al., 2007) have similar mutation densities to *Arabidopsis*; ranging from one mutation every 135-294kb. Here, in *C. rubella* a mutation density of one mutation every 259kb was calculated which falls within the variation of mutation densities recorded in TILLING populations in *Arabidopsis* and rice. However, this is likely to be an under estimate as mutations in the introns of *FUL* were not recorded. Given this mutation load this TILLING population in *C. rubella* will be a valuable resource for the scientific community.

3.3.2 Forward screen and new factors

The identification of new genetic factors controlling fruit shape in *Capsella* was explored in this study through a forward genetic screen. A few lines were identified that had fruit shape phenotypes. Due to time restrictions these mutants could not be characterised during this study. Cr.25 500 and Cr.25 0307 will be characterised by Lukasz Langowski.

Fruits of mutant Cr.25 0307 are flattened parallel to the septum at the base but perpendicular to the septum at the top of the fruit (Figure 3.6). Fruit flattened perpendicular to the septum are called angustiseptate, and fruit flattened parallel to the septum are called latiseptate. The mutant Cr.25 0307 looks like it is almost latiseptate in the basal region. In the Brassicaceae the trait latiseptate has evolved 23 times independently (Al-Shehbaz, 2003). However, no factors have been identified to be important for controlling this phenotype. The identification of the gene controlling the trait seen in Cr.25 307 may shed light on the regulation of angustiseptate to latiseptate evolution.

3.3.3 *FRUITFULL*

Here, it has been shown that *FUL* is important for the proper valve development of the *Capsella* fruit post-anthesis. The allele *crful1* produces a snuff bottle shaped gynoecium like wildtype. However, following anthesis the valves do not expand and the fruit does not develop into a heart-shaped fruit. This type of mutant was first described by Shull in 1914 where he reported on non-Mendelian inheritance of 'capsule-form' fruit in *Capsella bursa-pastoris*. Shull reasoned that there were two loci controlling the trait, which makes sense given that *C. bursa-pastoris* is tetraploid. Considering the close phenotypic resemblance of the 'capsule-form' fruit reported by Shull and the mature fruit phenotype of *crful* it is likely that Shull was describing a *ful* mutation in *C. bursa-pastoris.* 100 years on the gene controlling this trait has been identified by forward and reverse genetics (Adrien Sicard and Nicola Stacey) and characterised here.

3.3.4 *FUL* function

FUL functions with another MADS box transcription factor *SHATTERPROOF* (*SHP*) as an evolutionary module to regulate late fruit development and fruit dehiscence (Ferrandiz and Fourquin, 2014). In the Brassicaceae *FUL* restricts the expression of *SHP* and *INDEHISCENT* (*IND*) to the valve margin. Ectopic expression of *SHP* and *IND* in the valves is correlated with more lignification and reduced cell size. This characteristic phenotype of *ful* described here in *Capsella* is also evident with reduced activity of *FUL* in *Lepidium campestre* and *Arabidopsis* (Gu et al., 1998; Lenser and Theissen, 2013). The *FUL*/*SHP*/*IND* network also functions in the same way in *Brassica* species (Girin et al., 2010; Ostergaard et al., 2006).

Beyond the Brassicaceae *FUL* has been shown to function in late fruit development of fleshy fruits by influencing anthocyanin production and fruit ripening in bilberry and tomato (Jaakola et al., 2010; Wang et al., 2014). In two species of the basal eudicots, opium poppy (*Papaver somniferum*) and Californian poppy (*Eschscholzia californica*), knock down of *FUL-like* genes have much reduced fruit and ectopic lignification (Pabon-Mora et al., 2012). In all these cases the expression of *FUL* functions to maintain valve identity but doesn't seem to have a direct effect on fruit shape with the exception of tomato (Wang et al., 2014). Likewise in *Capsella*, *FUL* has a role in late fruit development but has not been observed to have a direct role in controlling fruit shape.

3.3.7 i_{LPHASE}

In the model of *Capsella* fruit, i_{LPHASE} is important for overall growth in the late phase. This is similar to *FUL* where expression of *CrFUL* or *AtFUL* can rescue the shape phenotype of both *Arabidopsis* and *Capsella*. Therefore the expression of *FUL* is important for overall valve growth and does not influence orientations of growth.

In *ful* there is no valve expansion, the fruits remain small, shrunken and do not develop into the WT fruit shape in either *Arabidopsis* or *Capsella*. As discussed above, *FUL* functions by restricting the expression of valve margin factors IND and SHP to the valve margin. Ectopic expression of these factors leads to an inhibition of growth in the valves. In **i**$_{lphase}$ the model remains similar in shape from 8-11 DAI but grows to almost WT size. This is because there are no factors that inhibit growth when **i**$_{LPHASE}$ is not expressed. It would be interesting to implement a genetic interaction in the model where **i**$_{LPHASE}$ controls the presence or absence of a growth inhibitor.

One possibility is that *FUL* interacts with i_{LPHASE} to activate valve growth, where i_{LPHASE} is the trigger for valve expansion in later stages, possibly following fertilisation. If the ovules are not fertilised, growth of the fruit is actively inhibited (Vivian-Smith et al., 2001). **i**$_{LPHASE}$ may represent the signal that the seeds have been fertilised, and therefore influences growth of all regions. Two major players in triggering fruit growth after fertilisation are auxin signalling and GA signalling (Fuentes et al., 2012; Goetz et al., 2006; Sotelo-Silveira et al., 2014). Mutants in these pathways can be parthenocarpic, fruit expand without fertilisation. Alternatively parthenocarpy can be induced by emasculating flowers and spraying gynoecia with GA. To investigate if it is specifically fertilisation that plays the role of **i**$_{LPHASE}$ it would be interesting to conduct this experiment in *Capsella*.

A phenotype of *ful* in *Arabidopsis* is that the replum continues to grow and the valves do not. This gives the replum a zigzag, lumpy phenotype that is larger than WT (Gu et al., 1998). In the model this could be implemented as K_{par} in the region $\mathbf{i}_{REP}$ being independent of i_{LPHASE}. Given that a higher rate of K_{par} in the midvalve is sufficient to flatten the cross section of the model, it is likely that higher K_{par} in the replum and midvalve regions could circularise the cross section shape. Hence the circular cross section shape characteristic of *ful* fruits maybe a result of higher proximodistal growth in the replum compared to the valves.

Here, potential factors important for the fruit shape of *Capsella* have been explored. New potential candidates have been identified through a forwards genetic screen and a TILLING resource has been established. In *Capsella* the valve identity factor *FUL* is important for the late phase of growth. In *crful* gynoecia up to flower stage 12 develop like WT but following fertilisation the fruits do not produce a heart shape. The expression of *CrFUL* is not sufficient to generate heart shaped fruit in *Arabidopsis* indicating that *FUL* does not influence orientation of growth. In this way *FUL* has some similar characteristics to the role of $\mathbf{i}_{LPHASE}$ in the model, which acts as a switch from middle phase to late phase growth.

4. Evolution of Fruit Shape

4.1 Introduction

In previous chapters I explored the factors important for the heart-shaped fruit of *Capsella* by modelling and mutant analysis. To investigate the importance of these factors in the evolution of fruit shape, in this chapter I compare the development and genetic control of *Arabidopsis* and *Capsella* fruit.

4.1.1 Fruit shape in the Brassicaceae

Fruit shape is highly divergent in the Brassicaceae and has been classically divided into two main forms. (1) The silique, which are elongated fruit where the length of the fruit is more than twice as long as width. Siliques are characteristic of *Arabidopsis*, Cardamine and Brassica. (2) Silicula which are generally ovate and length of the fruit is less than twice as long as width (Bowman, 2006). Genera with silicula include *Capsella*, *Lepidium* and *Neslia*. The evolution of siliques and silicles has occurred many times in the Brassicaceae.

Another aspect of fruit shape in the Brassicaceae is the orientation in which the fruit is flattened. Fruits such as *Capsella*, Lepidium and *Arabidopsis* are flattened laterally, perpendicular to the septum (Bowman, 2006). Some fruits such as Alyssum are flattened medially, parallel to the septum (Bowman, 2006). The advent of medial flattened fruit has evolved many times independently within the Brassicaceae (Al-Shehbaz et al., 2006).

4.1.3 *FRUITFULL* in fruit shape evolution

FUL is known to be important for the expansion of the valves and final fruit shape in many Brassicaceae species including *Lepidium*, *Capsella* and *Arabidopsis* (Gu et al., 1998; Lenser and Theissen, 2013). There is also evidence that *FUL* can alter fruit shape as tagging *FUL* with *VP16* (a viral activator of transcription) generates shorter, triangular shaped fruit in a *ful* background in *Arabidopsis* (Cristina Ferrandiz unpublished results, Figure 4.1). Another MADS-box transcription factor *SHP* has been shown to be important for the evolution of fruit shape in *Medicago* species. The activity of the protein, determined by a region in the C-terminal domain of the protein, is correlated with twisted and none twisted pods in the genus (Fourquin et al., 2013). During this work I will explore if *FUL* can also play a role in the diversification of fruit shape between *Arabidopsis* and *Capsella*.

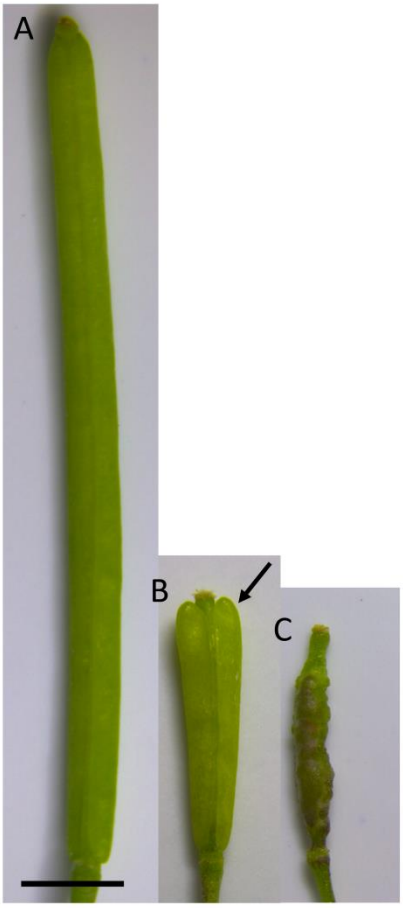

Figure 4.1 *Arabidopsis* WT, *FUL:VP16* and *ful-2* fruits (A) Col-0 (B) *ful* complemented with *FUL::FUL:VP16*. (C) *ful-2.* Scale bar 2mm

4.2 Results

4.2.1 Whole organ Growth Dynamics

To investigate how the development of the *Arabidopsis* fruit compares to *Capsella* fruit, it was first necessary to describe the timing and pattern of fruit shape changes. Using a method for staging *Arabidopsis* flowers (Sauret-Gueto et al., 2013), individual flowers were given an exact hours after sowing (HAS, see Section 3.2.1). From these flowers I measured the gynoecium length, along the longest axis from the gynophore to the top of the style, not including the stigmatic papillae and the gynoecium width at the widest point along the mediolateral axis. I used OPT images (by Susana Sauret-Gueto) for the earlier stages and whole mount images for fruit measurements.

For a better idea of gynoecium age and for ease of comparison with *Capsella*, the *Arabidopsis* gynoecia were classified according to time after gynoecium initiation. 0 days

after initiation (DAI) was defined as when the gynoecium is ~40µm long which corresponds to 330 HAS.

The natural logarithm of *Arabidopsis* and *Capsella* gynoecium length was plotted against DAI (Figure 4.2A,B). Two straight lines were fitted to the gynoecium length data for each species. One line was fitted to data 0-2.5 DAI, this is designated the early phase (Figure 4.2A,B). During the early phase the rate of growth in gynoecium length is ~2.2%/h and ~3%/h in *Arabidopsis* and *Capsella*, respectively. The second line fitted to the gynoecium length data is from 2.5 DAI to 16/18 DAI (Figure 4.2A,B) and represents the rate of growth in the middle phase (2.5-9 DAI for *Arabidopsis* and 2.5-10 DAI for *Capsella*) and late (post fertilisation) phase (9-18 DAI for *Arabidopsis* and 10-16 DAI for *Capsella*). The rate of growth length during middle and late phase is ~1.26%/h and ~1%/h for *Arabidopsis* and *Capsella*, respectively.

The length of the *Capsella* fruit at maturity is ~8mm and for *Arabidopsis* is ~14mm. This difference in final length is partly due to the rate of growth in length in *Arabidopsis* being slightly greater than *Capsella*, and mostly due to the *Arabidopsis* fruit growing for 2 days more before reaching maturity (Figure 4.2B).

Plotting the natural logarithm of gynoecium width against time for *Arabidopsis* and *Capsella* reveals a major difference in growth rates between the species (Figure 4.2C). The rate of growth in gynoecium width for both *Arabidopsis* and *Capsella* is constant from initiation to fruit maturity (0-16 or 18 DAI). However the rate of growth in gynoecium width in *Capsella* (~1.15%/h) is almost double the rate of growth in gynoecium width in *Arabidopsis* (~0.6%).

To compare growth rates in gynoecium length versus width in *Arabidopsis* and *Capsella*; the natural logarithm of length was plotted against the natural logarithm of width (Figure 4.3). A gradient of 1 would mean length is growing at an equal rate to width, represented by a red dotted line in Figure 4.3. Deviation from 1 would mean growth is anisotropic with one axis growing more than the other. Using this plot differences in relative growth rates between the species are observed. In *Capsella* gynoecium length is growing at a greater rate than width in the early phase (green line, 0-2 DAI) and then at 2 DAI there is a switch to width growing at a greater rate than length (blue line, Figure 4.3). However in *Arabidopsis* gynoecium the rate of growth in length is greater than the rate of growth in width throughout development (orange line, Figure 4.3).

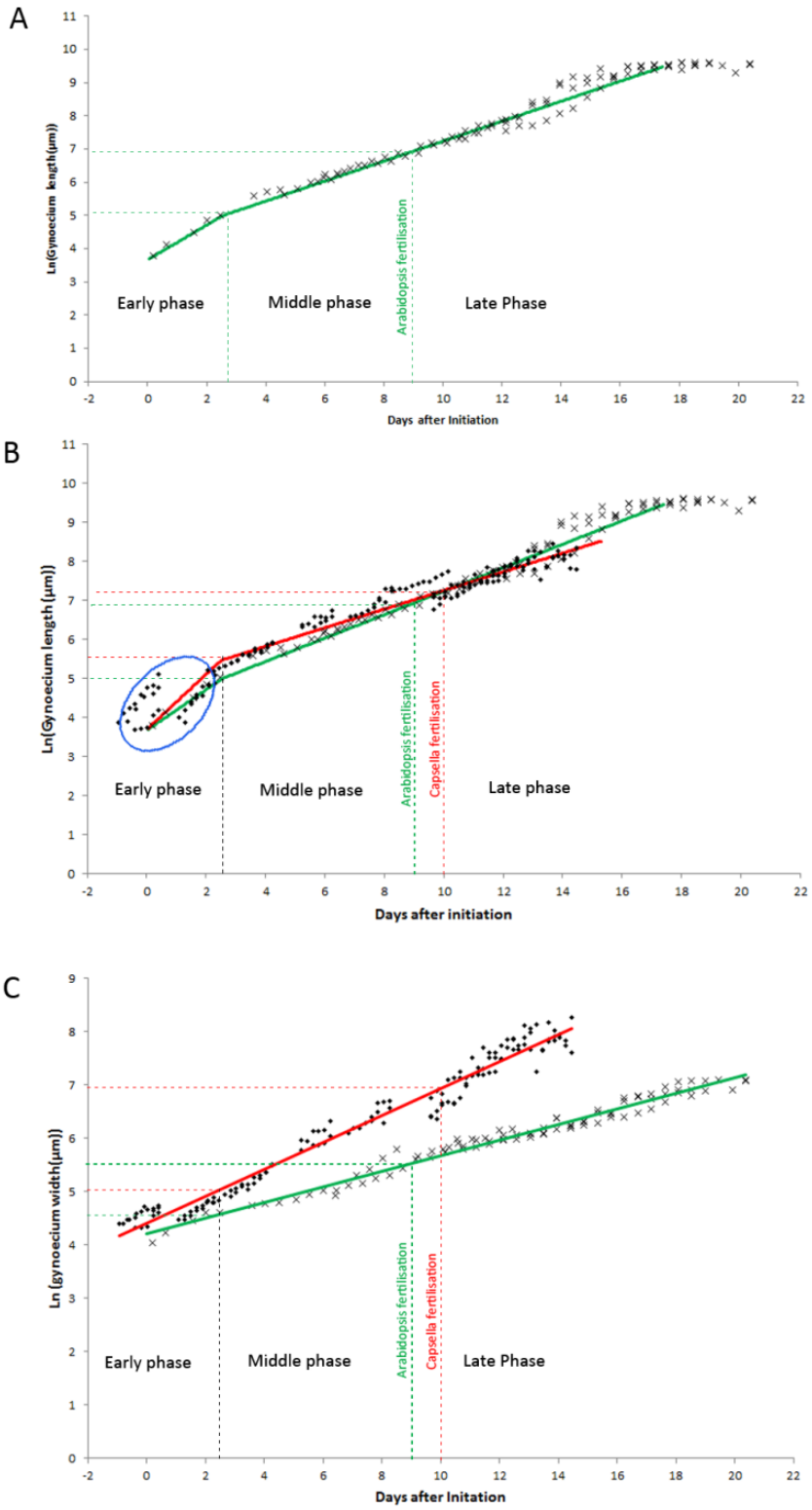

Figure 4.2 Growth of Arabidopsis and Capsella fruit. Natural logarithm of gynoecium length in Arabidopsis (A) and Arabidopsis and Capsella (B) and width of Arabidopsis and Capsella (C) at days after initiation. Black dots (Capsella) and black crosses (Arabidopsis) are data points for individual gynoecia. A straight line was fitted to the data: red line for Capsella (not including the early phase data) and green line for Arabidopsis (not including data after 16 DAI). Fertilisation occurs at ~9 DAI in Arabidopsis and ~10 DAI in Capsella. Blue ellipse shown discrepancy in early phase growth of Capsella, see section 2.2.1 for explanation.

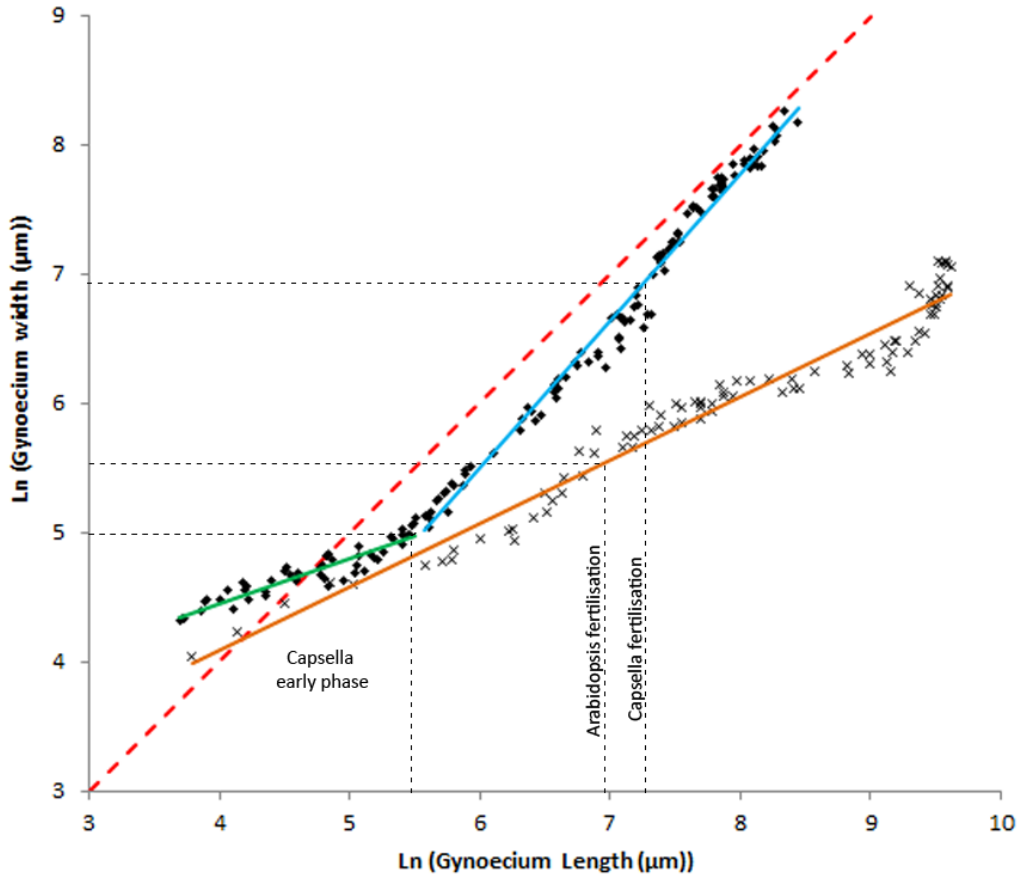

Figure 4.3 Natural logarithm of length vs. width during Arabidopsis and Capsella gynoecium development. Each data point represents one gynoecium of Arabidopsis (black crosses) and Capsella (black dots). The red dotted line plots length and width growing at an equal rate. The gradient of the orange fitted line is 0.49 showing that the Arabidopsis gynoecium is growing more in length than width throughout development. For Capsella the gradient of the green fitted line is 0.33 showing that the growth rate in length is greater than width at early stages of development. The gradient of the blue fitted line is 1.14 showing that in later stages of development the growth rate is greater in width than length.

4.2.2 Differences in fruit morphology

A timeframe has been established for the development of *Arabidopsis* and *Capsella* fruit from gynoecium initiation (0 DAI) to maximum fruit size (16 and 15 DAI, respectively). Next, to compare patterns of shape changes within this framework it was necessary to compare the morphology of the *Arabidopsis* and *Capsella* gynoecia/fruit. Thorough morphological descriptions of *Arabidopsis* gynoecia/fruit have already been detailed using SEM and sectioning (Roeder and Yanofsky, 2006; Smyth et al., 1990). Here, I have used OPT images to compare the 3D gynoecium development of *Arabidopsis* and *Capsella*.

I stained young inflorescences of *Arabidopsis* (ecotype Columbia) and *Capsella rubella* with propidium iodide and imaged them using OPT. Some *Arabidopsis* images were taken from OPT scans by Susana Sauret-Gueto. Included in the description is the corresponding floral developmental stage (Smyth et al., 1990), which uses landmark features to stage floral development from *Arabidopsis*.

In the earliest phases of *Capsella* and *Arabidopsis* gynoecium development (0-2 DAI) the morphology of the gynoecia is very similar (Figure 4.4). In both species the gynoecium initiates as an oval ridge with a central groove (Figure 4.4A-D). The gynoecium grows into a hollow cylinder in both *Arabidopsis* and *Capsella* by 2 DAI (flower stage 8, Figure 4.4E-H). During this early phase of gynoecium development (0-2 DAI) the only feature that can distinguish the flower buds of the two species is the relative length of the stamens which are much shorter relative to the gynoecium in *Arabidopsis* (Figure 4.4B,F).

By 6 DAI the *Capsella* and the *Arabidopsis* gynoecium have become morphologically distinct. The *Capsella* gynoecium develops a snuff-bottle shape (Figure 4.5A,C) and the *Arabidopsis* gynoecium continues to grow as a long thin cylindrical shape (Figure 4.5B,D). By 11.5 DAI (fertilisation), the *Capsella* gynoecium has become flattened in cross section (Figure 4.5E). The *Arabidopsis* gynoecium has a circular-oval shaped cross section shape through to 11 DAI (Figure 4.5D,F). By maturity, the *Arabidopsis* fruit is twice as long as the fruit if *Capsella* and has maintained a cylindrical shape (Figure 4.6).

In summary, the *Arabidopsis* and *Capsella* gynoecium have a very similar primordium and early phase of development to generate a cylindrical shape by 2 DAI. After this stage the gynoecium shapes diverge, and by fertilisation the *Capsella* gynoecium is much wider and flatter than the *Arabidopsis* gynoecium. After Fertilisation, where the *Capsella* fruit grows into a heart-shaped fruit the *Arabidopsis* fruit remains a cylindrical shape and elongates.

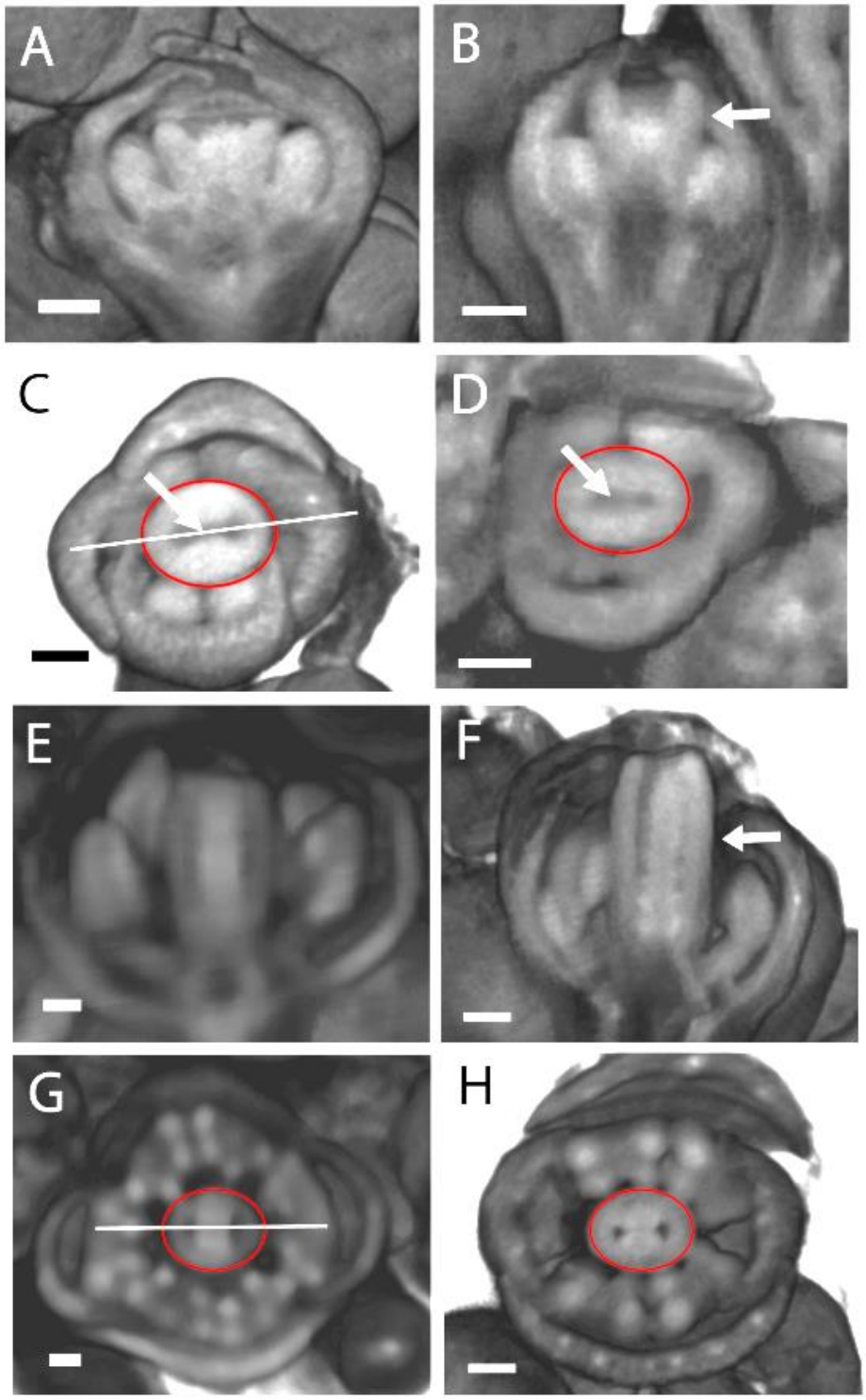

Figure 4.4 Arabidopsis and Capsella gynoecium 0-2 DAI. All images on the left are Capsella and right are Arabidopsis at the corresponding stage. (A, B) gynoecia ~0.5 DAI, flower stage 7: virtual longitudinal section of the mediolateral plane indicated by white line in (C). (C, D) gynoecia ~0.5 DAI, flower stage 7: virtual cross section. White arrows indicate central groove. (E, F) gynoecia ~2 DAI, flower stage 8: virtual longitudinal section indicated by line in (G). (G, H) Gynoecia ~2 DAI, flower stage 8: virtual cross section. White arrows in (B & F) indicates the gynoecium of Arabidopsis is longer than the stamens. Red oval outlines indicates cross sectional shape of gynoecia. Scale bars 50µm.

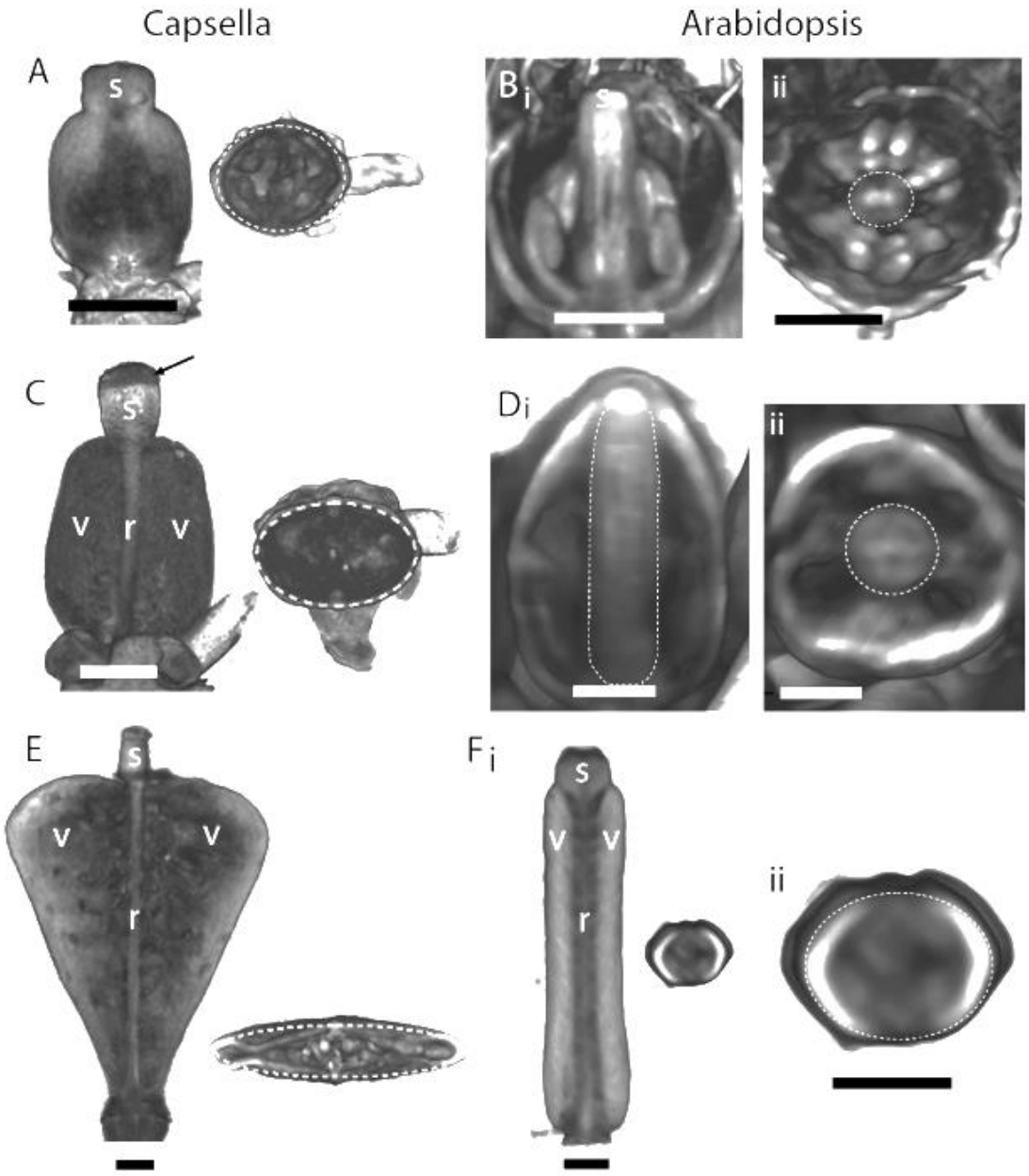

Figure 4.5 Capsella and Arabidopsis fruit. OPT images of dissected Capsella gynoecia and Arabidopsis flower buds of longitudinal image (left) and virtual cross section(right). (A, B) Gynoecia 6 DAI, flower stage 10. (C, D) 9 DAI, flower stage 12. Black arrow shows stigmatic papillae. (E) 11.5 DAI and (F) 11 DAI, flower stage 14. White dotted line shows outline of the gynoecium. Labels: style (s), replum (r) and valves (v). Scale bars 250µm.

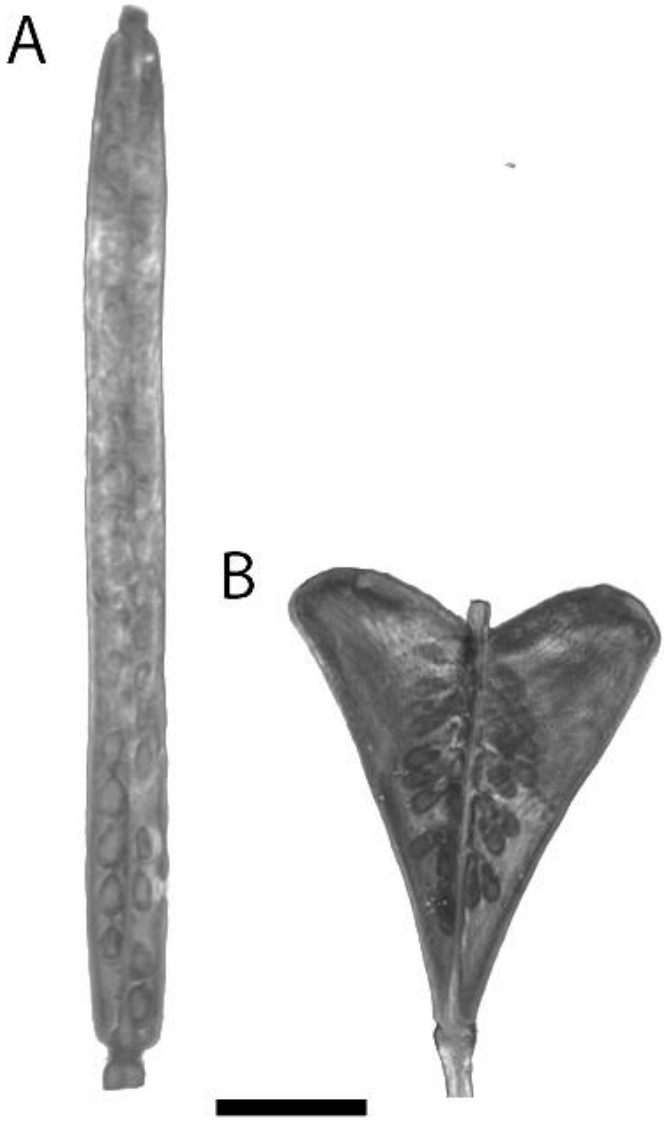

Figure 4.6 Mature fruit of Arabidopsis and Capsella. OPT images of mature fruit of (A) *Arabidopsis thaliana* Col-0 and (B) *Capsella rubella*. Scale bar 2mm.

4.2.3 Clonal Analysis

To investigate the differences in regional growth dynamics of *Arabidopsis* and *Capsella* I carried out clonal analysis in both species. I have given a detailed description of local growth dynamics in *Capsella* rubella by imaging clones through development (Section 3.2.4). To compare dynamics with *Arabidopsis* I have used the transgenic line BOB (Wachsman et al., 2011) and induced clones by heat shock. I imaged the clones in *Arabidopsis* at equivalent stages of development to *Capsella*.

I divided the growth of the gynoecium in each species into doubling lengths. The sizes that I chose were 300µm, 500µm, 1mm, 2mm and 4mm. The time to reach these lengths in the two species is different. For *Capsella* it takes 4, 6, 8.5 11.5 and 14 DAI and for *Arabidopsis* it takes 5, 6.5, 9, 11 and 13.5 DAI, respectively. Growth rates are calculated based on clones, assuming that the starting cell shape is isodiametric.

4.2.3.1 Imaging clones at 4 or 4.5 DAI

At 4 DAI the *Capsella* gynoecium is almost cylindrical in shape with a slightly tapered apex where the style will probably form (Figure 4.7A). The gynoecium has reached ~300µm in length. At 4.5 DAI the *Arabidopsis* is also cylindrical in shape but the apex is not tapered (Figure 4.7B), and has reached ~300µm in length. I induced clones 4 days prior to imaging; however I only imaged two individual samples at 4.5 DAI in *Arabidopsis*. The clones capture the early phase of growth and some of the middle phase.

Clones imaged at 4 DAI in *Capsella* are elongated along the proximodistal axis throughout the gynoecium (Figure 4.7). The clones imaged at 4.5 DAI in *Arabidopsis* have a similar shape and orientation, elongated along the proximodistal axis. This is represented by the average L/W ratio of the clones; which is 5.2 and 7.7 for *Capsella* and *Arabidopsis*, respectively. The average growth rate along the major axis of the clones is 2%/h and 2.4%/h and the average growth rate along the minor axis is 0.4%/h and 0.3%/h for *Capsella* and *Arabidopsis*, respectively.

The anisotropic shape of the clones correlates with cell division rates along the two axis with 2-3 rounds of cell division along the proximodistal axis and 1 or 0 rounds of cell division along the mediolateral axis in both species.

Where the style will probably form in Capsella the clones are shorter than the rest of the gynoecium (Figure 4.7A), a trend that seems to be common in *Arabidopsis*; however I only imaged one clone in the style of *Arabidopsis* (Figure 4.7B).The yellow region in Figure 4.7 represents where the style will probably form, based on the shape of the clones.

In summary, the clones induced prior to 4 or 4.5 DAI, which capture the early phase of growth in *Capsella* and *Arabidopsis*, have a similar orientation. Growth is predominately proximodistal across the whole organ and this is correlated with more cell division along this axis.

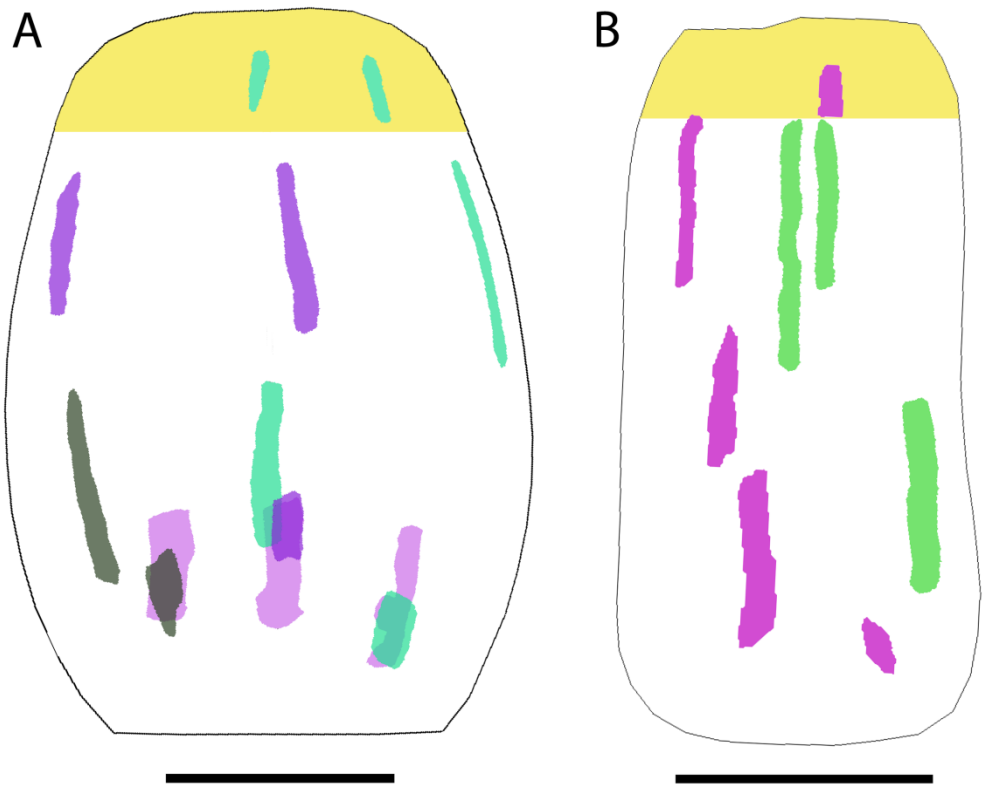

Figure 4.7 Clones images at 4 DAI and 4.5 DAI in Capsella and Arabidopsis gynoecium. The black outline marks the mean shape of the gynoecium and the clones have been warped on the mean shape in sector analysis toolbox. The coloured patches represent individual clones and clones of the same colour are from the same sample. Clones were induced at -1 and 0 DAI in Capsella (A) and Arabidopsis (B) gynoecium, respectively. Yellow region indicates the probable style. Scale bars 100µm

4.2.3.2 Imaging clones at 6 or 6.5 DAI

I induced clones 6 and 4 days prior to imaging the *Capsella* gynoecium at 6 DAI and the *Arabidopsis* gynoecium at 6.5 DAI when the gynoecia are ~500µm. Clones induced 6 days prior to imaging capture the early phase and the middle phase. Clones induced 4 days prior to imaging capture mostly the middle phase of growth. At 6 DAI the *Capsella* gynoecium is clearly different to the *Arabidopsis* gynoecium. The gynoecium is rounded in shape with a distinct narrow style region at the distal end (Figure 4.8A,C). The replum region is also distinct. The *Arabidopsis* gynoecium at 6.5 DAI is elongated along the proximodistal axis (Figure 4.8B,D). The style is defined; however it is difficult to identify the replum at this stage.

In the style the clones induced 6 and 4 days prior to imaging are anisotropic in shape and elongated along the proximodistal axis in both *Capsella* and *Arabidopsis* gynoecia (Figure 4.8). This is reflected in the L/W ratio of the clones in the style induced 6 days prior to imaging at 8.9 and 7.2 and the clones induced at 4 days prior to imaging 5.4 and 6.3 for *Capsella* and *Arabidopsis*, respectively. This is correlated with 3 rounds of cell division along the proximodistal axis and no cell division along the mediolateral axis in both species.

In the valves, clones induced 6 days prior to this stage are elongated along the proximodistal axis in both *Arabidopsis* and *Capsella* (Figure 4.8A,B). However the clones are relatively wider along the mediolateral axis in *Capsella*. This can be observed by comparing the L/W ratio of the clones which are 2.5 and 9.8 for *Capsella* and *Arabidopsis*, respectively. The average growth rate along the major axis of the clones is 1.4%/h and 1.8%/h whereas the average growth rate along the minor axis is 0.8%/h and 0.3%/h for *Capsella* and *Arabidopsis*, respectively. Cell division rates along the axes are correlated with the sector shape and growth rates. The clones in *Capsella* and *Arabidopsis* were 6-10 cells long indicating ~3 rounds of cell division. In width the clones of *Capsella* were 2-4 cells wide indicating 1-2 rounds of cell divisions along minor axis. Whereas in *Arabidopsis* the clones were 1-2 cells wide indicating a maximum of 1 round of cell division.

Clones in the valves induced 4 days prior to imaging (capturing the middle phase of growth) the gynoecia are isotropic in *Capsella* and anisotropic along the proximodistal axis in *Arabidopsis* (Figure 4.8C,D). This is reflected in the L/W ratio of 1.4 and 4.4 for *Capsella* and *Arabidopsis*, respectively. The clone shape is correlated with cell division patterns where after 4 days the clones were 2-5 cells long and 2-4 cells wide in *Capsella* indicating 1-2 rounds of cell divisions along both axes. Whereas in *Arabidopsis* the clones were 2-6 cells long and 1-2 cells wide indicating 1-3 rounds of cell divisions along the proximodistal axis and 0-1 rounds of cell divisions along the mediolateral axis.

The clones in valves of *Capsella* are not all completely parallel to the long axis of the gynoecium and splay out near the base. In *Arabidopsis* the clones are all parallel to the long axis of the gynoecium.

In summary, the style region of the gynoecium in *Capsella* and *Arabidopsis* are growing in a similar orientation, preferentially along the proximodistal axis of the gynoecium. In the valves, both species have a similar growth rate along the proximodistal

axis of the gynoecium. However, in *Capsella* there is more growth along the mediolateral axis compared to *Arabidopsis*. This is correlated with higher cell division along the mediolateral axis in *Capsella* compared with *Arabidopsis*.

4.2.3.3 Imaging clones at 8.5 and 9 DAI

At 8.5 and 9 DAI, the gynoecia of *Capsella* and *Arabidopsis* have reached 1mm. I induced clones 8, 6 and 4 days prior to imaging the gynoecia (Figure 4.9). Clones induced 8 days prior to imaging capture the early phase and the middle phase growth. The clones induced at 6 and 4 days prior to imaging capture the middle phase growth. In both species the style and replum tissues are defined and easily distinguished from the valves. For the quantative clonal analysis I focus on clones induced 6 and 4 days before imaging.

4.2.3.3.1 Style

In *Arabidopsis* there were no clones in the style induced 6 days prior to imaging and only 1 clone induced 4 days prior to imaging. For this reason I cannot do a comparison between *Capsella* and *Arabidopsis* in the style for this stage. The clones induced 8 days prior to imaging have an anisotropic shape orientated along the proximodistal axis in both species.

4.2.3.3.2 Replum

In both species the shape of the clones in the replum are anisotropic along the proximodistal axis (Figure 4.9) with L/W ratio at 6 days of 2.3 and 5.7 for *Capsella* and *Arabidopsis*, respectively. The clones are 2-4 cells long and 1-2 cells wide indicating 1-2 rounds of cell division along the major axis and 0-1 rounds of cell division along the minor axis in both species for clones induced 6 days prior to imaging.

4.2.3.3.3 Valve

The clones induced 6 days prior to imaging in the valves of *Capsella* are isotropic in shape (Figure 4.9C) and have a L/W ratio of 1.0. In *Arabidopsis* clones induced 6 days prior to imaging are anisotropic in shape along the proximodistal axis (Figure 4.9D) and have a L/W ratio of 3.0. The growth rate along the major and minor axis of clones in *Capsella* is equal at ~0.9%/h whereas in *Arabidopsis* the growth rate along the major axis (~1.2%/h) is greater than the growth rate along the minor axis (~0.5%/h).

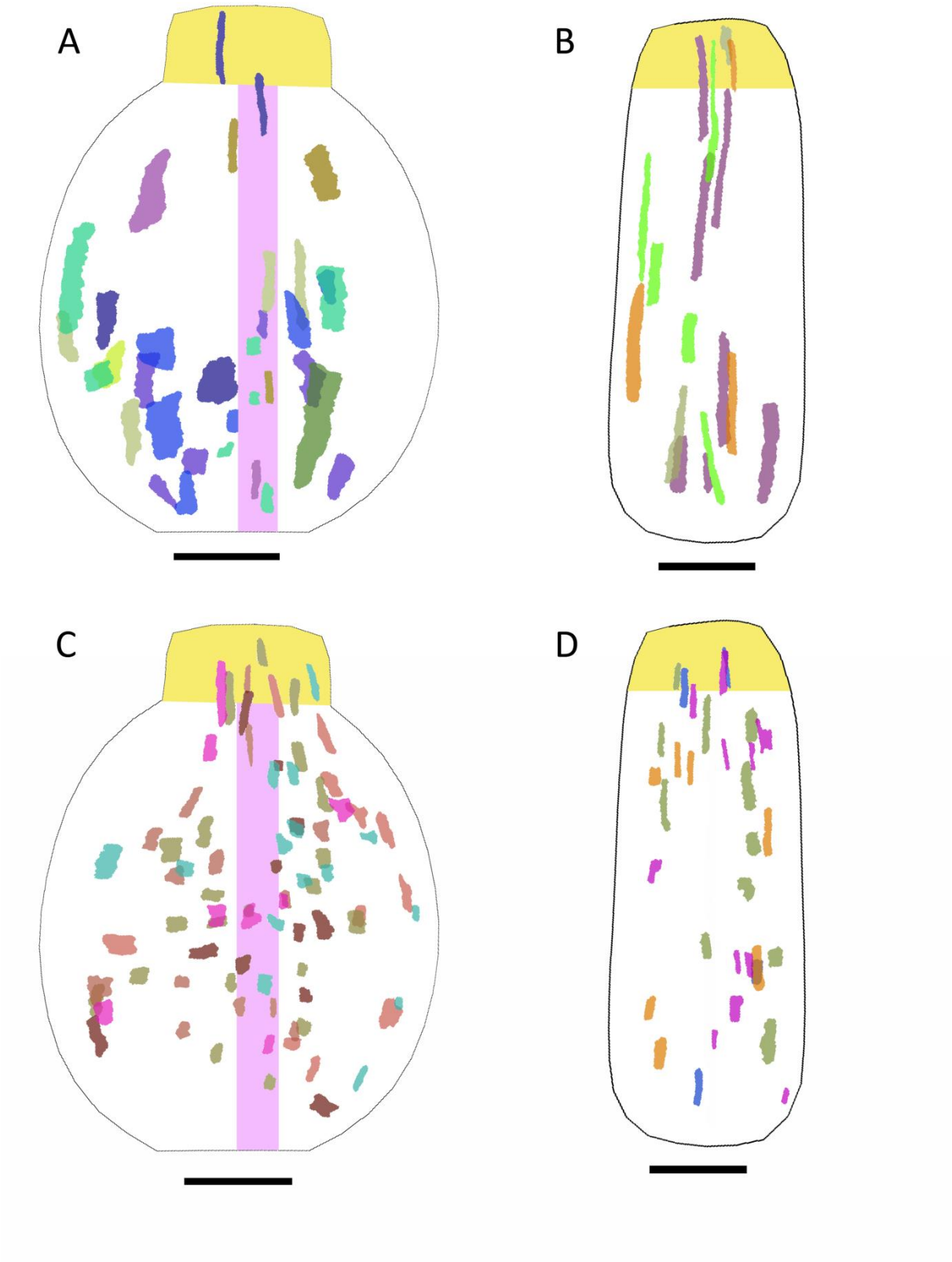

Figure 4.8 Clones imaged at 6 and 6.5 DAI in Capsella (left) and Arabidopsis (right) gynoecia. The black outline represents the mean organ shape at 6 DAI in Capsella (A, C) and 6.5 DAI in Arabidopsis (B, D) gynoecium. The coloured patches are individual clones and clones with the same colour are from the same sample. Clones were induced at 0 DAI (A) and 0.5 DAI (B) and imaged after 6 days. Clones were induced at 2 DAI (C) and 2.5 DAI (D) and imaged after 4 days. Yellow region: style, pink region: replum and white region: valves. Scale bars 100µm

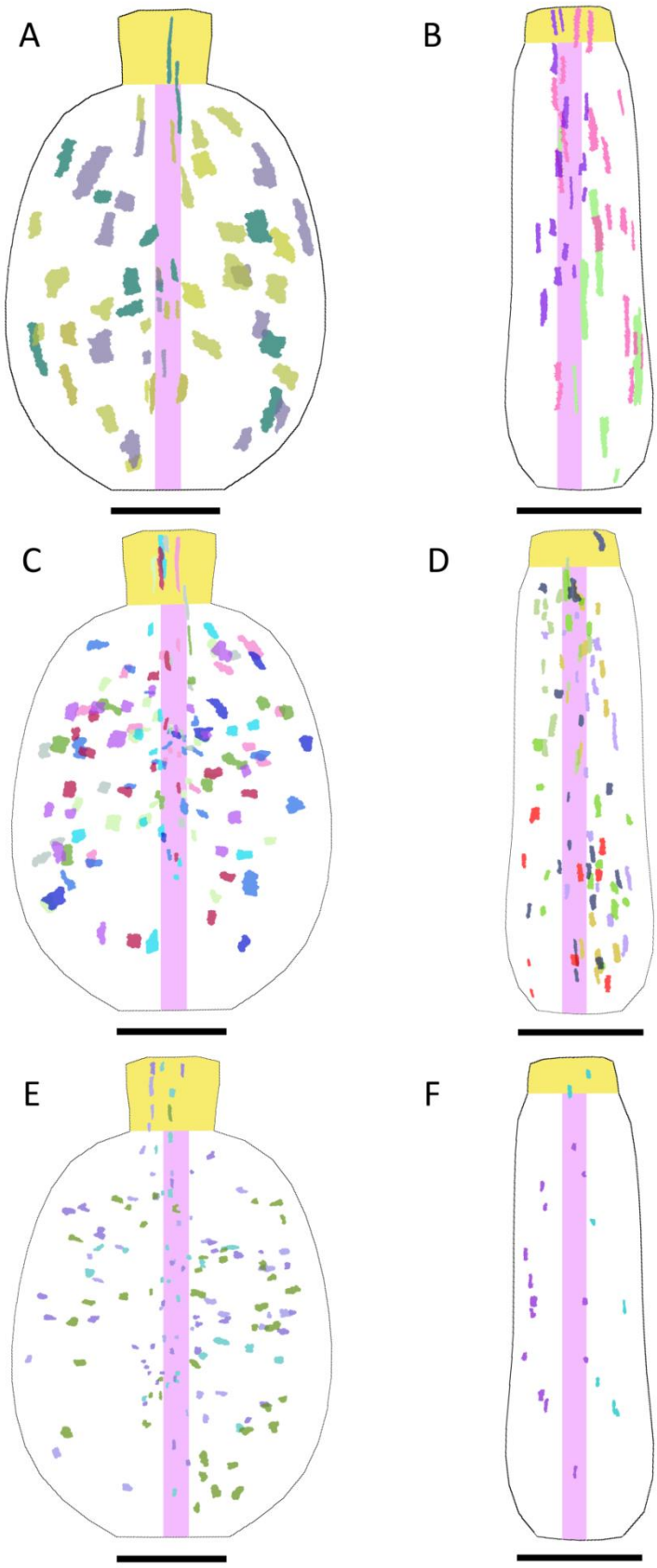

Figure 4.9 Clones imaged at 9 DAI in Capsella (left) and Arabidopsis (right) gynoecia. The black outline represents the mean organ shape at 9 DAI of Capsella (A,C,E) and Arabidopsis (B,D,F). The coloured patches are individual clones and clones with the same colour are from the same sample. Clones were induced at 1 DAI (A,B), 3 DAI (C,D) and 5 DAI (E,F) and imaged after 8, 6 and 4 days, respectively. Yellow region: style, pink region: replum and white region: valves. Scale bars 250µm

The clones induced 4 days prior to imaging in the valves of *Capsella* are anisotropic in shape along the mediolateral axis (Figure 4.9E) with a L/W ratio of 0.6. The mediolateral axis of the clones in *Capsella* is the major axis and the average growth rate along this is ~1.4%/h. This is in contrast to *Arabidopsis* where the clones are anisotropic in shape along the proximodistal axis (Figure 4.9F) and a L/W ratio of 3.6. In *Arabidopsis* the major axis is the proximodistal axis and the average growth rate along this axis is ~1.2%/h.

The cells in the clones are no longer isotropic in shape, some have a major and a minor axis and there are many asymmetrical stomatal divisions. Therefore the growth in the valves in both species at 9 DAI is correlated with both cell divisions and cell expansion.

In summary, clones in the replum reveal a similar pattern of growth in *Capsella* and *Arabidopsis*, elongating preferentially along the proximodistal axis. In the valves, during the middle phase of growth, the mediolateral axis of *Capsella* becomes the major axis of growth compared to *Arabidopsis* where the proximodistal axis is maintained as the major axis of growth. This growth is correlated with cell division and cell expansion.

4.2.3.4 Imaging clones at 11.5 DAI and 11 DAI

At 11.5 DAI and 11 DAI the *Capsella* and *Arabidopsis* gynoecium have reached 2mm in length. Both fruits have been fertilised at this stage. The *Capsella* fruit has started to develop a heart shape and the *Arabidopsis* fruit has continued to develop a long narrow fruit. I induced clones at 3.5 and 3 DAI in *Capsella* and *Arabidopsis*, respectively and images the clones after 8 days (Figure 4.10). The clones capture the middle phase and the late phase of growth.

4.2.3.4.1 Replum

Clones induced in the replum at 8 days prior to imaging of both *Capsella* and *Arabidopsis* have an anisotropic shape, elongated along the proximodistal axis (Figure 4.10) with a L/W ratio of 7.2 and 12.9, respectively.

4.2.3.4.2 Valve

Clones induced 8 days prior to imaging in the valves of *Capsella* have mixed orientations. In most cases the clones splay out towards the shoulders with clones elongated along the proximodistal axis near the base and along the mediolateral axis in the middle and distal part of the fruit (Figure 4.10A). This is reflected in the L/W ratio of clones near the base of 2.5 compared to 0.7 of clones in middle to distal parts of the fruit. Clones

induced 8 days prior to imaging in the valves of the *Arabidopsis* fruit are anisotropic in shape elongated along the proximodistal axis (Figure 4.10B) with an average L/W ratio of 4.5.

In both *Capsella* and *Arabidopsis* the growth rate along the major axis of the clones is ~1.5%/h. The orientation of the major axis is proximodistal for the clones near the base of the *Capsella* fruit and across the whole fruit of *Arabidopsis* but is mediolateral for clones in the upper half of the *Capsella* fruit. Growth along the minor axis is generally higher in *Capsella*, ~1.0%/h compared to 0.7%/h in *Arabidopsis*.

In summary, orientation of growth in the replum is proximodistal in both *Capsella* and *Arabidopsis*. The growth in the valves of *Capsella*, in the middle to late phase, is preferentially in a proximodistal orientation at the base and mediolateral in the middle and distal regions of the fruit. In *Arabidopsis* the orientation of growth is consistently proximodistal in the valves.

4.2.3.5 Imaging clones 14 and 13.5 DAI

The *Capsella* and *Arabidopsis* fruits have reached 4mm in length at 14 DAI and 13.5 DAI, respectively. The *Capsella* fruit has developed a heart shape and the *Arabidopsis* fruit has a very long narrow shape (Figure 4.11). I induced clones at 6 DAI and 5.5 DAI and imaged the clones after 8 days in *Capsella* and *Arabidopsis* fruit, respectively. The clone capture half middle phase growth and half late phase growth.

4.2.3.5.1 Replum

Clones induced in the replum 8 days prior to imaging in *Capsella* and *Arabidopsis* have an anisotropic shape, elongated along the proximodistal axis (Figure 4.11). This is reflected in the L/W ratio of the replum clones of 7.5 and 12.6 for *Capsella* and *Arabidopsis*, respectively.

4.2.3.5.2 Valves

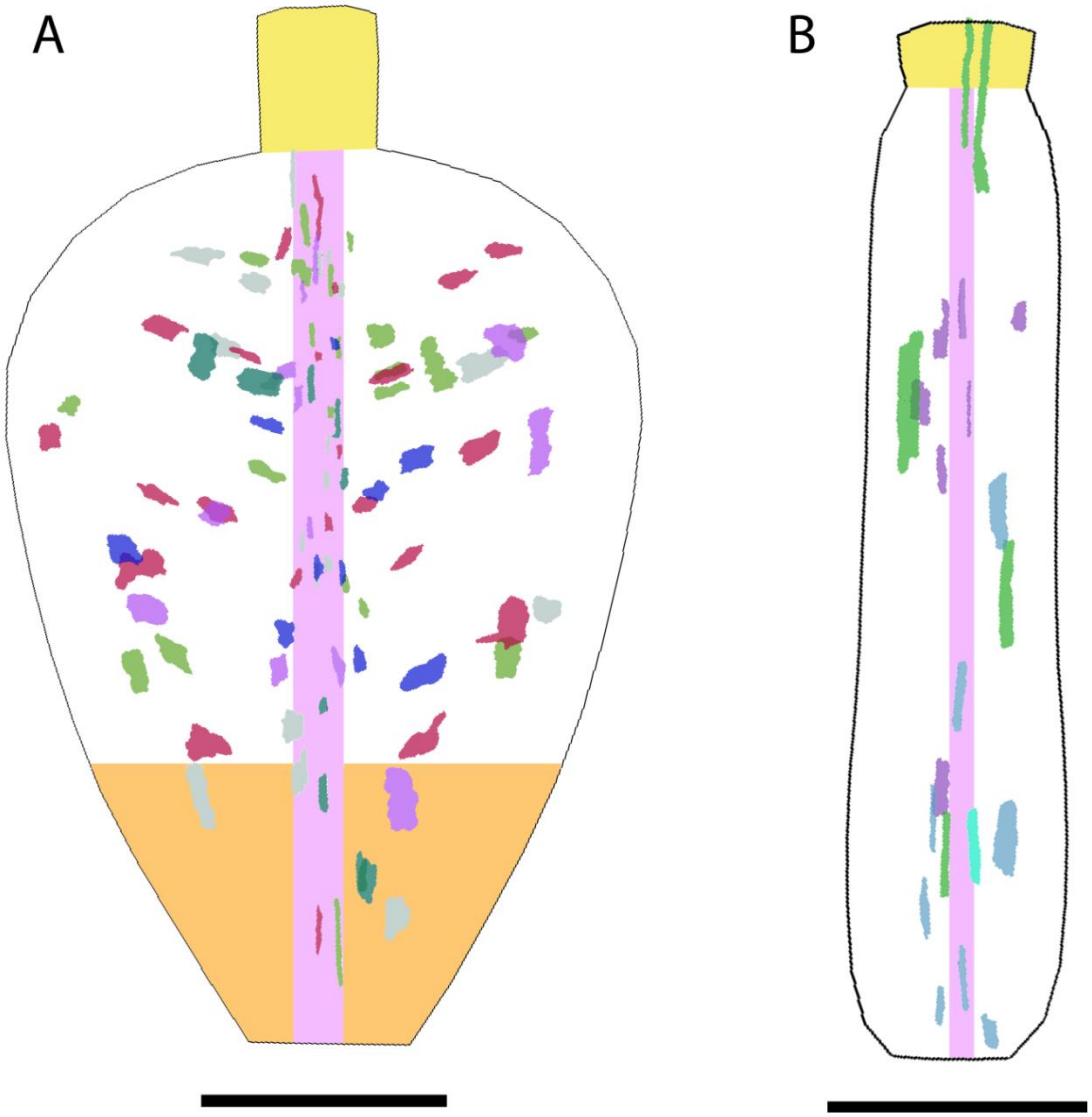

Figure 4.10 Clones imaged at 11.5 and 11 DAI in Capsella and Arabidopsis fruit The black outline represents the mean organ shape at 11.5 DAI of Capsella (A) and 11 DAI Arabidopsis (B). The coloured patches are individual clones and clones with the same colour are from the same sample. Clones were induced at 3.5 DAI (A), 3 DAI and imaged after 8 days. Yellow region: style, pink region: replum, orange region: base of valve where growth is preferentially proximodistal and white region: valves. Scale bars 500µm

Clones induced in the valves 8 days prior to imaging in the *Capsella* fruit are anisotropic in shape and splay out towards the distal shoulders of the heart (Figure 4.11A). The average growth rate of the major axis of the clones is 1.7%/h and the average growth rate of the minor axis of the clones is 1.0%/h. The major axes of the clones are not parallel to the proximodistal axis or the mediolateral axis of the fruit but rotated towards the distal shoulders. Clones induced in the valves 8 days prior to imaging in *Arabidopsis* are

anisotropic in shape and orientated along the proximodistal axis (Figure 4.11B). The average growth rate of the major axis of the clones is 1.6%/h and average growth rate of the minor axis of the clones is 0.7%/h. The major axes of the clones are parallel to the proximodistal axis of the fruit.

The areal growth rate of the *Capsella* clones is ~2.7%/h and in *Arabidopsis* is ~2.1%/h. The greater areal growth rate of the *Capsella* clones can be mostly accounted for by the higher growth rate along the minor axis compared to *Arabidopsis*.

In Summary, like previous stages the growth in the replum of both *Capsella* and *Arabidopsis* fruit is anisotropic along the proximodistal axis of the fruit. Clones induced in the valves of *Capsella*, capturing middle and late phases of growth, splay out towards the

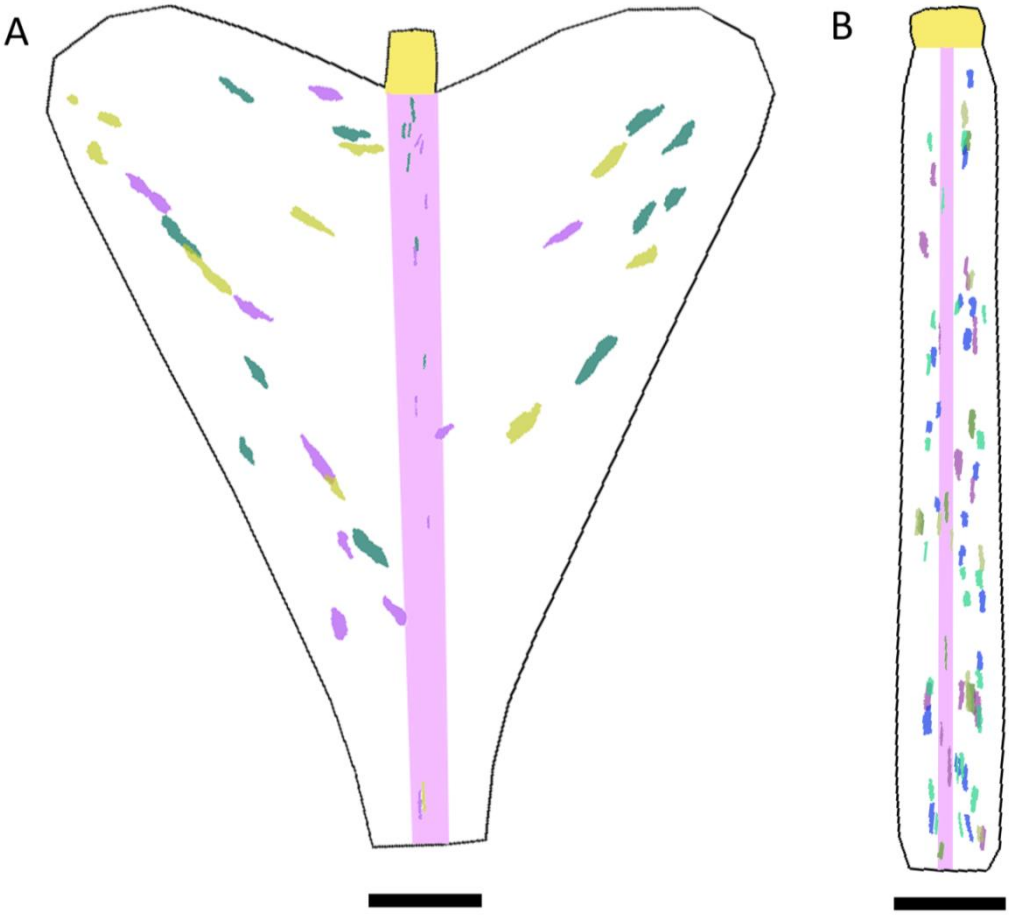

Figure 4.11 Clones imaged at 14 and 13.5 DAI in Capsella and Arabidopsis fruit The black outline represents the mean organ shape at 14 DAI of Capsella (A) and 13.5 DAI Arabidopsis (B). The coloured patches are individual clones and clones with the same colour are from the same sample. Clones were induced at 6 DAI (A), 5.5 DAI (B) and imaged after 8 days. Yellow region: style, pink region: replum and white region: valves. Scale bars 500µm

distal shoulders and have a greater areal growth rate than *Arabidopsis* mostly due to more growth along the minor axis. Growth in the valves of *Arabidopsis* is orientated parallel to the proximodistal axis through the middle and late phase.

Clonal analysis has revealed regional similaries and differences in the growth of the *Capsella* and *Arabidopsis* fruits. The replum and the style of both species have growth orientated in a proximodistal orientation throughout development. In the valves, *Capsella* and *Arabidopsis* gynoecium both grow preferentially in a proximodistal orientation in the early stages of development (0-2.5 DAI). In middles stages, while *Arabidopsis* maintains a proximodistal orientation of growth throughout the development of the gynoecium, *Capsella* grows more in a mediolateral orientation after 2.5 DAI. In the later stages, growth in the distal half of the valves in *Capsella* is orientated along the mediolateral axis and along the proximodistal axis near the base. In *Arabidopsis* growth in all regions of the valve are orientated along the proximodistal axis during the later stages.

4.2.4 Modelling the *Arabidopsis* fruit

Whole organ growth dynamics and clonal analysis have revealed the similarities and differences in overall and regional growth orientations that give rise to the different fruit shapes of *Capsella* and *Arabidopsis*. The experimental data collected for *Capsella* can be explained by the model developed in Section 3.2.6. To understand if the *Capsella* fruit model can also account for the divergent fruit shape and clone patterns of *Arabidopsis*, GPT framework was used to generate a model for the *Arabidopsis* fruit.

To generate a model for the *Arabidopsis* fruit, I altered the *Capsella* model in the following ways. I used the rates of growth in length and width from the whole organ growth data to specify K_{par} at 1.26%/h and K_{per} at 0.6%/h (in the *Capsella* model K_{par} is 1.4%/h and K_{per} is 1.15%/h). I ran the model with the following interactions, where blue indicates parameters I set to 0:

K_{par} = 0.0126 .pro(p_{EPHASE} , $\mathbf{i}_{EPHASE}$)

.inh(h_{BASE} , $\mathbf{i}_{BASE}$. $\mathbf{i}_{MPHASE}$) .pro($p_{MIDVALVE}$, $\mathbf{i}_{MIDVALVE}$. $\mathbf{i}_{MPHASE}$)

.pro($p_{GMIDVALVE}$, $\mathbf{i}_{GMIDVALVE}$. $\mathbf{i}_{LPHASE}$) .inh(h_{BASE} , $\mathbf{i}_{BASE}$. $\mathbf{i}_{LPHASE}$) .inh(h_{STYLE} , $\mathbf{i}_{STYLE}$. $\mathbf{i}_{LPHASE}$)

.inh(h_{GDIST} , $\mathbf{i}_{GDIST}$. $\mathbf{i}_{LPHASE}$) .pro(p_{GPROX} , $\mathbf{i}_{GPROX}$. $\mathbf{i}_{LPHASE}$)

K_{per} = 0.006 .inh(h_{STYLE} , $\mathbf{i}_{STYLE}$. $\mathbf{i}_{MPHASE}$) .inh(h_{BASE} , $\mathbf{i}_{BASE}$. $\mathbf{i}_{MPHASE}$) .inh(h_{REP} , $\mathbf{i}_{REP}$. $\mathbf{i}_{MPHASE}$)

.inh($h_{MIDVALVE}$, $\mathbf{i}_{MIDVALVE}$. $\mathbf{i}_{MPHASE}$)

.inh($h_{MIDVALVE}$, $\mathbf{i}_{MIDVALVE}$. $\mathbf{i}_{LPHASE}$) .inh(h_{STYLE} , $\mathbf{i}_{STYLE}$. $\mathbf{i}_{LPHASE}$) .inh(h_{BASE} , $\mathbf{i}_{BASE}$. $\mathbf{i}_{LPHASE}$)

.inh(h_{REP} , $\mathbf{i}_{REP}$. $\mathbf{i}_{LPHASE}$) .pro(p_{GDIST} , $\mathbf{i}_{GDIST}$. $\mathbf{i}_{LPHASE}$) .inh(h_{GPROX} , $\mathbf{i}_{GPROX}$. $\mathbf{i}_{LPHASE}$)

K_{knor} = 0.01

Alternatively, the *Arabidopsis* model could be viewed as a simplified version of the *Capsella* fruit model and can be defined as:

K_{par} = 0.0126 .pro(p_{EPHASE} , $\mathbf{i}_{EPHASE}$) .inh(h_{BASE} , $\mathbf{i}_{BASE}$. $\mathbf{i}_{MPHASE}$).inh(h_{BASE} , $\mathbf{i}_{BASE}$. $\mathbf{i}_{LPHASE}$)

K_{per} = 0.006 .inh(h_{STYLE} , $\mathbf{i}_{STYLE}$. $\mathbf{i}_{MPHASE}$) .inh(h_{BASE} , $\mathbf{i}_{BASE}$. $\mathbf{i}_{MPHASE}$) .inh(h_{REP} , $\mathbf{i}_{REP}$. $\mathbf{i}_{MPHASE}$)

.inh(h_{STYLE} , $\mathbf{i}_{STYLE}$. $\mathbf{i}_{LPHASE}$) .inh(h_{BASE} , $\mathbf{i}_{BASE}$. $\mathbf{i}_{LPHASE}$).inh(h_{REP} , $\mathbf{i}_{REP}$. $\mathbf{i}_{LPHASE}$)

K_{knor} = 0.01

The key differences in the *Arabidopsis* model compared to the *Capsella* model are: (1) the basic values of K_{par} and K_{per} are different, (2) K_{par} is not promoted in the midvalve and (3) $\mathbf{i}_{GDIST}$ and $\mathbf{i}_{GPROX}$ are not used to make alternative gradients of K_{par} and K_{per}, in other words K_{par} and K_{per} are uniform across the valves.

For a comparison of the *Capsella* fruit model and the *Arabidopsis* fruit model I have modelled from 0-8 DAI (Figure 4.12) and from 8-11 DAI (Figure 4.13), respectively.

From 0-2 DAI the *Capsella* and the *Arabidopsis* models have a similar cylindrical shape (Figure 4.12A,B). By 4 DAI the *Capsella* model starts to become rounded where the *Arabidopsis* model becomes elongated (Figure 4.12A,B). At 8 DAI the *Arabidopsis* model is much narrower than the *Capsella* model. Instead of producing a snuff bottle shape it produces a cylindrical shape (Figure 4.12A,B). The cross section shape of the *Arabidopsis* model becomes progressively circular by 8 DAI. Resultant areal growth is lower in the *Arabidopsis* model than *Capsella* (Figure 4.12A,B) because it has a lower basic K_{per}.

I induced clones in the *Arabidopsis* model at the corresponding stages as the experimental clones. Clones induced in the model at 0.5 DAI are anisotropic along the proximal distal axis (Figure 4.12D). However, they are not as elongated as the experimental clones (Figure 4.12C). This may be due to the starting cell shape of the experimental clones being square, compared to the circular model clones. Clones induced in the model at 3 DAI, and imaged at 7 DAI are slightly anisotropic along the proximal distal axis (Figure 4.12F).

The experimental clones are more elongated during this period (Figure 4.12E), again this may be due to the starting cell shape.

In the *Capsella* model, between 8-11 DAI the snuff bottle shape grows into a flattened heart shape (Figure 4.13A). In the *Arabidopsis* model, the resultant shape after 11 DAI is a longer cylindrical shape with a rounded cross-section (Figure 4.13B). The resultant areal growth rates are again higher in the shoulders and the base of the *Capsella* model where there K_{per} and K_{par} are high (Figure 4.13A). In *Arabidopsis* K_{per} has a lower basic rate and so the areal growth rates are lower (Figure 4.13B).

The polarity field remains parallel to the proximodistal axis throughout all stages of the *Arabidopsis* model (Figure 4.13C) which results in the clones always aligning with the proximodistal axis. Clones induced at 3 DAI and imaged at 9 DAI in the *Arabidopsis* model have anisotropic shape along the proximal distal axis (Figure 4.13D) and match clone orientations in the experimental data (Figure 4.13E). Also clones induced at 5 DAI and images at 11 DAI in the *Arabidopsis* model (Figure 4.13F) also have proximal distal orientation matching the experimental clones (Figure 4.13G). Clones in the replum region of the model are narrower than clones in the valve regions (Figure 4.13E) due to the inhibition of K_{per} by $\mathbf{i}_{REP}$. This is a common feature observed in the experimental clones where in many cases the clones in the replum are only one cell file wide (Figure 4.13F).

In Summary, the growth specified in this model of *Arabidopsis* fruit is sufficient to explain the final fruit shape up to 11 DAI and most clonal patterns observed experimentally. One problem with the model is that by 11 DAI it has a rounded cross section whereas the *Arabidopsis* fruit has a more oval cross section (Figure 4.5F). In the *Capsella* model promoting K_{par} in the mid valve region was enough to flatten the cross section shape. This principle could be applied to the *Arabidopsis* model to generate the oval cross section.

The model developed for *Capsella* fruit identified key principles for fruit growth that could explain clonal patterns. By simplifying this model it is possible to generate the cylindrical shape of the *Arabidopsis* fruit and explain the observed experimental clones.

4.2.6 Investigating FUL in fruit shape evolution

The modelling has revealed factors that are important for generating the differences in fruit shape between *Arabidopsis* and *Capsella*. In Chapter 4, *CrFUL* was

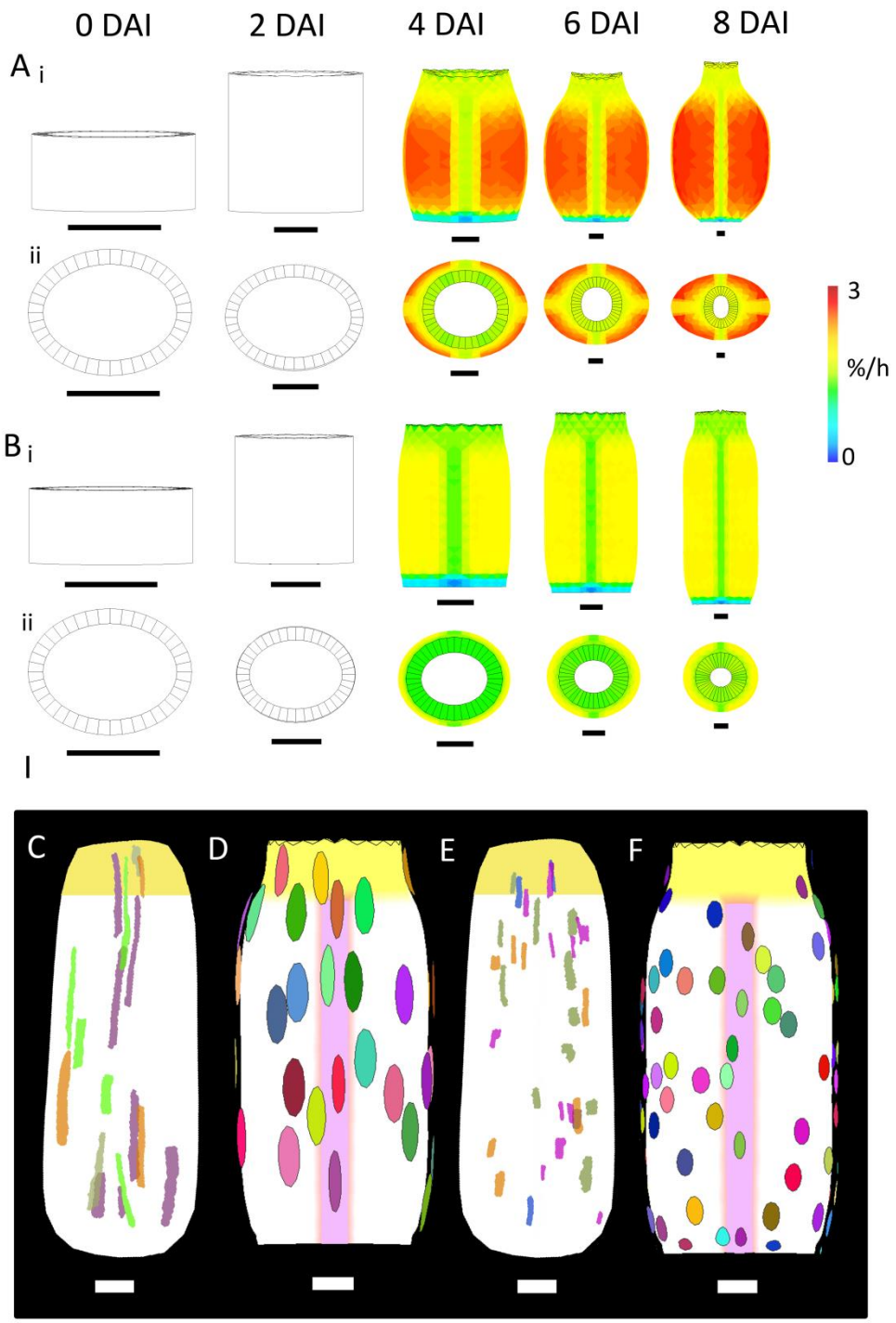

Figure 4.12 Model of Capsella and Arabidopsis fruit growth 0-8 DAI (A) Capsella model resultant shapes and areal growth. (B) Arabidopsis model resultant shapes and areal growth rates. Clones induced at 0.5 DAI and imaged at 7 DAI experimentally (C) and in the Arabidopsis fruit model (D). Clones induced at 3 DAI and imaged at 7 DAI experimentally (E) and in the Arabidopsis fruit model (F).). Yellow region: style, pink region: replum. Coloured scale bar represents resultant areal growth in %/h. Scale bars 50µm

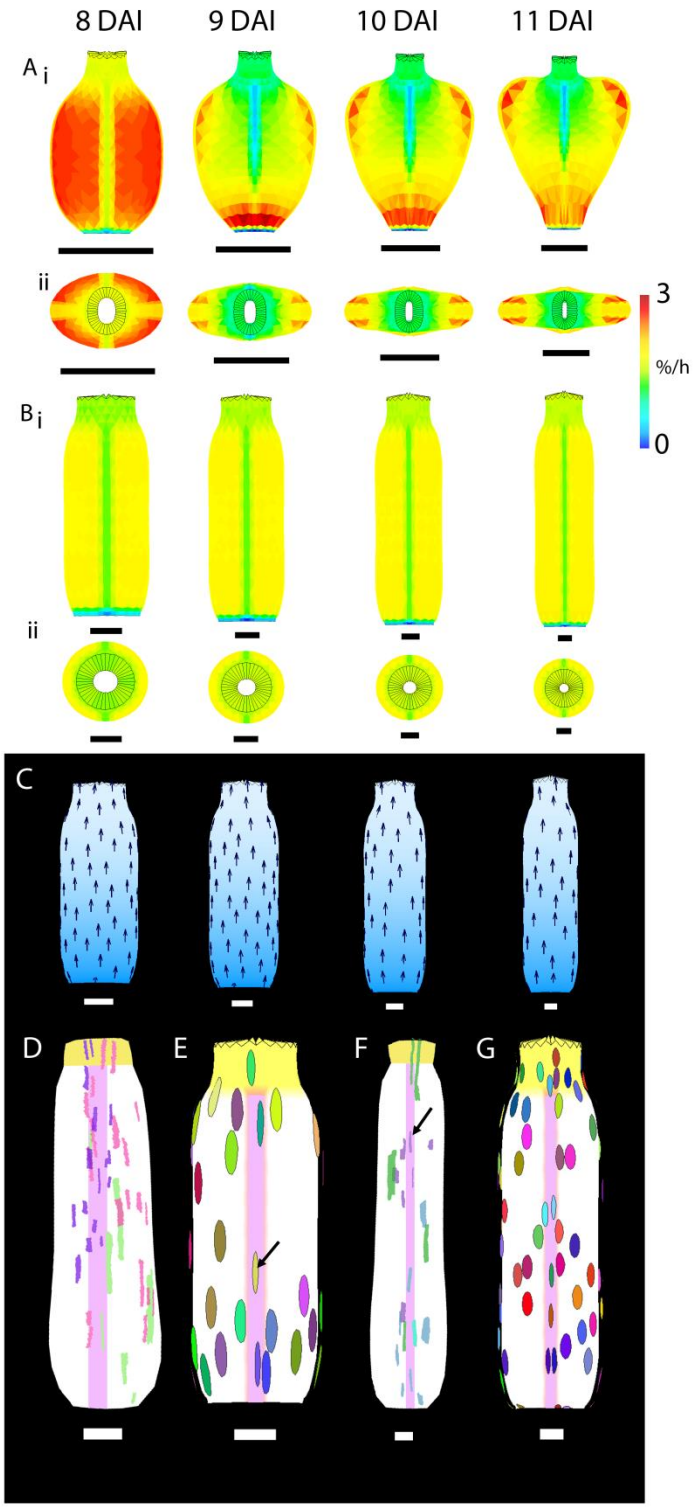

Figure 4.13 Model of Capsella and Arabidopsis fruit 8-11 DAI (A) Capsella model resultant shapes and areal growth. (B) Arabidopsis model resultant shapes and areal growth rates. (C) $\mathbf{s}_{POL}$ (blue colour) and polarity field (arrows. Clones induced at 3 DAI and imaged at 9 DAI experimentally (D) and in the Arabidopsis fruit model (E). Clones induced at 5 DAI and imaged at 11 DAI experimentally (F) and in the Arabidopsis fruit model (G). Yellow region: style, pink region: replum. Black arrows mark narrow clones in the replum region. Coloured scale bar represents resultant areal growth in %/h. Scale bars 100µm

shown to be important for specifying the heart-shape fruit of *Capsella*. *AtFUL* is also known to be important for the elongation of the *Arabidopsis* fruit (Gu et al., 1998) and it has been observed that altering the activity of *AtFUL* with VP16 can result in altered fruit shape in *Arabidopsis* (Cristina Ferrandiz unpublished results, Figure 4.1). This suggests that *FUL* could be a factor important for the evolution of divergent fruit shapes.

4.2.6.1 FUL sequence comparison

Phenotypic differences in *Arabidopsis* and *Capsella* fruit may arise from differences in protein sequence of *FUL*. Alternatively, differences in fruit shapes between the species may be the result of differences downstream of *FUL*. To investigate if there are differences, the protein sequence of *CrFUL* was compared to *AtFUL* and the three copies of *Brassica FUL: BraA.FUL.a*, *BraA.FUL.b* and *BraA.FUL.c* (Brassica gene nomenclature by Østergaard and King, 2008).

CrFUL protein sequence is 97% similar to *AtFUL*. The majority of the sequence variation between species compared in this analysis is in the C-terminal domain of the proteins (Figure 4.14). There are 8 amino acid substitutions specific to *Capsella* FUL that are not observed in the other species analysed; five of these are for similar residues. However, three substitutions are specific to *Capsella* and have a change in charge and polarity. At positions 180, 208 and 214 non polar neutral residues of *BraFUL* and *AtFUL* are substituted with negatively charged acidic residues, glutamic acid and aspartic acid in *CrFUL*. This trend towards acidic residues in the C-terminal tail of *CrFUL* may lead to phenotypic differences in the fruit shape between the species.

4.2.6.2 Complementation of *ful2* and *crful1*

To investigate the contribution of *CrFUL* and *AtFUL* protein sequence to fruit shape I designed a complementation experiment. I cloned the coding DNA sequence (CDS) of *AtFUL*, a 2kb promoter of *AtFUL* (Urbanus et al., 2009) and *CrFUL* CDS into the TOPO 4 cloning vector with appropriate restriction sites. The promoter of *CrFUL* could not be cloned due to difficulties in amplifying the sequence. Recently, the *pCrFUL* has been synthesised but was not available for the complementation experiments before writing. I combined *pAtFUL* with either *CrFUL* CDS or *AtFUL* CDS in the pEGAD plant expression vector. I transformed *Capsella* and *Arabidopsis* plants (genotypes *crful-1* and *atful-2*, respectively) with the constructs *pAtFUL::AtFUL* or *pAtFUL::CrFUL*.

```
AtFUL            MGRGRVQLKRIENKINRQVTFSKRRSGLLKKAHEISVLCDAEVALIVFSSKGKLFEYSTDS 61
BraA.FUL.a       MGRGRVQLKRIENKINRQVTFSKRRSGLLKKAHEISVLCDAEVALIVFSSKGKLFEYSTDS 61
BraA.FUL.b       MGRGRVQLKRIENKINRQVTFSKRRPGLLKKAHEISVLCDAEVALVIFSSKGKLFEYSTDS 61
BraA.FUL.c       MGRGRVQLKRIENKINRQVTFSKRRSGLLKKAHEISVLCDAEVALVVFSSKGKLFEYSTDS 61

CrFUL            MGRGRVQLKRIENKINRQVTFSKRRSGLLKKAHEISVLCDAEVALIVFSSKGKLFEYSTDS 61
                 ************************.******************::************** 

AtFUL            CMERILERYDRYLYSDKQLVGRDVSQSENWVLEHAKLKARVEVLEKNKRNFMGEDLDSLSL 122
BraA.FUL.a       CMERILERYDRYLYSDKQLVGRDISQSENWVLEHAKLKARVEVLEKNKRNFMGEDLDSLSL 122
BraA.FUL.b       CMERILERYDRYLYSDKQLVGRDISQSENWVLEHAKLKARVEVLEKNKRNFMGEDLDSLSL 122
BraA.FUL.c       SMERILERYDRYLYSDKQLVGRDISQSENWVLEHAKLKARVEVLEKNKRNFMGEDLDSLSI 122

CrFUL            CMERILERYDRYLYSDKQLVGREVSQSENWVLEHAKLKARVEVLEKNKRNFMGEDLDSLSL 122
                 .**********************::************************************: 

AtFUL            KELQSLEHQLDAAIKSIRSRKNQAMFESISALQKKDKALQDHNNSLLKKIKERE--KKTGQ 181
BraA.FUL.a       KELQSLEHQLDAAIKSIRSRKNQAMFESISALQKKDKALQDHNNTLLKKIKERE--KKTGH 181
BraA.FUL.b       KELQSLEHQLHAAIKSIRSRKNQAMFESISALQKKDKALQDHNNALLKKIKERE--KNTVQ 181
BraA.FUL.c       KELQSLEHQLDAAIKSIRSRKNQAMFESISALQKKDKALQDHNNTLLKKIKEKEKEKNTGQ 183

CrFUL            KELQSLEHQLDAAIKSIRSRKNQAMFESISALQKKDKALQDHNNSLLKKIKERE--KKTDQ 181
                 **********.**********************************:*******:*  *:* : 

AtFUL            QEGQLVQCSNSSSVLLPQYCVTSSRDGFVERVGGENGGASSLTEPNSLLPAWMLRPTTTNE 242
BraA.FUL.a       QEGQLNHCSNNSSIVQPQYCLTSSRDGFVGRVGAENGGASSLTQPNSLLPAWMLP--TTNE 240
BraA.FUL.b       QEGQLIQCSNNSSILQPQYCLTSSRDGFVGRVGGDDGGASSLAEPNSLLPAWMLRLATNE- 241
BraA.FUL.c       QEGQLIQCSNNSSVLQPQYCVTASRDGLVERVVGENGGASSLIEPNSLLPAWMLR------ 238

CrFUL            QEGQLNQCSNSCSVLLPQYCLSSSRDDFVERVEGENGSAPSLTEPNSLLPAWMLRPTTTNE 242
                 ***** :***..*:: ****:::***.:* ** .::*.*.** :********** 
```

Figure 4.14 Interspecific *FUL* Protein sequence alignment. *FUL* protein is highly conserved between *Brassica*, Arabidopsis and Capsella. Blue letters indicate amino acid substitutions specific to Capsella that do not carry a change in polarity. Red letters and yellow highlighted letters indicate amino acid substitutions specific to Capsella that carry a change in polarity with a general pattern of neutral to acidic residues. Analysis carried out by Lars Ostergaard.

If protein sequence of *FUL* was important for the generation of fruit shape it would be expected that expression of *CrFUL* in *Arabidopsis ful* background would generate fruit that were partially heart shaped or triangular. Likewise, expression of *AtFUL* in *Capsella ful* background would generate longer, narrower fruit.

4.2.6.2.1 *atful-2*

In the *atful-2* background I generated 5 and 11 transformants of *pAtFUL::AtFUL* and *pAtFUL::CrFUL*, respectively. Both constructs partially complemented the *ful* mutant phenotype as the siliques elongated more than *atful-2* (Figure 4.15). In the T1 generation both transgenic constructs did not reach WT length however there was a tendency for *pAtFUL::AtFUL* to elongate more compared to lines expressing *pAtFUL::CrFUL* (Figure 4.15). To confirm this many more lines would have to be measured and a statistical test carried out.

There was no difference in the shape of the siliques in either *pAtFUL::AtFUL* or *pAtFUL::CrFUL* (Figure 4.15). There was no indication of distal shoulders or a tapered proximal base in *pAtFUL::CrFUL*.

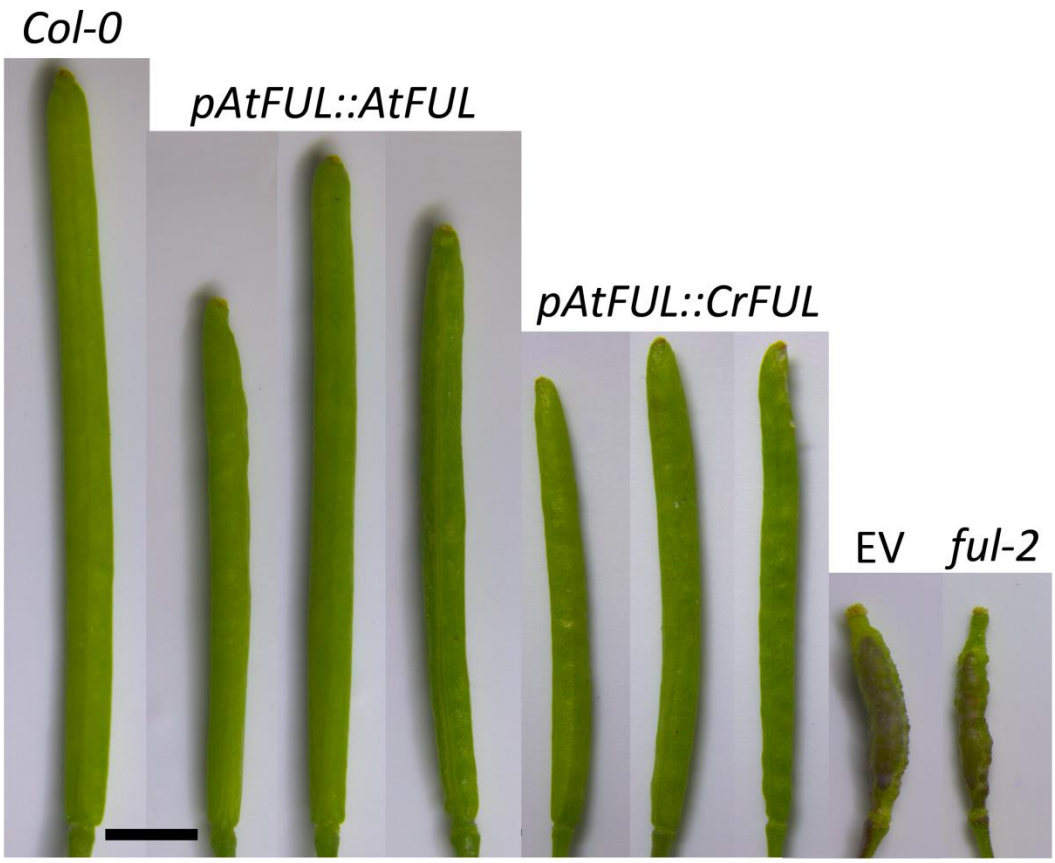

Figure 4.15 Transgenic complementation of *atful2.* Arabidopsis *ful* mutant was complemented with either *pAtFUL::AtFUL* CDS or *pAtFUL::CrFUL* CDS. Col-0 is wildtype, the three fruit for each construct represent three individual transgenic lines in T1 generation. EV: empty vector control. Scale bar 2mm

In WT *Arabidopsis* fruits lignification is restricted to the endocarp b layer and the lignification layer of the valve margin (Figure 4.16A). In *ful2* fruit there is ectopic lignification of valve tissues (Figure 4.16B). To investigate if the lignification phenotype is complemented by *pAtFUL::AtFUL* and *pAtFUL::CrFUL*, mature fruit of transformants were sectioned and stained with Alcian blue and Safranin-O by André Kuhn. Transformants of either *pAtFUL::AtFUL* and *pAtFUL::CrFUL* had lignin staining restricted to the endocarp b layer and the lignification layer of the valve margin (Figure 4.16C,D). Therefore the expression of *AtFUL* or *CrFUL* is sufficient to generate the correct lignification pattern of *Arabidopsis* fruit.

The cross section shape of *Arabidopsis* WT fruit is oval and one seed either side of the septum is in the sectional plane (Figure 4.16A). In *ful2* the cross section shape of the fruit is rounded and multiple seeds are in the section plane (Figure 4.16B). Plants expressing *pAtFUL::AtFUL* or *pAtFUL::CrFUL* have oval cross section shape and a single seed in plane either side of the septum (Figure 4.16C,D).

The degree to which the *ful* phenotype was complemented in terms of silique length and cross section shape varied between transgenic lines in both *pAtFUL::AtFUL* and *pAtFUL::CrFUL* (Figure 4.15). This variation may be due to expression levels of the

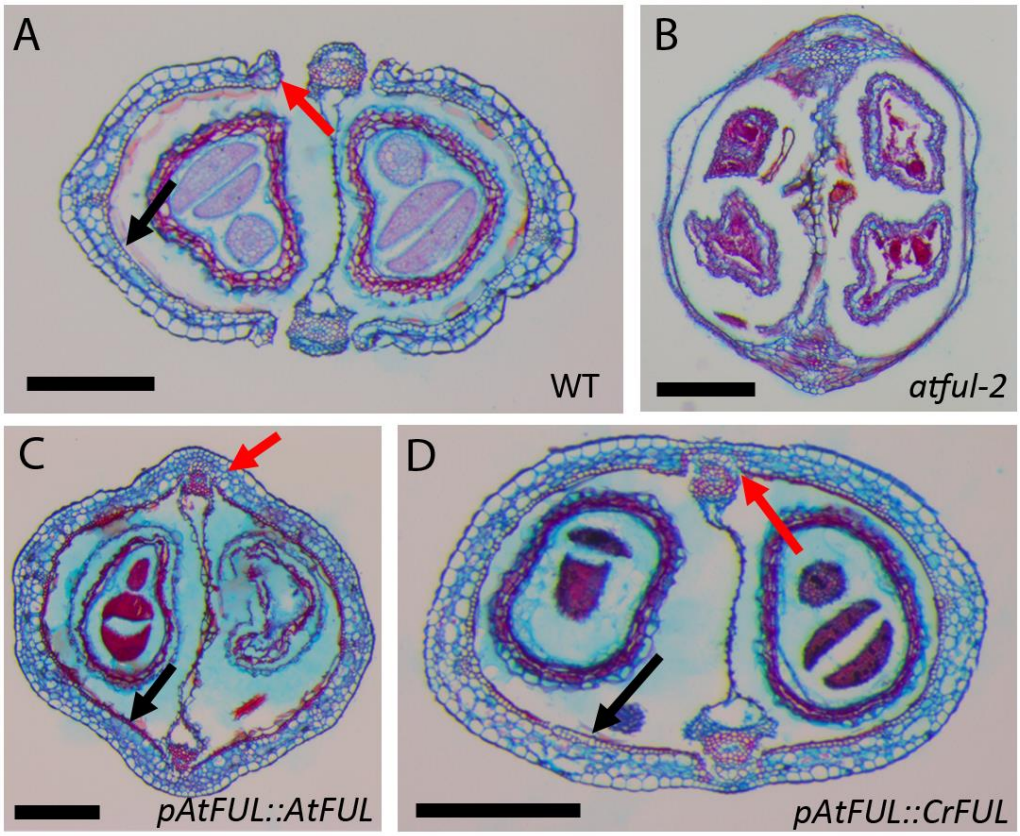

Figure 4.16 Cross sections and lignin staining of Arabidopsis transgenic lines. Fruits were sectioned and stained with Alcian blue and Safranin. Lignin is stained pink. (A) wildtype has an oval cross section shape and has two seeds either side of septum. (B) *ful2* has a rounded cross section and 4 seeds in plane (C) *ful2* complemented with *pAtFUL::AtFUL* CDS (D) *ful2* complemented with *pAtFUL::CrFUL* CDS. Both transgenic lines (C, D) partially rescue the oval cross section shape, have two seeds on either side of septum and lignification is restricted to endocarp *b* layer. Black arrow indicate staining of lignin in the endocarp b layer. Red arrows indicate where the valve margin should be. Scale bars 200µm.

transgenes.

Although fruit elongation, lignification pattern and cross sectional shape could be complemented by the expression of either construct, all fruits were indehiscent. This is because the valve margin did not form properly in any of the transgenic lines (Figure 4.16C,D). This may be due to misexpression of *FUL* reported when a promoter of less than 3.9kb is used (Woods, 2010) or the use of CDS instead of genomic sequence. Over-expression of *FUL* causes fruit to be indehiscent and may also be a reason from this phenotype in the transgenic lines (Ferrandiz et al., 2000).

In summary, expression of *CrFUL* CDS in *Arabidopsis* is not sufficient to generate a heart-shaped fruit but partially complements the silique elongation, cross section shape and lignification patterning of the *atful-2* fruits.

4.2.6.2.2 *crful-1*

In *Capsella* plants with *crful1* background, Nicola Stacey and I generated 3 and 14 transformants of *pAtFUL::AtFUL* and *pAtFUL::CrFUL*, respectively.

In the *crful-1* background, expression of *pAtFUL::CrFUL* CDS or *pAtFUL::AtFUL* CDS partially complemented the mutant phenotype (Figure 4.17). The fruit of the transgenic lines expanded, shoulders of the heart shape were partially formed and had a tapered based. In both transgenic lines the shoulders did not extend to the full size of WT and the fruits were indehiscent (Figure 4.17). The growth conditions in the Basta selection glasshouse (where transgenic lines were grown) were not ideal in the summer months. Many of the fruit did not fully expand due to fluctuation in temperatures affected fertility. Hence it was difficult to make a direct comparison of the fruit length in lines expressing either construct. Also it would be desirable to have many more transgenic lines for a statistical comparison.

In summary, the heart-shaped fruit was partially rescued by *pAtFUL::CrFUL* CDS and *pAtFUL::AtFUL* CDS. This observation shows that *pCrFUL* and *CrFUL* CDS are not required for the shape of *Capsella* fruit. The expression of *FUL* from either species is sufficient to generate a heart shaped fruit in a *crful-1* background.

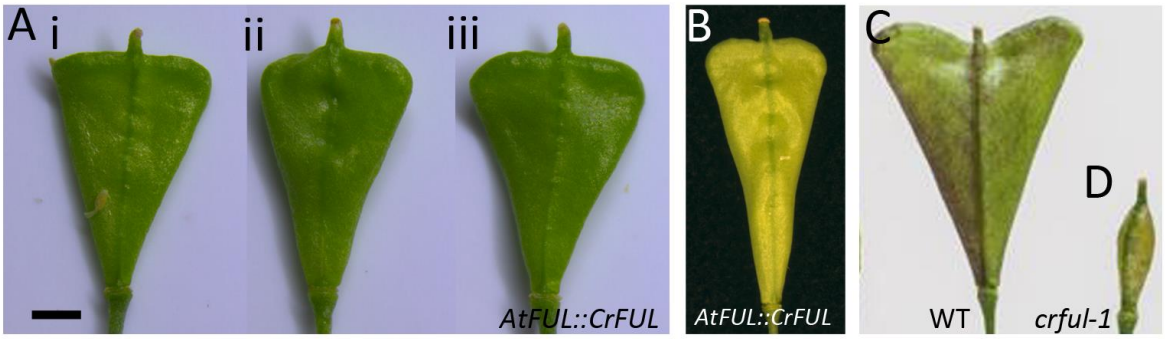

Figure 4.17 Transgenic complementation of *crful-1*. Capsella *ful* mutant was complemented with either *pAtFUL::AtFUL* CDS or *pAtFUL::CrFUL* CDS. (A) Three individual transgenic lines of *crful1* expressing *pAtFUL::CrFUL* CDS (i-iii, T1 generation). (B) A single line of *crful1* expressing *pAtFUL::AtFUL* CDS, image not to scale. *Capsella rubella* wildtype (C) and *crful-1* (D), images not to scale. (C,D) picture by André Kuhn. Scale bar 1mm

4.2.7 Flattening fruit

The spatiotemporal dynamics of fruit development in *Capsella* and *Arabidopsis* can be explained by a model with a small number of parameters. If this model of fruit development is of general importance it should be able to predict growth patterns of divergent fruit forms in closely related species. In the Brassicaceae family there are many other divergent fruit forms, for example flat rounded fruit is common in the multiple genres (Figure 4.18A-D).

Fruits can either be flattened laterally (perpendicular to the septum) or medially (parallel to the septum). *Lepidium* are flattened laterally like *Capsella* and the at fruit maturity have a rounded shape (Figure 4.18B). Before the gynoecium is fertilised it already has a laterally flattened cross section (Figure 4.18A). In the *Capsella* model to flatten the shape K_{par} was promoted by $\mathbf{i}_{MIDVALVE}$. To generate the heart shape K_{per} was promoted in the distal half of the model by $\mathbf{i}_{GDIST}$ and K_{par} promoted in the proximal base by $\mathbf{i}_{GPROX}$. To explore the generation of a flat rounded shape I reduced h_{GDIST}, h_{GPROX}, p_{GDIST} and p_{GPROX} to 0 (highlighted in blue) and maintained the promotion of K_{par} by $\mathbf{i}_{MIDVALVE}$. Interactions highlighted in red show the parameters that were altered from the *Capsella* model:

$$K_{par} = 0.014 .\text{pro}(p_{EPHASE} , \mathbf{i}_{EPHASE}) .\text{inh}(h_{BASE} , \mathbf{i}_{BASE}. \mathbf{i}_{MPHASE}) .\text{pro}(p_{MIDVALVE} , \mathbf{i}_{MIDVALVE}. \mathbf{i}_{MPHASE})$$

$$.\text{pro}(p_{MIDVALVE} , \mathbf{i}_{MIDVALVE}. \mathbf{i}_{LPHASE}) .\text{inh}(h_{BASE} , \mathbf{i}_{BASE}. \mathbf{i}_{LPHASE}) .\text{inh}(h_{STYLE} , \mathbf{i}_{STYLE}. \mathbf{i}_{LPHASE})$$

$$.\text{inh}(h_{GDIST} , \mathbf{i}_{GDIST}. \mathbf{i}_{LPHASE}) .\text{pro}(p_{GPROX} , \mathbf{i}_{GPROX}. \mathbf{i}_{LPHASE})$$

$$K_{per} = 0.0125 .\text{inh}(h_{STYLE} , \mathbf{i}_{STYLE}. \mathbf{i}_{MPHASE}) .\text{inh}(h_{BASE} , \mathbf{i}_{BASE}. \mathbf{i}_{MPHASE}) .\text{inh}(h_{REP} , \mathbf{i}_{REP}. \mathbf{i}_{MPHASE})$$

.inh($h_{MIDVALVE}$, $\mathbf{i}_{MIDVALVE}$. $\mathbf{i}_{MPHASE}$) .inh($h_{MIDVALVE}$, $\mathbf{i}_{MIDVALVE}$. $\mathbf{i}_{LPHASE}$)

.inh(h_{STYLE} , $\mathbf{i}_{STYLE}$. $\mathbf{i}_{LPHASE}$) .inh(h_{BASE} , $\mathbf{i}_{BASE}$. $\mathbf{i}_{LPHASE}$) .inh(h_{REP} , $\mathbf{i}_{REP}$. $\mathbf{i}_{LPHASE}$)

.pro(p_{GDIST} , $\mathbf{i}_{GDIST}$. $\mathbf{i}_{LPHASE}$) .inh(h_{GPROX} , $\mathbf{i}_{GPROX}$. $\mathbf{i}_{LPHASE}$)

K_{knor} = 0.01

The resultant shape of the model is rounded and flattened laterally with the replum central to the flattened face. The model has a flattened cross section by 8 DAI. For the early stages of growth the model predicts that the clones induced at 0 DAI and grown to 8 DAI would be narrow in the replum, like *Arabidopsis* and *Capsella*, anisotropic along the proximodistal axis in the valves and more elongated in the midvalve region. The anisotropic clones in the early phase are due to $\mathbf{i}_{EPHASE}$ promoting K_{par} from 0-2 DAI. To my knowledge no one has studied the growth dynamics in *Lepidium* so it is difficult to say if there is an early phase of high K_{par} in Lepidium. The model also predicts that the clones would splay out towards the middle and converge towards the style. For the later stages the model predicts that clones induced at 8 DAI and grown to 15 DAI would be isotropic in the valves, anisotropic along the proximodistal axis in the replum and midvalves.

Fruits can also be flattened laterally for example *Alyssum linifolium* have rounded fruits like *Lepidium* however the replum is on the ridge equivalent to the midvalve in *Capsella* and *Lepidium*. It has been observed that fruits of *A. linifolium* are rounded in cross section before fertilisation (Figure 4.18C) and then after fertilisation become flattened medially (Figure 4.18D). Since, promoting K_{par} in the midvalve by varying $p_{MIDVALVE}$ has a large effect on the flattening the model laterally, to flatten the model medially I explored the effect of promoting K_{par} in the replum only by $\mathbf{i}_{LPHASE}$. Terms highlighted in blue were reduced to 0 for this model compared to the *Capsella* fruit model:

K_{par} = 0.014 .pro(p_{EPHASE} , $\mathbf{i}_{EPHASE}$) .inh(h_{BASE} , $\mathbf{i}_{BASE}$. $\mathbf{i}_{MPHASE}$) .pro($p_{MIDVALVE}$, $\mathbf{i}_{MIDVALVE}$. $\mathbf{i}_{MPHASE}$)

.pro($p_{GMIDVALVE}$, $\mathbf{i}_{GMIDVALVE}$. $\mathbf{i}_{LPHASE}$) .inh(h_{BASE} , $\mathbf{i}_{BASE}$. $\mathbf{i}_{LPHASE}$) .inh(h_{STYLE} , $\mathbf{i}_{STYLE}$. $\mathbf{i}_{LPHASE}$)

.inh(h_{GDIST} , $\mathbf{i}_{GDIST}$. $\mathbf{i}_{LPHASE}$) .pro(p_{GPROX} , $\mathbf{i}_{GPROX}$. $\mathbf{i}_{LPHASE}$) .pro(p_{REP} , $\mathbf{i}_{REP}$. $\mathbf{i}_{LPHASE}$)

K_{per} = 0.0125 .inh(h_{STYLE} , $\mathbf{i}_{STYLE}$. $\mathbf{i}_{MPHASE}$) .inh(h_{BASE} , $\mathbf{i}_{BASE}$. $\mathbf{i}_{MPHASE}$) .inh(h_{REP} , $\mathbf{i}_{REP}$. $\mathbf{i}_{MPHASE}$)

.inh($h_{MIDVALVE}$, $\mathbf{i}_{MIDVALVE}$. $\mathbf{i}_{MPHASE}$) .inh($h_{MIDVALVE}$, $\mathbf{i}_{MIDVALVE}$. $\mathbf{i}_{LPHASE}$)

.inh(h_{STYLE} , $\mathbf{i}_{STYLE}$. $\mathbf{i}_{LPHASE}$) .inh(h_{BASE} , $\mathbf{i}_{BASE}$. $\mathbf{i}_{LPHASE}$) .inh(h_{REP} , $\mathbf{i}_{REP}$. $\mathbf{i}_{LPHASE}$)

.pro(p_{GDIST} , $\mathbf{i}_{GDIST}$. $\mathbf{i}_{LPHASE}$) .inh(h_{GPROX} , $\mathbf{i}_{GPROX}$. $\mathbf{i}_{LPHASE}$)

K_{knor} = 0.01

Where p_{REP} is the amount of promotion by $\mathbf{i}_{REP}$. This function can be simplified to:

K_{par} = 0.014 .pro(p_{EPHASE} , $\mathbf{i}_{EPHASE}$)

.inh(h_{BASE} , $\mathbf{i}_{BASE}$. $\mathbf{i}_{MPHASE}$)

.inh(h_{BASE} , $\mathbf{i}_{BASE}$. $\mathbf{i}_{LPHASE}$) .inh(h_{STYLE} , $\mathbf{i}_{STYLE}$. $\mathbf{i}_{LPHASE}$) .pro(p_{REP} , $\mathbf{i}_{REP}$. $\mathbf{i}_{LPHASE}$)

K_{per} = 0.0125 .inh(h_{STYLE} , $\mathbf{i}_{STYLE}$. $\mathbf{i}_{MPHASE}$) .inh(h_{BASE} , $\mathbf{i}_{BASE}$. $\mathbf{i}_{MPHASE}$)

.inh(h_{STYLE} , $\mathbf{i}_{STYLE}$. $\mathbf{i}_{LPHASE}$) .inh(h_{BASE} , $\mathbf{i}_{BASE}$. $\mathbf{i}_{LPHASE}$) .inh(h_{REP} , $\mathbf{i}_{REP}$. $\mathbf{i}_{LPHASE}$)

The resultant shape is rounded by 8 DAI and the model predicts that the clones are anisotropic along the proximodistal axis across the valves (Figure 4.18G). Again this is due to the effect of $\mathbf{i}_{EPHASE}$. This model predicts that clones would be similar in size and shape across the whole gynoecium (replum, midvalve and valves) before fertilisation (Figure 4.18G), unlike the laterally flattened model where clones in the replum and midvalve are narrower compared to the valves (Figure 4.18E).

From 8 to 15 DAI the model becomes flattened medially with the replum on the ridge (Figure 4.18H). The model predicts that the clones would be similar in a medially flattened fruit and a laterally flattened fruit in the valves in the later stages (Figure 4.18F,H).

In both laterally and medially flattened models in the later phases there is a bulging out of the model near the base which is not seen in the fruits (Figure 4.18Fii,Hi). This may be resolved by searching for better parameters although I did not have time to investigate this. Also in the fruit the septum links the two sides of the fruit together and may hold the two valves together. This cannot be investigated in this model as it would require a volumetric 3D modelling framework.

In summary, by promoting Kpar in the replum region instead of the midvalve region the orientation that the fruit is flattened is changed from lateral to medial. In different species the time that the gynoecium or fruit becomes flattened varies from before fertilisation in *Lepidium* to after fertilisation in *Alyssum*. By using $\mathbf{i}_{MPHASE}$ and $\mathbf{i}_{LPHASE}$ to control

parameters it is possible to separate these pre and post fertilisation growth patterns that are also evident in *Capsella*.

Simplified versions of the model developed for *Capsella* can generate fruit shapes that are comparable with fruit shapes observed in the Brassicaceae. To test the model predictions it would be necessary to have a clonal analysis system in species with different fruit shapes. Lukasz Langowski in the lab is currently trying to transform *Lepidium campestre* with the *BOB Cre* recombinase system.

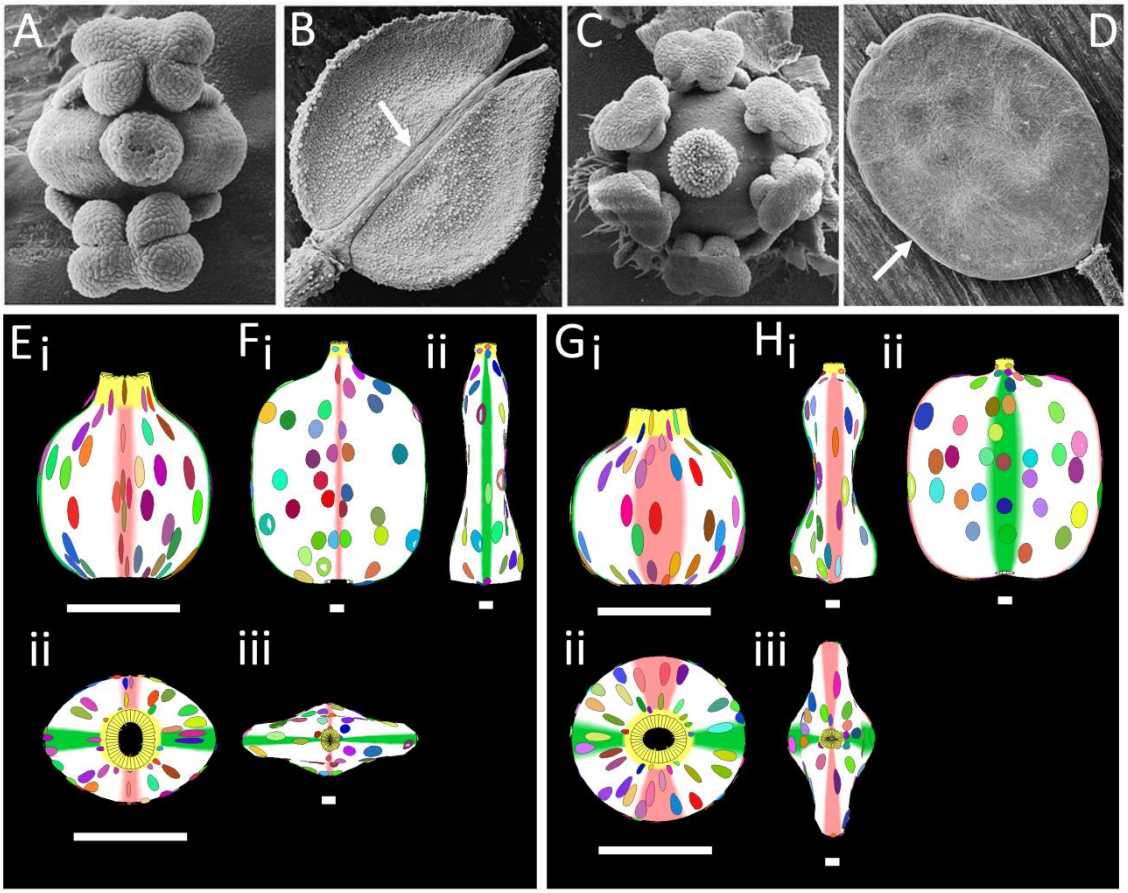

Figure 4.18 Models of fruit flattened laterally and medially (A) *Lepidium fasciculatum* gynoecium is flattened laterally before fertilisation. (B) *Lepidium phlebopetalum* fruit is flattened laterally at maturity. (C) *Alyssum linifolium* gynoecium is rounded before fertilisation. (D) *A. linifolium* fruit are flattened medially at maturity. White arrows indicate the position of the replum. (E-H) Resultant shapes and clone patterns of laterally flattened model at 8 DAI (E) and 15 DAI (F) and medially flattened model at 8 DAI (G) and 15 DAI (H). Clones induced at 0 DAI (E,G) and 8 DAI (F,H). Yellow: style, pink: replum, green: midvalve. (A-D) taken from Bowman 2006. Scale bars 500µm

4.3 Discussion

This study has provided a dynamic morphological comparison of fruit and gynoecium development between: *Arabidopsis thaliana* and *Capsella rubella*. Three phases of fruit growth have been identified in *Capsella*. The early phase is shared with *Arabidopsis*: where growth parallel to the polarity is greater than growth perpendicular to the polarity. During the middle and late phases of growth the *Capsella* fruit generates a snuff-bottle shape and then a heart-shape through higher growth perpendicular to the polarity. The cylindrical shape of the *Arabidopsis* fruit is maintained by lower growth rates perpendicular to the polarity.

To understand the genetic component that causes the difference in fruit shape between *Arabidopsis* and *Capsella* I investigated the coding sequence of *FUL*. *FUL* is important for the formation of the elongated silique of *Arabidopsis* and the heart-shape fruit of *Capsella*, but may not be important for the difference between the two.

The model for *Capsella* fruit development has provided a framework to understand the key features of fruit growth. By simplifying the model it has been possible to generate a range of different fruit forms in the Brassicaceae family including the long thin siliques of *Arabidopsis* and the round flat fruit of *Lepidium*.

4.3.1 Regional differences in growth

Arabidopsis and *Capsella* have very different fruit shapes. However, the structure of the fruits is very similar. The replum and the style have a similar growth pattern in both species. *BP* and *RPL* are likely to control this conserved pattern of growth in the replum (Gonzalez-Reig et al., 2012). Expression and function of the transcription factor *RPL* are conserved in the Brassicaceae (Arnaud et al., 2011). The style has such an essential role in catching pollen and providing an environment for pollen tubes to grow, it is unsurprising that there is little variation in the development between closely related species.

The valves show the greatest variation in growth patterns between the species. However, a pattern common to the *Arabidopsis* and the *Capsella* gynoecia is that growth rates are relatively uniform across the whole organ. This differs from leaf development where the base of the leaf grows more than the tip, leading to larger clones near the base (Kuchen et al., 2012). This difference may be due to selective constraints on the different organs. The leaf needs to be photosynthetically active from an early stage, the tip of the

leaf rapidly differentiates as it is exposed, slowing down growth (Andriankaja et al., 2012). The gynoecium is protected within the flower bud and has to rapidly generate a structure that can protect the ovules and seeds. The entire gynoecium becomes exposed as the flower opens and differentiation can be more uniform. This may allow a more uniform growth rate across the gynoecium/fruit.

4.3.2 Starting shape

The gynoecium primordia of *Capsella* and *Arabidopsis* are very similar with an oval shaped ridge which early on in development grows into a cylinder. This shape is likely to be common throughout the Brassicaceae family and is at least also common in *Lepidium* (Bowman, 2006). This starting primordium shape is common for organs that have to enclose or protect organs. For example in maize the leaf primordium begins as a ring around the vegetative meristem and as it grows encloses and protects the younger leaves which develop in the middle (Scanlon et al., 1996). The gynoecium primordium also grows as a ring to enclose and protect the developing ovules in the centre. Since this starting shape is tightly linked with the function of the organ it constrains the shape of the fruit.

Although there are many divergent fruit forms in the Brassicaceae there is a general pattern of either long and thin or rounded fruits. It is probable that the starting shape of the gynoecium primordium and gynoecium function constrains the fruit to these major forms. For example, many species in the Brassicaceae can have complex leaves with many leaflets and serrations along the leaf margin (Sicard et al., 2014; Vlad et al., 2014). The leaf primordium is a dome shape and the margin can grow more or less to give rise to this complexity (Kuchen et al., 2012; Vlad et al., 2014). In the fruit primordium, the leaf margin is equivalent to each of the carpels valve margin or replum, which are united together. This is likely to constrain the complexity of shape that can be generated along this margin compared to leaves and petals.

4.3.3 Multiple phases

In models for each *Capsella*, *Arabidopsis* and the flattened fruit there are three phases: $\mathbf{i}_{EPHASE}$, $\mathbf{i}_{MPHASE}$ and $\mathbf{i}_{LPHASE}$. In *Capsella* and *Arabidopsis* there is evidence for an $\mathbf{i}_{EPHASE}$ from the initially high growth rate in length. $\mathbf{i}_{MPHASE}$ is transient in the model. In the *Arabidopsis* model $\mathbf{i}_{MPHASE}$ and $\mathbf{i}_{LPHASE}$ interact in the same way to other factors and so it is not necessary to have both. In the same way in the clonal analysis it is not possible to separate a middle phase and a late phase in growth patterns. However, when the fruit is

not fertilised growth of the fruit is stunted (Vivian-Smith et al., 2001) and a late phase is more obvious. In many other species in the Brassicaceae, such as *Capsella* and Alyssum the late phase is highlighted by altered growth patterns (Bowman, 2006). The switch to late phase probably occurs in all species and some species have used this genetic switch to alter fruit morphology, creating more fruit form diversity.

4.3.4 FUL protein activity

I investigated *FUL* as a factor that could be important for the differences in fruit shape observed in *Arabidopsis* and *Capsella*. The activity of *FUL* can alter fruit shape, this has been demonstrated in *Arabidopsis* by tagging *FUL* with the viral constitutive activator VP16 (Christina Ferrándiz unpublished data). A positive result in the complementation experiments would have been an altered shape in *atful-2* fruit expressing *CrFUL* and *crful-1* plants expressing *AtFUL*.

In sequence comparisons orthologs of *CrFUL* in *Arabidopsis* and Brassica are highly conserved apart from the C-terminal domain of the proteins. This region is known to interact with activators of transcription and influence the activity of MADS box transcription factors (Kaufmann et al., 2005). A change in protein sequence in one MADS box transcription factor *SHP* in *Medicago spp.* has been correlated with the divergent fruit morphologies curled or straight pods (Fourquin et al., 2013). A sequence difference in the C-terminal domain protein confers greater protein activity from species that have curled fruits. The amino acid substitution that affects protein activity in *SHP* is in the same region that is divergent in *Capsella* compared to other Brassicaceae species. Therefore, the sequence divergence of *CrFUL* may have an effect on protein activity. However, sequence differences between the coding regions of *AtFUL* and *CrFUL* did not affect fruit morphology in complementation tests. This negative result shows that the *FUL* protein sequence differences do not drive the differences in fruit shapes between *Capsella* and *Arabidopsis. FUL* from both species can rescue fruit shape phenotypes of the complementary mutants showing that its role is convserved between the species. It does not discount that expression patterns may play a role in shape differences.

FUL has a differential effect on orientations of growth dependent on the background it is in. It is not clear if FUL has a differential effect on the orientation of growth in *Arabidopsis* and *Capsella* due to direct interactors or if it just expands a pre-pattern laid down in early stages of development. In either, proximodistal elongation of cells in

Arabidopsis or Mediolateral elongations of cells in the distal half of *Capsella*, FUL seems to have a differential effect on the cellular axis. This suggests that the targets of FUL modulating anisotropy by weakening or strengthening cell walls relative to one another. *FUL* genes have been implicated in cell wall modifications: in tomato over expression of *FUL2* alters levels of expansin, plant cell wall modifying enzymes (Wang et al., 2014).

4.3.5 FUL expression

Differences in expression patterns of *FUL* may underlie the differences in fruit shape between *Capsella* and *Arabidopsis*. Evidence that *FUL* expression can alter fruit shape comes from tomato where over expression of *FUL2* generates pointed fruit (Wang et al., 2014). However, *FUL* overexpression lines in *Arabidopsis* and *Brassica juncea* does not show any fruit shape phenotypes but fail to specify valve margin identity (Ferrandiz et al., 2000; Ostergaard et al., 2006).

In *Arabidopsis* the *FUL* is expressed throughout in the gynoecium primordium and in the valves of the gynoecium throughout development (Figure 4.19A,B). However, a phenotype of the mutant is not observed until just before fertilisation. By fertilisation a bipolar expression pattern, with high expression at the top and base of the valves (Figure 4.19C), has been reported for *FUL* in *Arabidopsis* by promoter GUS fusions (Woods, 2010). *CArG* boxes and *AuxRE* elements in the promoter (3.9kb) drive this bipolar expression and removal of any one of these elements results in expression along the whole length of the valve. Mutation of both *CArG* boxes resulted in no expression of *FUL* in the valves (Woods, 2010). However, protein localisation experiments with a reduced promoter (2kb) that did not include either *CArG* box show protein localisation across the entire valve (Urbanus et al., 2009). As the protein localisation of *FUL* with the entire 3.9kb promoter has not been studied it is difficult to say if *FUL* protein has a bipolar localisation. Using a 2kb promoter driving *gFUL:GFP* fusion rescues the *ful-1* phenotype (Urbanus et al., 2009) and this was the reason for choosing the promoter for this study. Retrospectively it may have been more informative to use the entire 3.9kb promoter to elucidate if *FUL* expression had a role in fruit shape.

Many attempts were made to clone the *Capsella FUL* promoter with no success. A golden gate cloning system was designed to test the expression pattern of *pCrFUL:CrFUL:GFP* but this was not completed on time and is an on-going study of the lab.

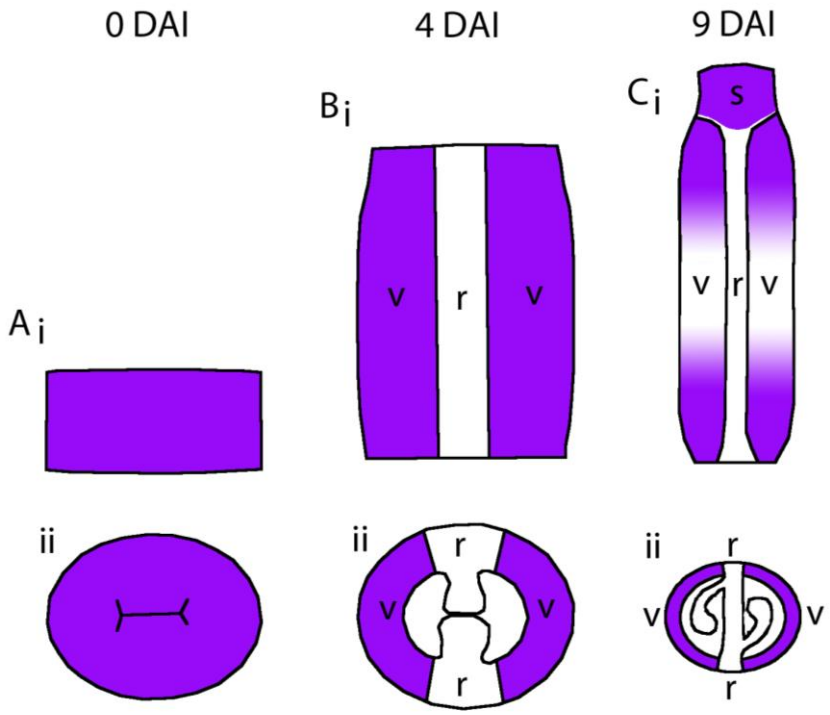

Figure 4.19 Schematic of *FUL* expression at different stages of *Arabidopsis* gynoecium development. (A) At 0 DAI (stage 6) *FUL* is expressed across the whole gynoecium primordia. (B) At 4 DAI (stage 8) *FUL* expression is restricted to the valves. (C) At 9 DAI (stage 13, anthesis) *FUL* expression shows a bipolar pattern in the valves and is expressed in the style. Above: longitudinal view, Below: cross section view, Purple regions: *FUL* expression, v: valve, r: replum, s: style. (A,B) Figure adapted from Ferrandiz et al 1999 and (C) from Woods 2010

4.3.6 Modelling FUL

In Chapter 3, *FUL* was discussed as a potential candidate for $\mathbf{i}_{LPHASE}$ by being required to switch growth rates and orientations in the *Capsella* model. However, the expression pattern of *FUL* in *Arabidopsis* (Figure 4.19) does not match an expected expression pattern of a factor only acting in $\mathbf{i}_{LPHASE}$. In the *Arabidopsis* model $\mathbf{i}_{LPHASE}$ is require to switch growth rates in the late phase but orientations are not switched as $\mathbf{i}_{GDIST}$ and $\mathbf{i}_{GPROX}$ are set to 0. However, the interaction of $\mathbf{i}_{LPHASE}$ and $\mathbf{i}_{GDIST}$/$\mathbf{i}_{GPROX}$ are maintained in the model. This means that $\mathbf{i}_{LPHASE}$ from both models has the same role. The complementation experiments support *FUL* as a candidate for or to interact with $\mathbf{i}_{LPHASE}$ as *FUL* from both species can complement the mutant phenotype of the other species.

In *Arabidopsis*, the bipolar expression pattern of *FUL* does not seem to have any effect on growth as the clones reveal uniform growth across the valves. In *Capsella* this

bipolar expression may have been exploited by different interactions with *FUL* to generate the heart-shape fruit.

Since, *FUL* has a bipolar expression pattern an alternative is that *FUL* is a potential candidate for or interacting with $\mathbf{i}_{GDIST}$ and $\mathbf{i}_{GPROX}$. *FUL* could play a role to activate $\mathbf{i}_{GDIST}$ and $\mathbf{i}_{GPROX}$ in the presence of $\mathbf{i}_{LPHASE}$.

4.3.7 Evolutionary origin of the heart-shaped fruit

Capsella is a member of the Camelineae tribe which also contains *Arabidopsis*, *Neslia*, *Catolobus* and *Camelina* (Al-Shehbaz et al., 2006; Gupta, 2009). In multiple phylogenetic analysis the genus *Neslia* has grouped together with *Capsella* (Bailey et al., 2006). Although little work has been done on the development of *Neslia* fruit it is clear from pictures that superficially they have many similarities to *Capsella* (www.agroatlas.ru). The fruits are silicles, spherical in shape and slightly compressed laterally (Francis and Warwick, 2003). The nearest relative to *Capsella* seems to be *Catabolus pendula*, which has elongated siliques that are flattened medially (Al-Shehbaz et al., 2006). This is just one example of the evolutionary plasticity of fruit shape within the family.

In phylogenetic analysis the nearest extant ancestoral genre to the Brassicaceae family is *Aethionema*. The split between *Aethionema* and the core Brassicaceae occurred between 15-60 mya (Franzke et al., 2011). Members of the *Aethinema* have flattened rounded fruit with wings. Many of them contain two seeds per pod. This suggests that the ancestoral state of Brassicaceae fruit is round and flat and the other fruit shapes evolved from this ancestoral shape It would be interesting to carry out a clear comparison of fruit shapes of the basal members of the Brassicaceae to investigate this hypothesis. However, the resolution of the early divergent Brassicaceae is still unclear.

Modelling fruit shape in GFtbox has shown that to generate the fruit form of *Capsella,* extra growth interactions have to be added with $\mathbf{i}_{GDIST}$ and $\mathbf{i}_{GPROX}$ compared to other Brassicaceae species. Therefore, the Capsella fruit is a more elaborate form of the basic underlying mechanisms of fruit development in the Brassicaceae. A possible intermediate evolutionary phase between long fruit and heart-shaped fruit is rounded. It would be interesting to characterise *N. microcarpa* gynoecium and fruit development to understand if this rounded form has similarities in development to the heart-shape fruit of *Capsella*.

4.3.8 Flattening the fruit

Fruit of the Brassicaceae can be flattened laterally, perpendicular to the septum (augustiseptate) or medially, parallel to the septum (latiseptate). The evolution of latiseptate fruit has occurred at least 23 times independently in the Brassicaceae (Al-Shehbaz, 2003). This apparent evolutionary plasticity between the two forms suggests the trait could be under a simple genetic control.

In the models, shapes could be generated that were flattened in either orientation by having higher K_{par} in the midvalve region or in the replum region relative to the valves. The replum and the valves are under distinct genetic control: in *ful* the valves do not expand, the replum continues to elongate, bulges out and forms a zigzag pattern of cells (Gu et al., 1998). This potentially could be the reason for the rounded cross section shape. If so, this shows that the relative growth rates in the replum and valve are important for maintaining the orientation the fruit is flattened in.

REPLUMLESS (*RPL*) is a factor important for establishing the replum in *Arabidopsis* and Brassica species (Arnaud et al., 2011; Roeder et al., 2003). In *Arabidopsis*, *rpl* fruit have a wildtype cross section shape (Roeder et al., 2003) as the fruit is partly flattened laterally the removal of the replum would not be expected to alter fruit flatness. It would be interesting to identify *rpl* alleles in the species that are flattened medially such as *Alyssum linifolium* as the removal of the replum would likely have more of an effect on the cross section shape of the fruit.

4.3.8.1 Comparing leaves and fruits

Since the evolutionary origin of the carpel is thought to be a leaf like structure, it is possible to compare the tissues and growth of the leaves and gynoecium. The valves, replum and midvalve of the fruit are analogous to the lamina, leaf margin and midvein of the leaf, respectively. Also the Arabidopsis leaf is thought to have a proximodistal polarity field (Kuchen et al., 2012). In a mutant of *PEAPOD* (*PPD*) there is more growth in the lamina of the leaf and midvein (White, 2006) which causes the leaf to curl over and produce a dome-shaped leaf. If two of these leaves were joined together, like the gynoecium, you would expect the midveins to protrude out, like the midvalve in the Capsella fruit. Interestingly the fruits of *ppd* are more flattened than wildtype *Arabidopsis* fruit (White, 2006).

In the leaf if there is higher growth along the leaf margin, the leaf becomes wrinkled at the edges such as in *jaw-D* mutants of *Arabidopsis* (Palatnik et al., 2003). This is similar to lily petals which are wrinkled at the edges of the petals due to higher growth in this region (Liang and Mahadevan, 2011). If the leaves with higher growth along the leaf margin were united like the gynoecium, you would expect the margins would protrude out like the replum does in *Alyssum* fruit.

In the leaf and petals the relative growth of the lamina, leaf margin and the midvein are important for the 3D shape of the organs (Liang and Mahadevan, 2009; Liang and Mahadevan, 2011). Also, relative growth rates and orientations in the comparable tissues; valve, replum and midvalve are also important for generating the 3D form of the fruit.

During this work I have made a comparative analysis of fruit growth in *Arabidopsis* and *Capsella*. There are similarities in the growth phases and regional growth patterns in the replum and the style between the two species. Much of the difference in fruit shapes is driven by growth in width or in the model K_{per}. *FUL* protein was investigated as a genetic factor that is important for the fruit shape differences between species but has been ruled out as the direct genetic control of this phenotypic difference. By simplifying the *Capsella* fruit model it has been possible to explain the clone patterns of *Arabidopsis* and make predictions of how other fruit shapes in the Brassicaceae are generated.

5. Discussion

5.1 Summary of work

In this work I have used whole organ growth dynamics and clonal analysis to understand regional growth patterns to generate a model of fruit growth for *Capsella rubella*. This model has shown how orientations of growth relative to a polarity field change through time to generate the morphological features of the *Capsella* fruit. The growth can be divided into three phases: an early phase where growth is parallel to the polarity, a middle phase where growth is more isotropic and the late phase where near the base growth is orientated parallel to the polarity and at the distal half growth is orientated perpendicular to the polarity. Simplifying this model can generate models for divergent fruit forms such as *Arabidopsis thaliana* and *Lepidium campestre.*

Factors important for the development of the heart-shaped fruit of *Capsella* were investigated by forward and reverse genetics. Three alleles of *ful* were identified which can no longer produce a heart-shaped fruit. *CrFUL* is important in the third phase of growth leading to the hypothesis that *FUL* could be or interact with $\mathbf{i}_{LPHASE}$ in the model, which is important for switching growth orientations and rates in the late phase of growth. *FUL* was also investigated in the context of evolution by a complementation study. Sequence differences in the *FUL* coding region are not sufficient to drive heart-shaped fruit in *Arabidopsis* and cylindrical fruit in *Capsella*.

Altogether, I have used an integrated approach by combining imaging, growth analysis, genetics and computational modelling to generate hypothesis for how divergent fruit forms are generated in the Brassicaceae.

5.2 Validity of computational models

The three dimensional structure of the fruit is modelled as a continuous sheet divided into finite elements for computational purposes. Computational power is saved by ignoring the large number of cells that make up the fruit at later stages and allows growth to be captured at a tissue level. Generalising tissues as a continuum is validated by observations of spatial distributions of growth rates where growth rates are relatively uniform within regions of a tissue (Kuchen et al., 2012; Kwiatkowska and Dumais, 2003; Schmundt et al., 1998). Also, plant cells are mechanically constrained by the neighbouring cells due to the tight junctions between the cell walls. These observations suggest that

plant tissues can be treated as a continuum (Silk and Erickson, 1979). Introducing cells into the model could potentially have some interesting results as shown by Bassel et al 2014 where cell geometries direct genetically driven growth. Cell shapes in the shoulders of the heart on *Capsella* may influence the protrusion of the outgrowths. However in order to introduce cells it would be necessary to generate a clear map of cells across the whole gynoecium.

Treating plant tissues in a continuum in this way has allowed the generation of models for the development of the *Arabidopsis* leaf and petal (Kuchen et al., 2012; Sauret-Gueto et al., 2013). Both of these organs could be considered as a two-dimensional structure, the fruit is a more three-dimensional volumetric structure. However, the fruit has been modelled as a 2D sheet that deforms in 3D. The two fused carpels that make up the gynoecium/fruit in Brassicaceae are thought to originate from leaf-like structures that are congenitally united to produce the gynoecium. There is mounting genetic evidence to support this hypothesis such as leaf margin genes expressed at the valve margins (Moubayidin and Ostergaard, in revision) and lateral factors expressed in the valves (Gonzalez-Reig et al., 2012). This supports the hypothesis that the valves, which make up the majority of the fruit area, could be considered as 2D sheets similar to the leaf and petal. The medial tissue of the fruit, including the style, septum and ovules are perhaps not accurately portrayed in the 2D modelling framework as considerable growth occurs in a different plane, internally to the fruit. Modelling the full 3D structure of the fruit including the internal structures could potentially influence the medial region (style, replum and septum). During the development of the gynoecium, the septum grows and fuses between the two repla. This may influence the flatness of fruit as it could pin the medial region together in laterally flattened fruit or growth in this region could push the medial region out in medially flattened fruit. Nevertheless, much of the fruit growth could be explained using a 2D modelling framework that deforms in 3D.

Another simplification of the modelling framework is to generalise factors that control growth and polarity. The roles of the factors in the model are likely to be carried out by many genetic components in the fruit. Several components of fruit growth and patterning have been described in a genetic network (Gonzalez-Reig et al., 2012; Roeder and Yanofsky, 2006) and could be incorporated into the model. However, by abstracting from the specific genetic components this has allowed the core mechanisms controlling fruit shape to be explored without the complication of many genetic interactions. Also in

Capsella, there is little known about the genetic pathways that control fruit development and so genetic interactions would have to be assumed from *Arabidopsis*.

5.3 Polarity in the fruit

In the *Arabidopsis* gynoecium there is evidence of a distal organiser of polarity at the distal end of the gynoecium as there is high expression of the auxin response marker *DR5rev::GFP* at the apex (Girin et al., 2011) as well as high *PIN3* expression (Moubayidin and Ostergaard, in revision). The polarity field is directly parallel with the proximodistal axis of the organ (Grieneisen et al., 2013). The clones reveal this by also aligning parallel with the long axis of the fruit. The polarity field does not deform much as the *Arabidopsis* fruit grows as the cylindrical shape parallel to the proximodistal axis (K_{par}) throughout development. This is a very simple pattern of growth and polarity.

In *Capsella* the interaction of polarity and growth is more complex to understand. Due to the boosted K_{per} (growth perpendicular to the polarity), the polarity field deforms with the tissue and splays out before converging back at the style. It is likely that this diverging and then converging polarity field is a prerequisite for the formation of the heart as it feeds back to K_{per} no longer being exactly perpendicular to the long axis of the gynoecium. This gives a potential angle for the shoulders to form. Therefore, the shoulders form by the polarity field changing by deformation with the growing tissue and the organisers of polarity remain constant (Figure 5.1A,B).

An alternative hypothesis, which has not been explored in this work, is that the polarity field could change through a new organiser of polarity in a broad region in the midvalves. Auxin is generally thought to be critical in the organisation of tissue polarity (Benkova et al., 2003; Heisler et al., 2005; Petrasek and Friml, 2009). and so you would possibly expect *DR5rev::GFP* and *PIN* expression (Sauret-Gueto et al., 2013) in the presumptive shoulder or midvalve region in this hypothesis (Figure 5.1C,D). The explanation for the clonal patterns in this hypothesis would be K_{par} is greater than K_{per} as the polarity would diverge out towards the midvalve. A short coming of this work is that *PIN* localisation has yet to be studied in the context of the *Capsella* gynoecium. Addressing this would validate one of these hypotheses.

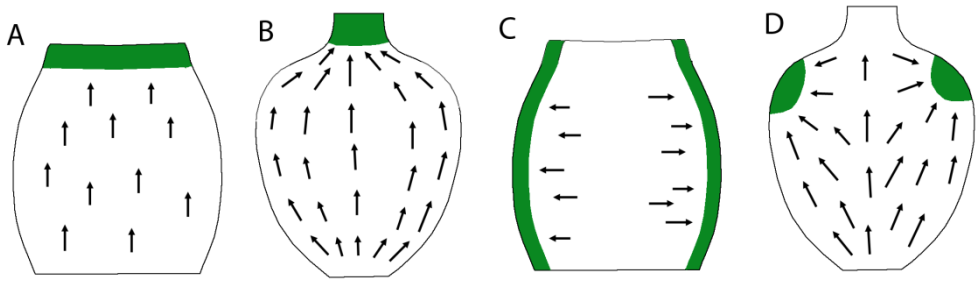

Figure 5.1 Alternative models of polarity organisation in Capsella (A, B) proximodistal organisation of polarity. (C) mediolateral organisation of polarity, with polarity diverging towards midvalve region. (D) Organiser of polarity in the presumptive shoulders. Green represents the expected pattern of *DR5rev::GFP* expression.

At the beginning of this work, and in previous studies, the fruit was described as growing along three straight axes: the proximodistal, mediolateral and ab-adaxial axes. However, growth does not occur in straight lines and becomes complicated to explain. For example, in the late phase of growth, clones in the Capsella fruit are elongated along the mediolateral axis but are not exactly parallel to the mediolateral. Instead the clones are orientated towards the shoulders of the heart. Therefore, perhaps a more natural description of growth is to consider the internal polarity field. As the polarity field deforms with the growing tissue, describing growth as parallel or perpendicular to this polarity field is a more accurate explanation of the growth patterns observed in the fruit.

5.4 Structure of the fruit

There is a vast diversity in fruit shape in the Brassicaceae, however the structural components of the fruit almost invariable. The two valves are joined to a central replum which is generally a narrow strip of tissue connecting the base of the gynoecium to the style. I have shown that in two divergent fruit forms, *Capsella* and *Arabidopsis*, the growth of the replum and the style is very similar.

Mutants that do not produce a replum in *Arabidopsis* are similar in shape fruit to wildtype (Arnaud et al., 2011; Roeder et al., 2003). However, mutants that have defects in the style have many morphological abnormalities including longer gynophores, an open apex and smaller valves (Alvarez et al., 2009; Sohlberg et al., 2006; Trigueros et al., 2009). This is possibly due to the disruption of the polarity organiser at the distal end of the gynoecium (Moubayidin and Ostergaard, in revision) which would affect polarity and growth orientations not only in the style region but the rest of the gynoecium. Also, in the

Capsella model the style provides a constriction point at the apex and this is very important for the final fruit shape.

The majority of differences in fruit shape in the Brassicaceae can be explained by differences in relative growth rates parallel or perpendicular to the polarity field in the valve tissue. This evolutionary plasticity of the shape may relate to the seed dispersal methods of the species, which would be under selective pressures in different environments. There is no agreed hypothesis as to why the *Capsella* fruit is heart-shaped; the shoulders are hollow as the seeds are all lined up down the septum. It could be speculated that it has a function in seed dispersal; the pods need a good knock for the valves to dehisce and it may provide a larger surface area for agitation. The heart-shape of the fruit equally may confer no selective advantage and may be a consequence of flattening the fruit. There are no functional studies available to test these hypotheses.

5.6 *FUL*

FUL and FUL-like proteins have been found in all families of Angiosperms, right back to the basal angiosperms (Pabon-Mora et al., 2014). In the core eudicots *euFUL* is important for the development of the fruit wall in the dry fruit species *Arabidopsis*, *Antirrhinum*, *Nicotiana* and *Brassica* (Gu et al., 1998; Muller et al., 2001; Ostergaard et al., 2006; Smykal et al., 2007) as well as fruit ripening and colouration in fleshy fruit species Tomato, peach, Bilberry and apple (Cevik et al., 2010; Dardick et al., 2010; Jaakola et al., 2010; Wang et al., 2014). In basal eudicots *FUL-like* genes are also important for fruit wall development. *FUL-like* genes are also expressed in the fruit of early divergent angiosperms and it has been suggested that the advent of *FUL* was integral to the evolution of fruit in the angiosperms (Pabon-Mora et al., 2014).

5.7 Modelling loop

During this work I have used clonal patterns to make predictions of the specified growth that underlies the resultant orientations and sizes of the clones. I have tested these predictions in the GPT framework and generated models of the *Capsella* and *Arabidopsis* fruits. If the models are accurate and robust, they should be able to make predictions and generating hypothesis that can be tested experimentally. Experimental results should be fed back into the model, validating or disproving certain aspects to improve the model. This is a continual loop of hypothesis driven research is often limited by the experimental data

that can be collected. However, it provides a good framework in which to design focused experiments to answer the important questions.

5.8 Future Directions

The work described in this study has helped develop hypothesis through experiments and computational modelling on the evolution and development of fruit shape. The modelling has highlighted some important questions that I would like to answer in future experimental work:

The *Capsella* fruit model generated a key prediction that relatively higher K_{par} in the midvalve region is necessary to flatten the fruit. Experimentally this can be tested by collecting clone data for this region. It has been difficult to image the midvalve region when imaging the gynoecia and fruits under coverslips. However, imaging with a dipping lens on the confocal microscope gives the possibility of imaging this region. I have made a preliminary attempt at this method and would like to image many samples to calculate if the clones are significantly longer along the proximodistal axis in this region.

It would be interesting to generate an alternative model, exploring different patterns of polarity organisers. Specifically to test if clonal patterns can be explained through an organiser of polarity in the midvalve region. I have attempted this type of model, without success. However, it would be necessary to try a larger array of parameters to rule out if organisers of polarity have a specific role in generating the heart shape. Experimental evidence that would validate one of these models would be to look at PIN localisations and auxin signalling in the gynoecium and fruit throughout development. A *PIN1:GFP* line has been developed for *Capsella rubella* (Adrien Sicard, personal communication) and immunolocalisation studies would elucidate the localisation of other PIN proteins. This is an essential component of the *Capsella* fruit model and needs to be addressed.

I have used the model developed for *Capsella* to make predictions on growth patterns in species with different fruit shapes, such as the rounded fruit of Lepidium. Clonal analysis lines are being generated by Lukasz Langowski (a postdoc in the lab) in Lepidium and it will be an important validation of the model if clonal patterns match.

A large missing component of understanding the role of *CrFUL* in fruit shape is the analysis of the promoter and expression patterns. Cloning *pCrFUL* has been problematic,

synthesising the promoter should resolve this. Alternatively *in situ* hybridisation could help resolve the expression pattern of *CrFUL*. *FUL* in the *Capsella* model could be or interact with $\mathbf{i}_{LPHASE}$ which is important for the switch in growth orientations and rates or $\mathbf{i}_{GDIST}$ and $\mathbf{i}_{GPROX}$. It is difficult to tease apart these two possibilities. In *Arabidopsis* a double mutant *ful ind* almost rescues to WT fruit length. It would be interesting to generate a *ful ind* double mutant in *Capsella* to investigate the above hypotheses. Currently *ind* alleles have been identified by TILLING (by Nicola Stacey) and crosses are being made.

Therefore, the work started here is not the end. The experimental work and computational models have generated many hypotheses that will be investigated in future work.

6. Materials and Methods

6.1 General methods

6.1.1 Plant material

6.1.1.1 *Arabidopsis*

Arabidopsis thaliana ecotype Col-0 was used in all experiments. *atful-2* mutants are in Col-0 background. Plants were grown in glasshouse conditions at ~22˚C, 16h photoperiod. Plants for clonal analysis were grown in a controlled environment rooms at 20˚C in long day conditions (8 h dark and 16 h light under fluorescent light at a photon fluence rate of 100 mmol m^{-2} s^{-1}) and 80% humidity.

6.1.1.2 *Capsella*

Capsella rubella SAS 52 seeds were kindly provided by Dr Adrien Sicard and Prof. Michael Lenhard (University of Potsdam). *C. rubella* SAS 52 line was used in all *Capsella* experiments. Plants were grown in glasshouse conditions at ~22˚C, 16h photoperiod. Plants for clonal analysis and growth curve were grown in a controlled environment rooms at 22˚C in long day conditions (8 h dark and 16 h light under fluorescent light at a photon fluence rate of 100 mmol m^{-2} s^{-1}) and 80% humidity.

6.1.2 Edwards' quick DNA extraction

One to two young leaves of the plants were collected in Eppendorf tubes. The tissue was ground using a blue plastic grinder for 15 seconds. Genomic DNA extraction buffer (200mM Tris HCL pH7.5, 250mM NaCl, 25mM EDTA, 0.5% SDS) was added to the ground tissue and vortexed for 5 seconds. This mixture was centrifuged at 13,000rpm for 1 minute. 300µl of the supernatant was transferred to a fresh Eppendorf tube and mixed with 300µl isopropanol. The mixture was left at room temperature for 5 minutes, centrifuges for 5 minutes at 13,000rpm and the supernatant was removed. The pellet was washed with 180µl 70% ethanol before a second 5 minutes centrifugation at 13,000rpm. The pellet was air dried and resuspended in 50µl H_2O and stored at -20^{o}C. (Edwards et al., 1991)

6.1.3 PCR

Generally, PCR reactions (20µl) contained 1µl taq DNA polymerase, 1xPCR buffer, 0.5mM total dNTPs, 1mM of each specific primer, 2µl genomic DNA or in the case of a colony PCR a tip touched on a colony was rubbed on the bottom of the PCR tube. PCR reactions were carried out in a G-Storm GS482 thermal cycler and amplified products were analysed by agarose gel electrophoresis.

6.1.4 Sequencing reactions

Sequencing reactions (10µl) contained 1µl DNA (approx. 50-100 ng/µl), 1µl Big Dye v3.1, 1.5µl 5x sequencing reaction buffer and 0.32µM of specific primer. Sequencing reactions were carried out in a G-Storm GS482 thermal cycler with the following cycle:

96^{o}C (1min)	x1
96^{o}C (10sec), 50^{o}C (5sec), 60^{o}C (4min)	x25
10^{o}C forever	

The reactions were sequenced by eurofins mwg|operon.

6.1.5 RNA extraction and cDNA synthesis

This work was carried out by George Averill, a summer student I was partially supervising for 8 weeks. Total RNA was extracted from 2 small leaves using RNAeasy® Plant Mini Kit (Qiagen) according to the manufactures protocol. A total of 1µg of RNA was used for first-strand synthesis in a 11µl reaction volume with 1µl oligo dT (18) primers. After an incubation at 65^{o}C for 15 min, 1µl of MMLV-RT (Invitrogen), 1µl of 10mM dNTP mix, 2µl 0.1mM DTT, 4µl 2.5mM $MgCl_2$, 2µl 10x RT Buffer was added to the reaction to make a reaction volume of 20µl.This was incubated at 50^{o} for 50min and 80µl of RNAse-free water was added to the reaction mixture making 100µl of total cDNA.

6.1.6 *E. coli* heat shock and electroporation transformation

For transformation DH5α or TOP10 *E. coli* competent cells were used. Competent cells were thawed on ice for 5-10min. 1-5µl of the plasmid or DNA ligation was added to 50-100µl of competent cells, mixed gently and incubated on ice for 15min. Chemically competent cells heat shocked for 45sec at 42^{o}C and placed on ice for 2min. Electro-competent cells were placed in pre-chilled electroporation cuvette and subjected to a pulse length of 4-6ms in Biorad GenePulser (settings 2.50kV, 25µFD and 200 Ohms). In both cases

250-500µl of LB was added to the cells and incubated at 37°C for 1hr. The transformed cells were plated on selective media and incubated at 37°C overnight.

6.1.7 Agrobacterium electroporation transformation

GV3101 (25µg/ml gentamycin, 25µg/ml rifampicin) or AGL1 (25µg/ml carbenicillin, 25µg/ml rifampicin) electro-competent cells were used for transformation. After 5-10min thaw on ice 50µl of electro-competent cells was mixed gently with 50-200ng of the DNA to be transformed and left on ice for 30min. The cells were transferred to a pre-chilled cuvette and pulsed for 8-12ms using Biorad GenePulser (settings 2.50kV, 25µFD and 400 Ohms). 1ml LB was immediately added to the cells which were subsequently incubated at 28°C for 2-4hr. Transformed cells were plated on selective media (including the cell specific antibiotics and plasmid specific antibiotics) and incubated at 28°C for 2days until colonies appeared.

6.1.8 *Arabidopsis* floral dip transformation

A single colony of *A. tumefaciens* containing the plasmid to be transformed was grown in 10ml LB with the appropriate antibiotics and incubated at 28°C with 250rpm shaking for 24-48hr. 2ml of this preculture was used to inoculate 500ml LB containing appropriate antibiotics and grown overnight at 28°C until an OD_{600} >1.5 was reached. The culture was centrifuged at 5000rpm for 20min at room temperature and the pellet was resuspended in 5% sucrose to OD_{600} of approximately 0.8. Silwet L77 was added to 0.05% before dipping. Five pots containing ten plants of *Arabidopsis* were dipped in the culture for approximately 1min with some agitation. The plants were moved to containment and bagged overnight.

6.1.9 *Capsella* floral dip transformation

For transformation of *Capsella* the preculture of *A. tumefaciens* was prepared as for as *Arabidopsis* dipping. 4ml of the preculture was added to 600ml LB containing appropriate antibiotics and grown overnight at 28°C until an OD_{600} >1.5 was reached. The culture was centrifuged at 5000rpm for 20min at room temperature and the pellet was resuspended in 10% sucrose to OD_{600} of approximately 0.8. Silwet L77 was added to 0.05% before dipping. For each transformation 30-60 individual *Capsella* plants were dipped for approximately 15sec with agitation. This was repeated twice more with an interval of 4-

7days. The plants were moved to containment and bagged overnight. The method was adapted from (Bartholmes et al., 2008).

6.1.10 Screening for transformants

For *C. rubella* transformants selected for by antibiotics, 0.09g (approx. 1000) of T_0 seeds were sterilised in Eppendorf tubes in 1ml sterilisation solution (6.25mg/ml dichloroisocyanuric acid, 50% ethanol) for 15min on a rotor. Following three washes in 70% ethanol the seeds were left to air dry in a laminar flow hood. The seeds were transferred to large sterile pipette tips (1ml) and tapped over five 140mm petri dishes (~200seeds/plate) containing ½ MS media, Gibberellic acid (50µg/ml) and the appropriate antibiotics. This method of spreading the seeds was developed by Nathan Sukhnandan. This method avoids hydrating the seeds which produce a large sticky mucilage after 5 second of hydration making them difficult to spread (Deng et al., 2012). The plates were sealed with micropore tape, left at 5^{o}C for 48h before being transferred to a controlled environment room (23^{o}C, 8 h dark and 16 h light under fluorescent light at a photon fluence rate of 100 mmol m^{-2} s^{-1}).

6.1.11 Propidium iodide (PI) staining

Material was fixed in 10% acetic acid, 50% methanol and left at 5^{o}C for up to a month. After two washes with H_2O the sample was dehydrated in an ethanol series (40%, 60%, and 80%) and boiled in 80% ethanol at 80^{o}C for 10min. Following rehydration (60%, 40%, 20% ethanol, 2 x H_2O) the material was incubated overnight at 37^{o}C in alfa-amylase solution (20mM pH7 phosphate buffer, 2mM NaCl, 0.25mM Ca_2Cl, 2mg/ml alfa-amylase). The next day the material was washed (3 x H_2O) and treated with 1% periodic acid for 1h at room temperature and washed (2 x H_2O). The material was treated for 5hr at room temperature with Shiff reagent (PI) (0.33mM sodium metabisulfite, 0.5M HCl, 0.1mg/ml propidium iodide). Finally the material was washed (2 x H_2O), left at 5^{o}C overnight.

6.1.12 Optical projection tomography (OPT)

Samples were collected in 100% ethanol and stored at 4^{o}C until use, collected in water to be used immediately or stained with propidium iodide. Samples in ethanol were rehydrated in a series (80%, 60%, 40%, 20% ethanol, 2 x H_2O for 30 min each at room temperature) before being embedded in 1% low-melting-point agarose as described by (Sharpe et al., 2002). The mounted specimens were dehydrated overnight in 100% Methanol and cleared for 24h in a mixture of 1:2 benzyl alcohol and benzyl benzoate

(Sigma-Aldrich). Specimens smaller than 1cm in width were scanned with a prototype OPT device described previously by (Lee et al., 2006). Specimens between 1cm and 2cm width were scanned using a Commercial Scanner Biooptimics 3001.

To visualise the OPT scans in 3D a freely available software package VolViewer (http://cmpdartsvr3.cmp.uea.ac.uk/wiki/BanghamLab/index.php/Software#Viewing_and_measuring_volume_images:_VolViewer) was used.

6.1.13 Scanning Electron Microscopy

Samples were fixed in Formalin Acetic Acid (FAA, 50% Ethanol, 5% Acetic acid, 3.7% formaldehyde) for 24 h. The samples were washed in 50% ethanol and then dehydrated in an ethanol series (50%, 70%, 80%, 90%, 2 x 100% ethanol, 2 x 100% dry ethanol for 30 min each at room temperature). Samples were critical point dried using Leica EM CPD300. Gynoecia were dissected from dried samples and mounted on stubs for coating in gold using Agar High Resolution Splutter Coater and imaged using the Zeiss Supra 55VP FEG Scanning Electron Microscope.

6.1.14 Lignin staining

This work was carried out by André Kuhn, a Masters student I was supervising for a 10 week project. Fruits of *Arabidopsis* and *Capsella* at stage 17 were fixed in FAA and dehydrated in an ethanol series (50%, 70%, 80%, 90%, 2 x 100% ethanol for 30 min each at room temperature). The tissue was cleared with Histoclear and embedded in paraffin. The embedded material was sectioned on a RM 2255 rotary microtome (Leica). The sections were deparaffinised with Histoclear, and stained with an Alcian Blue 8GX/Safranin-O solution (0.05% Alcian Blue 8GX, 0.05 Safranin-O, 0.1 M acetate buffer, pH 5.0). I imaged the sections using Leica M205C stereo microscope.

6.1.15 Heat shocking plant inflorescences

Pots containing a single plant of either *Arabidopsis* or *Capsella* were covered in Clingfilm. A small cross-shaped hole was pierced through the Clingfilm and the young plant inflorescence (1-3cm in height) was thredded through the hole. The inflorescences were heat-shocked by turning the whole plant upside down in a 37^{o}C waterbath for varying times between 30 sec and 4 min.

6.2 Generating resources

6.2.1 Clonal analysis line in *C. rubella*

60 plants of *C. rubella* SAS52 were transformed with *pBOB* (Wachsman et al., 2011) or HS-*Cre* (Gallois et al., 2002). *pBOB* (CrBOB) and HS-*Cre* (*CrHS-Cre*) transformants were selected on methotrexate (MTX, 0.5µg/ml) or Kanamycin (Kan, 100µg/ml) respectively (T1 plants). For each construct >100,000 seeds were screened on plates. 3 individual *CrBOB* transformants and 6 individual *CrHS-Cre* transformants were identified. Therefore efficiency of Agro-transformation of *C.rubella* with *pBOB* was 0.002% and with HS-*Cre* was 0.006%.

To check if *pBOB* was expressed, the roots of transformants were screened for YFP expression. YFP was expressed with nuclear localisation in the roots of all three lines. To check if the transformants were from a single or multiple insertion events 100 T2 seeds were plated on respective selective media. If the lines are single insertion events the expected proportion of resistant plant segregating is 75%. If there has been more than one insertion event this proportion increases to more than 90%. All of the *CrBOB* and 5 of the *CrHS-Cre* transgenic lines have a single insertion of the construct.

CrHS-Cre-1 was crossed with both *CrBOB*-1 and *CrBOB*-2 as these were the first lines to mature. The F1 seeds were grown on selective media containing Kan (100µg/ml) and MTX (0.5µg/ml) for 1 week. A few of the seedlings were heat shocked in a 38˚C water bath for up to 1h. After 48h the seedlings were checked for fluorescence markers using Zeiss LSM 5 EXCITER Laser Scanning Confocal Microscope. Sectors of CFP and RFP were visible in the roots and the shoot revealing that the sector analysis line is functional. No CFP or RFP sectors were visible in the seedling that had not been heat shocked.

6.2.2 EMS mutagenesis

The EMS mutagenesis was carried out on seeds of *C. rubella* SAS52. 820mg of seeds (~10,000 seeds) were treated with 0.2%, 0.25% or 0.3% EMS diluted in 20ml of 0.02% Tween solution. The seeds were continually agitated for 18h in 50ml falcon tubes before a series of 14 x 20-minute washes with 0.02% Tween. The seeds excreted mucilage which prevented them from settling to the bottom of the tube so before each wash the seeds were spun down before the liquid could be removed. Finally the seeds were mixed with 150ml of fine vermiculite to facilitate even distribution over 348mm x 220mm seeds trays.

The seeds were sown at an approximate density of 500 seeds/tray. After 25 days 730, 898 and 770 seedlings of 0.2%, 0.25% and 0.3% EMS treatments, respectively were transferred to individual (size) compartments. Each individual M1 plant was harvested and threshed separately and given an individual line number (by myself, Pauline Stephenson, Nicola Stacey and Nathan Sukhnandan).

6.2.3 Screening for mutants

Twelve M2 plants were screened for changes in fruit shape from each M1 seed pool. Recessive mutations would be expected to segregate 1:3 so if 12 plants were grown from each M1 line there would be a 97% chance of finding at least one homozygous mutation $(1-(1-1/4)^{12})$. However, some M1 plants maybe chimeric as germline is likely formed by two cells as in *Arabidopsis*. In this case if 12 plants were grown there would be 80% chance of finding at least one homozygous mutation $(1-(1-1/8)^{12})$. Therefore ideally 22 plants should be screened to increase the probability to 95% chance $(1-(1-1/8)^{22})$. However, due to glasshouse restraints it was decided to growth 12 plants for each line. In the interest of glasshouse space and time the sowing of the M2 plants were staggered in batches of 96 lines at once and planted every 2-3 weeks.

6.2.4 Setting up TILLING platform

The TILLING platform was set up as described by Stephenson et al (2010) and modified as follows. Two M2 plants were selected and grown in pots, two young leaves were taken for DNA extraction using a DNeasy Plant 96 Qiagen kit using manufacturer's instructions (Qiagen, UK) making a total of 32 plates (by Richard Goram, JIC genotyping platform). DNA was quantified using SPECTROstar^{Nano} and normalised to 0.5ng/µl or 5ng/µl by Nicola Stacey. Four eight-pool plates were made up to a final concentration of 0.5 ng/µl or 5ng/µl (by Nicola Stacey). The M3 seeds from these lines were harvested and threshed individually (by myself, Nicola Stacey, Friederike Jantzen, George Averill and Nathan Sukhnandan).

6.2.5 TILLING

Mutation detection was carried out as described by Mutant detection was carried out using Cel1 digestion to identify DNA mismatches, followed by analysis on a capillary ABI3730 sequencer (Applied Biosystems, Foster City, California, USA) as described in (Le Signor et al., 2009). TILLING was carried out on four amplicons covering all exons of

FRUITFULL by Nicola Stacey. The corresponding lines for mutants identified by sequencing were confirmed by sequencing by Nicola Stacey. All lines tested by sequencing matched those identified by TILLING.

Name	Description	Exons covered	Sequence
FUL 1	F for 1st Amplicon	1	CCCCCACTCTGGTCTCTTCCCACTC
FUL 1	R for 1st Amplicon	1	GATTTAGTTCCAAGGCTGTCGACGATCG
FUL 2	F for 2nd Amplicon	2,3	GCTTTGGTAACCGAGTCAGGAGGGAAATTCG
FUL 2	R for 2nd Amplicon	2,3	ACGGAGGAGTCAATATTCAAATCGC
FUL 3	F for 3rd Amplicon	4,5,6	GCGATTTGAATATTGACTCCTCCGT
FUL 3	R for 3rd Amplicon	4,5,6	GCTAACCCCATTCGTTTAGAGTACATC
FUL 4	F for 4th Amplicon	7,8	GATGTACTCTAAACGAATGGGGTTAGC
FUL 4	R for 4th Amplicon	7,8	ATCTTTGTGATCTTAAGAAAACGCAGTCG

Table 6.1 Primers used for TILLING of *FUL* with four amplicons

6.2.6 Complementation experiments

This work was carried out by myself, André Kuhn, George Averill and Friederike Jantzen. A 2kb promoter of *AtFUL* (Urbanus et al., 2009), *AtFUL* CDS and *CrFUL* CDS were cloned into the TOPO PCR4 vector with the corresponding restriction sites (for primers see Table 6.2). The pEGAD plant expression vector (Cutler et al., 2000) was used to assemble the components (Figure 6.1). *pAtFUL* was cloned by restriction digest into Pac I and Age I sites and the CDS sequences into Age I and EcoRI sites.

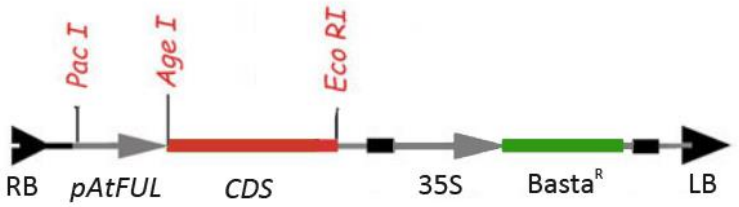

Figure 6.1 Complementation experiment construct design. Vector backbone *pEGAD* from (Cutler et al., 2000)

atful-2 and *crful-1* plants were transformed with *pAtFUL::AtFUL*, *pAtFUL::CrFUL* or *pEGAD* empty vector control. T0 seeds were spread thickly on soil and young seedlings were sprayed with Basta three times to select for transformants. The T1 generation were imaged using Leica M205C stereo microscope.

Name	Description	Sequence
pAtFUL	F with PacI site for promoter cloning	TTAATTAATCGATCAGAATTTGAGCTG
pAtFUL	R with AgeI site for promoter cloning	ACCGGTatctctctctcttcaaaatctc
AtFUL_CDS	F with AgeI site for cloning CDS	ACCGGTCTCGTTCGTAGTGGTA
AtFUL_CDS	R with EcoRI site for cloning CDS	GAATTCCTACTCGTTCGTAGTGGTA
CrFUL_CDS	F with AgeI site for cloning CDS	ACCGGTCTCATTCGTGGTGGTAGGGC
CrFUL_CDS	R with EcoRI site for cloning CDS	GAATTCCTACTCATTCGTGGTGGTAGGGC

Table 6.2 PCR primers used to clone pAtFUL and the coding sequences of AtFUL and CrFUL

6.3 Data collection

6.3.1 Gynoecium growth curves

Capsella plants were grown in a controlled environment room were grown on soil in a controlled environment room (Section 6.1.1.2). The plants were standardised by selecting those at a similar stage, for example the plants that had 4 leaves at the same time. Whole inflorescences were collected and fixed for PI staining at two day intervals at about the same time of day starting from 19 to 32 days after sowing. This method was developed from a protocol for staging *Arabidopsis* flower buds (Sauret-Gueto et al., 2013). Whole inflorescences were PI stained and imaged using OPT. *Arabidopsis* inflorescences were collected and imaged in the same way by Susana Sauret-Gueto.

The timing of the first flower of the main inflorescence was given in exact time in hours after sowing (HAS). The timing for subsequent flowers on the same inflorescence was calculated using the plastochron (timing interval between initiation of successive flower primordia) and the flower position. The plastochron was calculated by counting the number of newly open flowers in a 24h period on 10 inflorescences and averaged over several days. Under these conditions the plastochron of *Capsella* was 4.8h. The position of the individual flowers is the order that the flowers were initiated; so that the first flower on the inflorescence (oldest) would be at position 1, the second flower (second oldest) would be at position 2. Since, the flower at position 2 is initiated one plastochron after the first flower (456 HAS), the timing of the second flower would be 456 h – 4.8 h = 451.2 HAS.

The length and width along the mediolateral axis of gynoecia were measured using the measuring tool in Volviewer. For later stages, when inflorescences were too large for imaging by OPT, the individual fruits along the inflorescence were imaged using Leica M205C stereo microscope and measured in the Leica LAS V4 software. Gynoecium initiation, 0 days after initiation (0 DAI) was assumed to be when the gynoecium is ~40µm in length which corresponds to 450 HAS.

6.3.2 Clonal Analysis

For clonal analysis the plants were grown in the same conditions as those used for the growth curve. Following heat shock treatment plants were placed back in the growth rooms and left for 4, 6 or 8 days before imaging. The gynoecia at lengths 300µm, 500µm, 1mm, 2mm and 4mm were dissected and mounted on glass slides with a coverslip in water.

Samples were imaged using a Leica DM6000 compound microscope, a Zeiss LSM 5 EXCITER Laser Scanning Confocal Microscope, or the Zeiss LSM 780 Laser Scanning Confocal microscope.

Clones on the *Capsella* and *Arabidopsis* fruit were analysed using *Sector Analysis Toolbox* implemented in MATLAB (http://www.uea.ac.uk/cmp/research/cmpbio/SectorAnalysisToolbox). The organ outline and individual clones were segmented manually in Image J software. For each fruit project, fruit were warped to a mean fruit shape by placing 50 points around the segmented fruit outlines, with 5 points following the replum and several reference points. For 300µm there were 4 reference points, 1 on each corner of the rectangular shape. For gynoecia larger than 300µm there were 7 reference points with 2 at base, 2 where the style met the valves, 2 on the corners of the style and 1 at the apex of the style in line with the replum. These placed points were subjected to Procrustes Alignment (Gower, 1975) and normalised for scale. For clones were warped to the corresponding mean shape using a Piecewise Linear Warp (Goshtasby, 1986).

The area of clones was calculated from the outline in image J, and the length and width were measured using the line tool in Image J.

6.4 Computational modelling

Details of each of the models are given in the appropriate chapters. Here, general methods and the parameters for each of the models are described. All modelling was carried out with GPT-framework, implemented in the MATLAB toolbox, *GFtbox* (Kennaway et al., 2011). The *GFtbox* is available at http://www.uea.ac.uk/cmp/research/cmpbio/GFtbox

6.4.1 The Canvas

In all models the same starting canvas was used, an oval cylindrical shape with the base of the cylinder parallel to *xy*-axis and the long axis parallel to the *z*-axis. Growth at the baseline is constrained to be parallel to the *xy*-axis. The dimensions of the starting canvas are 40 µm length and 80µm x 60µm width. The starting canvas consists of 2000 elements and is locally subdivided at 160h at the midvalve generating a mesh of 2960 elements.

6.4.2 The Factors

Growth and Polarity in all models is controlled by factors. Factors have a value for each vertex and are distributed over the canvas. Factors can either retain fixed values: $\mathbf{i}_{FACTORNAME}$ for identity, or propagate through the canvas: $\mathbf{s}_{FACTORNAME}$ for signalling. It is assumed that factor levels do not dilute with growth. Factors promote growth through the function *pro*, which is defined as:

$$\text{pro}(p_F, \mathbf{x}_F) = 1 + p_F \times \mathbf{x}_F$$

where p_F is the promotion coefficient of the factor $\mathbf{x}_F$. Factors can inhibit growth through the function *inh*, which is defined as:

$$\text{inh}(h_F, \mathbf{x}_F) = 1 /(1 + h_F \times \mathbf{x}_F)$$

where h_F is the inhibition coefficient of the factor $\mathbf{x}_F$.

In *GFtbox* models have two interconnected networks: the Polarity Regulatory Network which specifies tissue polarity and the Growth Regulatory Network (KRN) which specifies how factors influence growth rates. These networks determine the specified growth and polarity fields across the canvas. Due to the connectedness of the canvas the specified growth rates differ from the resultant growth rates.

6.4.3 Simulation details

The canvas starting size corresponds to the size of the gynoecium at 0 DAI. The model starts at -1 DAI with the starting canvas size and goes through an initial set up phase where factor distributions are established before the canvas starts to grow at 0 DAI. Growth was simulated up to 11 DAI which corresponds to when the fruit is 2mm in length.

The models take around 10 mins to run on a CORE^{TM}i7 laptop for 72 steps (the period simulated, each step is 4h), solving the diffusion and elasticity equations with a tolerance of 10^{-4} relative to the magnitude of the numbers.

At each simulation step, calculations are carried out in the following order (the simulation loop):

- Calculate values and distribution of growth factors as specified
- Calculate extent of diffusion during the time step
- Specified by the factors, calculate the growth tensor field

- To obtain the computed growth field, calculate the resulting displacement of each vertex
- Calculate the region of identity factor expression in the new volume after growth from the displacement field.

6.4.4 Polarity Parameters

The polarity field was specified the same in each of the models. The parameter values are given in Table 6.3

Parameter	Description	Value
b_{pol}	$\mathbf{s}_{POL}$ production by $\mathbf{i}_{PROXORG}$ (maximum value)	1
D_{pol}	$\mathbf{s}_{POL}$ diffusion rate	0.005 mm^2h^{-1}

Table 6.3 Polarity parameters used in fruit models

6.4.5 Growth parameters

In the core *Capsella* wildtype fruit model the growth was specified as:

K_{par} = 0.014 .pro(h_{EPHASE} , $\mathbf{i}_{EPHASE}$)

.inh(h_{BASE} , $\mathbf{i}_{BASE}$. $\mathbf{i}_{MPHASE}$) .pro($h_{MIDVALVE}$, $\mathbf{i}_{MIDVALVE}$. $\mathbf{i}_{MPHASE}$)

.pro($h_{GMIDVALVE}$, $\mathbf{i}_{GMIDVALVE}$. $\mathbf{i}_{LPHASE}$) .inh(h_{BASE} , $\mathbf{i}_{BASE}$. $\mathbf{i}_{LPHASE}$) .inh(h_{STYLE} , $\mathbf{i}_{STYLE}$. $\mathbf{i}_{LPHASE}$)

.inh(h_{GDIST} , $\mathbf{i}_{GDIST}$. $\mathbf{i}_{LPHASE}$) .pro(h_{GPROX} , $\mathbf{i}_{GPROX}$. $\mathbf{i}_{LPHASE}$)

K_{per} = 0.0115 .inh(h_{STYLE} , $\mathbf{i}_{STYLE}$. $\mathbf{i}_{MPHASE}$) .inh(h_{BASE} , $\mathbf{i}_{BASE}$. $\mathbf{i}_{MPHASE}$) .inh(h_{REP} , $\mathbf{i}_{REP}$. $\mathbf{i}_{MPHASE}$)

.inh($h_{MIDVALVE}$, $\mathbf{i}_{MIDVALVE}$. $\mathbf{i}_{MPHASE}$)

.inh($h_{MIDVALVE}$, $\mathbf{i}_{MIDVALVE}$. $\mathbf{i}_{LPHASE}$) .inh(h_{STYLE} , $\mathbf{i}_{STYLE}$. $\mathbf{i}_{LPHASE}$) .inh(h_{BASE} , $\mathbf{i}_{BASE}$. $\mathbf{i}_{LPHASE}$)

.inh(h_{REP} , $\mathbf{i}_{REP}$. $\mathbf{i}_{LPHASE}$) .pro(h_{GDIST} , $\mathbf{i}_{GDIST}$. $\mathbf{i}_{LPHASE}$) .inh(h_{GPROX} , $\mathbf{i}_{GPROX}$. $\mathbf{i}_{LPHASE}$)

K_{knor} = 0.01

This model is the most complex and all models that build up to this full version of the *Capsella* fruit model and the simplified versions of *Arabidopsis* fruit and fruit flattened laterally and medially models use the same parameters values, except where specified in the appropriate sections. The timing of the phases was specified by $\mathbf{i}_{EPHASE}$, $\mathbf{i}_{MPHASE}$ and $\mathbf{i}_{LPHASE}$. The parameter values at different times are shown in Table 6.4. The growth factors parameter and parameter values for the core model are shown in Table 6.4 Factors $\mathbf{i}_{STYLE}$, $\mathbf{i}_{STYLE}$, $\mathbf{i}_{BASE}$, $\mathbf{i}_{GMIDVALVE}$, $\mathbf{i}_{GDIST}$, $\mathbf{i}_{GPROX}$ were set up as a gradient with a diffusible factor ($\mathbf{s}_{FACTORNAME}$) in the initial set up phase (-1-0DAI) then at 0DAI the diffusion rate was set to 0. Therefore at 0DAI $i_{FACTORNAME} = \mathbf{s}_{FACTORNAME}$. The gradients were established with the parameters shown in Table 6.4

	Factor values		
Time	$\mathbf{i}_{EPHASE}$	$\mathbf{i}_{MPHASE}$	$\mathbf{i}_{LPHASE}$
>0h <48h	1	0	0
>48h <192h	0	1	0
>192h <264h	0	0	1

Table 6.4 Factors controlling phases

Parameter	Description	Value
b_{STYLE}	$\mathbf{s}_{STYLE}$ production by $\mathbf{i}_{STYLE}$ (maximum value)	1
D_{STYLE}	$\mathbf{s}_{STYLE}$ diffusion rate	0.0004 mm^2h^{-1}
b_{BASE}	$\mathbf{s}_{BASE}$ production by $\mathbf{i}_{BASE}$ (maximum value)	1
D_{BASE}	$\mathbf{s}_{BASE}$ diffusion rate	0.0004 mm^2h^{-1}
b_{GPROX}	$\mathbf{s}_{GPROX}$ production by $\mathbf{i}_{GPROX}$ (maximum value)	1
D_{GPROX}	$\mathbf{s}_{GPROX}$ diffusion rate	0.005 mm^2h^{-1}
b_{GDIST}	$\mathbf{s}_{GDIST}$ production by $\mathbf{i}_{GDIST}$ (maximum value)	1
D_{GDIST}	$\mathbf{s}_{GDIST}$ diffusion rate	0.015 mm^2h^{-1}
$b_{GMIDVALVE}$	$\mathbf{s}_{GMIDVALVE}$ production by $\mathbf{i}_{GMIDVALVE}$ (maximum value)	1
$D_{GMIDVALVE}$	$\mathbf{s}_{GMIDVALVE}$ diffusion rate	0.015 mm^2h^{-1}
$\boldsymbol{p}_{EPHASE}$	growth promotion by $\mathbf{i}_{EPHASE}$	1
$\boldsymbol{p}_{MIDVALVE}$	growth promotion by $\mathbf{i}_{MIDVALVE}$	0.2
$\boldsymbol{p}_{GMIDVALVE}$	growth promotion by $\mathbf{i}_{GMIDVALVE}$	0.5
$\boldsymbol{p}_{GPROX}$	growth promotion by $\mathbf{i}_{GPROX}$	2
$\boldsymbol{p}_{GDIST}$	growth promotion by $\mathbf{i}_{GDIST}$	0.2
$\boldsymbol{h}_{STYLE}$	growth inhibition by $\mathbf{i}_{STYLE}$	3
$\boldsymbol{h}_{BASE}$	K_{par} inhibition by $\mathbf{i}_{BASE}$	5 (mphase), 100 (lphase)
$\boldsymbol{h}_{BASE}$	K_{per} inhibition by $\mathbf{i}_{BASE}$	1
$\boldsymbol{h}_{REP}$	growth inhibition by $\mathbf{i}_{REP}$	5
$\boldsymbol{h}_{MIDVALVE}$	growth inhibition by $\mathbf{i}_{MIDVALVE}$	1
$\boldsymbol{h}_{GPROX}$	growth inhibition by $\mathbf{i}_{GPROX}$	2
$\boldsymbol{h}_{GDIST}$	growth inhibition by $\mathbf{i}_{GDIST}$	6

Table 6.4 Growth parameters used in fruit models

List of Abbreviations

Abbreviation	Full Name
ALC	ALCATRAZ
ARF	AUXIN RESPONSE FACTOR
AS1	ASYMMETRIC LEAF 1
BOB	BROTHER OF BRAINBOW
BP	BREVIPEDICELLUS
CDS	coding sequence
Cre	Cre-recombinase
CUC	CUP-SHAPED COTYLEDON
DAI	days after initiation
DR5	auxin response marker
DVL	DEVIL
EMS	ethyl methanesulfonate
en*a*	endocarp*a*
en*b*	endocarp*b*
ETT	ETTIN
EV	empty vector
FEM	finite element method
FIL	FILAMENTOS
FUL	FRUITFULL
GA	gibberellic acids
GFP	green florescent protein
GPT framework	Growing Polarised Tissue framework
HAI	hours after initiation
HAS	hours after sowing
HD ZIP III	class III homeodomain leucine zipper
HS	heat shock
IND	INDEHISCENT
JAG	JAGGED
KAN	KANADI
L/W	length/width ratio

NGA	NGATHA
NUB	NUBBIN
OPT	optical projection tomography
PID	PINOID
PIN	PINFORMED
PPD	PEAPOD
RCO	REDUCED COMPLEXITY
REP	REPLUMLESS
RFP	red florescent protein
ROT	ROTUNDIFOLIA
SAM	shoot apical meristem
SEM	scanning electron microscopy
SHP	SHATTERPROOF
SPL	SQUAMOSA PROMOTER BINDING PROTEIN LIKE
STY	STYLISH
TILLING	targeting induced local lesions in genomes
VP16	viral activator of transcription
YAB	YABBY
YFP	yellow florescent protein
YUC	YUCCA

References

Abley, K., de Reuille, P. B., Strutt, D., Bangham, A., Prusinkiewicz, P., Maree, A. F. M., Grieneisen, V. A., and Coen, E. (2013). An intracellular partitioning-based framework for tissue cell polarity in plants and animals. Development *140*, 2061-2074.

Agren, J. A., Wang, W., Koenig, D., Neuffer, B., Weigel, D., and Wright, S. I. (2014). Mating system shifts and transposable element evolution in the plant genus Capsella. BMC genomics *15*, 602.

Al-Shehbaz, I. A. (2003). Transfer of Most North American Species of Arabis to Boechera (Brassicaceae). Novon *13*, 381-391.

Al-Shehbaz, I. A., Beilstein, M. A., and Kellogg, E. A. (2006). Systematics and phylogeny of the Brassicaceae (Cruciferae): an overview. Plant Syst Evol *259*, 89-120.

Al-Shehbaz, I. A., Mummenhoff, K., and Appel, O. (2002). Cardaria, Coronopus, and Stroganowia are united with Lepidium (Brassicaceae). Novon *12*, 5-11.

Alonso-Cantabrana, H., Ripoll, J. J., Ochando, I., Vera, A., Ferrandiz, C., and Martinez-Laborda, A. (2007). Common regulatory networks in leaf and fruit patterning revealed by mutations in the Arabidopsis ASYMMETRIC LEAVES1 gene. Development *134*, 2663-2671.

Alonso, J. M., Stepanova, A. N., Leisse, T. J., Kim, C. J., Chen, H., Shinn, P., Stevenson, D. K., Zimmerman, J., Barajas, P., Cheuk, R.*, et al.* (2003). Genome-wide insertional mutagenesis of Arabidopsis thaliana. Science *301*, 653-657.

Alvarez, J. P., Goldshmidt, A., Efroni, I., Bowman, J. L., and Eshed, Y. (2009). The NGATHA distal organ development genes are essential for style specification in Arabidopsis. Plant Cell *21*, 1373-1393.

Andriankaja, M., Dhondt, S., De Bodt, S., Vanhaeren, H., Coppens, F., De Milde, L., Muhlenbock, P., Skirycz, A., Gonzalez, N., Beemster, G. T., and Inze, D. (2012). Exit from proliferation during leaf development in Arabidopsis thaliana: a not-so-gradual process. Developmental cell *22*, 64-78.

Arnaud, N., Lawrenson, T., Ostergaard, L., and Sablowski, R. (2011). The Same Regulatory Point Mutation Changed Seed-Dispersal Structures in Evolution and Domestication. Current Biology *21*, 1215-1219.

Asl, L. K., Dhondt, S., Boudolf, V., Beemster, G. T., Beeckman, T., Inze, D., Govaerts, W., and De Veylder, L. (2011). Model-based analysis of Arabidopsis leaf epidermal cells reveals distinct division and expansion patterns for pavement and guard cells. Plant Physiol *156*, 2172-2183.

Bailey, C. D., Koch, M. A., Mayer, M., Mummenhoff, K., O'Kane, S. L., Jr., Warwick, S. I., Windham, M. D., and Al-Shehbaz, I. A. (2006). Toward a global phylogeny of the Brassicaceae. Molecular biology and evolution *23*, 2142-2160.

Bartholmes, C., Nutt, P., and Theissen, G. (2008). Germline transformation of Shepherd's purse (Capsella bursa-pastoris) by the 'floral dip' method as a tool for evolutionary and developmental biology. Gene *409*, 11-19.

Baskin, T. I. (2005). Anisotropic expansion of the plant cell wall. Annual review of cell and developmental biology *21*, 203-222.

Bassel, G. W., Stamm, P., Mosca, G., Barbier de Reuille, P., Gibbs, D. J., Winter, R., Janka, A., Holdsworth, M. J., and Smith, R. S. (2014). Mechanical constraints imposed by 3D cellular geometry and arrangement modulate growth patterns in the Arabidopsis embryo. Proceedings of the National Academy of Sciences of the United States of America *111*, 8685-8690.

Bayer, E. M., Smith, R. S., Mandel, T., Nakayama, N., Sauer, M., Prusinkiewicz, P., and Kuhlemeier, C. (2009). Integration of transport-based models for phyllotaxis and midvein formation. Genes & development *23*, 373-384.

Beilstein, M. A., Al-Shehbaz, I. A., and Kellogg, E. A. (2006). Brassicaceae phylogeny and trichome evolution. Am J Bot *93*, 607-619.

Benkova, E., Michniewicz, M., Sauer, M., Teichmann, T., Seifertova, D., Jurgens, G., and Friml, J. (2003). Local, efflux-dependent auxin gradients as a common module for plant organ formation. Cell *115*, 591-602.

Bossinger, G., and Smyth, D. R. (1996). Initiation patterns of flower and floral organ development in Arabidopsis thaliana. Development *122*, 1093-1102.

Bowman, J. L. (2006). Molecules and morphology: comparative developmental genetics of the Brassicaceae. Plant Syst Evol *259*, 199-215.

Bowman, J. L., Smyth, D. R., and Meyerowitz, E. M. (1989). Genes directing flower development in Arabidopsis. Plant Cell *1*, 37-52.

Cevik, V., Ryder, C., Popovich, A., Manning, K., King, G., and Seymour, G. (2010). A FRUITFULL-like gene is associated with genetic variation for fruit flesh firmness in apple (Malus domestica Borkh.). Tree Genetics & Genomes *6*, 271-279.

Cheng, Y., Dai, X., and Zhao, Y. (2006). Auxin biosynthesis by the YUCCA flavin monooxygenases controls the formation of floral organs and vascular tissues in Arabidopsis. Genes & development *20*, 1790-1799.

Chew, Y. H., Wenden, B., Flis, A., Mengin, V., Taylor, J., Davey, C. L., Tindal, C., Thomas, H., Ougham, H. J., de Reffye, P*., et al.* (2014). Multiscale digital Arabidopsis predicts individual organ and whole-organism growth. Proceedings of the National Academy of Sciences of the United States of America.

Colbert, T., Till, B. J., Tompa, R., Reynolds, S., Steine, M. N., Yeung, A. T., McCallum, C. M., Comai, L., and Henikoff, S. (2001). High-throughput screening for induced point mutations. Plant Physiol *126*, 480-484.

Coquillat, M. (1951). Sur les plantes les plus communes a la surface du globe. Bulletin Mensual Societe Linneenne *20*, 165-170.

Cosgrove, D. J. (2005). Growth of the plant cell wall. Nature reviews Molecular cell biology *6*, 850-861.

Cosgrove, D. J., Li, L. C., Cho, H. T., Hoffmann-Benning, S., Moore, R. C., and Blecker, D. (2002). The growing world of expansins. Plant & cell physiology *43*, 1436-1444.

Cutler, S. R., Ehrhardt, D. W., Griffitts, J. S., and Somerville, C. R. (2000). Random GFP::cDNA fusions enable visualization of subcellular structures in cells of Arabidopsis at a high frequency. Proceedings of the National Academy of Sciences *97*, 3718-3723.

Dardick, C. D., Callahan, A. M., Chiozzotto, R., Schaffer, R. J., Piagnani, M. C., and Scorza, R. (2010). Stone formation in peach fruit exhibits spatial coordination of the lignin and flavonoid pathways and similarity to Arabidopsis dehiscence. BMC biology *8*, 13.

Deng, W., Jeng, D.-S., Toorop, P. E., Squire, G. R., and Iannetta, P. P. M. (2012). A mathematical model of mucilage expansion in myxospermous seeds of Capsella bursa-pastoris (shepherd's purse). Annals of Botany *109*, 419-427.

Dinneny, J. R., Weigel, D., and Yanofsky, M. F. (2006). NUBBIN and JAGGED define stamen and carpel shape in Arabidopsis. Development *133*, 1645-1655.

Edwards, K., Johnstone, C., and Thompson, C. (1991). A SIMPLE AND RAPID METHOD FOR THE PREPARATION OF PLANT GENOMIC DNA FOR PCR ANALYSIS. Nucleic Acids Research *19*, 1349-1349.

Eshed, Y., Baum, S. F., Perea, J. V., and Bowman, J. L. (2001). Establishment of polarity in lateral organs of plants. Current biology : CB *11*, 1251-1260.

Ferrandiz, C., and Fourquin, C. (2014). Role of the FUL-SHP network in the evolution of fruit morphology and function. J Exp Bot.

Ferrandiz, C., Gu, Q., Martienssen, R., and Yanofsky, M. F. (2000). Redundant regulation of meristem identity and plant architecture by FRUITFULL, APETALA1 and CAULIFLOWER. Development *127*, 725-734.

Ferrandiz, C., Pelaz, S., and Yanofsky, M. F. (1999). Control of carpel and fruit development in Arabidopsis. Annual review of biochemistry *68*, 321-354.

Fourquin, C., del Cerro, C., Victoria, F. C., Vialette-Guiraud, A., de Oliveira, A. C., and Ferrandiz, C. (2013). A change in SHATTERPROOF protein lies at the origin of a fruit morphological novelty and a new strategy for seed dispersal in medicago genus. Plant Physiol *162*, 907-917.

Fourquin, C., and Ferrandiz, C. (2014). The essential role of NGATHA genes in style and stigma specification is widely conserved across eudicots. The New phytologist *202*, 1001-1013.

Foxe, J. P., Slotte, T., Stahl, E. A., Neuffer, B., Hurka, H., and Wright, S. I. (2009). Recent speciation associated with the evolution of selfing in Capsella. Proceedings of the National Academy of Sciences of the United States of America *106*, 5241-5245.

Francis, A., and Warwick, S. I. (2003). The biology of Canadian weeds. 120. Neslia paniculata (L.) Desv. Canadian Journal of Plant Science *83*, 441-451.

Franzke, A., Lysak, M. A., Al-Shehbaz, I. A., Koch, M. A., and Mummenhoff, K. (2011). Cabbage family affairs: the evolutionary history of Brassicaceae. Trends in plant science *16*, 108-116.

Fuentes, S., Ljung, K., Sorefan, K., Alvey, E., Harberd, N. P., and Ostergaard, L. (2012). Fruit growth in Arabidopsis occurs via DELLA-dependent and DELLA-independent gibberellin responses. Plant Cell *24*, 3982-3996.

Gallois, J. L., Woodward, C., Reddy, G. V., and Sablowski, R. (2002). Combined SHOOT MERISTEMLESS and WUSCHEL trigger ectopic organogenesis in Arabidopsis. Development *129*, 3207-3217.

Gilchrist, E. J., O'Neil, N. J., Rose, A. M., Zetka, M. C., and Haughn, G. W. (2006). TILLING is an effective reverse genetics technique for Caenorhabditis elegans. BMC genomics *7*, 262.

Gillaspy, G., Bendavid, H., and Gruissem, W. (1993). FRUITS - A DEVELOPMENTAL PERSPECTIVE. Plant Cell *5*, 1439-1451.

Girin, T., Paicu, T., Stephenson, P., Fuentes, S., Korner, E., O'Brien, M., Sorefan, K., Wood, T. A., Balanza, V., Ferrandiz, C*., et al.* (2011). INDEHISCENT and SPATULA interact to specify carpel and valve margin tissue and thus promote seed dispersal in Arabidopsis. Plant Cell *23*, 3641-3653.

Girin, T., Stephenson, P., Goldsack, C. M., Kempin, S. A., Perez, A., Pires, N., Sparrow, P. A., Wood, T. A., Yanofsky, M. F., and Ostergaard, L. (2010). Brassicaceae INDEHISCENT genes specify valve margin cell fate and repress replum formation. The Plant journal : for cell and molecular biology *63*, 329-338.

Goetz, M., Hooper, L. C., Johnson, S. D., Rodrigues, J. C., Vivian-Smith, A., and Koltunow, A. M. (2007). Expression of aberrant forms of AUXIN RESPONSE FACTOR8 stimulates parthenocarpy in Arabidopsis and tomato. Plant Physiol *145*, 351-366.

Goetz, M., Vivian-Smith, A., Johnson, S. D., and Koltunow, A. M. (2006). AUXIN RESPONSE FACTOR8 is a negative regulator of fruit initiation in Arabidopsis. Plant Cell *18*, 1873-1886.

Gonzalez-Reig, S., Ripoll, J. J., Vera, A., Yanofsky, M. F., and Martinez-Laborda, A. (2012). Antagonistic gene activities determine the formation of pattern elements along the mediolateral axis of the Arabidopsis fruit. PLoS genetics *8*, e1003020.

Goshtasby, A. (1986). Piecewise linear mapping functions for image registration. Pattern Recognition *19*, 459-466.

Gower, J. C. (1975). Generalized procrustes analysis. Psychometrika *40*, 33-51.

Gramzow, L., and Theissen, G. (2010). A hitchhiker's guide to the MADS world of plants. Genome Biology *11*.

Green, A. A., Kennaway, R., Hanna, A. I., Bangham, J. A., and Coen, E. (2010). Genetic Control of Organ Shape and Tissue Polarity. Plos Biology *8*.

Greene, E. A., Codomo, C. A., Taylor, N. E., Henikoff, J. G., Till, B. J., Reynolds, S. H., Enns, L. C., Burtner, C., Johnson, J. E., Odden, A. R.*, et al.* (2003). Spectrum of chemically induced mutations from a large-scale reverse-genetic screen in Arabidopsis. Genetics *164*, 731-740.

Grieneisen, V. A., Maree, A. F., and Ostergaard, L. (2013). Juicy stories on female reproductive tissue development: coordinating the hormone flows. Journal of integrative plant biology *55*, 847-863.

Grieneisen, V. A., Xu, J., Maree, A. F. M., Hogeweg, P., and Scheres, B. (2007). Auxin transport is sufficient to generate a maximum and gradient guiding root growth. Nature *449*, 1008-1013.

Gu, Q., Ferrandiz, C., Yanofsky, M. F., and Martienssen, R. (1998). The FRUITFULL MADS-box gene mediates cell differentiation during Arabidopsis fruit development. Development *125*, 1509-1517.

Guo, Y. L., Bechsgaard, J. S., Slotte, T., Neuffer, B., Lascoux, M., Weigel, D., and Schierup, M. H. (2009). Recent speciation of Capsella rubella from Capsella grandiflora, associated with loss of self-incompatibility and an extreme bottleneck. Proceedings of the National Academy of Sciences of the United States of America *106*, 5246-5251.

Gupta, S. K. (2009). Biology and Breeding of Crucifers: Taylor & Francis).

Hawkins, C., and Liu, Z. (2014). A model for an early role of auxin in Arabidopsis gynoecium morphogenesis. Front Plant Sci *5*, 327.

Hay, A. S., Pieper, B., Cooke, E., Mandakova, T., Cartolano, M., Tattersall, A. D., Ioio, R. D., McGowan, S. J., Barkoulas, M., Galinha, C.*, et al.* (2014). Cardamine hirsuta: a versatile genetic system for comparative studies. The Plant journal : for cell and molecular biology *78*, 1-15.

Heisler, M. G., Hamant, O., Krupinski, P., Uyttewaal, M., Ohno, C., Jönsson, H., Traas, J., and Meyerowitz, E. M. (2010). Alignment between PIN1 Polarity and Microtubule Orientation in the Shoot Apical Meristem Reveals a Tight Coupling between Morphogenesis and Auxin Transport. PLoS Biol *8*, e1000516.

Heisler, M. G., Ohno, C., Das, P., Sieber, P., Reddy, G. V., Long, J. A., and Meyerowitz, E. M. (2005). Patterns of auxin transport and gene expression during primordium development revealed by live imaging of the Arabidopsis inflorescence meristem. Current biology : CB *15*, 1899-1911.

Hintz, M., Bartholmes, C., Nutt, P., Ziermann, J., Hameister, S., Neuffer, B., and Theissen, G. (2006). Catching a 'hopeful monster': shepherd's purse (Capsella bursa-pastoris) as a model system to study the evolution of flower development. J Exp Bot *57*, 3531-3542.

Honma, T., and Goto, K. (2001). Complexes of MADS-box proteins are sufficient to convert leaves into floral organs. Nature *409*, 525-529.

Hunter, C., Willmann, M. R., Wu, G., Yoshikawa, M., de la Luz Gutierrez-Nava, M., and Poethig, S. R. (2006). Trans-acting siRNA-mediated repression of ETTIN and ARF4 regulates heteroblasty in Arabidopsis. Development *133*, 2973-2981.

Ito, T., and Meyerowitz, E. M. (2000). Overexpression of a gene encoding a cytochrome p450, CYP78A9, induces large and seedless fruit in arabidopsis. Plant Cell *12*, 1541-1550.

Jaakola, L., Poole, M., Jones, M. O., Kamarainen-Karppinen, T., Koskimaki, J. J., Hohtola, A., Haggman, H., Fraser, P. D., Manning, K., King, G. J.*, et al.* (2010). A SQUAMOSA MADS box gene involved in the regulation of anthocyanin accumulation in bilberry fruits. Plant Physiol *153*, 1619-1629.

Jansen, J. G., Vrieling, H., van Teijlingen, C. M., Mohn, G. R., Tates, A. D., and van Zeeland, A. A. (1995). Marked differences in the role of O6-alkylguanine in hprt mutagenesis in T-lymphocytes of rats exposed in vivo to ethylmethanesulfonate, N-(2-hydroxyethyl)-N-nitrosourea, or N-ethyl-N-nitrosourea. Cancer research *55*, 1875-1882.

Johnston, J. S., Pepper, A. E., Hall, A. E., Chen, Z. J., Hodnett, G., Drabek, J., Lopez, R., and Price, H. J. (2005). Evolution of genome size in Brassicaceae. Ann Bot *95*, 229-235.

Johri, M. M., and Coe Jr, E. H. (1983). Clonal analysis of corn plant development: I. The development of the tassel and the ear shoot. Dev Biol *97*, 154-172.

Jonsson, H., Heisler, M. G., Shapiro, B. E., Meyerowitz, E. M., and Mjolsness, E. (2006). An auxin-driven polarized transport model for phyllotaxis. Proceedings of the National Academy of Sciences of the United States of America *103*, 1633-1638.

Kaufmann, K., Melzer, R., and Theißen, G. (2005). MIKC-type MADS-domain proteins: structural modularity, protein interactions and network evolution in land plants. Gene *347*, 183-198.

Kayes, J. M., and Clark, S. E. (1998). CLAVATA2, a regulator of meristem and organ development in Arabidopsis. Development *125*, 3843-3851.

Kelley, D. R., Arreola, A., Gallagher, T. L., and Gasser, C. S. (2012). ETTIN (ARF3) physically interacts with KANADI proteins to form a functional complex essential for integument development and polarity determination in Arabidopsis. Development *139*, 1105-1109.

Kennaway, R., Coen, E., Green, A., and Bangham, A. (2011). Generation of Diverse Biological Forms through Combinatorial Interactions between Tissue Polarity and Growth. Plos Computational Biology *7*.

Kerstetter, R. A., Bollman, K., Taylor, R. A., Bomblies, K., and Poethig, R. S. (2001). KANADI regulates organ polarity in Arabidopsis. Nature *411*, 706-709.

Kesel, A. B., Philippi, U., and Nachtigall, W. (1998). Biomechanical aspects of the insect wing: an analysis using the finite element method. Computers in Biology and Medicine *28*, 423-437.

Koornneef, M. (2002). Classical mutagenesis in higher plants. Molecular plant biology *1*, 1-11.

Kuchen, E. E., Fox, S., de Reuille, P. B., Kennaway, R., Bensmihen, S., Avondo, J., Calder, G. M., Southam, P., Robinson, S., Bangham, A., and Coen, E. (2012). Generation of Leaf Shape Through Early Patterns of Growth and Tissue Polarity. Science *335*, 1092-1096.

Kurowska, M., Daszkowska-Golec, A., Gruszka, D., Marzec, M., Szurman, M., Szarejko, I., and Maluszynski, M. (2011). TILLING: a shortcut in functional genomics. Journal of applied genetics *52*, 371-390.

Kwiatkowska, D., and Dumais, J. (2003). Growth and morphogenesis at the vegetative shoot apex of Anagallis arvensis L. J Exp Bot *54*, 1585-1595.

Larsson, E., Franks, R. G., and Sundberg, E. (2013). Auxin and the Arabidopsis thaliana gynoecium. J Exp Bot *64*, 2619-2627.

Larue, C. T., Wen, J., and Walker, J. C. (2010). Interactions between a NAC-Domain Transcription Factor and the Putative Small Protein Encoding DVL/ROT Gene Family. Plant Molecular Biology Reporter *28*, 162-168.

Le Signor, C., Savois, V., Aubert, G., Verdier, J., Nicolas, M., Pagny, G., Moussy, F., Sanchez, M., Baker, D., Clarke, J., and Thompson, R. (2009). Optimizing TILLING populations for reverse genetics in Medicago truncatula. Plant biotechnology journal *7*, 430-441.

Lee, K., Avondo, J., Morrison, H., Blot, L., Stark, M., Sharpe, J., Bangham, A., and Coen, E. (2006). Visualizing plant development and gene expression in three dimensions using optical projection tomography. Plant Cell *18*, 2145-2156.

Lenser, T., and Theissen, G. (2013). Conservation of fruit dehiscence pathways between Lepidium campestre and Arabidopsis thaliana sheds light on the regulation of INDEHISCENT. Plant Journal *76*, 545-556.

Liang, H., and Mahadevan, L. (2009). The shape of a long leaf. Proceedings of the National Academy of Sciences of the United States of America *106*, 22049-22054.

Liang, H., and Mahadevan, L. (2011). Growth, geometry, and mechanics of a blooming lily. Proceedings of the National Academy of Sciences *108*, 5516-5521.

Liljegren, S. J., Roeder, A. H. K., Kempin, S. A., Gremski, K., Ostergaard, L., Guimil, S., Reyes, D. K., and Yanofsky, M. F. (2004). Control of fruit patterning in Arabidopsis by INDEHISCENT. Cell *116*, 843-853.

Lockhart, J. A. (1965). An analysis of irreversible plant cell elongation. J Theor Biol *8*, 264-275.

Marée, A. F. M., Panfilov, A. V., and Hogeweg, P. (1999). Phototaxis during the slug stage of Dictyostelium discoideum: a model study. Proceedings of the Royal Society of London Series B: Biological Sciences *266*, 1351-1360.

Marti, C., Orzaez, D., Ellul, P., Moreno, V., Carbonell, J., and Granell, A. (2007). Silencing of DELLA induces facultative parthenocarpy in tomato fruits. The Plant journal : for cell and molecular biology *52*, 865-876.

Martin, B., Ramiro, M., Martinez-Zapater, J. M., and Alonso-Blanco, C. (2009). A high-density collection of EMS-induced mutations for TILLING in Landsberg erecta genetic background of Arabidopsis. BMC plant biology *9*, 147.

Martinez-Fernandez, I., Sanchis, S., Marini, N., Balanza, V., Ballester, P., Navarrete-Gomez, M., Oliveira, A. C., Colombo, L., and Ferrandiz, C. (2014). The effect of NGATHA altered activity on auxin signaling pathways within the Arabidopsis gynoecium. Front Plant Sci *5*, 210.

McCallum, C. M., Comai, L., Greene, E. A., and Henikoff, S. (2000). Targeting induced local lesions IN genomes (TILLING) for plant functional genomics. Plant Physiol *123*, 439-442.

McConnell, J. R., and Barton, M. K. (1998). Leaf polarity and meristem formation in Arabidopsis. Development *125*, 2935-2942.

McConnell, J. R., Emery, J., Eshed, Y., Bao, N., Bowman, J., and Barton, M. K. (2001). Role of PHABULOSA and PHAVOLUTA in determining radial patterning in shoots. Nature *411*, 709-713.

McQueen-Mason, S., Durachko, D. M., and Cosgrove, D. J. (1992). Two endogenous proteins that induce cell wall extension in plants. Plant Cell *4*, 1425-1433.

Muhlhausen, A., Lenser, T., Mummenhoff, K., and Theissen, G. (2013). Evidence that an evolutionary transition from dehiscent to indehiscent fruits in Lepidium (Brassicaceae) was caused by a change in the control of valve margin identity genes. The Plant journal : for cell and molecular biology *73*, 824-835.

Muller, B. M., Saedler, H., and Zachgo, S. (2001). The MADS-box gene DEFH28 from Antirrhinum is involved in the regulation of floral meristem identity and fruit development. The Plant journal : for cell and molecular biology *28*, 169-179.

Nahar, M. A., Ishida, T., Smyth, D. R., Tasaka, M., and Aida, M. (2012). Interactions of CUP-SHAPED COTYLEDON and SPATULA genes control carpel margin development in Arabidopsis thaliana. Plant & cell physiology *53*, 1134-1143.

Narita, N. N., Moore, S., Horiguchi, G., Kubo, M., Demura, T., Fukuda, H., Goodrich, J., and Tsukaya, H. (2004). Overexpression of a novel small peptide ROTUNDIFOLIA4 decreases cell proliferation and alters leaf shape in Arabidopsis thaliana. Plant Journal *38*, 699-713.

Nemhauser, J. L., Feldman, L. J., and Zambryski, P. C. (2000). Auxin and ETTIN in Arabidopsis gynoecium morphogenesis. Development *127*, 3877-3888.

Nole-Wilson, S., Azhakanandam, S., and Franks, R. G. (2010). Polar auxin transport together with aintegumenta and revoluta coordinate early Arabidopsis gynoecium development. Dev Biol *346*, 181-195.

Oleykowski, C. A., Bronson Mullins, C. R., Godwin, A. K., and Yeung, A. T. (1998). Mutation detection using a novel plant endonuclease. Nucleic Acids Res *26*, 4597-4602.

Ostergaard, L., Kempin, S. A., Bies, D., Klee, H. J., and Yanofsky, M. F. (2006). Pod shatter-resistant Brassica fruit produced by ectopic expression of the FRUITFULL gene. Plant biotechnology journal *4*, 45-51.

Pabon-Mora, N., Ambrose, B. A., and Litt, A. (2012). Poppy APETALA1/FRUITFULL orthologs control flowering time, branching, perianth identity, and fruit development. Plant Physiol *158*, 1685-1704.

Pabon-Mora, N., Wong, G. K. S., and Ambrose, B. A. (2014). Evolution of fruit development genes in flowering plants. Front Plant Sci *5*.

Palatnik, J. F., Allen, E., Wu, X., Schommer, C., Schwab, R., Carrington, J. C., and Weigel, D. (2003). Control of leaf morphogenesis by microRNAs. Nature *425*, 257-263.

Pekker, I., Alvarez, J. P., and Eshed, Y. (2005). Auxin response factors mediate Arabidopsis organ asymmetry via modulation of KANADI activity. Plant Cell *17*, 2899-2910.

Petrasek, J., and Friml, J. (2009). Auxin transport routes in plant development. Development *136*, 2675-2688.

Pyke, K. A., Marrison, J. L., and Leech, R. M. (1991). Temporal and spacial development of the cells of the expanding first leaf of Arabidopsis thaliana (L.) Heynh. J Exp Bot *42*, 1407-1416.

Rajani, S., and Sundaresan, V. (2001). The Arabidopsis myc/bHLH gene ALCATRAZ enables cell separation in fruit dehiscence. Current biology : CB *11*, 1914-1922.

Redei, G. P., and Koncz, C. (1992). Classical Mutagenesis. In Methods in Arabidopsis Research, C. Koncz, N.-H. Chua, and J. Schell, eds. (Singapore

London: World Scientific Publishing), pp. 16-82.

Robinson, S., Barbier de Reuille, P., Chan, J., Bergmann, D., Prusinkiewicz, P., and Coen, E. (2011). Generation of spatial patterns through cell polarity switching. Science *333*, 1436-1440.

Roeder, A. H., Ferrandiz, C., and Yanofsky, M. F. (2003). The role of the REPLUMLESS homeodomain protein in patterning the Arabidopsis fruit. Current biology : CB *13*, 1630-1635.

Roeder, A. H. K., Chickarmane, V., Cunha, A., Obara, B., Manjunath, B. S., and Meyerowitz, E. M. (2010). Variability in the Control of Cell Division Underlies Sepal Epidermal Patterning in Arabidopsis thaliana. Plos Biology *8*.

Roeder, A. H. K., and Yanofsky, M. F. (2006). Fruit Development in *Arabidopsis*. The Arabidopsis Book *4*.

Rolland-Lagan, A. G., Bangham, J. A., and Coen, E. (2003). Growth dynamics underlying petal shape and asymmetry. Nature *422*, 161-163.

Rolland-Lagan, A. G., and Prusinkiewicz, P. (2005). Reviewing models of auxin canalization in the context of leaf vein pattern formation in Arabidopsis. The Plant journal : for cell and molecular biology *44*, 854-865.

Romera-Branchat, M., Ripoll, J. J., Yanofsky, M. F., and Pelaz, S. (2012). The WOX13 homeobox gene promotes replum formation in the Arabidopsis thaliana fruit. The Plant journal : for cell and molecular biology.

Sahlin, P., Söderberg, B., and Jönsson, H. (2009). Regulated transport as a mechanism for pattern generation: Capabilities for phyllotaxis and beyond. Journal of Theoretical Biology *258*, 60-70.

Sauret-Gueto, S., Schiessl, K., Bangham, A., Sablowski, R., and Coen, E. (2013). JAGGED Controls Arabidopsis Petal Growth and Shape by Interacting with a Divergent Polarity Field. Plos Biology *11*.

Scanlon, M. J., Schneeberger, R. G., and Freeling, M. (1996). The maize mutant narrow sheath fails to establish leaf margin identity in a meristematic domain. Development *122*, 1683-1691.

Schiessl, K., Kausika, S., Southam, P., Bush, M., and Sablowski, R. (2012). JAGGED controls growth anisotropyand coordination between cell sizeand cell cycle during plant organogenesis. Current biology : CB *22*, 1739-1746.

Schmundt, D., Stitt, M., Jähne, B., and Schurr, U. (1998). Quantitative analysis of the local rates of growth of dicot leaves at a high temporal and spatial resolution, using image sequence analysis. The Plant Journal *16*, 505-514.

Scutt, C. P., Vinauger-Douard, M., Fourquin, C., Finet, C., and Dumas, C. (2006). An evolutionary perspective on the regulation of carpel development. J Exp Bot *57*, 2143-2152.

Sessions, A., Nemhauser, J. L., McColl, A., Roe, J. L., Feldmann, K. A., and Zambryski, P. C. (1997). ETTIN patterns the Arabidopsis floral meristem and reproductive organs. Development *124*, 4481-4491.

Sessions, R. (1997). Arabidopsis (Brassicaceae) flower development and gynoecium patterning in wild type and Ettin mutants. Am J Bot *84*, 1179.

Sharpe, J., Ahlgren, U., Perry, P., Hill, B., Ross, A., Hecksher-Sorensen, J., Baldock, R., and Davidson, D. (2002). Optical projection tomography as a tool for 3D microscopy and gene expression studies. Science *296*, 541-545.

Shull, G. H. (1914). Duplicate genes for capsule-form in *Capsella bursa-pastoris*. Z Abst u Vererbl *12*, 97-149.

Sicard, A., Stacey, N., Hermann, K., Dessoly, J., Neuffer, B., Baurle, I., and Lenhard, M. (2011). Genetics, evolution, and adaptive significance of the selfing syndrome in the genus Capsella. Plant Cell *23*, 3156-3171.

Sicard, A., Thamm, A., Marona, C., Lee, Y. W., Wahl, V., Stinchcombe, J. R., Wright, S. I., Kappel, C., and Lenhard, M. (2014). Repeated evolutionary changes of leaf morphology caused by mutations to a homeobox gene. Current biology : CB *24*, 1880-1886.

Sieburth, L. E., Drews, G. N., and Meyerowitz, E. M. (1998). Non-autonomy of AGAMOUS function in flower development: use of a Cre/loxP method for mosaic analysis in Arabidopsis. Development *125*, 4303-4312.

Silk, W. K., and Erickson, R. O. (1979). Kinematics of plant growth. Journal of Theoretical Biology *76*, 481-501.

Slotte, T., Hazzouri, K. M., Agren, J. A., Koenig, D., Maumus, F., Guo, Y. L., Steige, K., Platts, A. E., Escobar, J. S., Newman, L. K.*, et al.* (2013). The Capsella rubella genome and the genomic consequences of rapid mating system evolution. Nature genetics *45*, 831-835.

Smith, R. S., Guyomarc'h, S., Mandel, T., Reinhardt, D., Kuhlemeier, C., and Prusinkiewicz, P. (2006). A plausible model of phyllotaxis. Proceedings of the National Academy of Sciences of the United States of America *103*, 1301-1306.

Smykal, P., Gennen, J., De Bodt, S., Ranganath, V., and Melzer, S. (2007). Flowering of strict photoperiodic Nicotiana varieties in non-inductive conditions by transgenic approaches. Plant molecular biology *65*, 233-242.

Smyth, D. R., Bowman, J. L., and Meyerowitz, E. M. (1990). Early flower development in Arabidopsis. Plant Cell *2*, 755-767.

Sohlberg, J. J., Myrenas, M., Kuusk, S., Lagercrantz, U., Kowalczyk, M., Sandberg, G., and Sundberg, E. (2006). STY1 regulates auxin homeostasis and affects apical-basal patterning of the Arabidopsis gynoecium. Plant Journal *47*, 112-123.

Sotelo-Silveira, M., Cucinotta, M., Chauvin, A. L., Chavez Montes, R. A., Colombo, L., Marsch-Martinez, N., and de Folter, S. (2013). Cytochrome P450 CYP78A9 is involved in Arabidopsis reproductive development. Plant Physiol *162*, 779-799.

Sotelo-Silveira, M., Marsch-Martínez, N., and de Folter, S. (2014). Unraveling the signal scenario of fruit set. Planta *239*, 1147-1158.

Spence, J., Vercher, Y., Gates, P., and Harris, N. (1996). 'Pod shatter' in Arabidopsis thalianaBrassica napus and B. juncea. Journal of Microscopy *181*, 195-203.

Stadler, L. J. (1930). Some genetic effects of xrays in plnats. Journal of Heredity *21*, 3-20.

Steffensen, D. M. (1968). A Reconstruction of Cell Development in the Shoot Apex of Maize. Am J Bot *55*, 354-369.

Stein, O. L., and Steffensen, D. M. (1959). THE ACTIVITY OF X-RAYED APICAL MERISTEMS - A GENETIC AND MORPHOGENETIC ANALYSIS IN ZEA-MAYS. Zeitschrift Fur Vererbungslehre *90*, 483-502.

Stephenson, P., Baker, D., Girin, T., Perez, A., Amoah, S., King, G. J., and Ostergaard, L. (2010). A rich TILLING resource for studying gene function in Brassica rapa. BMC plant biology *10*, 62.

Sternberg, N., and Hamilton, D. (1981). BACTERIOPHAGE-P1 SITE-SPECIFIC RECOMBINATION .1. RECOMBINATION BETWEEN LOXP SITES. Journal of Molecular Biology *150*, 467-486.

Suzuki, T., Eiguchi, M., Kumamaru, T., Satoh, H., Matsusaka, H., Moriguchi, K., Nagato, Y., and Kurata, N. (2008). MNU-induced mutant pools and high performance TILLING enable finding of any gene mutation in rice. Mol Genet Genomics *279*, 213-223.

Till, B. J., Cooper, J., Tai, T. H., Colowit, P., Greene, E. A., Henikoff, S., and Comai, L. (2007). Discovery of chemically induced mutations in rice by TILLING. BMC plant biology *7*, 19.

Till, B. J., Reynolds, S. H., Greene, E. A., Codomo, C. A., Enns, L. C., Johnson, J. E., Burtner, C., Odden, A. R., Young, K., Taylor, N. E*., et al.* (2003). Large-scale discovery of induced point mutations with high-throughput TILLING. Genome research *13*, 524-530.

Till, B. J., Reynolds, S. H., Weil, C., Springer, N., Burtner, C., Young, K., Bowers, E., Codomo, C. A., Enns, L. C., Odden, A. R*., et al.* (2004). Discovery of induced point mutations in maize genes by TILLING. BMC plant biology *4*, 12.

Trigueros, M., Navarrete-Gomez, M., Sato, S., Christensen, S. K., Pelaz, S., Weigel, D., Yanofsky, M. F., and Ferrandiz, C. (2009). The NGATHA genes direct style development in the Arabidopsis gynoecium. Plant Cell *21*, 1394-1409.

Uauy, C., Paraiso, F., Colasuonno, P., Tran, R. K., Tsai, H., Berardi, S., Comai, L., and Dubcovsky, J. (2009). A modified TILLING approach to detect induced mutations in tetraploid and hexaploid wheat. BMC plant biology *9*, 115.

Urbanus, S. L., de Folter, S., Shchennikova, A. V., Kaufmann, K., Immink, R. G., and Angenent, G. C. (2009). In planta localisation patterns of MADS domain proteins during floral development in Arabidopsis thaliana. BMC plant biology *9*, 5.

van der Knaap, E., and Tanksley, S. D. (2001). Identification and characterization of a novel locus controlling early fruit development in tomato. Theoretical and Applied Genetics *103*, 353-358.

van Dijk, A. D. J., Morabito, G., Fiers, M., van Ham, R. C. H. J., Angenent, G. C., and Immink, R. G. H. (2010). Sequence Motifs in MADS Transcription Factors Responsible for Specificity and Diversification of Protein-Protein Interaction. Plos Computational Biology *6*.

Vivian-Smith, A., and Koltunow, A. M. (1999). Genetic analysis of growth-regulator-induced parthenocarpy in arabidopsis. Plant Physiology *121*, 437-451.

Vivian-Smith, A., Luo, M., Chaudhury, A., and Koltunow, A. (2001). Fruit development is actively restricted in the absence of fertilization in Arabidopsis. Development *128*, 2321-2331.

Vlad, D., Kierzkowski, D., Rast, M. I., Vuolo, F., Dello Ioio, R., Galinha, C., Gan, X., Hajheidari, M., Hay, A., Smith, R. S.*, et al.* (2014). Leaf shape evolution through duplication, regulatory diversification, and loss of a homeobox gene. Science *343*, 780-783.

Wachsman, G., Heidstra, R., and Scheres, B. (2011). Distinct Cell-Autonomous Functions of RETINOBLASTOMA-RELATED in Arabidopsis Stem Cells Revealed by the Brother of Brainbow Clonal Analysis System. Plant Cell *23*, 2581-2591.

Walpole, J., Papin, J. A., and Peirce, S. M. (2013). Multiscale computational models of complex biological systems. Annual review of biomedical engineering *15*, 137-154.

Wang, S., Lu, G., Hou, Z., Luo, Z., Wang, T., Li, H., Zhang, J., and Ye, Z. (2014). Members of the tomato FRUITFULL MADS-box family regulate style abscission and fruit ripening. J Exp Bot *65*, 3005-3014.

Wen, J. Q., Lease, K. A., and Walker, J. C. (2004). DVL, a novel class of small polypeptides: overexpression alters Arabidopsis development. Plant Journal *37*, 668-677.

White, D. W. (2006). PEAPOD regulates lamina size and curvature in Arabidopsis. Proceedings of the National Academy of Sciences of the United States of America *103*, 13238-13243.

Winkler, S., Schwabedissen, A., Backasch, D., Bokel, C., Seidel, C., Bonisch, S., Furthauer, M., Kuhrs, A., Cobreros, L., Brand, M., and Gonzalez-Gaitan, M. (2005). Target-selected mutant screen by TILLING in Drosophila. Genome research *15*, 718-723.

Woods, J. C. (2010). Analysis of FRUITFULL promoter motifs and their influence on valve expression during fruit development. In.

Xing, S., Salinas, M., Garcia-Molina, A., Hohmann, S., Berndtgen, R., and Huijser, P. (2013). SPL8 and miR156-targeted SPL genes redundantly regulate Arabidopsis gynoecium differential patterning. The Plant journal : for cell and molecular biology *75*, 566-577.

Yang, X. Y., Wang, Y., Jiang, W. J., Liu, X. L., Zhang, X. M., Yu, H. J., Huang, S. W., and Liu, G. Q. (2013). Characterization and expression profiling of cucumber kinesin genes during early fruit development: revealing the roles of kinesins in exponential cell production and enlargement in cucumber fruit. J Exp Bot *64*, 4541-4557.